Inorganic and Stable Isotope Geochemistry of Tropical Atlantic/Caribbean Planktonic Foraminifera: Implications for the Reconstruction of Upper Ocean Temperatures and Stratification

Dissertation

zur Erlangung des Doktorgrades

der Mathematisch-Naturwissenschaftlichen Fakultät

der Christian-Albrechts-Universität

zu Kiel

vorgelegt

von

Marcus Regenberg

Kiel, Dezember 2006

Abstract

The reconstruction of paleoceanographic and environmental parameters from marine sediments depends on the reliability of proxy indicators from planktonic foraminifera. Therefore, the aim of this thesis is to improve our confidence in planktonic foraminiferal proxies as indicators of upper ocean temperatures and stratification. This requires the understanding of parameters originating the proxy signal and of secondary processes, which potentially comprise the fidelity of the proxy signal. To achieve this goal, geochemical analyses of multiple species of planktonic foraminifera from marine surface sediments and sediment cores were performed.

Planktonic foraminifera from the examined tropical Atlantic and Caribbean sediment-surface samples (0–1 cm) are shown to reflect the modern hydrographic conditions. Planktonic foraminiferal Mg/Ca and δ^{18}O reveal the systematic succession of the different species according to their expected increased calcification depths. The general westward-directed increase in their calcification depths is depending on the east-west increase in thermocline depth.

Decreasing planktonic foraminiferal Mg/Ca related to decreasing carbonate ion concentration in the Caribbean generates a dissolution pattern with preserved ratios down to depths $\sim$1.5 km above the lysocline. Below carbonate ion concentrations of 26–18 μmol/kg, Mg/Ca starts to decrease linearly, which allows to recalculate originate Mg/Ca from a dissolution-affected ratio.

Calibration of Mg/Ca with δ^{18}O-derived calcification temperatures reveals similar exponential temperature sensitivities of 7–11% per 1°C for species examined, yet significantly different preexponential constants for shallow- and thermocline-dwelling (0.23–0.65) compared to deep-dwelling species (0.83–1.31). Corresponding multispecies calibrations indicate that a 'warm water' calibration is valid for temperatures above 19°C, and a 'cold water' calibration for temperatures below 15°C.

The changing depth of the modern westward-directed deepening of the tropical Atlantic thermocline is reflected in planktonic foraminiferal δ^{18}O and δ^{13}C from different preferred calcification depths. Interspecific δ^{18}O differences of intermediate or thermocline dwellers minus shallow-dwelling (deep-dwelling) species show decreased (increased) values, when the thermocline deepens. A zonal decrease in δ^{13}C differences between shallow- and deep-dwelling species is observed for decreasing vertical nutrient gradients towards the Caribbean, which are associated with the increasing thermocline depth.

Alteration of downcore deep-sea sediments in the vicinity of the Bahama platform results in micro-scale inorganic crystallites on planktonic foraminiferal test. Mg/Ca and Sr/Ca of the

crystallites are 4–6 times elevated and 2–3 times depleted, respectively, compared to the original foraminiferal test. This causes a anomalous elevation of the planktonic foraminiferal Mg/Ca above 6 mmol/mol, when crystallite proportion is 10–20 percent. The absence of high-magnesium calcite from the sediment synchronizes these anomalous Mg/Ca ratios. Prior to ∼550 thousand years, changed geochemical characteristics of the foraminifera suggest export of pore fluid to the overlying sediment column.

Zusammenfassung

Die Rekonstruktion von Umwelt- und paläozeanographischen Parametern mittels mariner Sedimente ist von der Zuverlässigkeit der dafür genutzten Proxy-Indikatoren in planktonischen Foraminiferen abhängig. Ziel dieser Arbeit ist daher das Vertrauen in Proxys planktonischer Foraminiferen als Anzeiger von Ozeantemperaturen und -stratifizierung zu verbessern. Dazu wird ein gutes Verständnis der Parameter, die das Proxy-Signal erzeugen, sowie über sekundäre Prozesse, die möglicherweise die Auflösung dieses Signals einschränken, benötigt. Um dieses Ziel zu erreichen, wurden geochemische Analysen verschiedener Arten planktonischer Foraminiferen aus marinen Oberflächensedimenten und Sedimentkernen durchgeführt.

Für planktonische Foraminiferen aus den untersuchten Sediment-Oberflächenproben (0–1 cm) konnte gezeigt werden, dass diese die moderne Hydrographie des tropischen Atlantiks und der Karibik widerspiegeln. Mg/Ca und δ^{18}O unterschiedlicher Arten planktonischer Foraminiferen zeigen die systematische Abfolge hinsichtlich ihrer zu erwartenden zunehmenden Kalzifizierungstiefen. Die allgemein westwärts gerichtete Zunahme ihrer Kalzifizierungstiefen ist abhängig von der Ost-West-Vertiefung der Thermokline.

Die Abnahme von Mg/Ca planktonischer Foraminiferen und der dazu in Beziehung stehenden Karbonationenkonzentration erzeugen ein Lösungsmuster mit gleichbleibenden Verhältnissen bis zu einer Tiefe von $\sim$1.5 km oberhalb der Lysokline. Bei einer Karbonationenkonzentration unterhalb von 26–18 μmol/kg beginnt Mg/Ca linear abzunehmen, was eine Berechnung des originalen Mg/Ca aus einem lösungsbeeinflussten Verhältnis erlaubt.

Die Kalibrierung der Mg/Ca mit δ^{18}O-Kalzifizierungstemperaturen der untersuchten Arten zeigt untereinander ähnliche exponentielle Temperaturempfindlichkeiten von 7–10% pro 1°C, jedoch signifikant unterschiedliche preexponentielle Konstanten für flach und innerhalb der Thermokline lebende Arten (0.23–0.65) im Vergleich zu tief lebenden Arten (0.83–1.31). Zugehörige Kalibrationen verschiedener Arten zeigen, dass eine 'Warmwasser'-Kalibration für Temperaturen oberhalb von 19°C und eine 'Kaltwasser'-Kalibration für Temperaturen unterhalb von 15°C gelten.

Die Änderung der Tiefe der modernen, nach Westen abgesenkten Thermokline des tropischen Atlantiks wird in den δ^{18}O und δ^{13}C der planktonischen Foraminiferen, welche unterschiedliche Kalzifizierungstiefen bevorzugen, widergespiegelt. Bei einer Vertiefung der Thermokline zeigen die δ^{18}O-Differenzen der intermediären Arten und der Thermoklinenarten minus den flach (tief) lebenden Arten geringe (hohe) Beträge. Eine zonale Abnahme der δ^{13}C-Differenzbeträge

zwischen flach- und tieflebenden Arten in Richtung Karibik wurde mit einer gleichzeitigen Verringerung des vertikalen Nährstoffgradienten, die mit der zunehmenden Thermoklinentiefe zusammenhängt, beobachtet.

Veränderungen von Tiefsee-Sedimenten in der Nähe der Bahama-Plattform resultieren aus mikroskaligen inorganischen Kristallen auf planktonischen Foraminiferengehäusen. Mg/Ca und Sr/Ca der Kristalle sind vier- bis sechsfach erhöht bzw. zwei- bis dreifach erniedrigt im Vergleich zur originalen Foraminiferenprobe. Dies bedingt eine anomale Zunahme des Mg/Ca planktonischer Foraminiferen über 6 mmol/mol bei Kristallanteilen von 10–20%. Das Fehlen von Hochmagnesium-Kalzit im Sediment verläuft synchron mit diesen anomalen Mg/Ca-Verhältnissen. Für den Zeitraum vor $\sim$550 Tausend Jahren lassen veränderte geochemische Kennzeichen der Foraminiferen einen Export von Porenfluid in die überliegende Sedimentsäule vermuten.

Danksagung

Hier und jetzt möchte ich all denen danken, die mich die Jahre hindurch begleitet haben oder zumindest einen Teil des Weges.

Für die Übernahme des Referats und des Korreferats bin ich PD Dr. Dirk Nürnberg, Prof. Wolf-Christian Dullo und Prof. Wolfgang Kuhnt sehr verbunden.

Ein besonderer Dank gilt Prof. Wolf-Christian Dullo und PD Dr. Dirk Nürnberg für das Schaffen der Doktorandenstelle im Projekt RASTA. Darüber hinaus bedanke ich mich bei Dir, Dirk, dass Du Dir Zeit für meine Fragen und Probleme genommen hast. Die Gespräche und Diskussionen mit Dir halfen mir Sachverhalte aus anderen Blickwinkeln zu betrachten und neue Lösungswege zu finden.

Für hervorragende Zusammenarbeit bei der Fertigstellung der Manuskripte danke ich Dr. Silke Steph. Mit Dir ging die großartige Diskussionspartnerin weg von Kiel. Gern denke ich an intensive und bereichernde Diskussionen mit Prof. Ralf Tiedemann, Dr. Stefan Mulitza, Dr. Joachim Schönfeld, Dr. Jeroen Groeneveld, Dr. Lars Reuning und Dr. Arne Sturm zurück. Dr. Uwe Pflaumann danke herzlich für die Einführung in die Taxonomie von Foraminiferen. Von der Einweisung in das Programm co2sys durch Prof. Douglas Wallace und insbesondere Anke Schneider profitierte meine Arbeit in ganz erheblichem Maße.

All den Personen ein ganz großes Dankeschön, die mir bei den Laborarbeiten hilfreich zur Seite standen: Allen voran Silvia Koch, die das Mg-Labor 'zu meiner Zeit' stets in Schuss gehalten hat, und Lulzim Haxhiaj, der meinen Isotopenmessungen freudig entgegensah. Bei den Messungen an der ICP der Uni Kiel hatte ich das Vergnügen der Zusammenarbeit mit Dr. Dieter Garbe-Schönberg und Karin Kißling. Langwierige Vorbereitungen für XRD-Messungen wurden mir versüßt durch die freundliche Unterstützung von Jutta Heinze.

Meine fleißigen HiWis haben mir lange Nächte am Mikroskop erspart. Danke dafür an Daniel Oesterwind, Stefan Dennenmoser, Annekatrin und Silke Meier.

Andeas Hoelzl und Ulf Ehlers erläuterten mir immer wieder gern mathematische Zusammenhänge - vielen Dank!!

Für stets hilfsbereites Auftreten, das mir ein wohliges Betriebsklima vermittelte, möchte ich Pallass Ray Eddie, Maren Dalock und Barbara Moll herzlich grüßen.

Ich hoffe, dass meine geschätzten Mitdoktoranden Anke Dürkop, Rina Zuraida, Jeannette Lezius, Reinhard Kozdon, Lester Lembke-Jene und Steffen Hetzinger auch ihre Arbeit in der Güte abschließen können wie es mir vergönnt war.

Diese Doktorarbeit wurde mit Mitteln des Bundesministeriums für Bildung und Forschung im Rahmen des Forschungsprojektes RASTA finanziert. Insbesondere danke ich Prof. Wolf-Christian Dullo für die Finanzierung meines dritten Doktorandenjahres mit Geldern aus seinem Leibnizpreis.

Contents

List of Figures

List of Tables

Chapter 1

Introduction

1.1 The Use of Proxies in Paleoceanography

The primary objective of paleoceanography is the reconstruction of physico-chemical seawater conditions. In order to deduce the states of past oceans and climates, secondary indicators, which are in close relationship to certain seawater conditions, are employed for this challenge. Such a measurable descriptor for a desired (but unobservable) variable is called "proxy" (*Wefer et al.*, 1999). One of the most desired tasks in paleoceanography is to determine the temperature evolution of past oceans, since oceans are crucial components of the global climate system and their temperatures are representative for the climatic state. Earth scientists have developed a suite of inorganic, organic, and isotope geochemical proxies to determine past ocean temperatures with a great deal of recent progress. Heightened by the threat of global warming, the understanding of the global climate system is one of the striking challenges. Since such knowledge is strongly entailed with paleoceanographic research, paleotemperature studies will remain important and vivid for future research.

In order to contribute to these demanding questions, this thesis was accomplished within the framework of the project 'RASTA – Rapid climate change in the western tropical Atlantic', funded by the German Ministry of Education and Research (BMBF), and the ongoing allowance by the Leibniz Award Du 129/33 of Professor Wolf-Christian Dullo. Inorganic and stable isotope geochemistry of planktonic foraminifera was investigated to assess relevant primary and secondary effects on the signature of their proxies.

1.2 Structure of the Thesis

The main objectives of this thesis are

- the evaluation of the effect of dissolution on planktonic foraminiferal Mg/Ca ratios,
- the calibration of Mg/Ca ratios of multiple planktonic foraminifera from different preferred habitat depths,

- the description of a stratified upper ocean with δ^{18}O and δ^{13}C of planktonic foraminifera, and
- the characterization of diagenetic alteration of shallow-burial deep-sea sediments.

Dissolution Effect on Planktonic Foraminiferal Mg/Ca

As dissolution on foraminiferal Mg/Ca ratios is accompanied by calcite loss, two approaches of quantifying the dissolution effect on foraminiferal Mg/Ca ratios have been pursued. *Rosenthal and Lohmann* (2002) detected that the loss in mass of foraminiferal tests is associated with the decrease in their Mg/Ca. *Dekens et al.* (2002) implemented dissolution-correcting factors for planktonic foraminiferal Mg/Ca in the calibrations of the species, indicating that dissolution starts right at the surface of the ocean. The approach in this thesis relies on the relatively constant thermal structure of the Caribbean with only small spatial variation in temperatures at the calcification depths of modern shallow-, thermocline-, intermediate-, and deep-dwelling foraminifera, which reduces the temperature-induced variability in Mg/Ca to a minimum. The results are introduced and disscussed in Chapter 2, which was published in *Geochemistry Geophysics Geosystems* (*Regenberg et al.*, 2006a).

Temperature Calibration of Multispecies Planktonic Foraminiferal Mg/Ca

Calibration of Mg/Ca ratios with temperatures is crucial to recalculate past ocean temperatures from fossil foraminifera. Empirical assessment of temperature associated with a Mg/Ca ratio is based on two kinds of foraminiferal studies: Cultivating studies with prescribed conditions in an artificial environment and studies of settled material that reflects known temperatures. Like *Elderfield and Ganssen* (2000) and *Anand et al.* (2003), this thesis used multiple planktonic foraminifera from shallow, thermocline, intermediate, and deep habitats from sediment-surface samples in combination with δ^{18}O-derived calcification temperatures. Presentation and discussion of this modern tropical Atlantic and Caribbean data set is presented in Chapter 3, which was submitted to *Earth and Planetary Science Letters* (*Regenberg et al.*, 2006b).

Stable Isotopes of Planktonic Foraminifera

Previously published plankton-tow and core-top studies from the tropical Atlantic (*Ravelo et al.*, 1990; *Ravelo and Fairbanks*, 1992, 1995; *Niebler et al.*, 1999; *Ravelo and Andreasen*, 1999) demonstrated that changes in stable isotope gradients between planktonic foraminifera from different preferred habitats are valuable indicators for changes in upper ocean stratification. This thesis compares planktonic foraminiferal species covering all habitat depths from tropical Atlantic and Caribbean sediment-surface samples with a changing stratification regime along the same area. The results and their discussion is presented in Chapter 4, which is in preparation for publication.

Effect of Diagenesis on Planktonic Foraminiferal Geochemistry

Another process possibly affecting the planktonic foraminiferal geochemical composition next to dissolution is the diagenetic alteration by addition to and/or (partial) replacement of the initial test. A demanding issue in the examination of foraminifera involved in diagenesis is the assessment of the extent of the alteration. Shallow-burial deep-sea alteration of Atlantic sediment cores in the vicinity of the Bahamian platform and its effect on the changing effect on the geochemical composition on planktonic foraminifera is described and estimated in Chapter 5. This manuscript is in preparation for publication.

1.3 Planktonic Foraminifera

Planktonic foraminifera are found in marine pelagic environments. In general, their classification is based on that of *Loeblich and Tappan* (1964). Foraminifera are testate protozoa, which possess granuloreticulose pseudopodia consisting of ectoplasm. Bi-directional cytoplasmic flow along these pseudopodia, which may include symbiotic dinoflagellates (e.g., shallow-dwelling species), carries granules for vacuolization. The name foraminifera is derived from the foramen, the connecting hole through the wall (septa) between each chamber.

The geochemical analyses of this thesis were performed on planktonic foraminifera from different preferred habitats. Shallow-dwelling species are *Globigerinoides ruber* as pink and white varieties, and *Globigerinoides sacculifer*. *Globorotalia menardii* and *Neogloboquadrina dutertrei* are indicative of the thermocline. Intermediate to deep habitats are supposed for *Globorotalia tumida*, *Globorotalia scitula*, *Globorotalia truncatulinoides* (dextral variety) and *Globorotalia crassaformis*. For summary and illustration of the habitats of the planktonic species used in this study, see Figure 1.1.

1.3.1 Planktonic Foraminiferal Geochemical Signature

Planktonic foraminifera pass through complex ontogenetic cycles with vertical migration (of tens to hundreds of meters) through the water column and precipitation of different kinds of calcite crusts at different depth levels (*Bé and Ericson*, 1963; *Bé and Lott*, 1964; *Bé*, 1977, 1980; *Fairbanks and Wiebe*, 1980a; *Fairbanks et al.*, 1980b, 1982; *Duplessy et al.*, 1981; *Erez and Honjo*, 1981; *Bé et al.*, 1983; *Hemleben et al.*, 1989; *Bijma et al.*, 1990, 1994; *Schweitzer and Lohmann*, 1991; *Lohmann*, 1995; *LeGrande et al.*, 2004; *Lončarić et al.*, 2006).

The associated varying geochemical signature within a single test (*Curry and Crowley*, 1987; *Spero and Williams*, 1989; *Lohmann*, 1995; *Nürnberg et al.*, 1996a; *Rosenthal et al.*, 2000; *Benway et al.*, 2003; *Eggins et al.*, 2003; *Reichart et al.*, 2003; *Klinkhammer et al.*, 2004; *LeGrande et al.*, 2004; *Mulitza et al.*, 2004; *McKenna and Prell*, 2004; *Sadekov et al.*, 2005; *Lončarić et al.*, 2006) may represent a mixture of carbonate that was precipitated under different temperature and salinity conditions within (sub)surface, thermocline and subthermocline waters. The calcification depth derived by the oxygen isotope composition (δ^{18}O), thus, represents an integrated and mass

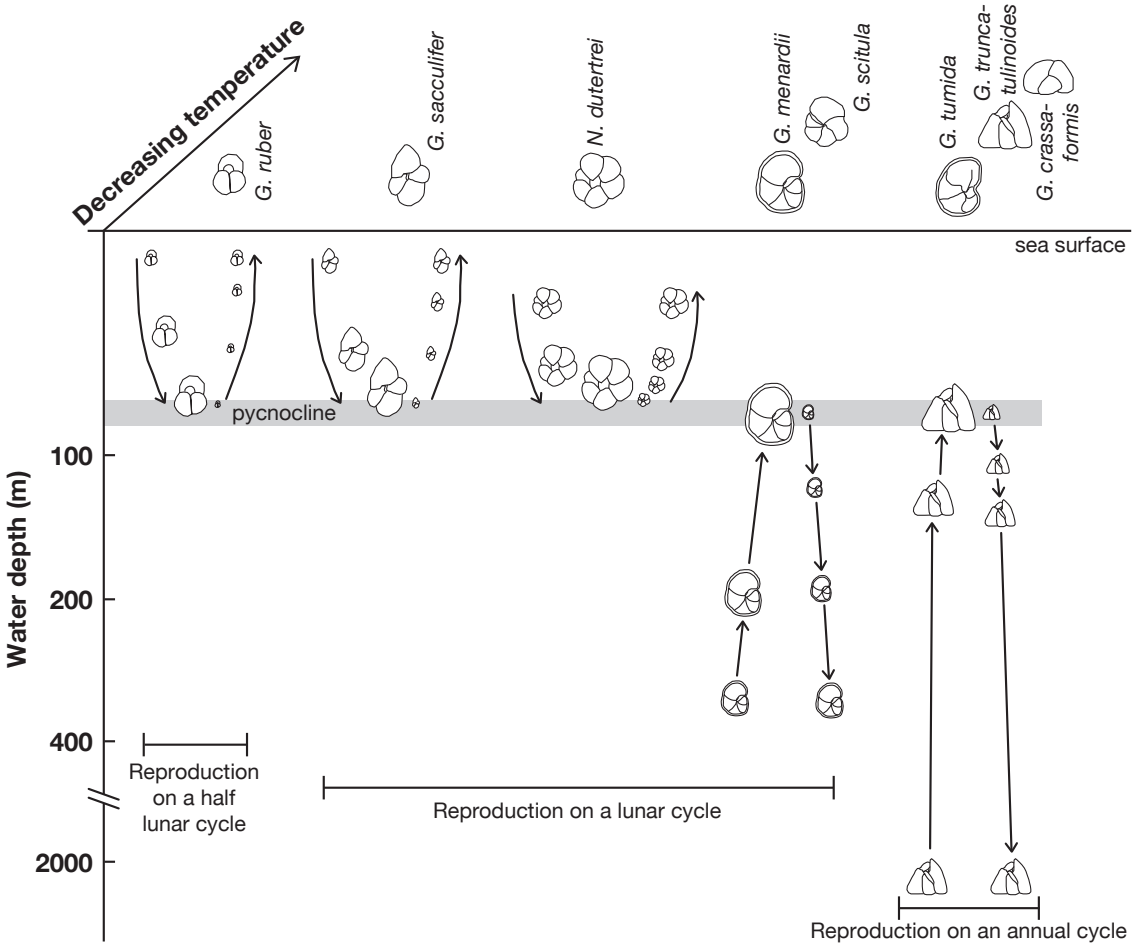

Figure 1.1 Sketch of planktonic foraminiferal habitats and their distribution in the upper water column according to water depth and relative temperature succession. Their different inhabited ecological niches are characterized by species-specific demands on light, chlorophyll concentrations, salinity, temperature, and food availability. Indicated ontogenetic cycles are supposedly emanating from reproduction close to the pycnocline, where feeding conditions are optimal. Figure modified after *Schiebel and Hemleben* (2005).

weighted signal that potentially records all variation (e.g., secondary or gametogenic calcite crusts) of the habitat depth Figure 1.1 by calcite precipitation.

Planktonic Foraminifera as Temperature Indicator

Oxygen bears three stable isotopes that appear in certain proportions compared to each other. The lightest isotope ^{16}O is the most abundant (99.76%), whereas ^{17}O and ^{18}O account for only 0.04% and 0.2%, respectively. The isotopic composition of an oxygen-bearing phase, denoted in permil (‰), is expressed as:

$$\delta^{18}O = [\frac{(^{18}O/^{16}O)_{phase} - (^{18}O/^{16}O)_{standard}}{(^{18}O/^{16}O)_{standard}}] \cdot 1000$$

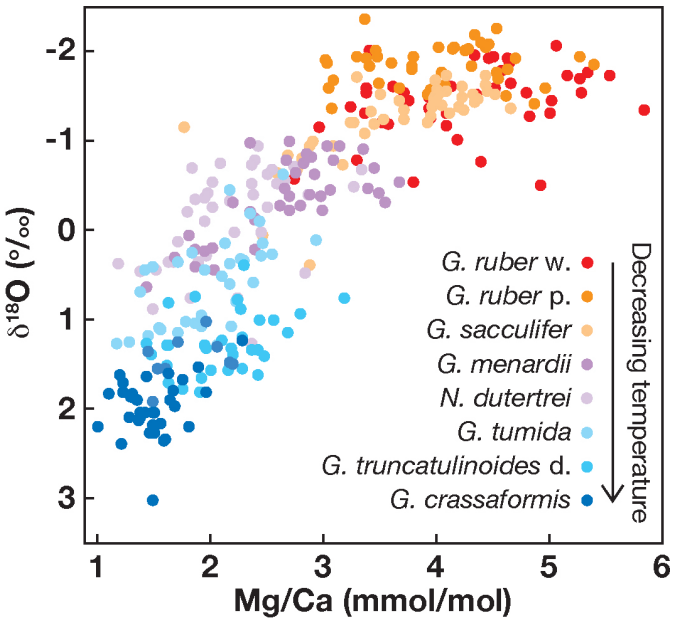

Figure 1.2 Measured sediment-surface planktonic foraminiferal Mg/Ca *vs.* δ^{18}O for all examined species of this thesis: Both geochemical proxies indicate higher (red colors) to lower (blue colors) temperatures according to the different expected calcification depths of the species.

The use of oxygen isotope ratios as a paleotemperature indicator in carbonate minerals is based on the thermodynamic fractionation between ^{16}O and ^{18}O that occurs during precipitation (e.g., *Urey*, 1947; *O'Neil et al.*, 1969; *Shackleton*, 1974; *Kim and O'Neil*, 1997; *Zhou and Zheng*, 2003). The δ^{18}O of marine carbonates is dependent, among temperature, on the δ^{18}O of the ambient seawater. The δ^{18}O of the seawater depends on the volume of globally fixed ice that deprives the ^{16}O content of seawater, and on the local precipitation/evaporation ratio for water masses close to the sea surface.

Mg/Ca ratios of foraminifera are common for the use as paleotemperature indicator, since the Mg^{2+} content of the biogenic calcite is governed by the systematics of a partition coefficient D_{Mg} between the solid (calcite) and the fluid phase (seawater):

$$D_{Mg} = \frac{(Mg/Ca)_{solid}}{(Mg/Ca)_{fluid}}$$

Modern seawater Mg/Ca amounts to 5.1 mol/mol. Partition coefficients for inorganic calcites range from 0.01–0.06 (e.g., *Katz*, 1973; *Mucci*, 1987), which is an order of magnitude higher than for planktonic foraminiferal calcite. Application of planktonic foraminiferal Mg/Ca of the studied species is based on empirical calibrations (e.g., *Nürnberg et al.*, 1996a; *Lea et al.*, 1999; *Elderfield and Ganssen*, 2000; *Lea et al.*, 2000; *Nürnberg et al.*, 2000; *Dekens et al.*, 2002; *Whitko et al.*, 2002; *Rosenthal and Lohmann*, 2002; *Anand et al.*, 2003; *McKenna and Prell*, 2004; *McConnell and Thunell*, 2005).

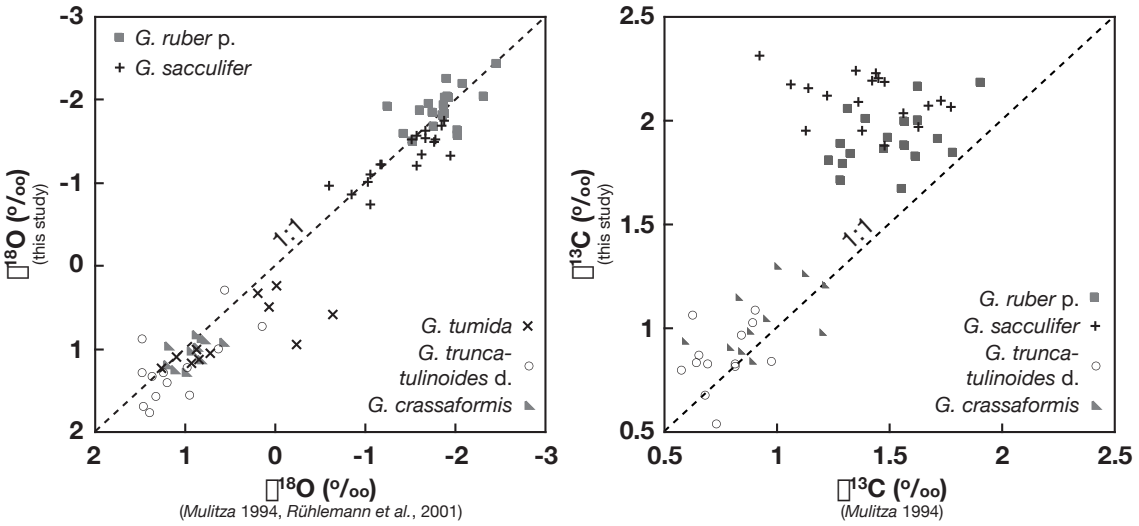

Figure 1.3 Measured δ^{13}C and δ^{18}O values of replicate planktonic foraminiferal samples: Specimens from this study are form the 315–400 μm fraction, tests in *Mulitza* (1994) and *Rühlemann et al.* (2001) have been selected if the longest elongation of a specimen was 400 μm.

To illustrate the close relation of both temperature proxies, we plotted planktonic foraminiferal Mg/Ca *vs.* δ^{18}O from the same sample. Using those paired measurements, possible habitat and seasonal effects are excluded with respect to combined records e.g., of alkenone temperatures and foraminiferal δ^{18}O (*Nürnberg et al.*, 2000).

Planktonic Foraminifera and the Size Effect

The carbon isotope composition (δ^{13}C) of planktonic foraminifera is dependent on the dissolved inorganic carbon (DIC) content at their preferred calcification depths. $\delta^{13}C_{DIC}$ near the surface, however, is discriminated against $^{12}CO_2$ by phytoplankton. Deeper in the water column, ^{13}C-depleted CO_2 gets reintroduced to the DIC pool by respiration of heterotrophic organisms (*Kroopnick*, 1974; *Spero et al.*, 2003). It is, thus, commonly assumed that the most positive δ^{13}C values correspond to the nutrient-depleted surface mixed-layer, and that lowest δ^{13}C values occur at greater depths, where the nutrient supply and recycling is highest.

Complications arise by the fact that fractionation of δ^{13}C occurs during calcite precipitation of foraminifera. Such fractionation is strongly size-dependent in several planktonic foraminiferal species (*Shackleton and Vincent*, 1978; *Ravelo and Fairbanks*, 1995; *Mulitza et al.*, 1999; *Mielke*, 2001). Size fractionation is negligible for δ^{18}O values of the respective tests (Figure 1.3).

1.4 Sample Processing

Core-top (0–1 cm) and downcore sample material of R/V SONNE cruise SO164 (*Nürnberg et al.*, 2003) was sampled shipboard. Up to ~10 cm^3 of bulk sediment per sample was weighed

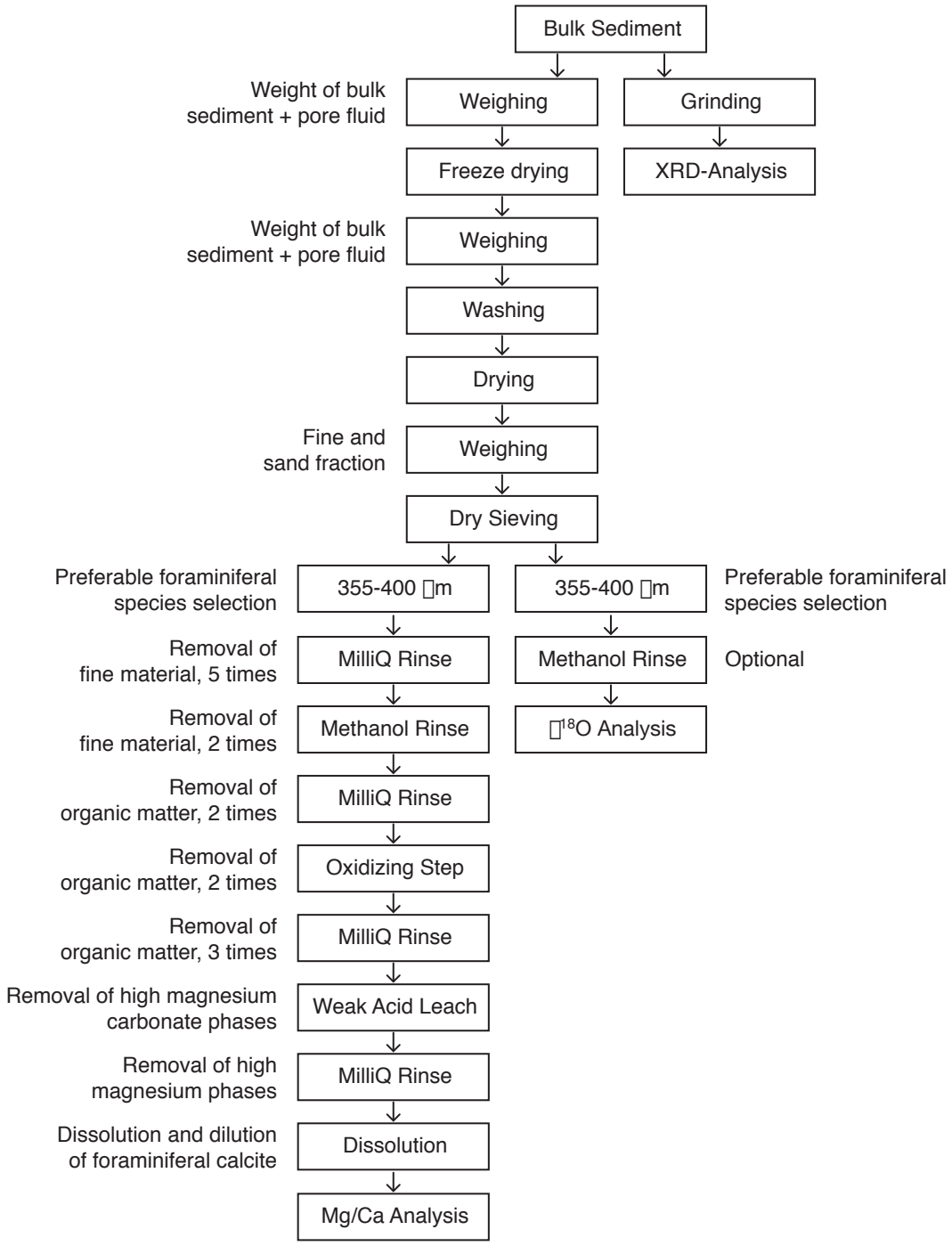

Figure 1.4 Scheme of routinely sample processing: Core-top and downcore sample material of this thesis was analysed for their foraminiferal test's element (i.e., Ca, Mg, Sr, Fe, Mn) and stable isotope compositions (i.e., δ^{18}O, δ^{13}C). Cleaning procedures prior to analyses are indicated. In addition, downcore bulk sediment was investigated for its carbonate mineralogy by X-ray diffraction.

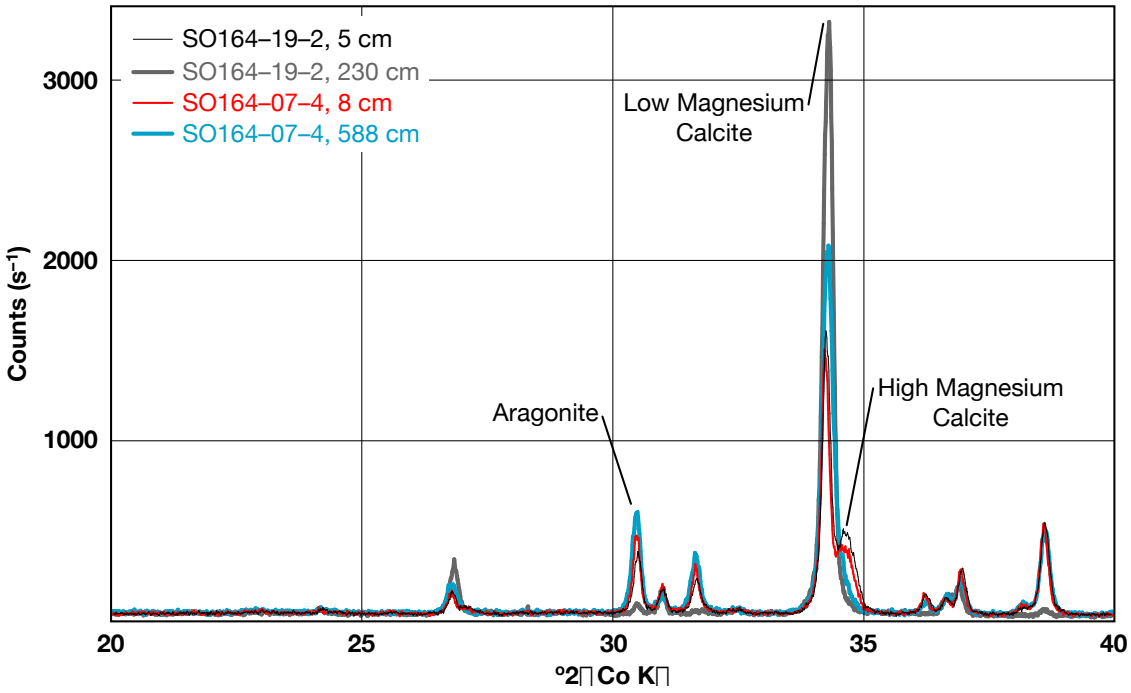

Figure 1.5 X-ray diffraction scans of Caribbean cores SO164–07–4, samples 8 cm and 588 cm (turbidite-corrected sample depth), and SO164–19–2, samples 5 cm and 230 cm. The characteristic peaks used for the calculation of the fractions of the carbonate phases are indicated (LMC = low-magnesium calcite, HMC = high-magnesium calcite). Typically, samples from near the sediment/seawater interface exhibit HMC, which is not detected in deeper-burial samples.

prior to freeze-drying. After freeze-drying, the samples were weighed again in order to calculate the weight of the pore waters. Subsequently, the samples were washed through a 63 μm mesh, the remainder was oven dried at $\sim$50°C, and weighed again in order to calculate the weight of the fine fraction (<63 μm) of each sample (Figure 1.5). The residue represents the dry sand fraction, which typically consists of nearly 100% carbonate in the investigated samples. The sand fraction was separated in different size fractions by dry sieving (63–125 μm, 125–250 μm, 250–315 μm, 315–355 μm, 355–400 μm, 400–450 μm, 450–500 μm, 500–1000 μm, and >1000 μm).

1.4.1 XRD

The relative abundance of a variety of minerals present in the sediment samples was quantified by X-ray diffraction (XRD). XRD typically was performed on $\sim$0.5 g of the bulk sediment. The analysis was carried out on a Philips PW 1710 X-ray diffractometer at IFM-GEOMAR, Kiel. The device contained a cobalt anode Kα tube (Co 1.7903 Å) at 40 KV and 35 mA. The samples were scanned from 20–40° at a scanning speed of 0.01 steps per second to cover the significant peaks of the various carbonate minerals. The peak-area method was deployed to quantify the aragonite content using the computer based integration program MacDiff version 4.2.5 of *Petschick* (2001).

1.4.2 co2sys for Calculation of the *in situ* Carbonate Ion Concentration

In order to calculate appropriate carbonate ion concentrations, we applied the co2sys program of *Lewis and Wallace* (1998). Optional parameter of the program were set to the constants of *Mehrbach et al.* (1973) refited by *Dickson and Millero* (1987) for the dissociation constants K_1 and K_2 of carbonic acid. The dissociation constant of ${SO_4}^{2-}$ is from *Dickson* (1990), and the pH is on the total scale.

Chapter 2

Assessing the Effect of Dissolution on Planktonic Foraminiferal Mg/Ca Ratios: Evidence from Caribbean Core-Tops

Marcus Regenberg[1], Dirk Nürnberg[1], Silke Steph[2], Jeroen Groeneveld[3], Dieter Garbe-Schönberg[4], Ralf Tiedemann[2], Wolf-Christian Dullo[1]

[1]Leibniz Institute of Marine Sciences IFM-GEOMAR, Kiel, Germany

[2]Alfred Wegener Institute for Polar and Marine Research AWI, Bremerhaven, Germany

[3]Research Center Ocean Margins RCOM, University of Bremen, Germany

[4]Institute of Geosciences, University of Kiel, Germany

Published in *Geochemistry Geophysics Geosystems*, *7*(7)
Q07P15, doi:10.1029/2005GC001019

Abstract. In order to assess the dissolution effect on foraminiferal Mg/Ca ratios, we analyzed Mg/Ca of seven planktonic foraminiferal species and four of their varieties from Caribbean core-tops from ∼900–4700 m water depth. Depending on the foraminiferal species and variety, Mg/Ca starts to decline linearly below $\Delta[CO_3^{2-}]$ levels of ∼18–26 μmol/kg by ∼0.04–0.11 mmol/mol per 1 μmol/kg $\Delta[CO_3^{2-}]$, similar to decreases of ∼0.5–0.8 mmol/mol per kilometer below ∼2500–3000 m water depth. Above these species-specific critical levels, Mg/Ca remains stable with higher intraspecific Mg/Ca variability than below. We developed routines to correct Mg/Ca from below these critical thresholds for dissolution effects, which reduce the overall intraspecific variability by ∼24–64%, and provide dissolution-corrected Mg/Ca appropriate to calculate Holocene paleotemperatures. When taking into account only dissolution-unaffected

Mg/Ca from <2000 m, the systematic succession of foraminiferal species according to their Mg/Ca reflects expected calcification depths.

2.1 Introduction

Mg/Ca ratios of planktonic foraminiferal tests have been developed as a powerful tool in paleoceanography to assess past ocean temperatures (e.g., *Elderfield and Ganssen*, 2000; *Nürnberg*, 2000; *Lea*, 2003). This proxy became widely used mainly due to the fact that both stable oxygen isotopes (δ^{18}O) and Mg/Ca can be measured within the same biotic carrier, which ensures the recording of the same seasonality and/or habitat effects that may occur when proxy data from different faunal groups are compared. Most advantageous, combined measurements of Mg/Ca and δ^{18}O allow to extract the δ^{18}O record of past upper ocean water, and accordingly salinity variations (e.g., *Nürnberg*, 2000; *Lea*, 2003; *Schmidt et al.*, 2004; *Pahnke and Zahn*, 2005; *Nürnberg and Groeneveld*, 2006).

The accurate assessment of paleotemperatures from different depth levels of the ocean is a pre-requisite to reconstruct and model past changes in salinity and density gradients, stratification patterns, and thus thermohaline circulation. The exponential dependence of Mg/Ca ratios on temperature within single planktonic foraminiferal species is well-studied, resulting in a variety of species-specific (*Nürnberg*, 1995; *Nürnberg et al.*, 1996a,b; *Lea et al.*, 1999; *Mashiotta et al.*, 1999; *Lea et al.*, 2000; *Nürnberg et al.*, 2000; *Dekens et al.*, 2002; *Rosenthal and Lohmann*, 2002; *Whitko et al.*, 2002; *McKenna and Prell*, 2004; *McConnell and Thunell*, 2005) and multi-species calibration curves (*Elderfield and Ganssen*, 2000; *Anand et al.*, 2003). The accuracy of the Mg/Ca paleothermometry is specified with $\pm$0.2–1.2°C (*Nürnberg*, 1995; *Nürnberg et al.*, 1996a; *Hastings et al.*, 1998; *Elderfield and Ganssen*, 2000; *Nürnberg et al.*, 2000; *Lea et al.*, 2000; *Dekens et al.*, 2002; *Anand et al.*, 2003). Nevertheless, the influence of factors on Mg/Ca other than temperature, which may affect the amount of magnesium incorporated into foraminiferal tests during calcification, is still debated. Primary effects such as intraspecies and ontogenetic variations (e.g., *Nürnberg et al.*, 1996a), pH, carbonate ion concentration ([CO_3^{2-}]), and salinity (e.g., *Nürnberg et al.*, 1996a,b; *Lea et al.*, 1999; *Russell et al.*, 2004) as well as secondary (diagenetic) effects such as preferential removal of Mg^{2+} during calcite dissolution (e.g., *Savin and Douglas*, 1973; *Cronblad and Malmgren*, 1981; *Brown and Elderfield*, 1996; *Rosenthal et al.*, 2000; *Rosenthal and Lohmann*, 2002; *Dekens et al.*, 2002; *de Villiers*, 2003) may influence foraminiferal Mg/Ca.

Several efforts have been made to correct the foraminiferal Mg/Ca ratios for the effect of dissolution. For example, *Rosenthal and Lohmann* (2002) established dissolution-corrected Mg/Ca *vs.* temperature calibrations for *Globigerinoides ruber* and *Globigerinoides sacculifer*, based on shell mass loss studies along depth transects, where the pre-exponential constant is a function of size-normalized shell weight. In an alternative core-top study along depth transects, *Dekens et al.* (2002) introduced water depth-dependent dissolution correction factors into the exponent of their Mg/Ca *vs.* temperature calibrations for *G. ruber*, *G. sacculifer*, and

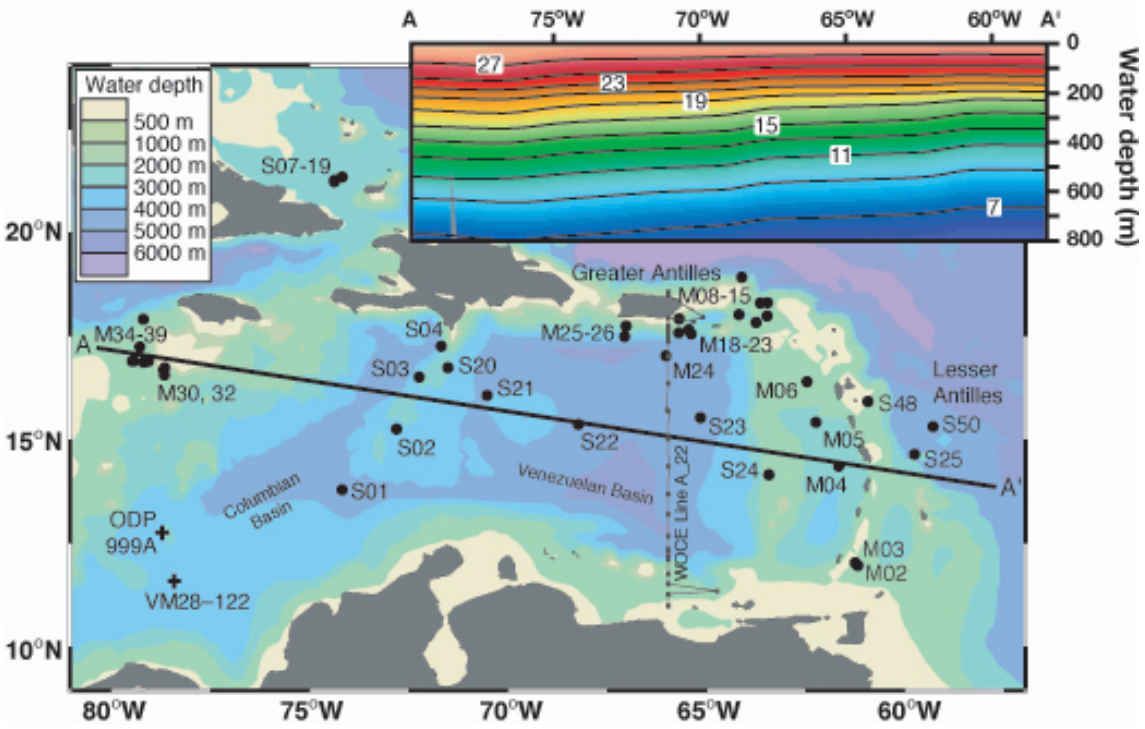

Figure 2.1 Bathymetric chart of the Caribbean (*Schlitzer*, 2002) showing the locations of the core-top samples from this study (black dots, station labels abbreviate the cruise stations: S: SO164-..; M: M35/1, M350..) and of two sediment cores (crosses; *Schmidt et al.* (2004)) discussed here. Inlet presents the annual mean temperature (*NODC*, 2001) *vs.* water depth along the profile AA'. WOCE Line A22 stations are used to compute the carbonate ion concentration considered to be representative for the Caribbean.

Neogloboquadrina dutertrei, differentiated into Atlantic and Pacific equations. Yet, only few core-top studies covered the upper 2000 m of the water column to a larger extent.

Our study focusses on the impact of water depth-related partial calcite dissolution on the Mg/Ca ratios of seven planktonic foraminiferal species and four of their varieties from water depths of ~900–4700 m. All selected foraminifers were collected from core-top sediments from the Caribbean and the adjacent tropical Atlantic (Figure 2.1). The thermal structure in the study area minimizes temperature-induced variability in the foraminiferal Mg/Ca, and allows to isolate the impact of calcite dissolution. Our results indicate that Mg/Ca remains stable down to species-specific water depths.

2.2 Hydrography

Although seasonal variability influences the strength of the trade winds and current patterns in the Caribbean (*Schott et al.*, 1988; *Molinari et al.*, 1990; *Morrison and Smith*, 1990; *Larsen*, 1992; *Johns et al.*, 2002), seasonal temperature changes are relatively small. Within the mixed layer, spatial temperature gradients at similar water depths are in the order of 1°C, increasing to ~4°C

within the thermocline (*NODC*, 2001) (Figure 2.1).

The Upper North Atlantic Deep Water (UNADW) with salinity values of 34.7–34.9 (*Wüst*, 1963; *Joyce et al.*, 1999; *Schmuker and Schiebel*, 2002) ventilates the Columbian and Venezuelan Basins *via* the Greater Antilles Passages (*Stalcup et al.*, 1975; *Morrison and Nowlin*, 1982; *Fratantoni et al.*, 1997). Above the UNADW, Antarctic Intermediate Water (AAIW) enters the Caribbean between ~550–1000 m (*Wüst*, 1963; *Bulgakov and Lomakin*, 1995; *Schmuker and Schiebel*, 2002). AAIW mixes with overlying Subtropical Under Water (SUW), forming the permanent thermo- and nutricline in the Caribbean (*Kameo*, 2002). The SUW with salinity values of >36.8 (*Corredor and Morell*, 2001; *Schmuker and Schiebel*, 2002) and temperatures of 18–23°C (*Morrison and Nowlin*, 1982) ranges between ~80–180 m (*Wüst*, 1964) or even down to ~300 m (*Schmuker and Schiebel*, 2002) (Figure 2.3). It emanates from the North Atlantic subtropical gyre and enters the Caribbean *via* the Greater Antilles Passages (*Wüst*, 1964; *Johns et al.*, 2002). The mixed layer is composed of Caribbean Water (CW) in the upper ~80 m of the water column with salinity values of ~35.5 and temperatures of ~28°C (*Wüst*, 1964; *Corredor and Morell*, 2001) (Figure 2.3).

2.3 Materials and Methods

2.3.1 Core-Top Sediments

Mg/Ca analyses were performed on tests of planktonic foraminiferal species or their varieties from 42 sediment surface samples (0–1 cm; Figure 2.1; Table 2.1) , collected during R/V SONNE SO164 (*Nürnberg et al.*, 2003) and R/V METEOR M35/1 cruises (*Hemleben et al.*, 1998). Based on 7 AMS^{14}C-dated core-tops revealing ages not older than 2–3 kyrs (Table 2.1), we assume the remaining core-top sediments to be within the same age range.

Twenty to 25 visually (magnification up to 40x) uncontaminated tests of the foraminiferal species or their varieties were selected from the narrow 355–400 μm size fraction (~550–800 μg) for Mg/Ca analyses to minimize size-related intraspecific elemental variations (*Elderfield et al.*, 2002). In case of insufficient material, we subsequently extended the selection of tests to a larger size range (maximum 250–500 μm; Figure 2.2; Table 2.2).

2.3.2 Foraminiferal Species Selection

Seven tropical to subtropical planktonic foraminiferal species and four of their varieties were selected for Mg/Ca analyses. Generic assignments of selected specimens in this study follow *Kennett and Srinivasan* (1983) and *Hemleben et al.* (1989). The specific adaptations to and demands of light, chlorophyll concentrations, salinity, temperature, and food availability (e.g., *Fairbanks et al.*, 1980b, 1982; *Fairbanks and Wiebe*, 1980a; *Curry et al.*, 1983; *Deuser*, 1987; *Deuser and Ross*, 1989; *Sautter and Thunell*, 1991a; *Ortiz et al.*, 1995, 1996, 1997; *Watkins and Mix*, 1998) determine the vertical distribution patterns and abundances of planktonic foraminiferal species in the water column. Their different preferred depth habitats, thus, allow the reconstruction

Table 2.1 Locations, depths, and ages of core-top samples of this study. ^{14}C-ages are calibrated after *Stuiver et al.* (2005), marine reservoir corrections after *Reimer et al.* (2004). Lab.-# a from *Schmuker* (2000).

Station	Longitude (W)	Latitude (N)	Water depth *d* (m)	Sample (cm)	^{14}C-age (years BP)	Lab.-#	2 sigma age ranges (years BP)	Marine reservoir correction (ΔR) (years)
M35006-6	62°27.2'	16°25.3'	888	0–1				
M35013-3	63°27.0'	18°18.9'	899	0–1				
SO164-04-2	71°39.09'	17°16.38'	1,013	0–1				
M35038-1	79°13.8'	17°15.7'	1,066	0–1				
M35012-6	63°37.6'	18°18.3'	1,121	0–1				
M35039-1	79°08.7'	17°55.6'	1,142	0–1				
M35023-4	65°41.0'	17°36.2'	1,183	0–1				
M35037-1	79°23.3'	16°54.8'	1,190	0–1				
M35023-3	65°40.9'	17°36.2'	1,192	0–1				
M35036-3	79°25.3'	16°55.0'	1,196	0–1				
M35034-3	79°03.5'	16°54.2'	1,212	0–1				
M35015-1	63°27.1'	17°59.6'	1,230	0–1				
M35035-1	79°07.9'	16°53.6'	1,252	0–1				
SO164-48-2	60°55.0'	15°57.02'	1,286	0–1				
M35030-1	78°36.6'	16°45.3'	1,298	0–1				
M35003-6	61°14.7'	12°05.1'	1,299	0–1				
M35032-1	78°36.9'	16°35.3'	1,363	0–1				
M35002-1	61°10.6'	12°01.9'	1,506	0–1				
SO164-24-3	63°25.43'	14°11.89'	1,545	0–1				
M35014-1	63°44.2'	17°50.5'	1,604	0–1				
SO164-18-1	74°21.0'	21°13.61'	1,629	0–1	1,350 ± 25	KIA23386	774–924	37 ± 14
SO164-19-3	74°20.98'	21°14.7'	1,706	0–1	> AD 1954	KIA23383		
M35018-1	65°22.2'	17°34.5'	1,728	0–1				
M35025-1	67°00.5'	17°45.2'	1,778	0–1	699 ± 30	a	280–445	–16 ± 23
M35019-1	65°26.1'	17°40.3'	1,815	0–1				
M35020-2	65°40.2'	17°55.8'	2,005	0–1				
M35005-3	62°13.9'	15°27.2'	2,289	0–1				
M35010-2	64°05.4'	18°56.0'	2,696	0–1				
SO164-25-3	59°44.48'	14°41.25'	2,720	0–1	1,915 ± 30	KIA23385	1,287–1,577	33 ± 60
SO164-07-3	74°08.76'	21°19.46'	2,722	0–1	720 ± 35	KIA23384	262–423	37 ± 14
SO164-03-3	72°12.31'	16°32.40'	2,744	0–1				
M35008-1	64°09.8'	18°01.9'	2,820	0–1				
M35004-1	61°39.7'	14°24.6'	2,885	0–1				
SO164-02-3	72°47.06'	15°18.29'	2,977	0–1	2,205 ± 25	KIA23382	1,717–1,914	–16 ± 23
SO164-20-2	71°29.22'	16°45.49'	3,357	0–1				
M35026-2	67°02.6'	17°30.5'	3,815	0–1	1,175 ± 70	a	628–900	–16 ± 23
SO164-21-3	70°30.0'	16°06.0'	3,995	0–1				
SO164-50-3	59°16.94'	15°21.25'	4,002	0–1				
SO164-01-3	74°09.028'	13°50.195'	4,026	0–1				
SO164-23-3	65°08.09'	15°34.01'	4,328	0–1				
SO164-22-2	68°12.0'	15°24.0'	4,506	0–1				
M35024-6	66°00.1'	17°02.6'	4,710	0–1	2,510 ± 45	a	2,059–2,318	–16 ± 23

Table 2.2 Measured Mg/Ca ratios and size fractions of selected specimens. Each single ratio is the average of three measurements, except the samples listed in Table 2.3. Mean Mg/Ca (Mg/Ca_{mean}) ± standard deviations (sd) from <2000 m are converted into temperatures after *Anand et al.* (2003) (Mg/Ca=0.38·exp(0.09T)).

Station	*d* (m)	*G. ruber* p.		*G. ruber* w.		*G. sacculifer*		*N. dutertrei*		*G. menardii*		*G. tumida*		*G. truncatulinoides* d.		*G. truncatulinoides* s.		*G. crassaformis*	
M35006-6	888	a	4.20	a	5.09	a	4.23	a	2.73	a	3.24	d	2.35	a	2.65	d	2.45	b	2.28
M35013-3	899	a	6.02	a	5.95	a	4.31	a	3.11	d	3.09			d	2.48				
SO164-04-2	1,013	a	5.26	a	5.27	a	4.43	a	2.74	a	3.35	i	2.93	c	2.68			b	2.28
M35038-1	1,066	a	4.70	a	5.23	a	4.34	a	3.41	a	3.20	a	2.76	g	2.85			g	2.18
M35012-6	1,121	a	5.84	a	5.87	a	4.31	a	3.87	i	3.20	a	2.27	a	2.59				
M35039-1	1,142	a	5.62	a	6.02	a	4.64	a	5.59*	a	4.10**	a	2.59	a	5.80*				
M35023-4	1,183	a	4.50											a	2.58	d	2.53	f	2.04
M35037-1	1,190	a	4.91	a	4.94	a	4.41	a	2.89	a	3.36	e	2.80	g	2.55			e	2.01
M35023-3	1,192	a	4.48	a	4.77	a	4.29	a	3.37	a	3.60	a	2.87	a	2.60	e	2.55	a	1.97
M35036-3	1,196	a	4.714	a	4.929	a	4.066	a	3.192	a	3.728	a	2.594	g	3.304			e	1.94
M35034-3	1,212	a	5.34	b	5.84	a	4.34	a	3.00	b	3.74								
M35015-1	1,230	a	4.41	a	5.01	a	4.39	a	3.03	c	3.41			c	2.71				
M35035-1	1,252	a	4.50	a	5.30	a	4.41	a	3.16	a	3.40	a	2.90	h	2.75				
SO164-48-2	1,286	a	5.39	a	5.33	a	4.43	a	3.00	a	3.66	c	2.55	c	2.36				
M35030-1	1,298	a	5.62	b	5.61	a	4.07	a	3.47	a	3.51	d	2.33						
M35003-6	1,299	a	4.53	a	4.72	a	3.80	a	2.51	e	2.67							e	1.77
M35032-1	1,363	a	4.51	a	4.91	a	4.33	a	2.75	a	3.61	c	2.40					d	2.26
M35002-1	1,506	a	4.47	a	5.17	a	4.15	a	2.93	c	2.75			d	2.20				
SO164-24-3	1,545	a	4.39	a	4.63	a	4.23	a	2.63	j	2.98			c	2.28			c	1.64
M35014-1	1,604	a	4.88	a	4.83	a	4.23	a	2.86	a	3.26	d	2.50	d	2.44				
SO164-18-1	1,629	a	4.86	a	5.83	a	4.55	b	3.27					b	2.79				
SO164-19-3	1,706			e	5.53	a	4.65	e	2.36					c	2.48				
M35018-1	1,728	a	4.91	a	4.62	a	4.54	a	3.35	a	3.51	c	2.46	c	2.67				
M35019-1	1,815	a	4.73	a	5.39	a	4.68	a	2.95	a	3.92	b	2.46	b	3.17	d	2.47		
M35020-2	2,005	a	5.14	a	5.28	a	4.38	a	2.71	a	3.45	c	2.28	b	2.95				
M35005-3	2,289	a	4.45	a	4.59	a	3.90	a	2.81	a	3.08	d	1.99	d	2.30				
M35010-2	2,696	a	4.77	a	4.70	a	4.38	a	3.15	a	4.66**	a	2.69	a	2.50	b	2.57		
SO164-25-3	2,720	a	4.46	a	5.05	a	4.36	a	2.55	a	3.54	b	2.35	a	2.28	c	2.17	c	1.81
SO164-07-3	2,722	a	4.96	b	5.28	a	4.51	b	2.66	c	3.39			c	3.19				
SO164-03-3	2,744	a	4.62	a	5.15	a	4.44	a	2.42	a	3.44	c	2.64					a	1.89
M35008-1	2,820	a	4.68	a	4.77	a	4.43	a	2.68	a	3.51	d	2.20	b	2.57				
M35004-1	2,885	a	4.34	a	4.78	a	3.98	a	2.91	c	2.94			b	2.20				
SO164-02-3	2,977	a	4.70	a	4.79	a	4.20	a	2.58	a	3.49	c	2.43	c	2.43	c	2.10	b	1.96
SO164-20-2	3,357	a	4.30	a	4.51	a	4.23	a	2.39	a	3.05	b	2.35	b	2.30	c	2.20	b	1.76
M35026-2	3,815	a	4.37	a	4.76	a	4.06	a	2.78	a	3.99**	d	2.46	g	2.62				
SO164-21-3	3,995	a	4.44	a	4.45	a	4.04	a	2.36	a	2.88	b	2.17	a	2.24	b	1.96	a	1.63
SO164-50-3	4,002	a	4.04	a	4.13	a	3.92	a	2.02	a	2.98	i	2.17	a	2.10	a	2.05	a	1.50
SO164-01-3	4,026	a	4.07	a	4.34	a	3.71	a	1.98	a	2.40	h	1.48					a	1.31
SO164-23-3	4,328	a	3.47	a	3.93	a	3.53	a	1.87	a	2.38	i	1.72	a	1.63	c	1.45	a	1.09
SO164-22-2	4,506	a	3.60	a	3.62	a	3.71	a	1.84	a	2.20	a	1.95	a	1.62	c	1.60	a	1.23
M35024-6	4,710	a	3.44	a	4.19	a	3.86	a	1.93	a	2.56	a	1.91	a	1.79	e	1.88	e	1.61
Mg/Ca_{mean}			4.9		5.25		4.34		3.03		3.36		2.58		2.64		2.5		2.04
sd			0.51		0.44		0.2		0.35		0.32		0.22		0.27		0.05		0.22
Temperature			28.41		29.18		27.06		23.07		24.22		21.28		21.54		20.93		18.67

* Not used for calculation of the mean <2,000 m. ** Not considered for the calculation of the linear regression.
Specimens size fractions a: 355-400 □m; b: 315-400 □m; c: 315-450 □m; d: 315-500 □m; e: 250-400 □m; f: 250-450 □m; g: 250-500 □m; h: 355-500 □m; i: 355-450 □m; j: 400-500 □m

of the upper ocean structure in detail, presupposing that the various foraminiferal habitats remain fixed through time and environmental change.

G. ruber and *G. sacculifer* are spinose and symbiont-bearing species. They commonly reach highest abundances in the upper 50 m of the mixed layer (*Bé*, 1977; *Fairbanks et al.*, 1982; *Deuser*, 1987; *Bijma et al.*, 1994; *Kroon and Darling*, 1995; *Kemle von Mücke and Oberhänsli*, 1999; *Schmuker and Schiebel*, 2002). An almost uniform occurrence throughout the year makes *G. ruber* suitable to reflect annual hydrographic conditions (*Hemleben et al.*, 1989; *Lin et al.*, 1997; *Tedesco and Thunell*, 2003). *Savin and Douglas* (1973) showed that *G. ruber* calcifies at shallower water depths than *G. sacculifer*.

Globorotalia menardii and *N. dutertrei* live within the tropical to subtropical thermocline (*Ravelo and Fairbanks*, 1992; *Chaisson and Ravelo*, 1997). *N. dutertrei* is known to occur in a well-stratified photic zone near the deep chlorophyll maximum (*Fairbanks et al.*, 1980b, 1982; *Fairbanks and Wiebe*, 1980a), often associated with the lower thermocline (*Sautter and Thunell*, 1991a; *Ravelo and Fairbanks*, 1992).

Globorotalia tumida calcifies near the bottom of the photic zone (*Ravelo and Fairbanks*, 1992; *Chaisson and Ravelo*, 1997). It shows distinct preferences for low water densities during summer (*Hilbrecht*, 1996). *Globorotalia truncatulinoides* and *Globorotalia crassaformis* are deep-dwelling species that reach maximum abundances below the photic zone (*Ganssen and Kroon*, 2000). According to *Mulitza et al.* (1997), *G. truncatulinoides* reflects mean ocean conditions at about 200 m, while *McKenna and Prell* (2004) assign the habitat to the permanent thermocline. In the Caribbean, *G. truncatulinoides* is linked to the SUW (*Schmuker*, 2000). Changing coiling directions do not indicate substantially different physical preferences (*Hilbrecht*, 1996). *G. crassaformis* calcifies below the photic zone and thermocline (*Ravelo and Fairbanks*, 1992). In general, *G. crassaformis* is supposed to behave like *G. truncatulinoides* (*Hemleben et al.*, 1989).

Impending gametogenesis is morphologically signaled by additional calcification of a diminutive final chamber for *G. ruber* (*Bijma et al.*, 1990), a sac-like final chamber for *G. sacculifer* (*Bé et al.*, 1983; *Hemleben et al.*, 1989), and by discarding of spines (*Bé*, 1980; *Duplessy et al.*, 1981). Secondary calcite crust formation, associated with reproduction, mainly occurs at greater depths (*Hemleben et al.*, 1989; *Lohmann*, 1995), and hence may affect the geochemical signature of the foraminiferal tests (e.g., *Curry and Crowley*, 1987; *Spero and Williams*, 1989; *Lohmann*, 1995; *Nürnberg et al.*, 1996a; *Rosenthal et al.*, 2000; *Eggins et al.*, 2003; *Mulitza et al.*, 2004; *McKenna and Prell*, 2004). Addition of secondary calcite accounts for about one third of the test's mass of *G. sacculifer* (*Bé*, 1980; *Erez and Honjo*, 1981; *Hemleben et al.*, 1989; *Schweitzer and Lohmann*, 1991; *Bijma et al.*, 1994), and doubles the test's mass of *G. truncatulinoides* (*Bé and Lott*, 1964). Large vertical migrations during their ontogenetic cycles were described for *G. menardii*, *G. tumida*, and *G. truncatulinoides* (*Bé and Ericson*, 1963; *Bé*, 1977; *Fairbanks et al.*, 1980b, 1982; *Fairbanks and Wiebe*, 1980a; *Erez and Honjo*, 1981; *Hemleben et al.*, 1989; *Schweitzer and Lohmann*, 1991; *Brown and Azmy*, 2005).

To prevent our analyses from biases due to different amounts of secondary calcite, we took

care upon specimen selection. For *G. ruber* (pink and white varieties) and *G. sacculifer*, tests with spines were preferentially selected. For the latter, specimens showing a sac-like final chamber were excluded. For *G. menardii* and for *G. tumida*, we chose thin-walled and thick-encrusted specimens, respectively. Due to the low numbers of tests of *G. truncatulinoides* (dextral and sinistral varieties) and *G. crassaformis*, we did not differentiate between encrusted and non-encrusted specimens, and different morphotypes. In general, specimens with kummerform chambers were rejected.

2.3.3 Mg/Ca Analyses

The foraminiferal samples were cleaned according to the cleaning protocol of *Barker et al.* (2003). Prior to cleaning, the tests were gently crushed between two glass plates in order to open all chambers. The foraminiferal fragments were rinsed 5 times with ultrapure water and twice with methanol (suprapure), including ultrasonic treatment after each rinse. Subsequently, samples were treated twice with 250 μL of a hot (97°C) oxidizing 1% NaOH/H_2O_2 reagent (10 mL 0.1 N NaOH (analytical grade); 100 μL 30% H_2O_2 (suprapure)) for 10 minutes. Every 2.5 minutes, the solution was cautiously agitated in order to release any gaseous build-up. After 5 minutes, the samples were placed in an ultrasonic bath for a few seconds in order to maintain the chemical reaction. Remaining oxidizing solution was removed by three rinsing steps with ultrapure water. After transferring the samples into clean vials, a weak acid leach with 250 μL 0.001 M nitric acid (HNO_3, subboiling distilled) was applied with 30 seconds ultrasonic treatment, followed by two rinses with ultrapure water. After removal of any remaining solution, the samples were dissolved in 500 μL 0.075 M HNO_3 (subboiling distilled), and diluted with ultrapure water to achieve Ca concentrations of 30–70 ppm.

Analyses were performed on two ICP OES devices showing no significant offset as revealed by replicate measurements of 21 samples (Table 2.3). Each single Mg/Ca ratio (Table 2.2, 2.3) is the average of three measurements, from which the analytical errors are deduced. One set of samples was measured on an ICP OES (ISA Jobin Yvon, Spex Instruments S.A. GmbH) with polychromator applying yttrium as an internal standard. Selected element lines for analyses (Ca: 317.93 nm; Mg: 279.55 nm; Y: 371.03 nm) were most intensive and undisturbed. Element detection was performed with photomultipliers, the high-tension of which was adapted to each element concentration range. The analytical error for Mg is $\sim$0.45% and for Ca $\sim$0.15%. Replicate samples showed an average standard deviation of $\sim$0.1 mmol/mol (Table 2.3). A second set of samples was measured on a simultaneous, radially viewing ICP OES (Spectro CirosCCD SOP). A cooled cyclonic spraychamber in combination with a microconcentric nebulizer (200 μL/min sample uptake) was optimized for best precision of analytical results and minimized uptake of sample solution. Sample introduction took place *via* autosampler (Spectro A.I.). For Mg, we used the most sensitive line (279.553 nm). For Ca, we used the spectral line at 183.801 nm with a sensitivity matching that of Mg. This allows a true simultaneous measurement during the same detector read-out phase (phase 3) as for Mg-279. Matrix effects caused by varying concentrations of Ca were cautiously checked and found to be insignificant. Drift of the machine during analytical

Table 2.3 Replicate Mg/Ca measurements on two ICP OES devices. The use of same sample solutions is indicated by asterisks.

Station	Species	Mg/Ca (mmol/mol) ISA Jobin Yvon		Mg/Ca (mmol/mol) Spectro Ciros			Mg/Ca (mmol/mol)	
		1	2	1	2	3	mean	sd
SO164-22-2	*G. crassaformis*			* 1.22	* 1.23		1.23	0.00
SO164-04-2	*G. crassaformis*			* 2.29	* 2.28		2.28	0.00
SO164-02-3	*G. crassaformis*			* 2.07	** 1.85		1.96	0.08
SO164-01-3	*G. crassaformis*			* 1.32	** 1.30		1.31	0.01
M35018-1	*G. menardii*			* 3.31	** 3.72		3.51	0.29
M35037-1	*G. menardii*			* 3.53	** 3.20		3.36	0.23
M35036-3	*G. menardii*			* 3.81	** 3.28	*** 4.09	3.73	0.41
SO164-20-2	*G. ruber* p.			* 4.30	* 4.30		4.30	0.00
SO164-02-3	*G. ruber* p.			* 4.81	** 4.59		4.70	0.08
SO164-18-1	*G. ruber* p.			* 4.87	* 4.85		4.86	0.00
SO164-25-3	*G. ruber* w.	* 4.75		* 5.35			5.05	0.21
SO164-23-3	*G. ruber* w.	* 3.58		** 4.33	*** 3.87		3.93	0.25
SO164-04-2	*G. ruber* w.	* 5.34		** 5.20			5.27	0.05
SO164-01-3	*G. ruber* w.	* 4.38		* 4.41	** 4.22		4.34	0.10
SO164-19-3	*G. ruber* w.	* 5.75		* 5.32			5.53	0.15
SO164-48-2	*G. sacculifer*			* 4.48	* 4.38		4.43	0.03
SO164-24-3	*G. sacculifer*	* 4.10		** 4.36			4.23	0.09
M35014-1	*G. sacculifer*			* 4.36	** 4.09		4.23	0.19
SO164-23-3	*G. sacculifer*	* 3.41		** 3.66	*** 3.52		3.53	0.08
SO164-22-2	*G. sacculifer*	* 3.90		** 3.53			3.71	0.13
M35037-1	*G. sacculifer*			* 4.39	** 4.44		4.41	0.04
SO164-50-3	*G. truncatulinoides* d.			* 2.14	** 2.07		2.10	0.02
SO164-48-2	*G. truncatulinoides* d.			* 2.35	** 2.27		2.31	0.03
M35023-4	*G. truncatulinoides* d.			* 2.59	** 2.56		2.58	0.02
M35023-4	*G. truncatulinoides* s.			* 2.41	** 2.65		2.53	0.17
SO164-50-3	*G. tumida*			* 2.17	* 2.16		2.17	0.01
SO164-25-3	*G. tumida*			* 2.36	* 2.35		2.35	0.00
SO164-48-2	*G. tumida*			* 2.55	* 2.54		2.55	0.00
SO164-23-3	*G. tumida*			* 1.64	* 1.64	** 1.87	1.72	0.12
SO164-22-2	*G. tumida*			* 1.96	* 1.94		1.95	0.01
SO164-20-2	*G. tumida*			* 2.35	* 2.35		2.35	0.00
SO164-03-3	*G. tumida*			* 2.66	* 2.63		2.64	0.01
SO164-02-3	*G. tumida*			* 2.44	* 2.43		2.43	0.00
SO164-01-3	*G. tumida*			* 1.49	* 1.48		1.48	0.00
SO164-50-3	*N. dutertrei*	* 1.99		* 2.05			2.02	0.02
SO164-25-3	*N. dutertrei*	* 2.49		* 2.60			2.55	0.04
SO164-48-2	*N. dutertrei*	* 3.30	** 2.85	* 3.17	** 2.84	** 2.87	3.00	0.19
SO164-23-3	*N. dutertrei*	* 1.84		* 1.89			1.87	0.02
SO164-22-2	*N. dutertrei*	* 1.82	** 1.87	* 1.82	** 1.85		1.84	0.02
SO164-21-3	*N. dutertrei*	* 2.38	* 2.33				2.36	0.02
SO164-20-2	*N. dutertrei*	* 2.55		* 2.35	* 2.36		2.42	0.04
SO164-04-2	*N. dutertrei*	* 2.74		* 2.73			2.74	0.00
SO164-03-3	*N. dutertrei*	* 2.38		* 2.47			2.42	0.03
SO164-02-3	*N. dutertrei*	* 2.57		* 2.59			2.58	0.01
SO164-01-3	*N. dutertrei*	* 1.91	** 1.99	* 1.95	** 2.07		1.98	0.05
SO164-07-3	*N. dutertrei*	* 2.62		* 2.69			2.66	0.02
SO164-19-3	*N. dutertrei*	* 2.32		* 2.40			2.36	0.03
SO164-18-1	*N. dutertrei*	* 3.28		* 3.26			3.27	0.01

sessions was negligible (<0.5%, as determined by analysis of an internal consistency standard after every 5 samples). The analytical error for the Mg/Ca analyses was ~0.1%. Replicate samples showed an average standard deviation of ~0.08 mmol/mol (Table 2.3).

2.4 Results and Discussion

2.4.1 Bathymetric Change in Mg/Ca Ratios

For all foraminiferal species and varieties studied, we observe a considerable decrease in Mg/Ca ratios with increasing water depth below certain depth levels. Depending on the species or variety, the change from stable to continuously decreasing Mg/Ca happens in the depth range between ~2000 m and ~3000 m. Statistical analyses of the intraspecific Mg/Ca reveal that means of samples from <2000 m water depth differ significantly from those from >2000 m. Related low probability values ($p < 0.015$) of these Mg/Ca means indicate that both data sets behave significantly different and that environmental factors other than temperature bias Mg/Ca at deeper sites. According to the bathymetric distribution of the core-top samples in combination with the pattern of the Mg/Ca data (Figure 2.2), we assign decreasing Mg/Ca to dissolution and differentiate between three water depth intervals: (i) Samples <2000 m with no signs of preferential removal of Mg^{2+} (number of core-top samples n = 23; Table 2.3), (ii) samples >3000 m with distinctively decreasing Mg/Ca (n = 8; Table 2.3), and (iii) samples between 2000–3000 m (n = 9; Table 2.3). The incomplete distribution pattern of the latter sample set prevents to directly infer the transition depth separating Mg/Ca unaffected and affected by dissolution, respectively.

2.4.2 Dissolution Unaffected Mg/Ca Ratios from Shallow Water Depths

Evidence for excellent carbonate preservation at shallow water depths is provided by the presence of aragonitic pteropod shells in our Caribbean core-top sediments down to ~2700 m. Likewise, species-specific Mg/Ca ratios do not systematically decrease with increasing water depth in the depth interval <2000 m (correlation coefficients $r^2 = <0.1$). We assume these shallow Mg/Ca to be unaffected by dissolution.

There are significant differences in Mg/Ca ratios between the species and varieties from <2000 m (Figure 2.2; Table 2.2). Mixed layer-dwelling *G. ruber* exhibits highest Mg/Ca of 4.20–6.02 mmol/mol. In accordance with increasing calcification depth and decreasing ambient seawater temperature, Mg/Ca successively decrease to 1.64–2.28 mmol/mol for the deepest-living species *G. crassaformis* (Figure 2.2). With respect to *G. ruber*, the other species show lower mean Mg/Ca in samples <2000 m water depth (Figure 2.3): *G. sacculifer* is lower in Mg/Ca by ~15%, *G. menardii* by ~34%, *N. dutertrei* by ~40%, *G. tumida* by ~49%, *G. truncatulinoides* by ~49%, and *G. crassaformis* by ~60%. *G. ruber* pink shows consistently lower mean Mg/Ca from <2000 m by ~7% with respect to the white variety. The left-coiling variety of *G. truncatulinoides* (sinistral) is lower by ~5% with respect to the right-coiling (dextral) variety (Figures 2.2, 2.3). These differences between species are in general agreement to previous multispecies core-top

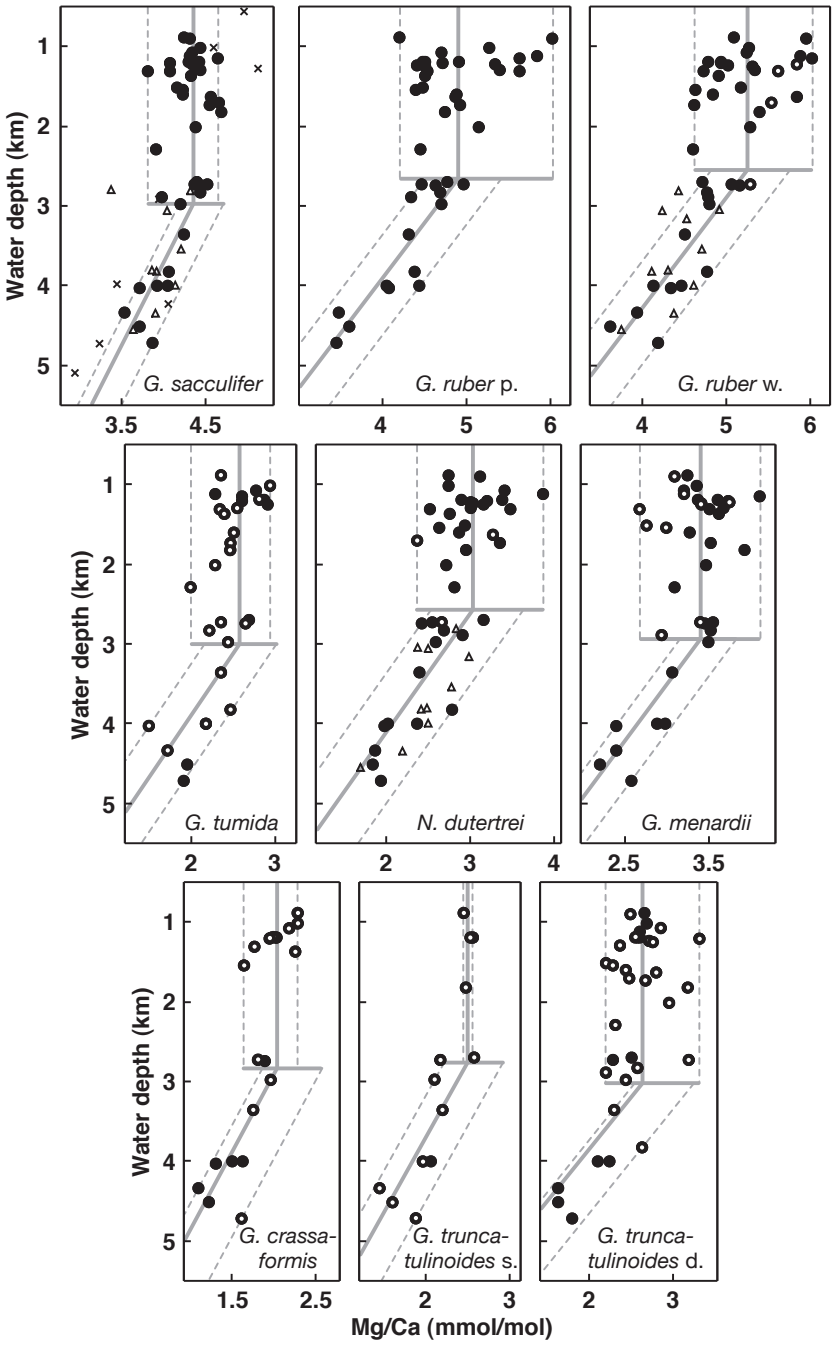

Figure 2.2 Mg/Ca ratios (black dots from 355–400 μm size fraction, open circles from enlarged size fractions; Table 2.2) *vs.* water depth for each planktonic foraminiferal species or variety: The data show significant decreases below species-specific water depth levels ($d_{critical}$ = horizontal line). $d_{critical}$ is defined as the intercept between the vertical (species-specific mean Mg/Ca calculated from samples <2000 m water depth (Table 2.2)) and diagonal lines (regression lines from Mg/Ca from >3000 m water depth). Below $d_{critical}$, the intraspecific scatter in Mg/Ca is significantly reduced. The dashed lines mark envelopes of measured Mg/Ca. For comparison, Mg/Ca of *Rosenthal et al.* (2000) (crosses) and *Dekens et al.* (2002) (triangles) are included. As the data of *Dekens et al.* (2002) are based on a foraminiferal cleaning protocol involving the reductive hydrazine step, we added 15% to their original Mg/Ca data according to the instructions of *Rosenthal et al.* (2004).

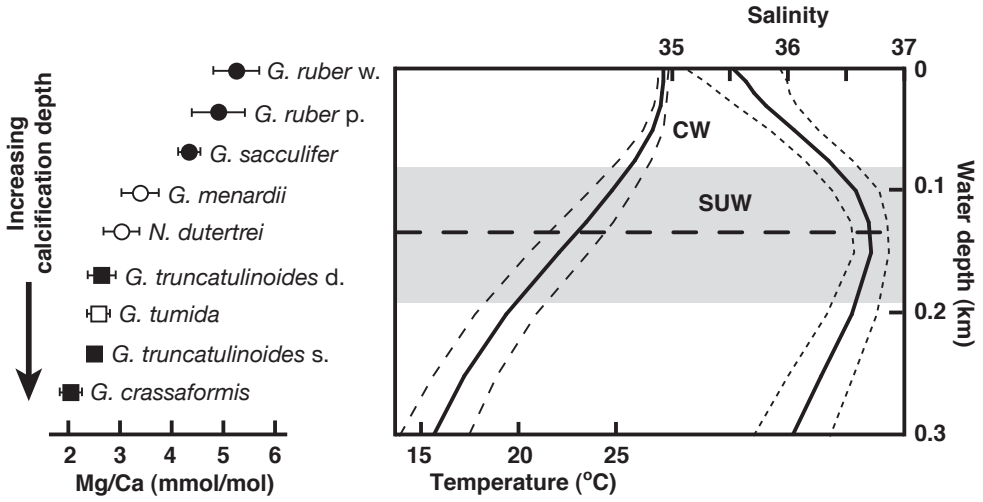

Figure 2.3 Species-specific mean Mg/Ca ratios from <2000 m water depth (error bars indicate standard deviations) ranked from highest to lowest Mg/Ca *vs.* relative calcification depth. Black dots: shallow-dwelling species; circles: thermocline-dwelling species; open square: bottom-of-photic-zone-dwelling species; black squares: deep-dwelling species. For comparison, eastern Caribbean annual mean temperatures and salinities (± standard deviations) (*NODC*, 2001) *vs.* water depth are shown. Shaded area indicates the thermocline. Horizontal dashed line marks the base of the photic zone (inferred from the irradiance value of 0.1%). CW: Caribbean Water; SUW: Subtropical Underwater.

studies of *Hecht et al.* (1975), *Lorens et al.* (1977), *Rosenthal and Boyle* (1993), *Russell et al.* (1994), *Brown and Elderfield* (1996), *Hastings et al.* (1996), *Dekens et al.* (2002), and *Anand et al.* (2003) (Figure 2.2).

2.4.3 Temperature *vs.* Mg/Ca Ratios Unaffected by Dissolution

The accuracy of Mg/Ca *vs.* temperature calibration curves depends on both the accuracy of Mg/Ca analyses and, more importantly, on the accuracy of the temperature assignment. The temperature assignment, however, is dependent on the foraminiferal habitat (e.g., water depth, season, life cycle, nutrient supply), which often comprises a broad range of water depths wherein calcification takes place. In Figure 2.4, we plotted the foraminiferal Mg/Ca ratios from <2000 m *vs.* Caribbean annual mean temperatures (*NODC*, 2001). These temperatures were converted from the specific foraminiferal habitat assignments found in the literature (*Fairbanks et al.*, 1980b, 1982; *Fairbanks and Wiebe*, 1980a; *Erez and Honjo*, 1981; *Hemleben et al.*, 1989; *Sautter and Thunell*, 1991a; *Schweitzer and Lohmann*, 1991; *Ravelo and Fairbanks*, 1992; *Mulitza et al.*, 1997; *Kemle von Mücke and Oberhänsli*, 1999; *Schmuker and Schiebel*, 2002; *Anand et al.*, 2003; *McKenna and Prell*, 2004). Considering only the habitat specifications of *Schmuker and Schiebel* (2002) inferred from abundance maxima of eastern Caribbean plankton tows (April-May 1996), an exponential multispecies Mg/Ca *vs.* temperature relationship suggests itself, which approaches the multispecies calibration curve of *Anand et al.* (2003) established for the Sargasso Sea (Figure 2.4).

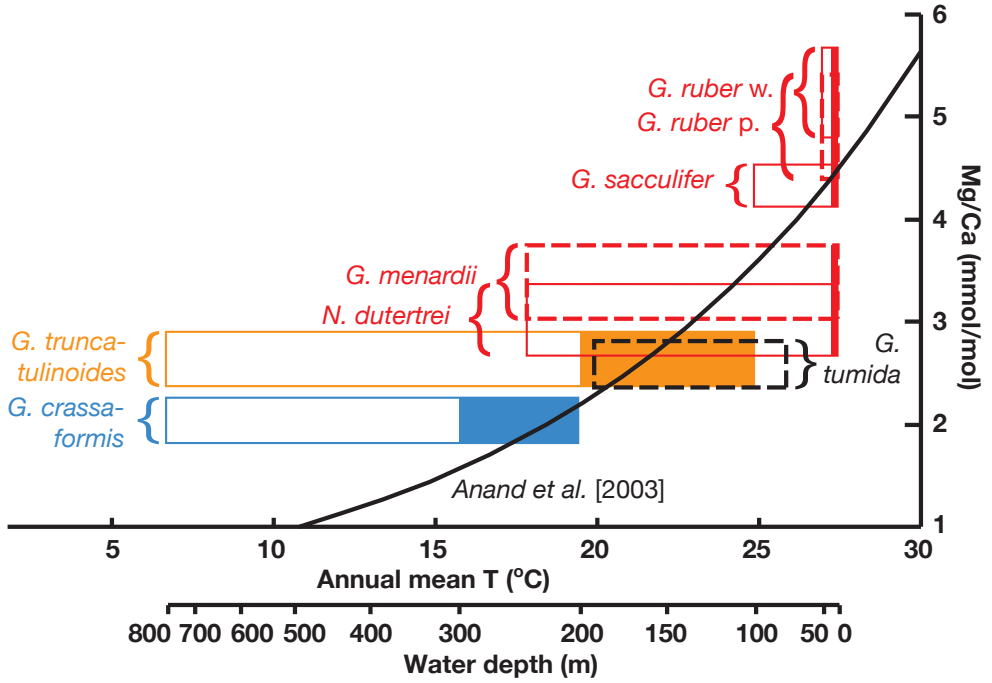

Figure 2.4 Species-specific mean Mg/Ca ratios from <2000 m water depth (box heights indicate Mg/Camean ± standard deviations) *vs.* eastern Caribbean annual temperatures (*NODC*, 2001). The eastern Caribbean annual temperatures were converted from the according habitat depths compiled for the different species and their varieties (widths of open and filled boxes, see Chapter 2.4.3). Considering only those habitat specifications (filled boxes) derived from eastern Caribbean plankton tows (*Schmuker and Schiebel*, 2002) (0–20 m (red bars); 100–200 m (orange bar); 200–300 m (blue bar)), the Mg/Ca *vs.* temperature relationship comes close to the multispecies calibration curve of *Anand et al.* (2003) (black curve).

The slope of such a calibration curve, however, is highly dependent on the determination of the foraminiferal habitat depths. In fact, while estimates on where foraminifers live and where calcification occurs are manifold or speculative, δ^{18}O data of primarily shallow-dwelling species indicate that planktonic foraminifera calcify in depth zones that are significantly narrower than the overall vertical distribution of these species implies (*Fairbanks et al.*, 1980b). From Mg/Ca of the thermocline-dwelling species *G. menardii* and *N. dutertrei*, which are lower than those of the shallow-dwelling species *G. ruber* and *G. sacculifer* (Figures 2.3, 2.4), we hypothesize that the potential calcification depths of these species, where the Mg/Ca signal is generated, are clearly deeper than the shallow abundance maxima given by *Schmuker and Schiebel* (2002).

Despite the overall correspondence between foraminiferal Mg/Ca ratios and temperature shown in Figure 2.4, which heavily relies on assumptions concerning the foraminiferal habitats, we note a broad intraspecific range of Mg/Ca in core-top samples from <2000 m water depth, in accordance to early observations of *Nürnberg* (1995) on the high variability of Mg/Ca in foraminiferal tests. The scatter appears to be largest in shallow- and thermocline-dwelling species with a range of ∼1.4 mmol/mol in *G. ruber* white, ∼1.8 mmol/mol in *G. ruber* pink,

~0.9 mmol/mol in *G. sacculifer*, ~1.3 mmol/mol in *G. menardii*, and ~1.5 mmol/mol in *N. dutertrei*, and a commonly smaller range in deep-dwelling species of ~0.7 mmol/mol in *G. tumida*, ~1.1 mmol/mol in *G. truncatulinoides* dextral, ~0.1 mmol/mol in *G. truncatulinoides* sinistral, and ~0.7 mmol/mol in *G. crassaformis* (Figure 2.2). The observed range of core-top Mg/Ca appears high, but is close to other shallow core-top and sediment-trap data from other ocean areas at similar temperatures showing a wide range of Mg/Ca of ~1 mmol/mol (e.g., *Elderfield and Ganssen*, 2000; *Whitko et al.*, 2002; *Anand et al.*, 2003) (Figure 2.5).

The observed scatter in the core-top Mg/Ca ratios may be due to several reasons: (i) An annual mixed layer temperature range of ~2–3°C at the respective core sites within the mixed layer (i.e., ~30–50 m water depth, assumed habitat of shallow-dwelling species (*Schmuker and Schiebel*, 2002)) and a smaller annual temperature range of only ~1–2°C at intermediate water depths (down to ~230 m water depth, assumed habitat of *G. crassaformis* (*Schmuker and Schiebel*, 2002)) (Figure 2.5) introduces a potential variability in Mg/Ca of ~0.1–0.4 mmol/mol when applying the Mg/Ca *vs.* temperature equation of *Anand et al.* (2003). (ii) The assumed age range of ~2–3 kyrs for the core-top sediments (see Chapter 2.3.1) might have introduced a certain variance in Mg/Ca due to short-term climate variations. Indeed, a cooling of Caribbean surface water temperatures of about 2°C during the Little Ice Age (*Watanabe et al.*, 2001) could account for a change in Mg/Ca of ~0.7 mmol/mol. (iii) A species-specific size-effect on Mg/Ca generally was avoided by selecting foraminiferal tests from narrow size ranges (see Chapter 2.3.1; Table 2.2). Especially for the deep-dwelling species, however, we were forced to widen the size range due to insufficient numbers of specimens for analysis (Table 2.2). Taking the published deviations from mean Mg/Ca of 12–36% by enlargement of the foraminiferal test sizes (*Elderfield et al.*, 2002; *Anand and Elderfield*, 2005), we estimate the size effect on our Mg/Ca to a maximum of ~0.2–0.7 mmol/mol. (iv) The presence of varying amounts of secondary, gametogenic calcite (see Chapter 3.2.1), which is added to the foraminiferal tests at greater water depths and, hence, records lower temperatures, biases Mg/Ca towards lower ratios. The quantitative effect on Mg/Ca, however, remains uncertain as we have no control on the amounts of gametogenic calcite. (v) Unintended mixing of morphotypes may have led to a widened scatter in Mg/Ca. Foraminiferal species are known to form different morphotypes showing different geochemical signatures (e.g., *Williams et al.*, 1981; *Deuser and Ross*, 1989). *Steinke et al.* (2005) presented a statistically significant difference in Mg/Ca for two morphotypes of *G. ruber* white of 0.38 ± 0.30 mmol/mol. In spite of all these factors potentially affecting Mg/Ca, the succession of foraminiferal species and varieties according to their Mg/Ca clearly reflects the expected depth habitats (Figure 2.3).

As we are not able to establish core-top Mg/Ca *vs.* temperature calibrations due to the restricted temperature range covered by our Caribbean samples, we compared our (dissolution-unaffected) core-top Mg/Ca data from <2000 m water depths to published Mg/Ca *vs.* temperature relationships. Mg/Ca ratios of the deep-dwelling species *G. truncatulinoides* dextral and sinistral, and *G. crassaformis* exhibit a clear relationship to temperature. Each species covers a regional temperature range of ~5–6°C when applying the habitat specification of *Schmuker and Schiebel* (2002) of ~160 m and ~230 m water depth, respectively (Figure 2.5a). The *G. truncatulinoides*

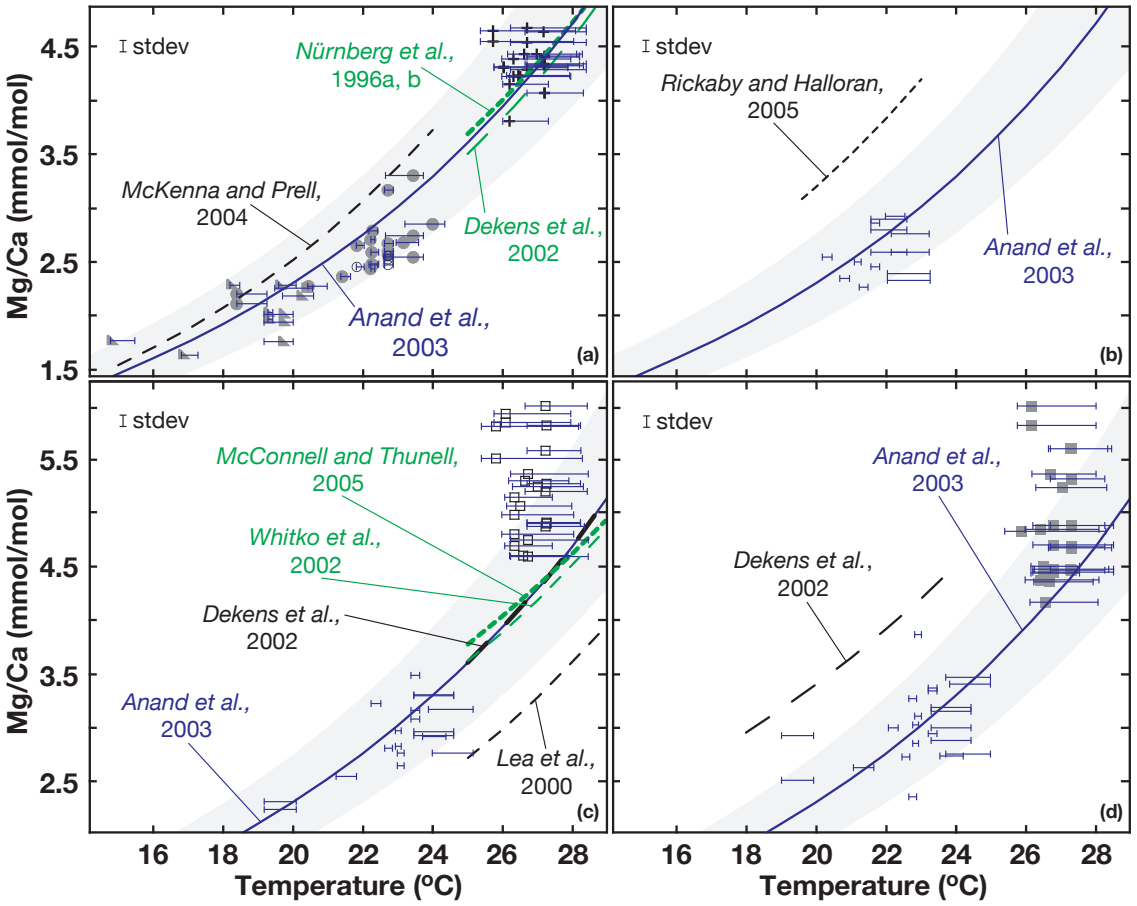

Figure 2.5 Caribbean core-top Mg/Ca ratios *vs.* temperature data of 9 planktonic foraminiferal species and varieties in comparison with published Mg/Ca-paleotemperature equations. Horizontal bars indicate entire annual temperature ranges (*NODC*, 2001) at the respective core locations from preferred living depths of the foraminiferal species and varieties. Symbols are placed at April-May temperatures when foraminiferal abundance maxima were observed (*Schmuker and Schiebel*, 2002). Shaded areas indicate the Mg/Ca data variability around the *Anand et al.* (2003) multispecies calibration curve (solid lines: Mg/Ca=0.38·exp(0.09T)). Average standard deviations of replicate Mg/Ca analyses (stdev) is indicated by vertical bars. (a) Deep-dwelling *G. crassaformis* (triangles), *G. truncatulinoides* dextral (dots) and sinistral (open circles), and shallow-dwelling *G. sacculifer* (crosses): Habitat depths of ∼230 m, ∼160 m, and ∼40 m, respectively (see Chapter 2.4.3); species-specific paleotemperature calibration curves for *G. truncatulinoides* dextral from *McKenna and Prell* (2004) (Mg/Ca=0.355·exp(0.098T)), and for *G. sacculifer* from *Dekens et al.* (2002) (Mg/Ca=0.37·exp(0.09T)) and *Nürnberg et al.* (1996a,b) (Mg/Ca=0.472·10^(0.036T)). (b) Deep-dwelling *G. tumida*: Habitat depth defined to ∼180 m; species-specific paleotemperature equation for *G. tumida* from *Rickaby and Halloran* (2005) (Mg/Ca=0.53·exp(0.09T)). (c) Thermocline-dwelling *G. menardii* and shallow-dwelling *G. ruber* white (open squares): Habitat depths defined to ∼150 m and ∼34 m, respectively; species-specific paleotemperature equations for *G. ruber* white from *Lea et al.* (2000) (Mg/Ca=0.3·exp(0.09T)), *Dekens et al.* (2002) (Mg/Ca=0.38·exp(0.09T)), *Whitko et al.* (2002) (Mg/Ca=0.57·exp(0.074T)), and *McConnell and Thunell* (2005) (Mg/Ca=0.69·exp(0.068T)). (d) Thermocline-dwelling *N. dutertrei* and shallow-dwelling *G. ruber* pink (squares): Habitat depths defined to ∼150 m and ∼37 m, respectively; species-specific paleotemperature equation for *N. dutertrei* from *Dekens et al.* (2002) (Mg/Ca=0.6·exp(0.08T)).

dextral and sinistral, and *G. crassaformis* data fall onto published Mg/Ca *vs.* temperature curves of *Anand et al.* (2003) proposed for multispecies planktonic foraminifers, and of *McKenna and Prell* (2004) for *G. truncatulinoides* dextral (Figure 2.5a). Also, the Mg/Ca data of Caribbean *G. sacculifer* agree with published calibration curves of *Nürnberg et al.* (1996a,b), *Dekens et al.* (2002), and *Anand et al.* (2003) when relating water temperatures from ∼40 m water depth (*Schmuker and Schiebel*, 2002) to the Mg/Ca ratios (Figure 2.5a).

The Mg/Ca ratios of *G. tumida* are very close to those of *G. truncatulinoides* (Figure 2.4), suggesting akin living depths. If we assume a living depth of ∼180 m, which is in accordance to *Ravelo and Fairbanks* (1992) and *Chaisson and Ravelo* (1997), than the according Mg/Ca *vs.* temperature data fall onto the *Anand et al.* (2003) calibration curve (Figure 2.5b). Thermocline-dwelling *G. menardii* and *N. dutertrei* have less well-defined habitat specifications. In view of the low Mg/Ca ratios, the extremely shallow abundance maximum of ∼40–50 m observed by *Schmuker and Schiebel* (2002) is highly unlikely to truly reflect the foraminiferal calcification depth (Figure 2.4). Assuming an average depth habitat of ∼150 m water depth inferred from various sources (*Fairbanks et al.*, 1980b, 1982; *Fairbanks and Wiebe*, 1980a; *Sautter and Thunell*, 1991b; *Ravelo and Fairbanks*, 1992; *Chaisson and Ravelo*, 1997) results in Mg/Ca *vs.* temperature data matching the *Anand et al.* (2003) calibration curve reasonably well (Figure 2.5c, 2.5d).

In contrast to the abovementioned foraminiferal species, *G. ruber* is different. First, the spread of Mg/Ca ratios in dissolution-unaffected core-top samples is largest among our studied species. Second, Mg/Ca of *G. ruber* white and pink deviate from existing Mg/Ca *vs.* temperature calibrations when considering depth habitats of ∼34 m and ∼37 m, respectively, which are the April-May abundance maxima in Caribbean plankton nets (*Schmuker and Schiebel*, 2002) (Figure 2.5c, 2.5d). Such depth estimates for *G. ruber* seem plausible as MOCNESS plankton tows from the western Gulf of Mexico show the depth preference for *G. ruber* white to be 0–45 m, for *G. ruber* pink to be slightly deeper (25–65 m) (*Tedesco and Thunell*, 2003). Even if one would assume a very shallow habitat of <10 m being ∼0.2°C warmer than at ∼30 m, the Mg/Ca data would still deviate from available calibration curves. The reason for that is not yet clear. It is evident, however, that *G. ruber* definitely occupies a shallower habitat than *G. sacculifer* as suggested by higher Mg/Ca (Figure 2.4) and generally lighter δ^{18}O values (*Anand et al.*, 2003). Their oxygen isotope signal commonly points to summer sea-surface conditions (*Deuser*, 1987), and both *Flower et al.* (2004) and *Anand et al.* (2003) pointed out that Mg/Ca of *G. ruber* white commonly represents warmer than average temperatures in the Orca Basin (Gulf of Mexico) and in the Sargasso Sea, respectively.

2.4.4 Correcting Deep Water Mg/Ca Ratios for the Effect of Dissolution

Dependent on the foraminiferal species and varieties, a major and systematic decrease in Mg/Ca ratios starts below species-specific critical water depths, which are situated in the depth interval between 2000–3000 m. This is far above the calcite saturation horizon (CSH) at ∼4600 m (Figure 2.6), which approximates the present-day top of the lysocline at a $\Delta[CO_3^{2-}]$ (difference

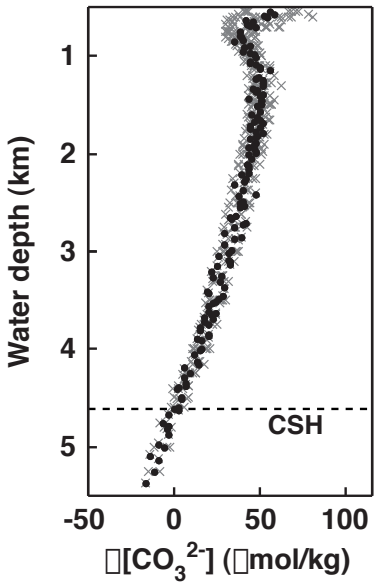

Figure 2.6 $\Delta[CO_3^{2-}]$, defined as the difference between the *in situ* carbonate ion concentration ($[CO_3^{2-}]$) and $[CO_3^{2-}]$ at saturation, *vs.* water depth. Total alkalinity (TA) and TCO_2 data necessary to calculate the *in situ* $[CO_3^{2-}]$ were obtained from the World Ocean Circulation Experiment (WOCE) Line number A22 and A22_2003A (Caribbean stations 1–38 and 2–37, respectively; available at: http://whpo.ucsd.edu/index.htm; Figure 2.1). The *in situ* $[CO_3^{2-}]$ was calculated using the program of *Lewis and Wallace* (1998) developed for CO_2 System Calculations. $[CO_3^{2-}]$ at saturation was calculated after *Jansen et al.* (2002). Grey crosses mark computed $\Delta[CO_3^{2-}]$ data, black dots indicate $\Delta[CO_3^{2-}]$ data averaged for every 20 m water depth. CSH = calcite saturation horizon (dashed line) as the approximate top of the lysocline.

between the *in situ* carbonate ion concentration ($[CO_3^{2-}]$) and the $[CO_3^{2-}]$ at saturation) of 0 μmol/kg, and is equal to a calcite solubility ratio (Ω) of 1 (*Lewis and Wallace*, 1998; *Tyrrell and Zeebe*, 2004). In fact, below >3000 m, Mg/Ca decreases linearly with increasing water depth (r^2 = 0.55–0.80; Figure 2.2; Table 2.4). This close relationship is also reflected in the linear decrease of Mg/Ca with decreasing $\Delta[CO_3^{2-}]$ (r^2 = 0.32–0.94; Figure 2.5; Table 2.4) below 20 μmol/kg (Figure 2.7; Table 2.4).

As only few Mg/Ca ratios cover the interval between 2000–3000 m (40–20 μmol/kg $\Delta[CO_3^{2-}]$), the onset of dissolution was determined by calculating the intersection between the unaffected Mg/Ca means from <2000 m (>40 μmol/kg) and the regressions through the dissolution-affected ratios from >3000 m (<20 μmol/kg). The decrease of Mg/Ca can be described as:

$$\Delta Mg/Ca \quad = \quad Mg/Ca_{initial} - Mg/Ca_{measured} \tag{2.1}$$

where ΔMg/Ca is the difference between the (unknown) initial, dissolution-unaffected Mg/Ca ($Mg/Ca_{initial}$) and the measured Mg/Ca ($Mg/Ca_{measured}$). A reasonable approximation for $Mg/Ca_{initial}$ is the mean Mg/Ca (Mg/Ca_{mean}) from <2000 m (Table 2.2). The intersection of

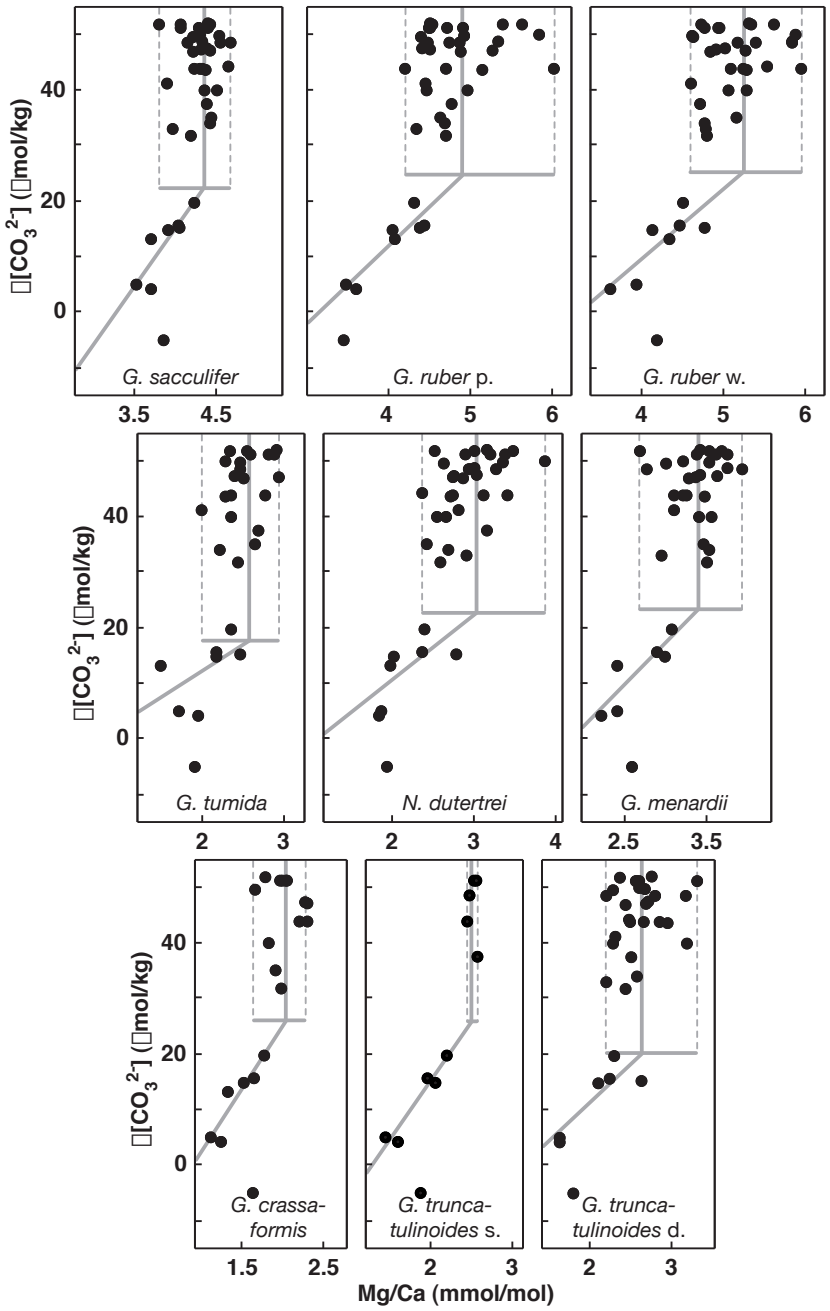

Figure 2.7 Mg/Ca ratios *vs.* $\Delta[CO_3{}^{2-}]$ for each planktonic foraminiferal species and variety indicating significant Mg_{2+} loss below species-specific $\Delta[CO_3{}^{2-}]$ levels ($\Delta_{critical}$ = horizontal lines). $\Delta_{critical}$ is defined by the intercept between the vertical lines (species-specific mean Mg/Ca calculated from samples <2000 m water depth, similar to $\Delta[CO_3{}^{2-}]$ >40 μmol/kg (Table 2.2)) and diagonal lines (regression lines from Mg/Ca at $\Delta[CO_3{}^{2-}]$ <20 μmol/kg). Deepest core-top sample M35024–6 from below the CSH was defined as an outlier and excluded from the calculation of the regressions.

Table 2.4 Species-specific parameters for Equations (2.2)–(2.7): a = y-axis intercepts; b = slope of the regression lines; r^2 = correlation coefficients; $d_{critical}$ = species-specific water depths where Mg^{2+} removal starts; $\Delta_{critical}$ = species-specific $\Delta[CO_3^{2-}]$ levels where Mg^{2+} removal starts.

Species	d-correction, equation (6)				□-correction, equation (7)			
	a	*b*	r^2	$d_{critical}$ (m)	*a*	*b*	r^2	□ $_{critical}$ (□mol/kg)
G. crassaformis	6,833	1,962	0.61	2,838	-20.00	22.70	0.86	26.31
G. menardii	7,734	1,413	0.8	2,939	-27.61	15.03	0.78	22.88
G. ruber p.	9,403	1,381	0.79	2,631	-44.08	14.03	0.84	24.67
G. ruber w.	9,793	1,382	0.76	2,535	-40.93	12.61	0.71	25.28
G. sacculifer	12,030	2,088	0.75	2,968	-68.50	20.87	0.78	22.10
G. truncatulinoides d.	6,456	1,303	0.56	3,019	-16.23	13.79	0.74	20.17
G. truncatulinoides s.	7,471	1,888	0.65	2,746	-27.43	21.28	0.94	25.77
G. tumida	6,985	1,547	0.55	2,989	-6.62	9.43	0.32	17.70
N. dutertrei	7,057	1,484	0.67	2,568	-12.73	11.65	0.48	22.58

the Mg/Ca_{mean} with the regression line calculated for Mg/Ca from >3000 m water depth and <20 μmol/kg $\Delta[CO_3^{2-}]$, respectively, provides the critical water depth ($d_{critical}$ in m) and the critical calcite saturation state ($\Delta_{critical}$ in μmol/kg), where Mg^{2+}-removal due to dissolution starts:

$$d_{critical} = a - b \cdot Mg/Ca_{mean} \tag{2.2}$$

$$\Delta_{critical} = a - b \cdot Mg/Ca_{mean} \tag{2.3}$$

where a is the y-axis intercept, and b is the slope of the regression lines (Figures 2.2, 2.7; Table 2.4). The levels of beginning preferential dissolution of Mg^{2+} appear to be species-specific. $\Delta_{critical}$ spans values of ~18–26 μmol/kg (Table 2.4) which correspond to Ω values of ~1.5, accompanied by $d_{critical}$ of ~2500–3000 m (Table 2.4).

Different susceptibility of calcitic tests from different planktonic foraminiferal species to dissolution is a well-known feature (e.g., *Berger*, 1968, 1970, 1971), likewise is the heterogeneous distribution of Mg^{2+} in foraminiferal tests (*Bender et al.*, 1975; *Duckworth*, 1977; *Nürnberg*, 1995; *Brown and Elderfield*, 1996; *Nürnberg et al.*, 1996a; *Rosenthal et al.*, 2000; *Eggins et al.*, 2003; *McKenna and Prell*, 2004; *Anand and Elderfield*, 2005; *Bentov and Erez*, 2005, 2006). *Sadekov et al.* (2005) recently illustrated by electron microprobe mapping that low-Mg/Ca (~1–5 mmol/mol) and high-Mg/Ca bands (~8–11 mmol/mol) alternate within tests of planktonic foraminifera. As Mg^{2+} has a pronounced effect on the stability of biogenic calcite (e.g., *Walter and Morse*, 1985), and as ion activity products increase with increasing Mg^{2+}, *Brown and Elderfield* (1996) deduced that Mg-enriched phases are less dissolution resistant. The selective removal of Mg^{2+}-enriched foraminiferal parts with increasing dissolution should thus cause the reduction of the intraspecific Mg/Ca scatter, which is observed in samples from >3000 m water depth in comparison to shallow samples from <2000 m. This reduction amounts to 36% for *G. ruber* white, 50% for *G. ruber* pink, 44% for *G. sacculifer*, 46% for *G. menardii*, 27% for *N. dutertrei*, 14%

for *G. tumida*, 36% for *G. truncatulinoides* dextral, while *G. crassaformis* shows no discernable change.

Nonetheless, the slopes b of the regression lines indicate a relatively uniform ~0.5–0.8 mmol/mol change in Mg/Ca ratios per kilometer water depth and ~0.04–0.11 mmol/mol per 1 μmol/kg decrease in $\Delta[CO_3^{2-}]$ with respect to Mg/Ca_{mean} for all studied foraminiferal species and varieties (Table 2.4). In contrast to observations of *Savin and Douglas* (1973), *Lorens et al.* (1977), *Brown and Elderfield* (1996), and *Rosenthal et al.* (2000), the relatively similar decline of Mg/Ca in combination with broadly the same $d_{critical}$ and $\Delta_{critical}$ (Figures 2.2, 2.7; Table 2.4) for all foraminifers studied does not support the notion that calcite of shallow-dwelling foraminifers with higher Mg/Ca dissolves preferentially with respect to deep-dwelling species bearing lower Mg/Ca.

The absolute change in Mg/Ca ratios of ~0.5–0.8 mmol/mol per kilometer water depth is equivalent to a relative decrease of ~11–29% per kilometer. Our results support previous core-top studies showing a decrease of Mg/Ca with increasing water depth (*Savin and Douglas*, 1973; *Bender et al.*, 1975; *Rosenthal and Boyle*, 1993). For *G. sacculifer*, *Lorens et al.* (1977) showed a decrease in Mg/Ca of ~40% in tropical East Pacific Rise and central Pacific samples over a depth range from ~600–4000 m. Both, *Lorens et al.* (1977) and *Brown and Elderfield* (1996) detected a decrease of 40% in Mg/Ca of *G. tumida* over a depth range from ~1900–4700 m, while the decline in Mg/Ca of *N. dutertrei* amounts to ~59% from ~600–3800 m, and ~25% for *G. ruber* from ~1900–4700 m (*Lorens et al.*, 1977), all from tropical Pacific samples. Assuming a linear Mg/Ca descent with depth, these numbers would convert to Mg/Ca reductions of ~12% for *G. sacculifer*, ~14% for *G. tumida*, ~18% for *N. dutertrei*, and ~9% for *G. ruber* per kilometer water depth. At Ontong Java Plateau, *Lea et al.* (2000) showed a decrease in Mg/Ca in tests of *G. ruber* by ~12% per kilometer water depth, while *Dekens et al.* (2002) revealed a decrease of ~14% per kilometer. At Sierra Leone Rise and Ceara Rise, a decrease in Mg/Ca of ~7% and ~5% per kilometer, respectively, was observed for G. ruber (*Dekens et al.*, 2002). For *N. dutertrei*, *Dekens et al.* (2002) found a Mg/Ca decline of up to ~23% per kilometer.

Our results on decreasing Mg/Ca ratios below species-specific $\Delta[CO_3^{2-}]$ levels of ~18–26 μmol/kg are in general accordance with *Dekens et al.* (2002), who also noted the onset of Mg^{2+} loss below ~20 μmol/kg $\Delta[CO_3^{2-}]$ at Ceara Rise (Atlantic) and Ontong Java Plateau (Pacific). In the South China Sea, *Whitko et al.* (2002) found declining Mg/Ca in core-top *G. ruber* below ~2000 m water depth, implying a strong dissolution effect below ~2000 m. This is considerably shallower than both, the present-day lysocline and the carbonate compensation depth in this ocean area at ~3000 m and ~3800 m, respectively (*Miao et al.*, 1994; *Feely et al.*, 2002, 2004). Although we do not have $\Delta[CO_3^{2-}]$ values for this ocean basin at hand, we speculate that the onset of Mg/Ca change observed by *Whitko et al.* (2002) might coincide with the approximate threshold in $\Delta[CO_3^{2-}]$ of ~20 μmol/kg. It needs to be proven, though, whether this threshold is globally valid.

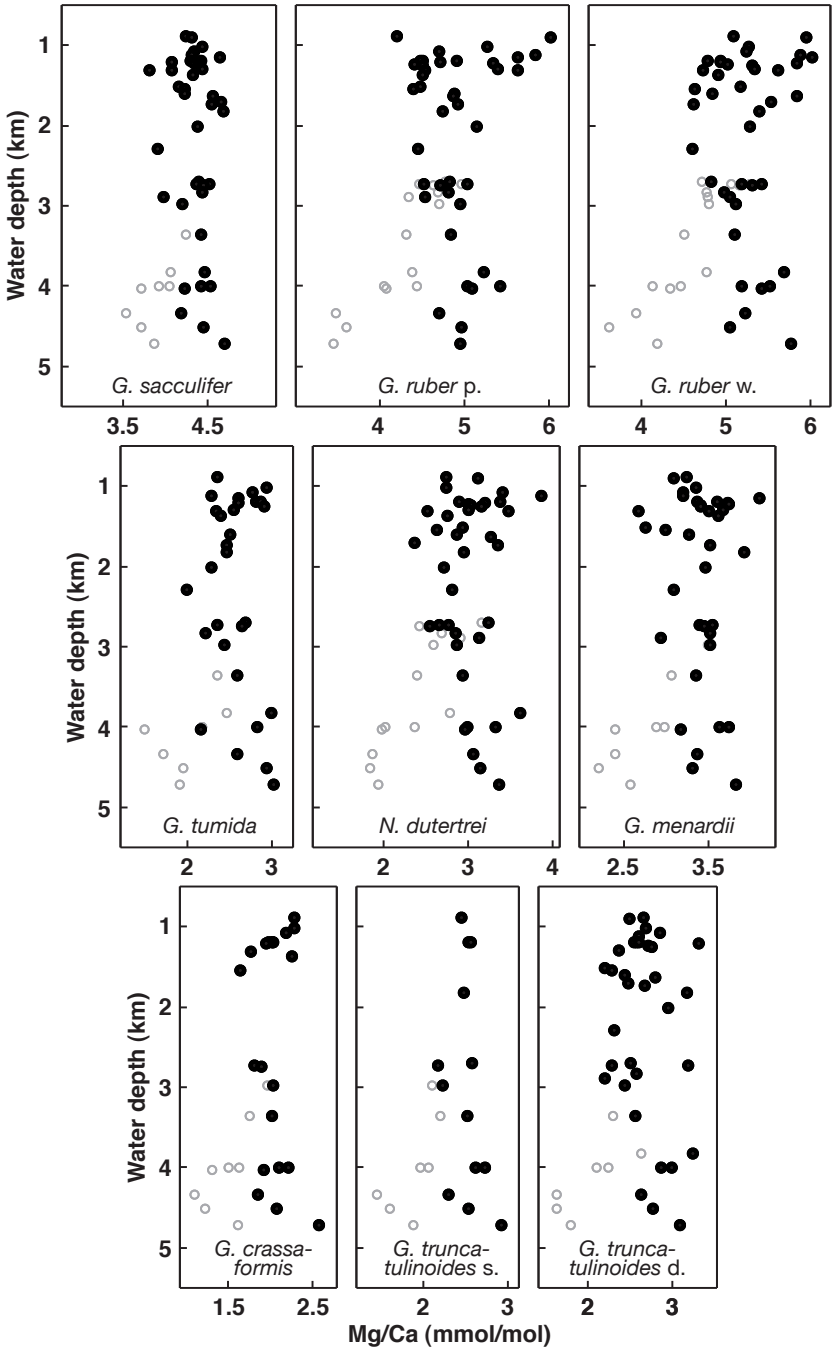

Figure 2.8 Foraminiferal Mg/Ca ratios *vs.* water depth (black dots): Mg/Ca from below $d_{critical}$ were corrected for water-depth induced calcite dissolution according to Equation (2.6). For comparison, the measured, non-corrected Mg/Ca data are included (circles). The application of the correction routine leads to a reduction of the intraspecific Mg/Ca variability by 24–64%.

In order to correct the measured Mg/Ca ratios for the selective loss of Mg^{2+} due to dissolution, ΔMg/Ca was calculated for every measured Mg/Ca from below $d_{critical}$ and $\Delta_{critical}$:

$$\Delta Mg/Ca = (d - d_{critical})/b \quad (2.4)$$

$$\Delta Mg/Ca = (\Delta_{critical} - \Delta)/b \quad (2.5)$$

where d is the water depth of the core-top sample in meter (with $d > d_{critical}$) (Table 2.1, 2.2), and Δ is the averaged $\Delta[CO_3^{2-}]$ in μmol/kg at the seafloor (with $\Delta < \Delta_{critical}$) (Figure 2.6). We then combined Equations (2.1) and (2.4), as well as (2.1) and (2.5) to re-calculate the dissolution-unaffected $Mg/Ca_{initial}$ (water depth correction (d-corrected) according to Equation (2.4) (Figure 2.8); and $\Delta_{critical}$ correction (Δ-corrected) according to Equation (2.5)):

$$Mg/Ca_{initial}\ (d\text{-}corrected) = Mg/Ca_{measured} + (d - d_{critical})/b \quad (2.6)$$

$$Mg/Ca_{initial}\ (\Delta\text{-}corrected) = Mg/Ca_{measured} + (\Delta_{critical} - \Delta)/b \quad (2.7)$$

Both independently developed routines for the correction of dissolution-induced Mg/Ca decline produce comparable results indicating that selective Mg^{2+} removal is mainly driven by the calcite saturation state (Figure 2.9). Application of the correction routines reduces the overall intraspecific variability of Mg/Ca by ~24–64% (Figure 2.8).

2.4.5 Implications for Paleo-Records

We chose the Mg/Ca records of *G. ruber* white of two Caribbean cores (*Schmidt et al.*, 2004) to test the downcore applicability of the proposed correction routine. Today, both records chart similar temperature conditions within the Columbian Basin (Figure 2.1), and hence, are expected to show similar Mg/Ca ratios. The impact of dissolution on the Holocene (3–6 kyrs) mean Mg/Ca from shallower ODP Site 999A (2827 m, 4.13 mmol/mol) appears to be less than on Mg/Ca from deeper site VM22–128 (3623 m, 3.75 mmol/mol), differing by 0.38 mmol/mol. Depth correction (Equation (6); parameters see Table 2.4) leads to higher Holocene Mg/Ca of 4.34 mmol/mol at ODP Site 999A and 4.53 mmol/mol at site VM28–122, reducing the offset to 0.19 mmol/mol. Such inter-site offset converts to a ~0.5°C difference (calculated after *Anand et al.* (2003); see Table 2.2), which is in accordance with the modern temperature pattern in the Columbian Basin.

For glacial times, instead, reduced pCO_2 and increased $[CO_3^{2-}]$ in Caribbean intermediate and deep waters (*Barker and Elderfield*, 2002; *Broecker and Clark*, 2002) suggest a better carbonate preservation (*Haddad and Droxler*, 1996; *Anderson and Archer*, 2002). Hence, Mg/Ca ratios should have been unaffected by dissolution effects even at greater water depths. This is reflected in the similar last glacial (19–21 kyrs) mean Mg/Ca of Caribbean cores ODP 999A and VM28–122 (*Schmidt et al.*, 2004), both revealing 3.36 mmol/mol.

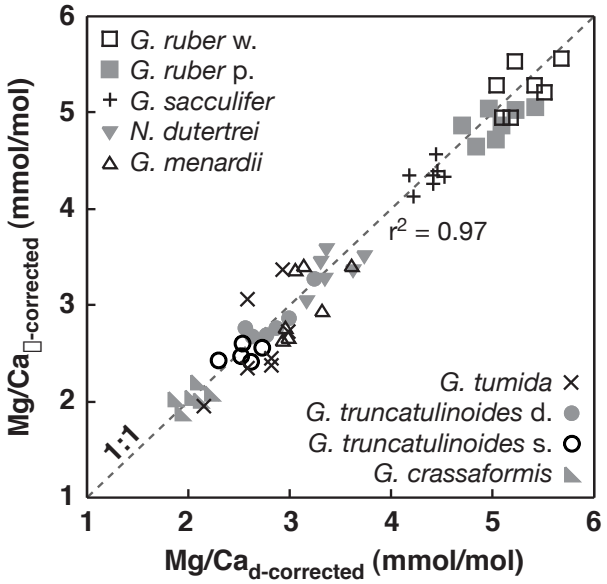

Figure 2.9 Depth-corrected (d-corrected, Equation (2.6)) *vs.* $\Delta[CO_3^{2-}]$-corrected (Δ-corrected, Equation (2.7)) Mg/Ca ratios: The independently corrected ratios from below $d_{critical}$ and $\Delta_{critical}$ highly correlate (r^2 = 0.97). Related high probability values (p = 0.77) imply that the corrected Mg/Ca means of all species and varieties do not statistically deviate from each other, implying that the selective removal of Mg^{2+} from foraminiferal calcite is mainly a function of the calcite saturation state $\Delta[CO_3^{2-}]$.

2.5 Conclusions

We analyzed Mg/Ca ratios in tests of seven planktonic foraminiferal species and four of their varieties from 42 Caribbean and tropical Atlantic core-top samples covering water depths of ~900–4700 m in order to quantify the effect of dissolution on Mg/Ca. As lateral temperature gradients at similar water depths in the study area are minor, the well-known temperature effect on intraspecific Mg/Ca variations is considered to be minimal. Shallow core-top samples from above 2000 m water depth being unaffected by dissolution processes, clearly reveal interspecific differences in Mg/Ca with high ratios in shallow-dwelling, and low ratios in deep-dwelling species. This pattern reflects the expected habitat depths, and clearly points to different calcification depths at different temperature regimes.

The core-top samples exhibit a linear decline of foraminiferal Mg/Ca ratios below water depths of ~2500–3000 m ($d_{critical}$) depending on the foraminiferal species or variety. Hence, the onset of selective Mg^{2+} removal ($d_{critical}$) takes place far above the present-day lysocline and concurs with calcite saturation state $\Delta[CO_3^{2-}]$ levels of ~18–26 μmol/kg ($\Delta_{critical}$). Mg/Ca from above these species-specific critical levels appear to remain stable, and hence, are considered to be unaffected by dissolution. Nonetheless, the intraspecific variability at shallow depths is larger than at greater water depths.

Below the species-specific levels ($\Delta_{critical}$ and $d_{critical}$) of apparent Mg^{2+} removal, Mg/Ca ratios decline linearly by ~0.04–0.11 mmol/mol per 1 μmol/kg decrease in $\Delta[CO_3^{2-}]$ and ~0.5–0.8 mmol/mol per kilometer water depth. The relatively similar rates of Mg/Ca change, and the broadly similar $d_{critical}$ and $\Delta_{critical}$ for all species and varieties studied, imply that low magnesium calcite of shallow-dwelling foraminifers showing higher Mg/Ca does not dissolve preferentially with respect to calcite of deep-dwelling species bearing lower Mg/Ca.

We developed independent routines to correct core-top Mg/Ca ratios from below $\Delta_{critical}$ and $d_{critical}$ for the effect of dissolution. Both routines produce comparable results, implying that the selective Mg^{2+} removal is mainly driven by the calcite saturation state at the seafloor. They may be used as robust approaches for the assessment and correction of the dissolution effect on planktonic Mg/Ca. The water-depth correction of Mg/Ca (Equation 2.6), however, should only be applied to samples from ocean areas with resembling calcite saturation states. Instead, the $\Delta[CO_3^{2-}]$ correction (Equation 2.7) is applicable to any ocean area as long as the $\Delta[CO_3^{2-}]$ levels are known. The critical $\Delta[CO_3^{2-}]$ level of ~20 μmol/kg as an effective threshold for the onset of Mg^{2+} removal from low magnesium foraminiferal calcite may be globally valid in this respect, even through geological time spans. The correction routines proposed here may help to improve core-top Mg/Ca *vs.* temperature calibrations, and to re-calculate initial Holocene Mg/Ca, from which paleotemperature estimates can be derived.

2.6 Acknowledgements

This study was funded by the German Ministry of Education and Research (BMBF) under project No. 03G0164, and the Leibniz Award Du 129/33. KIA-AMS ^{14}C analyses were performed at the Leibniz-Labor for Radiometric Dating and Isotope Research, Kiel, Germany. We thank Silvia Koch, Karin Kißling, Daniel Oesterwind, and Stefan Dennenmoser for technical support and laboratory assistance, and Anke Schneider and Douglas W. R. Wallace for assistance with the running of the co2sys-program. We are grateful for the useful comments of Joachim Schönfeld, Martin Ziegler, and the reviewers Robert C. Thunell and Luke C. Skinner, who considerably improved the manuscript.

Chapter 3

Calibrating Mg/Ca of Multiple Planktonic Foraminiferal Species with δ^{18}O-Calcification Temperatures: Paleothermometry for the Upper Water Column

Marcus Regenberg[1], Silke Steph[2], Dirk Nürnberg[1], Ralf Tiedemann[2]

[1]Leibniz Institute of Marine Sciences IFM-GEOMAR, Kiel, Germany

[2]Alfred Wegener Institute for Polar and Marine Research AWI, Bremerhaven, Germany

Submitted to *Earth and Planetary Science Letters*

Mg/Ca ratios of eight shallow-, thermocline-, and deep-dwelling planktonic foraminiferal species from 77 tropical Atlantic and Caribbean sediment-surface samples were calibrated *vs.* δ^{18}O-calcification temperatures derived after the *Shackleton* (1974) δ^{18}O-paleotemperature equation. The overall range of calcification temperatures amounts to ∼8–28°C. The species-specific exponential temperature dependencies are relatively similar for all species (∼7–11% per 1°C) and largely agree with existing calibrations, whereas the preexponential constants of the calibrations are significantly different for the deep-dwelling (0.83–1.31) with respect to the shallow- and thermocline-dwelling species (0.23–0.65). Combining the species-specific data sets, we extracted two multispecies calibrations, which differ in the preexponential rather than in the exponential constants: The 'warm water' multispecies calibration (Mg/Ca=0.223exp(0.113T), r=0.90) holds

for shallow and thermocline dwellers at temperatures >19°C, while the 'cold water' dual-species calibration (Mg/Ca=0.842exp(0.083T), r=0.85) is valid for deep-dwelling species at temperatures <15°C.

3.1 Introduction

The assessment of accurate seawater temperatures contributes as a major physical parameter to the understanding of past ocean dynamics. Especially the reconstruction of (sub)tropical upper ocean stratification, including vertical temperature, salinity, and density gradients, still suffers from inconsistencies in the quantification mainly of the temperature signal. This highlights the need of a detailed temperature reconstruction at different water depth levels. The seawater temperature, at which planktonic foraminifera calcify, is recorded in the Mg^{2+} content (Mg/Ca) and the oxygen isotope composition ($\delta^{18}O$) of their calcite tests (e.g., *Nürnberg*, 2000; *Elderfield and Ganssen*, 2000; *Lea*, 2003). Shallow-dwelling species generally exhibit increased Mg/Ca ratios and lower $\delta^{18}O$ values with respect to species calcifying at greater water depths and, hence, lower temperatures (e.g., *Emiliani*, 1954; *Savin and Douglas*, 1973; *Anand et al.*, 2003; *Regenberg et al.*, 2006a) (Chapter 2). Since $\delta^{18}O$ of foraminiferal calcite combines the temperature signal and the $\delta^{18}O$ signal of ambient seawater during calcification (e.g., *Shackleton and Opdyke*, 1973), the accurate determination of temperature requires a proxy controlled by temperature alone. Like in inorganic precipitates (e.g., *Katz*, 1973; *Mucci and Morse*, 1983), Mg/Ca of calcite foraminiferal tests increase at warmer temperatures due to the endothermic substitution of Mg^{2+}. As the incorporation of Mg^{2+} is biologically mediated, a temperature calibration of Mg/Ca based on foraminiferal calcite is required. Meanwhile, the dependence of the Mg^{2+} content in planktonic foraminiferal tests on temperature was established by core-top (*Nürnberg*, 1995; *Elderfield and Ganssen*, 2000; *Lea et al.*, 2000; *Rosenthal et al.*, 2000; *Rosenthal and Lohmann*, 2002; *Dekens et al.*, 2002; *Whitko et al.*, 2002), sediment trap (*Anand et al.*, 2003; *McConnell and Thunell*, 2005), and cultivating studies (*Nürnberg et al.*, 1996a,b; *Lea et al.*, 1999; *Mashiotta et al.*, 1999; *von Langen et al.*, 2005). Field-based studies with sediment-trap or core-top sample material rely on planktonic foraminifera that mainly passed through their complex life cycles, including vertical migration through the upper water column. Furthermore, core-top material contains foraminiferal tests that are deposited at the sea floor to form the paleoceanographic record. Mg/Ca of a core-top planktonic foraminiferal species reflects modern ocean temperatures at its preferred calcification depths, like downcore Mg/Ca records reflect past ocean temperature variability (e.g., *Elderfield and Ganssen*, 2000; *Lea et al.*, 2000; *Schmidt et al.*, 2004, 2006; *Pahnke and Zahn*, 2005; *Nürnberg and Groeneveld*, 2006). This offers the opportunity for the temperature calibration of Mg/Ca and, consequently, for the detailed paleoceanographic reconstruction of temperatures at different depth levels of the upper water column.

Elderfield and Ganssen (2000) and *Anand et al.* (2003) used combined N-Atlantic $\delta^{18}O$- and Mg/Ca-data sets of various foraminiferal species to establish Mg/Ca *vs.* temperature calibrations for core-top and sediment-trap samples, respectively. *Dekens et al.* (2002) published core-top

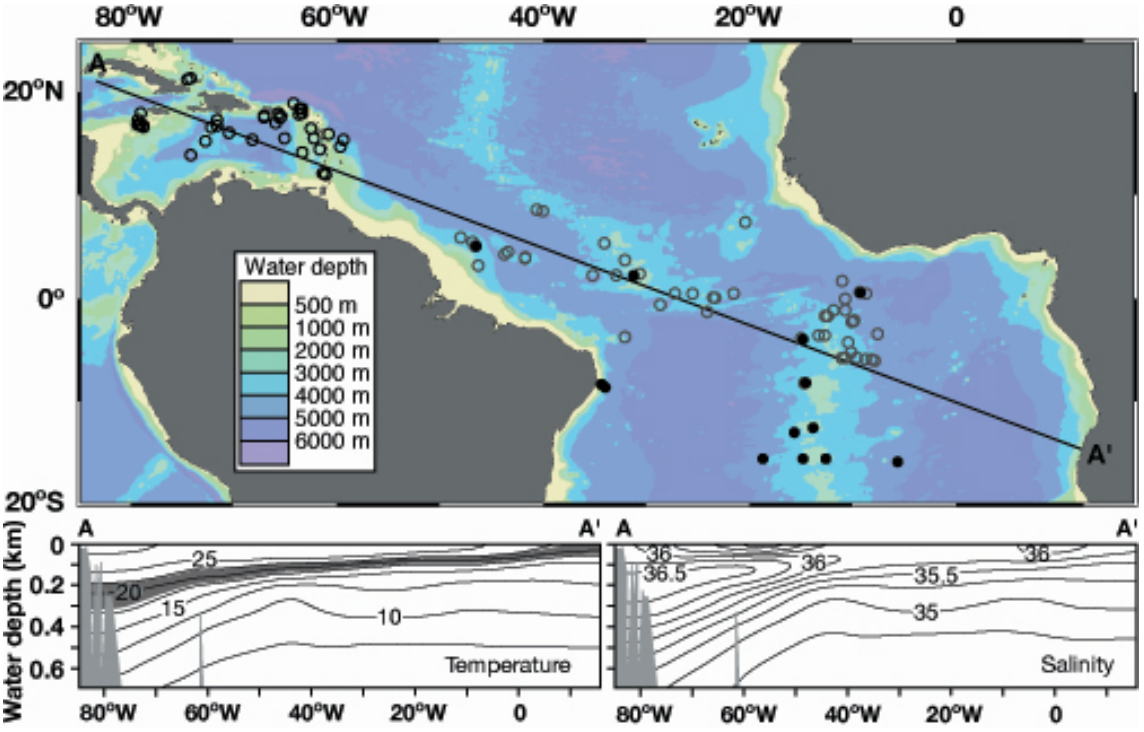

Figure 3.1 Bathymetric chart of the tropical Atlantic and the Caribbean (*Schlitzer*, 2002) showing the locations of the sediment-surface samples from which the analyses were performed (black dots: δ^{18}O values and Mg/Ca ratios are shown in Table 3.2 and 3.3; black circles: δ^{18}O are obtained from Chapter 4, Mg/Ca are obtained from *Regenberg et al.* (2006a) (Chapter 2); grey circles: Mg/Ca are shown in Table 3.3, δ^{18}O are given in Chapter 4). The hydrographic profiles AA' present the annual mean temperature and salinity (*NODC*, 2001) *vs.* water depth. Note the westward increasing depth of the thermocline, which is illustrated by the shaded area between the annual 22 and 18°C isotherms.

Mg/Ca *vs.* temperature calibrations for two shallow-dwelling and one thermocline-dwelling planktonic foraminifera for the tropical Atlantic. By now, there is still a lack of Mg/Ca *vs.* temperature calibrations for various foraminiferal species from different water depth levels of the tropical Atlantic.

For this study, we performed paired Mg/Ca and δ^{18}O measurements on abundant planktonic foraminifera of 77 tropical Atlantic and Caribbean sediment-surface (0–1 cm) samples (Figure 3.1). δ^{18}O signals were used to estimate absolute calcification depths by assigning the measured δ^{18}O values to expected equilibrium δ^{18}O of carbonate calculated from modern temperature and salinity data of the National Oceanographic and Data Center (*NODC*, 2001). Associating calcification temperatures and Mg/Ca ratios, we were able to establish Mg/Ca *vs.* temperature calibrations for eight planktonic foraminiferal species accurately tracking temperatures of the (sub)tropical mixed-layer, thermocline, subthermocline, and of deep waters.

Table 3.1 Locations, water depths (in m), and ^{14}C ages (in years BP) of the sediment-surface samples (0–1 cm) used in this study (*Mollenhauer*, 1999; *Schmuker*, 2000).

Station	Longitude	Latitude	Water depth	^{14}C Ages	Station	Longitude	Latitude	Water depth	^{14}C Ages
GeoB1103-3	9 15.6'W	0 36'N	4321		M35006-6	62 27.2'W	16 25.3'N	888	
GeoB1104-5	10 42.3'W	1 09.78'S	3724		M35008-1	64 09.8'W	18 01.9'N	2820	
GeoB1105-3	12 25.7'W	1 39.9'S	3232	2430±50[a]	M35010-2	64 05.4'W	18 56.0'N	2696	
GeoB1106-5	12 33.12'W	1 45.6'S	2471		M35012-6	63 37.6'W	18 18.3'N	1121	
GeoB1108-6	9 52.38'W	2 10.38'S	3897		M35013-3	63 27.0'W	18 18.9'N	899	
GeoB1111-5	8 39'W	5 50.52'S	3757		M35014-1	63 44.2'W	17 50.5'N	1604	
GeoB1112-3	10 44.58'W	5 46.68'S	3128	2730±40[a]	M35015-1	63 27.1'W	17 59.6'N	1230	
GeoB1113-7	11 02.1'W	5 44.7'S	2373		M35018-1	65 22.2'W	17 34.5'N	1728	
GeoB1114-3	10 12.18'W	5 16.98'S	3422		M35019-1	65 26.1'W	17 40.3'N	1815	
GeoB1115-4	12 34.8'W	3 33.48'S	2921		M35020-2	65 40.2'W	17 55.8'N	2005	
GeoB1116-1	13 11.22'W	3 37.38'S	3471		M35023-3	65 40.9'W	17 36.2'N	1192	
GeoB1117-3	14 54'W	3 49.2'S	3977		M35023-4	65 41.0'W	17 36.2'N	1183	
GeoB1417-2	12 42'W	15 31.8'S	2914		M35024-6	66 00.1'W	17 02.6'N	4710	2510±45[b]
GeoB1418-1	14 53.4'W	15 31.8'S	3524		M35025-1	67 00.5'W	17 45.2'N	1778	699±30[b]
GeoB1420-1	18 41.4'W	15 31.8'S	4587		M35026-2	67 02.6'W	17 30.5'N	3815	1175±70[b]
GeoB1503-2	30 38.88'W	2 18.6'N	2298		M35030-1	78 36.6'W	16 45.3'N	1298	
GeoB1504-1	31 17.4'W	2 17.4'N	2980		M35032-1	78 36.9'W	16 35.3'N	1363	
GeoB1505-3	33 00.42'W	2 16.38'N	3703	3090±40[a]	M35034-3	79 03.5'W	16 54.2'N	1212	
GeoB1506-1	35 10.92'W	2 12.3'N	4267		M35035-1	79 07.9'W	16 53.6'N	1252	
GeoB1508-1	34 01.5'W	5 19.98'N	3685		M35036-3	79 25.3'W	16 55.0'N	1196	
GeoB1511-6	46 20.58'W	3 10.68'N	3162		M35037-1	79 23.3'W	16 54.8'N	1190	
GeoB1512-1	48 02.58'W	5 54.18'N	3716		M35038-1	79 13.8'W	17 15.7'N	1066	
GeoB1513-2	46 55.62'W	5 25.92'N	3621		M35039-1	79 08.7'W	17 55.6'N	1142	
GeoB1514-5	46 34.8'W	5 08.4'N	3511		SO164-01-3	74 09.028'W	13 50.195'N	4025.7	
GeoB1515-2	43 39.9'W	4 14.28'N	3125	1750±40[a]	SO164-02-3	72 47.06'W	15 18.29'N	2977	2205±25[c]
GeoB1523-2	41 37.32'W	3 48.9'N	3291		SO164-03-3	72 12.31'W	16 32.40'N	2744	
GeoB1908-1	5 45'W	15 48.6'S	1231		SO164-04-2	71 39.09'W	17 16.38'N	1013	
GeoB2201-1	34 27.6'W	8 11.7'S	1127		SO164-07-3	74 08.76'W	21 19.46'N	2722	720±35[c]
GeoB2202-5	34 15.6'W	8 11.7'S	1127		SO164-18-1	74 21.0'W	21 13.61'N	1629	1350±25[c]
GeoB2204-1	34 01.38'W	8 31.92'S	2080		SO164-19-3	74 20.98'W	21 14.7'N	1706	<AD 1954[c]
GeoB4304-1	40 26.22'W	8 34.32'N	3365		SO164-20-2	71 29.22'W	16 45.49'N	3357	
GeoB4305-1	39 59.52'W	8 29.88'N	3042		SO164-21-3	70 30.0'W	16 06.0'N	3995	
GeoB5002-1	14 32.4'W	8 08.4'S	2851		SO164-22-2	68 12.0'W	15 24.0'N	4506	
GeoB5007-1	13 56.4'W	12 23.4'S	3668		SO164-23-3	65 08.09'W	15 34.01'N	4328	
GeoB5008-3	15 41.4'W	12 55.8'S	3407		SO164-24-3	63 25.43'W	14 11.89'N	1545	
M35002-1	61 10.6'W	12 01.9'N	1506		SO164-25-3	59 44.48'W	14 41.25'N	2720	1915±30[c]
M35003-6	61 14.7'W	12 05.1'N	1299		SO164-48-2	60 55.0'W	15 57.02'N	1286	
M35004-1	61 39.7'W	14 24.6'N	2885		SO164-50-3	59 16.94'W	15 21.25'N	4002	
M35005-3	62 13.9'W	15 27.2'N	2289						

^{14}C ages from [a]*Mollenhauer* (1999), [b]*Schmuker* (2000), [c]*Regenberg et al.* (2006).

3.2 Materials and Methods

Tests of shallow-dwelling planktonic foraminifera *Globigerinoides ruber* pink and white, *Globigerinoides sacculifer*, thermocline-dwelling *Globorotalia menardii* and *Neogloboquadrina dutertrei*, thermocline- to subthermocline-dwelling *Globorotalia tumida*, and deep-dwelling *Globorotalia truncatulinoides* dextral and *Globorotalia crassaformis* were investigated for this study, following generic assignments of *Kennett and Srinivasan* (1983) and *Hemleben et al.* (1989). The foraminiferal tests were selected from 42 Caribbean and 35 tropical Atlantic sediment-surface samples (0–1 cm; Figure 3.1; Table 3.1), collected during R/V SONNE cruise SO164 (*Nürnberg et al.*, 2003) and R/V METEOR cruises M06/6, M09/4, M16/2, M20/2, M35/1, M38/1, and M41/2 (*Mulitza*, 1994; *Rühlemann et al.*, 2001). Faunal assemblages and oxygen isotope stratigraphy indicate that the core-top samples used are of Holocene age (*Mulitza*, 1994; *Regenberg et al.*, 2006a) (Chapter 2).

Table 3.2 δ^{18}O values in ‰ of foraminiferal samples. The remainder of the δ^{18}O is given in Chapter 4.

Station	*G. ruber* w. □^{18}O	*G. ruber* p. □^{18}O	*G. sacculifer* □^{18}O	*G. menardii* □^{18}O	*N. dutertrei* □^{18}O	*G. tumida* □^{18}O	*G. truncatulinoides* d. □^{18}O	*G. crassaformis* □^{18}O
GeoB1103-3		-1.11						
GeoB1117-3		-1.51	-1.72					
GeoB1418-1		-1.08						
GeoB1504-1		-1.81	-1.58					
GeoB1514-5		-2.44	-1.53					
GeoB2201-1	-0.51	-1.51	-0.96	-0.30	1.26	0.13	1.65	1.96
GeoB2202-5	-1.30	-1.72	-1.28	-0.41	0.20	0.13		2.03
GeoB2204-1	-1.33	-1.77	-1.45	-0.80	0.46	0.14		2.03

Based on 12 AMS^{14}C dates, surface-sediment samples reveal ages not older than 2000–3000 years (Table 3.1).

3.2.1 δ^{18}O Analyses

For oxygen isotope analyses of the highly abundant *G. ruber* pink and white, *G. sacculifer* (without sac-like final chamber), and for *G. menardii*, ∼40 specimens were selected from the 355–400 μm size fraction, crushed and homogenized. For *N. dutertrei*, *G. tumida*, *G. truncatulinoides* dextral, and *G. crassaformis*, 8–12 specimens were separated from the 355–400 μm size fraction. All isotope measurements were run on a Finnigan MAT 252 Mass Spectrometer with automated Kiel carbonate preparation device at the IFM-GEOMAR (Kiel). Analytical precision was better than 0.07‰ for δ^{18}O ($\pm 1\sigma$, N=130). Calibration to the Vienna Pee Dee Belemnite (PDB) scale was performed *via* the National Bureau of Standards (NBS) 19 and an internal laboratory standard. The values are reported with respect to Vienna PDB and listed in Table 3.2 and Chapter 2.

3.2.2 Mg/Ca Analyses

For Mg/Ca analyses, ∼550–800 μg of intact monospecific foraminiferal tests (20–25 specimens) were selected from a preferably narrow size fraction (Table 3.3) (*Regenberg et al.*, 2006a) (Chapter 2) to minimize size-related intraspecific elemental variations (*Elderfield et al.*, 2002). The crushed samples were cleaned to remove clays (water and methanol wash) and organic matter (hydrogen peroxide treatment), followed by a weak acid leach prior to dissolution. The Mg-cleaning method (*Barker et al.*, 2003) is described in detail in *Regenberg et al.* (2006a) (Chapter 2).

Samples were measured on two ICP OES devices (ISA Jobin Yvon, Spex Instruments S.A. GmbH at IFM-GEOMAR, Kiel: Analytical error for Mg was ∼0.45% and for Ca ∼0.15%; Spectro CirosCCD SOP at the Institute for Geosciences, Kiel: Analytical error for Mg/Ca was 0.1%) showing no significant offset. Replicate Mg/Ca measurements showed an average standard deviation of ∼0.1 mmol/mol and ∼0.08 mmol/mol (Table 3.4) (*Regenberg et al.*, 2006a) (Chapter 2). Mg/Ca ratios are listed in Table 3.3 and in *Regenberg et al.* (2006a) (Chapter 2).

Table 3.3 Mg/Ca ratios in mmol/mol of foraminiferal samples: Measured Mg/Ca (meas) from below water depths of 2500–3000 m are corrected for the effect of dissolution (diss corr) by application of the species-specific dissolution-correction equations of *Regenberg et al.* (2006a) (Chapter 2). The remainder of the Mg/Ca is given in *Regenberg et al.* (2006a) (Chapter 2).

Station	*G. ruber* w. Mg/Ca			*G. ruber* p. Mg/Ca		*G. sacculifer* Mg/Ca		*G. menardii* Mg/Ca			*N. dutertrei* Mg/Ca			*G. tumida* Mg/Ca			*G. trunca-tulinoides* d. Mg/Ca			*G. crassa-formis* Mg/Ca	
		meas	diss corr	meas	diss corr	meas	diss corr		meas	diss corr		meas	diss corr		meas	diss corr		meas	diss corr	meas	diss corr
GeoB1103-3						2.91	3.56														
GeoB1104-5		3.52	4.38	3.67	4.47	2.87	3.23		1.95	2.50		1.48	2.26		1.45	1.93		1.75	2.29	1.21	1.66
GeoB1105-3		3.36	3.86	3.08	3.52	2.90	3.03		2.02	2.22		1.51	1.96		1.56	1.72		1.62	1.78	1.29	1.49
GeoB1106-5		4.09		3.04		3.17			2.39			1.82			1.77			2.19		1.60	
GeoB1108-6	a	3.23	4.22	3.41	4.33	2.69	3.13	a	1.87	2.54		1.37	2.26		1.28	1.87		1.62	2.30	1.22	1.76
GeoB1111-5		3.57	4.45	3.03	3.84	3.45	3.83		2.34	2.92		1.79	2.60		1.87	2.36				1.56	2.03
GeoB1112-3		3.71	4.14	3.29	3.65	3.26	3.34		2.69	2.82		2.21	2.59		1.91	2.00	a	1.96	2.05	1.50	1.65
GeoB1113-7		3.93		3.79		3.42			2.69			2.51			1.92			2.42		1.66	
GeoB1114-3	a	3.75	4.39	3.78	4.35	3.24	3.46		2.35	2.69		1.95	2.52		1.71	1.99				1.46	1.75
GeoB1115-4		3.37	3.65	3.37	3.58	3.36			2.04			1.66	1.90		1.54					1.35	1.39
GeoB1116-1		3.38	4.06	3.02	3.63	3.08	3.32		1.81	2.18		1.71	2.32		2.05	2.36		1.90	2.25	1.36	1.68
GeoB1117-3		4.11	5.15			3.29	3.77														
GeoB1417-2						3.48															
GeoB1418-1		3.94	4.66			3.39	3.66														
GeoB1420-1						2.88	3.66														
GeoB1503-2		3.79		3.94		4.11			3.03			2.24			2.29			2.00		1.59	
GeoB1504-1		3.87	4.19			4.00	4.01														
GeoB1505-3		4.18	5.02	3.79	4.56	3.97	4.33		2.75	3.29		2.17	2.94		2.09	2.55		1.95	2.47	1.39	1.83
GeoB1506-1		3.94	5.20	3.49	4.67	3.99	4.61		2.69	3.63		2.09	3.23		1.92	2.74		1.62	2.57	1.38	2.10
GeoB1508-1		4.08	4.91	3.46	4.22	3.50	3.84		2.67	3.20		2.02	2.77		1.84	2.29		2.15	2.66	1.27	1.70
GeoB1511-6		4.65	5.10	4.16	4.54	4.01	4.11		2.82	2.98		2.86	3.26		2.38	2.49		2.55	2.66	1.49	1.65
GeoB1512-1	a	4.64	5.50	4.53	5.31	4.08	4.44		2.89	3.44		2.37	3.14		2.26	2.73				1.35	1.80
GeoB1513-2	b	4.52	5.31	4.28	5.00	4.23	4.54		2.91	3.39		2.51	3.21		2.45	2.86	a	1.86	2.32	1.43	1.83
GeoB1514-5		4.23	4.94			4.32	4.58														
GeoB1515-2		4.57	5.00	4.33	4.69	4.08	4.16		2.84	2.97	j	3.33	3.71	c	2.16	2.25					
GeoB1523-2	a	5.01	5.56	4.14	4.62	3.98	4.14		3.14	3.38		1.95	2.44		2.38	2.57		2.27	2.48	1.37	1.60
GeoB1908-1		4.39																			
GeoB2201-1		4.92		4.62				a	2.80		a	2.37			2.45			1.92		1.68	
GeoB2202-5		4.82		4.55		3.94		a	2.88					b	2.12					1.42	
GeoB2204-1	a	5.00		4.53		4.34		a	3.09		a	2.83			2.47					1.48	
GeoB4304-1		4.35	4.95	4.02	4.55	3.67	3.86		2.61	2.91		1.96	2.50		2.19	2.43		2.19	2.45	1.44	1.71
GeoB4305-1		4.38	4.75	4.24	4.54	3.96	3.99	a	2.66	2.73		2.45	2.77		2.23	2.26		2.42	2.44	1.48	1.58
GeoB5002-1		3.91	4.14																		
GeoB5007-1		3.69	4.51																		
GeoB5008-3		3.89	4.52																		

All specimens from the 355–400 □m size fraction, except for a: 315–400 □m, b: 355–400 □m, c: 400–500 □m.

Planktonic foraminiferal Mg/Ca ratios are subject to dissolution (e.g., *Savin and Douglas*, 1973; *Rosenthal et al.*, 1997; *Rosenthal and Lohmann*, 2002). The close interrelationship of increasing water depth, decreasing carbonate ion concentration, and decreasing Mg/Ca (*Dekens et al.*, 2002) was finally quantified using Caribbean core-top samples (*Regenberg et al.*, 2006a) (Chapter 2). The resulting correction equations for depth-induced bias of Mg/Ca only affect samples from below species-specific water depths of 2500–3000 m, which is at least 1.5 km above the lysocline. Above these depths, Mg/Ca appears to be unaffected by dissolution without need of any dissolution correction (*Regenberg et al.*, 2006a) (Chapter 2). Measured tropical Atlantic Mg/Ca was corrected for the effect of dissolution applying the species-specific dissolution-correction equations of *Regenberg et al.* (2006a) ((Chapter 2); Table 3.3). This approach is most promising because the depth of the modern tropical Atlantic lysocline (*Broecker and Clark*, 2003)

Table 3.4 Replicate Mg/Ca measurements on two ICP OES devices[a]. For additional replicates, see *Regenberg et al.* (2006a) (Chapter 2).

Station	Species	Mg/Ca (mmol/mol) ISA Jobin Yvon		Mg/Ca (mmol/mol) Spectro Ciros			Mg/Ca (mmol/mol)	
		1	2	1	2	3	mean	sd
GeoB1105-3	*G. tumida*			* 1.57	* 1.55		1.56	0.01
GeoB1106-5	*G. menardii*			* 2.34	** 2.43		2.39	0.06
GeoB1106-5	*G. tumida*			* 1.78	* 1.77		1.77	0.00
GeoB1108-6	*G. tumida*			* 1.28	* 1.29		1.28	0.00
GeoB1108-6	*G. ruber* p.			* 3.74	** 3.08		3.41	0.47
GeoB1111-5	*G. menardii*			* 2.44	** 2.25		2.34	0.14
GeoB1111-5	*G. tumida*			* 1.87	* 1.86		1.87	0.01
GeoB1111-5	*G. ruber* p.			* 2.86	** 3.19		3.03	0.23
GeoB1112-3	*G. tumida*			* 1.93	* 1.90		1.91	0.02
GeoB1113-7	*G. ruber* p.			* 3.95	** 3.71	*** 3.71	3.79	0.14
GeoB1113-7	*N. dutertrei*			* 2.57	** 2.44		2.51	0.10
GeoB1114-3	*G. tumida*			* 1.71	* 1.70		1.71	0.01
GeoB1115-4	*G. tumida*			* 1.54	* 1.54		1.54	0.00
GeoB1116-1	*G. tumida*			* 2.06	* 2.04		2.05	0.01
GeoB1503-2	*G. menardii*			* 2.8	** 3.23	*** 3.04	3.03	0.22
GeoB1503-2	*G. ruber* p.			* 3.93	** 3.93	*** 3.94	3.94	0.01
GeoB1505-3	*G. ruber* w.	* 4.09		* 4.27			4.18	0.13
GeoB1506-1	*G. tumida*			* 1.91	* 1.92		1.92	0.00
GeoB1508-1	*G. tumida*			* 1.84	* 1.83		1.84	0.00
GeoB1512-1	*G. tumida*			* 2.27	* 2.25		2.26	0.01
GeoB1513-2	*G. tumida*			* 2.47	* 2.44		2.45	0.02
GeoB1513-2	*G. ruber* p.			* 4.28	** 4.28		4.28	0.00
GeoB1513-2	*G. sacculifer*	* 4.24	** 4.22				4.23	0.02
GeoB1523-2	*G. tumida*			* 2.39	* 2.36		2.38	0.02
GeoB2201-1	*G. tumida*			* 2.45	* 2.45		2.45	0.00
GeoB2202-5	*G. tumida*			* 2.13	* 2.11	* 2.12	2.12	0.01
GeoB2204-1	*G. menardii*			* 3.05	** 3.12		3.09	0.05
GeoB2204-1	*G. tumida*			* 2.48	* 2.45		2.47	0.01
GeoB4304-1	*G. ruber* p.			* 4.02	** 4.01		4.02	0.01
GeoB4305-1	*G. tumida*			* 2.23	* 2.22		2.23	0.01

[a]The use of same sample solutions is indicated by asterisks.

is close to the modern Caribbean lysocline depth of 4600 m (*Regenberg et al.*, 2006a) (Chapter 2). Thus, Mg/Ca *vs.* temperature relationships of this study are established with dissolution corrected Mg/Ca.

3.3 Results

3.3.1 Estimation of Planktonic Foraminiferal Calcification Depths and Temperatures

The estimation of calcification depths of the studied planktonic foraminifera is based on their δ^{18}O values (Chapter 4; Table 3.2). Since the δ^{18}O of calcite is dependent on the temperature and the δ^{18}O of the ambient seawater ($\delta^{18}O_w$) during calcification, the expected equilibrium (or thermodynamic) δ^{18}O signal of foraminiferal calcite ($\delta^{18}O_c$) precipitated from modern seawater can be calculated by solving established δ^{18}O-paleotemperature equations for $\delta^{18}O_c$, inserting modern temperatures and δ^{18}O of seawater (converted from modern salinity data). To determine appropriate $\delta^{18}O_w$ for the study area, we used the combined Atlantic $\delta^{18}O_w$ and salinity data from 30°N to 30°S of *Schmidt* (1999), excluding samples dominated by Amazon river discharge. As we

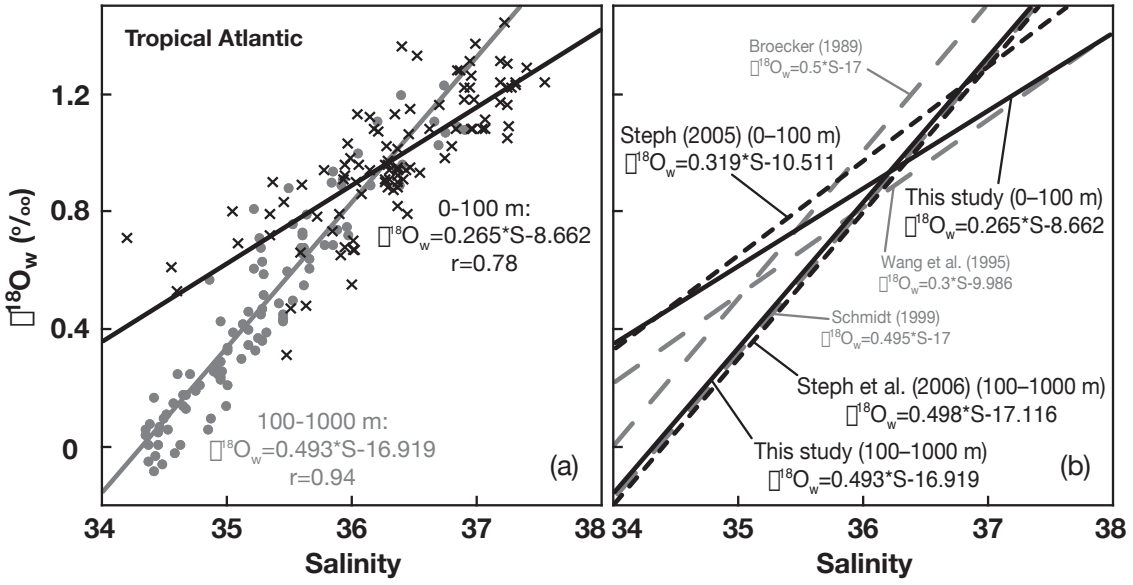

Figure 3.2 Salinity *vs.* $\delta^{18}O_w$ (in ‰ Vienna SMOW) relationships for (a) the tropical Atlantic (30°N–30°S), differentiated for 0–100 m (black line) and 100–1000 m water depth (grey line). Data are obtained from *Schmidt et al.* (1999), excluding Amazon river samples. (b) Relationships for the tropical Atlantic from this study (black solid lines) and for the Caribbean from *Steph* (2005) (0–100 m) and *Steph et al.* (2006) (100–1000 m) (black stippled lines) applied in this study. For comparison, the low-latitude Atlantic (40°N–40°S) relationship including Mediterranean samples (*Wang et al.*, 1995) and the global signal of upper ocean samples (*Broecker*, 1989; *Schmidt*, 1999) are given as grey stippled lines.

intend to calculate calcification depths of planktonic foraminiferal species which may dwell down to water depths of ∼800 m, we differentiated the $\delta^{18}O_w$-salinity database into the equations

$$\delta^{18}O_w = 0.265 \cdot S - 8.662 \tag{3.1}$$

for water depths 0–100 m (Figure 3.2a), and

$$\delta^{18}O_w = 0.493 \cdot S - 16.919 \tag{3.2}$$

for water depths 100–1000 m (Figure 3.2a), with $\delta^{18}O_w$ in ‰ reported with respect to the Vienna SMOW scale. For the calculation of Caribbean $\delta^{18}O_w$, we used the $\delta^{18}O_w$-salinity relationships of (*Steph*, 2005) for 0–100 m and *Steph et al.* (2006) for 100–1000 m water depth (Figure 3.2b). The tropical Atlantic Equation (3.2; 100–1000 m) is similar to the Caribbean relationship for 100–1000 m (*Steph et al.*, 2006) and matches well with the global signal of upper ocean samples (*Broecker*, 1989; *Schmidt*, 1999) (Figure 3.2b).

Using these $\delta^{18}O_w$-salinity relationships, modern water-column $\delta^{18}O_w$ was calculated from salinity data (*NODC*, 2001) and corrected to the PDB scale by subtracting $0.27\delta^{18}O_w$ (*Hut*, 1987). Subsequently, expected equilibrium $\delta^{18}O_w$ was calculated from temperature data (*NODC*,

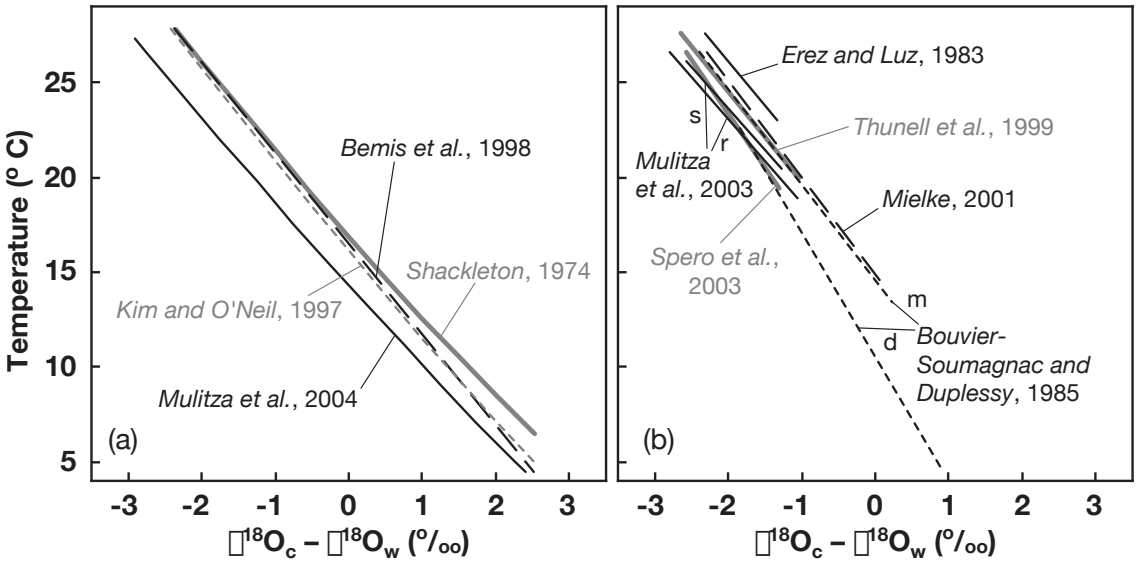

Figure 3.3 Difference between the oxygen isotope composition of calcite ($\delta^{18}O_c$) and ambient seawater ($\delta^{18}O_w$) *vs.* temperature: Illustrated δ^{18}O-paleotemperature relationships were used to assess calcification depths, from which calcification temperatures of the indicated range were extracted. (a) δ^{18}O-paleotemperature relationships for multispecies application of *Shackleton* (1974), *Kim and O'Neil* (1997), *Bemis et al.* (1998), and *Mulitza et al.* (2004). (b) Species-specific foraminiferal δ^{18}O-paleotemperature relationships for: *G. ruber* white of *Thunell et al.* (1999) and *Mulitza et al.* (2003) (r); *G. sacculifer* of *Erez and Luz* (1983), *Mulitza et al.* (2003) (s), and *Spero et al.* (2003); *G. menardii* of *Bouvier-Soumagnac and Duplessy* (1985) (m) and *Mielke* (2001); *N. dutertrei* of *Bouvier-Soumagnac and Duplessy* (1985) (d). Although most of the δ^{18}O-paleotemperature relationships are only slightly varying from each other, calcification temperatures can differ as much as 3°C.

2001) and the appropriate $\delta^{18}O_w$ using different δ^{18}O-paleotemperature equations (Figure 3.3) for multispecies application (*O'Neil et al.*, 1969; *Shackleton*, 1974; *Kim and O'Neil*, 1997; *Bemis et al.*, 1998; *Mulitza et al.*, 2004) and single species application (*Erez and Luz*, 1983; *Bouvier-Soumagnac and Duplessy*, 1985; *Bemis et al.*, 1998; *Thunell et al.*, 1999; *Mielke*, 2001; *Mulitza et al.*, 2003; *Spero et al.*, 2003). The estimated calcification depth, finally, is the water depth, where measured foraminiferal δ^{18}O equals expected equilibrium $\delta^{18}O_w$. The prevailing temperature at the assessed calcification depth, in turn, can be assumed as the calcification temperature of foraminiferal bulk calcite.

The relative succession of calcification depths of the planktonic foraminiferal species is consistent for each of the multispecies δ^{18}O-paleotemperature relationships applied (Figure 3.4). As expected, shallowest calcification depths of ∼10–100 m and ∼30–120 m are estimated for shallow-dwelling *G. ruber* (pink/white) and *G. sacculifer*, respectively. Intermediate calcification depths of ∼70–190 m are assessed for thermocline-dwelling *G. menardii* and *N. dutertrei*, followed by thermocline- to subthermocline-dwelling *G. tumida* (∼150–350 m). Deepest calcification depths of ∼220–590 m and ∼460–790 m are estimated for deep-dwelling *G. truncatulinoides*

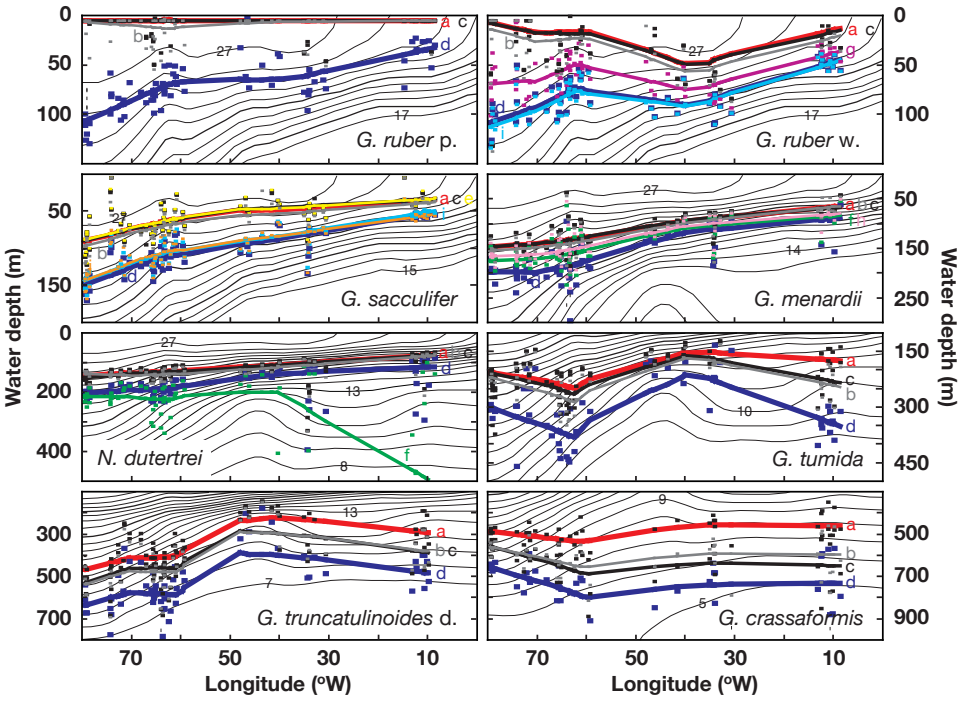

Figure 3.4 Longitudinal cross section through the upper water column: Trend lines illustrate the tropical Atlantic and Caribbean planktonic foraminiferal calcification depths deduced from their δ^{18}O values with respect to equilibrium $\delta^{18}O_c$. $\delta^{18}O_c$ was calculated with annual $\delta^{18}O_w$ and temperature data (*NODC*, 2001). Calcification depth was defined to the water depth where measured δ^{18}O equals $\delta^{18}O_c$. Differing intraspecific calcification depths emanate from the use of the various δ^{18}O-paleotemperature equations for multispecies application of a *Shackleton* (1974) (red), b *Kim and O'Neil* (1997) (grey), c *Bemis et al.* (1998) (black), and d *Mulitza et al.* (2004) (dark blue), and for species-specific application of e *Erez and Luz* (1983) (yellow), f *Bouvier-Soumagnac and Duplessy* (1985) (green), g *Thunell et al.* (1999) (violet), h *Mielke* (2001) (pink), i *Mulitza et al.* (2003) (light blue), and j *Spero et al.* (2003) (orange). Data were smoothed by using the locally weighted least squared error method (e.g., *Cleveland*, 1979) with a smoothing factor of 60%. For comparison, annual temperatures (*NODC*, 2001) of the hydrographic profile in Figure 3.1 are given as isotherms. Highlighted 18 and 22°C isotherms indicate the thermocline.

dextral and *G. crassaformis*, respectively (Figure 3.4).

Absolute calcification depths of single species, however, largely depends on the δ^{18}O-paleotemperature relationship used for calculation (Figure 3.3). The intraspecific differences in calcification depths (Figure 3.4) result from the up to 3°C differences in δ^{18}O-derived calcification temperatures, which are constant for the investigated temperature interval (Figure 3.3).

The variation in intraspecific calcification depths deduced from the multispecies δ^{18}O-paleotemperature relationships changes with increasing water depth. For shallow- and thermocline-dwelling species, all calcification depths are relatively similar, except those deduced from the *Mulitza et al.* (2004) relationship, which results in deeper calcification depths (offset to lower temperatures by up to 3°C (Figure 3.3)). For the subthermocline- and deep-dwelling species, all δ^{18}O-derived calcification depths diverge from each other. In this context, shallowest and deepest

calcification depths are deduced with the δ^{18}O-paleotemperature relationships of *Shackleton* (1974) and *Mulitza et al.* (2004), respectively. Additionally, calcification depths deduced from the species-specific δ^{18}O-paleotemperature equations available for shallow- and thermocline-dwelling species compare to the ranges indicated by the multispecies relationships of *Shackleton* (1974) and *Mulitza et al.* (2004) (Figure 3.4).

It is important to note that calcification depths of *G. sacculifer*, *G. menardii*, *N. dutertrei*, *G. truncatulinoides* dextral, and less pronounced for *G. ruber* pink and white, *G. tumida*, and *G. crassaformis*, are significantly deeper in the Caribbean than in the tropical Atlantic (Figure 3.4). This trend, unanimously obtained from each of the various δ^{18}O-paleotemperature equations, can be related to the westward deepening of the tropical Atlantic thermocline (Chapter 4); Figure 3.1).

3.3.2 Associated Mg/Ca Ratios and δ^{18}O-Calcification Temperatures

Association of the species-specific Mg/Ca ratios to annual mean temperature data (*NODC*, 2001) taken from the distinct calcification depths at each station reveals strong positive correlations, i.e. Mg/Ca increases with increasing temperature. The parameter of the calibration equations of the form

$$Mg/Ca \quad = \quad b \cdot exp^{(a \cdot T)} \tag{3.3}$$

are given in Table 3.5 for each single species, where Mg/Ca is in mmol/mol and T the δ^{18}O-derived calcification temperature in degree Celsius. The regression curve is defined by the slope a, which is the temperature sensitivity component, and the y-axis intercept b.

Since the δ^{18}O-derived calcification temperature, which is assigned to the foraminiferal Mg/Ca ratio, is dependent on the estimated calcification depth, our combined δ^{18}O- and Mg/Ca-data sets reveal different species-specific Mg/Ca *vs.* temperature relationships for every δ^{18}O-paleotemperature equation applied (Figure 3.5; Table 3.5). Due to the similarity of the various δ^{18}O-paleotemperature relationships, intraspecific variability in the temperature-sensitive slope a is relatively low. The y-axis intercepts b, in contrast, are varying significantly for one single species due to the distinct differences in the δ^{18}O-derived temperatures (Figure 3.5; Table 3.5). Using the same δ^{18}O-paleotemperature equation for each foraminiferal species, interspecific changes in the slopes a ($\sim$3–11% increase in Mg/Ca ratios per 1°C) as well as in the y-axis intercepts b ($\sim$1.4–1.6 mmol/mol increase) become obvious (Figure 3.5; Table 3.5). Such variability of regression curves points to species-specific differences in the incorporation mechanisms of Mg^{2+}.

3.4 Discussion

3.4.1 Refining Temperature Calibrations of Species-Specific Mg/Ca Ratios

The exponential fit of the presented calibrations (Figure 3.5) is consistent with the exponential nature of previous Mg/Ca calibration studies (*Nürnberg et al.*, 1996a,b; *Lea et al.*, 1999, 2000;

Table 3.5 Mg/Ca *vs.* temperature calibration parameter of Equation 3.3: Annual temperatures (*NODC*, 2001) are taken from the various equilibrium $\delta^{18}O_c$ derived calcification depths of each single station. a = slope of the regression curve, b = y-axis intercept, T range = temperature (in °C) range of calibration, r = correlation coefficient.

Calcification depths calculated after	Calibration parameter	*G. ruber* white	*G. ruber* pink	*G. sacculifer*	*G. menardii*	*N. dutertrei*	*G. tumida*	*G. truncatulinoides* dextral	*G. crassaformis*
Bemis et al., 1998	b	1.271	0.248	0.463	0.914	1.368	1.436	1.829	1.34
	a	0.05	0.108	0.083	0.055	0.034	0.03	0.028	0.043
	T range	22–28	23.5–28	23–27.5	17–27	10.5–25	10.5–24.5	7.5–18.5	4.5–12
	r	0.54	0.58	0.76	0.73	0.65	0.64	0.5	0.58
Kim and O'Neil, 1997	b	1.512	0.255	0.52	0.97	1.394	1.437	1.78	1.279
	a	0.045	0.107	0.08	0.053	0.033	0.031	0.031	0.048
	T range	21.5–28	23.5–28	22.5–27.5	16.5–27	10.5–24.5	10.5–23.5	7.5–18	5–11.5
	r	0.52	0.58	0.78	0.73	0.65	0.64	0.5	0.58
Mulitza et al., 2003b	b	2.323	1.369	0.737	1.18	1.504	1.506	1.8	1.255
	a	0.031	0.047	0.072	0.05	0.034	0.034	0.036	0.06
	T range	19–27	21.5–27.5	20–26	13.5–25.5	8.5–22.5	9–21	6–15	4.5–9.5
	r	0.49	0.29	0.78	0.71	0.63	0.63	0.49	0.58
Shackleton, 1974	b	1.278	0.251	0.436	0.863	1.255	1.326	1.642	1.172
	a	0.051	0.107	0.086	0.057	0.037	0.034	0.034	0.048
	T range	22–28	23.5–28	23–27.5	17.5–27	12–25	12–24	9.5–18.5	6.5–13
	r	0.53	0.58	0.78	0.72	0.65	0.64	0.51	0.58
Bouvier-Soumagnac and Duplessy, 1985	b				1.17	1.997			
	a				0.047	0.021			
	T range				13.5–26.5	4.5–22.5			
	r				0.72	0.63			
Erez and Luz, 1983	b			0.399					
	a			0.089					
	T range			23–27.5					
	r			0.78					
Mielke, 2001	b				1.134				
	a				0.048				
	T range				14.5–26.5				
	r				0.73				
Mulitza et al., 2003a	b	2.315		0.639					
	a	0.031		0.077					
	T range	19–26.5		20.5–26					
	r	0.48		0.78					
Spero et al., 2003	b			0.977					
	a			0.06					
	T range			19.5–26.5					
	r			0.78					
Bemis et al., 1998 *Thunell et al.*, 1999	b	2.043							
	a	0.034							
	T range	20–27.5							
	r	0.49							

Mashiotta et al., 1999; *Elderfield and Ganssen*, 2000; *Dekens et al.*, 2002; *Anand et al.*, 2003; *McKenna and Prell*, 2004; *McConnell and Thunell*, 2005; *Rickaby and Halloran*, 2005; *von Langen et al.*, 2005). In order to compare our Mg/Ca *vs.* temperature calibrations with previous studies, we selected only those calibrations based on calcification temperatures derived from the *Shackleton* (1974) δ^{18}O-paleotemperature equation. The according calcification depths of each species are relatively shallow (Figure 3.4) and, thus, match well with habitat specifications in the literature (e.g., *Fairbanks and Wiebe*, 1980a; *Fairbanks et al.*, 1980b, 1982; *Deuser and Ross*, 1989; *Sautter and Thunell*, 1991b; *Ravelo and Fairbanks*, 1992; *Mulitza et al.*, 1997; *Kemle von Mücke and Oberhänsli*, 1999; *Niebler et al.*, 1999; *Schmuker and Schiebel*, 2002; *Field*, 2004; *LeGrande et al.*, 2004; *McKenna and Prell*, 2004; *Lončarić et al.*, 2006). To further improve the correlation between δ^{18}O-derived calcification temperatures and Mg/Ca ratios, we applied

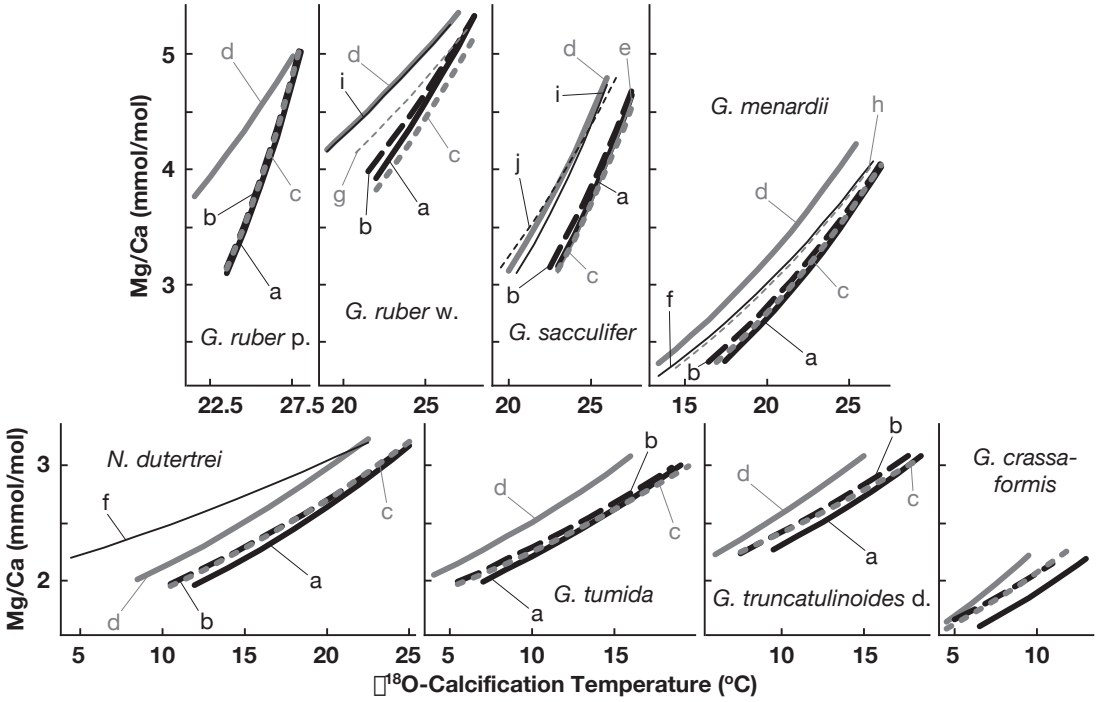

Figure 3.5 Species-specific exponential regression curves for the relationships between temperatures and planktonic foraminiferal Mg/Ca ratios of this study. The temperature was extracted from the δ^{18}O-derived calcification depth at each station, which is defined to the water depth where the measured δ^{18}O equals equilibrium $\delta^{18}O_c$. $\delta^{18}O_c$ was calculated with annual $\delta^{18}O_w$ and temperature data (*NODC*, 2001) after the various δ^{18}O-paleotemperature equations (Figure 3.3; Table 3.5). Thick curves indicate Mg/Ca *vs.* temperature calibrations deduced from δ^{18}O-paleotemperature equations for multispecies application: a) *Shackleton* (1974), black solid; b) *Kim and O'Neil* (1997), black dashed; c) *Bemis et al.* (1998), grey stippled; d) *Mulitza et al.* (2004), grey solid. Thin curves illustrate temperature calibrations of Mg/Ca deduced from species-specific δ^{18}O-paleotemperature equations: e) *Erez and Luz* (1983); f) *Bouvier-Soumagnac and Duplessy* (1985); g) *Thunell et al.* (1999); h) *Mielke* (2001); i) *Mulitza et al.* (2003); j) *Spero et al.* (2003). Differing calcification depths and, hence, temperatures for one single species aroused by the various δ^{18}O-paleotemperature equations generate varying intraspecific calibrations.

temperatures from mean calcification depths in the E-Atlantic, W-Atlantic, and Caribbean sector from our study area (Table 3.6), rather than temperatures from the calcification depths calculated for each station.

Using the *Shackleton* (1974) δ^{18}O-paleotemperature relationship with annual temperature and salinity data (*NODC*, 2001), 53 out of 70 core-top samples of *G. ruber* pink and 29 out of 64 samples of *G. ruber* white reveal lower δ^{18}O values than $\delta^{18}O_c$ calculated for the sea surface. In case of such discrepancies, calcification depths were set to 5 m water depth. To enhance the match between δ^{18}O and $\delta^{18}O_c$ for *G ruber* pink and white, we calculated *Shackleton* (1974) calcification depths with seasonal hydrographic data (*NODC*, 2001) using boreal winter to spring data for the E- and W-Atlantic sector, and boreal summer to autumn data from the Caribbean sector of the study area. Highest seawater temperatures during these seasons result in lower $\delta^{18}O_c$. This

Table 3.6 Mean calcification depths (±standard deviation) in meter deduced from $\delta^{18}O$ of the studied planktonic foraminifera. Reference equilibrium $\delta^{18}O_c$ was calculated from annual temperature and salinity data (*NODC*, 2001), except for seasonal calcification depths of *Shackleton* (1974), for which we used boreal E- and W-Atlantic winter to spring, and Caribbean summer to autumn temperature and salinity data (*NODC*, 2001).

Reference	Region	*G. ruber* white	*G. ruber* pink	*G. sacculifer*	*G. menardii*	*N. dutertrei*	*G. tumida*	*G. truncatulinoides* dextral	*G. crassaformis*
Bemis et al., 1998	E-Atlantic	15±12	8±9	33±10	69±11	88±36	235±50	374±85	667±167
	W-Atlantic	54±32	11±13	45±18	97±20	137±65	155±26	280±99	671±123
	Caribbean	21±26	11±14	69±24	136±28	138±17	236±47	477±99	631±88
Kim and O'Neil, 1997	E-Atlantic	20±13	8±10	36±11	67±15	98±45	245±48	370±76	599±118
	W-Atlantic	60±32	12±16	54±16	104±27	145±65	160±27	280±93	609±85
	Caribbean	27±28	16±18	75±24	144±28	141±16	254±54	490±92	616±72
Mulitza et al., 2003b	E-Atlantic	47±6	36±14	54±6	100±28	150±78	346±35	473±69	786±208
	W-Atlantic	98±24	60±23	91±18	125±30	175±83	202±45	372±126	781±140
	Caribbean	89±25	83±20	121±23	194±35	194±22	344±73	590±95	737±97
Shackleton, 1974	E-Atlantic	13±11	8±9	33±10	68±10	77±10	178±40	284±77	455±70
	W-Atlantic	54±32	11±14	47±18	99±20	133±54	147±24	216±62	458±43
	Caribbean	21±26	11±14	69±24	136±27	137±15	227±40	424±80	516±51
Shackleton, 1974 seasonal	E-Atlantic	33±5	12±12						
	W-Atlantic	52±31	12±16						
	Caribbean	38±28	32±21						
Bouvier-Soumagnac and Duplessy, 1985	E-Atlantic				89±21	450±339			
	W-Atlantic				114±27	281±226			
	Caribbean				167±32	223±43			
Erez and Luz, 1983	E-Atlantic			32±10					
	W-Atlantic			45±18					
	Caribbean			67±23					
Mielke, 2001	E-Atlantic				83±16				
	W-Atlantic				110±25				
	Caribbean				158±31				
Mulitza et al., 2003a	E-Atlantic	48±6		51±6					
	W-Atlantic	99±24		86±17					
	Caribbean	92±25		115±22					
Spero et al., 2003	E-Atlantic			56±8					
	W-Atlantic			87±18					
	Caribbean			114±24					
Thunell et al., 1999	E-Atlantic	37±6							
	W-Atlantic	81±25							
	Caribbean	59±27							

approach reduces the number of samples with lower measured $\delta^{18}O$ than expected equilibrium $\delta^{18}O_w$ at the sea surface to 23 and 8 samples of *G. ruber* pink and white, respectively. The resulting Mg/Ca *vs.* seasonal temperature calibrations, however, are similar to those generated with annual temperatures (Figure 3.6; Table 3.7).

We found a good agreement of the slopes of our Mg/Ca *vs.* temperature calibrations of shallow-dwelling *G. ruber* white and *G. sacculifer* (Figure 3.6; Table 3.7) with existing core-top (*Nürnberg et al.*, 2000; *Lea et al.*, 2000; *Dekens et al.*, 2002; *Whitko et al.*, 2002) and sediment-trap calibrations (*McConnell and Thunell*, 2005). Thus, relative temperature changes across the tropical Atlantic are consistently tracked by these species-specific calibrations. In general, our *G. ruber* white calibration shows a minor offset in temperature estimation at the cold end (<24°C), and an offset to lower temperatures by ∼1.5°C at the warm end with respect to previous calibrations.

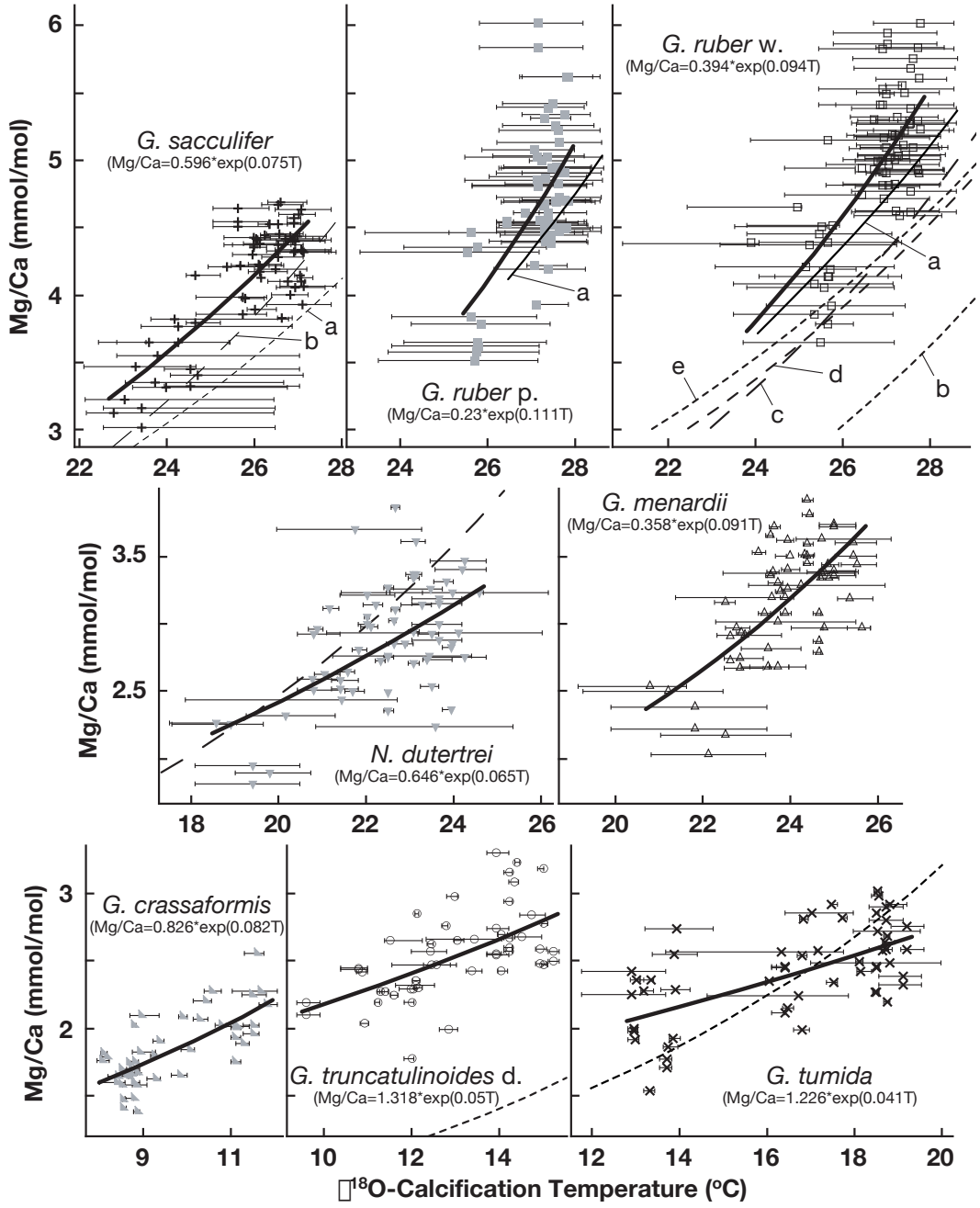

Figure 3.6 Species-specific Mg/Ca *vs.* annual temperature calibrations (thick solid lines): Symbols are set to the annual temperatures of the assigned mean calcification depths in the E-Atlantic, W-Atlantic, and Caribbean sector of the study area. Horizontal bars indicate the seasonal temperature range at the calcification depths of each sample location. For comparison, species-specific calibration curves (if available) are given for *G. sacculifer* (a: *Nürnberg et al.* (2000) Mg/Ca=0.491·exp(0.076T) and b: *Dekens et al.* (2002) Mg/Ca=0.37·exp(0.09T)), *G. ruber* pink (a: This study using seasonal temperatures), *G. ruber* white (a: This study using seasonal temperatures, b: *Lea et al.* (2000) Mg/Ca=0.3·exp(0.089T), c: *Dekens et al.* (2002) Mg/Ca=0.38·exp(0.09T), d: *Whitko et al.* (2002) Mg/Ca=0.57·exp(0.074T), and e: *McConnell and Thunell* (2005) Mg/Ca=0.69·exp(0.068T)), *N. dutertrei* (*Dekens et al.* (2002) Mg/Ca=0.6·exp(0.08T)), *G. tumida* (*Rickaby and Halloran* (2005) Mg/Ca=0.53·exp(0.09T)), and *G. truncatulinoides* dextral (*McKenna and Prell* (2004) Mg/Ca=0.355·exp(0.098T)).

Table 3.7 Species-specific Mg/Ca *vs.* temperature calibration parameter of Equation 3.3: Annual temperatures (*NODC*, 2001) assigned to the Mg/Ca ratios were taken from the equilibrium $\delta^{18}O_c$ derived mean calcification depths of the E-Atlantic, W-Atlantic, and Caribbean sector of the study area (Figure 3.1). Seasonal temperatures (*NODC*, 2001) assigned to *G. ruber* pink and white Mg/Ca were obtained from boreal winter to spring (E- and W-Atlantic), and boreal summer to autumn (Caribbean) equilibrium $\delta^{18}O_c$ derived mean calcification depths of the three study sectors. a = slope of the regression curve ±standard error at the 95% confidence interval, b = y-axis intercept ±standard error at the 95% confidence interval, r = correlation coefficient. Calibrations include temperatures (T) and Mg/Ca of the specified ranges, and the accuracy of Mg/Ca temperature estimate (±standard deviation). For comparison, the parameter of the multispecies Mg/Ca *vs.* temperature calibrations of *Elderfield and Ganssen* (2000) and *Anand et al.* (2003), both based on *Shackleton* (1974) derived calcification temperatures, are given.

Calcification depths calculated after	Calibration parameter	*G. ruber* white	*G. ruber* pink	*G. sacculifer*	*G. menardii*	*N. dutertrei*	*G. tumida*	*G. truncatulinoides* dextral	*G. crassaformis*
Shackleton, 1974 annual	b	0.394±0.283	0.23±0.458	0.596±0.163	0.358±0.309	0.646±0.261	1.226±0.122	1.318±0.124	0.826±0.116
	a	0.094±0.01	0.111±0.015	0.075±0.006	0.091±0.012	0.065±0.011	0.041±0.007	0.05±0.009	0.082±0.011
	r	0.72	0.61	0.8	0.66	0.55	0.61	0.59	0.73
	T range	24–28	25.5–28	23–27	21–26	19–25	13–19	9.5–15	8–12
	T accuracy	±0.8	±0.8	±0.8	±1.2	±1.9	±2.9	±2.0	±1.2
	Mg/Ca range	3.65–6.02	3.52–6.02	3.03–4.69	2.04–3.92	1.82–3.87	1.54–3.02	1.78–3.3	1.39–2.57
Shackleton, 1974 seasonal	b	0.536±0.325	0.343±0.688						
	a	0.081±0.011	0.094±0.022						
	r	0.63	0.42						
	T range	25.5–28.5	26.5–28.5						
	T accuracy	±0.8	±0.8						
	Mg/Ca range	3.65–6.02	3.52–6.02						
Shackleton, 1974	b			0.38					
	a	*Anand et al.*, 2003		0.09	mulitispecies				
	T range			15–28	calibration				
	T accuracy			±1.1					
Shackleton, 1974	b			0.52					
	a	*Elderfield and*		0.1	mulitispecies				
	T range	*Ganssen*, 2000		8–22	calibration				
	T accuracy			±1.13					

Interestingly, the *McConnell and Thunell* (2005) calibration for the 25–33°C temperature range shows the same exponential constant like our seasonal *G. ruber* white calibration (25.5–28.5°C). A good agreement of our *G. ruber* pink calibration is given with respect to the *Anand et al.* (2003) multispecies calibration (including *G. ruber* pink). Furthermore, *McConnell and Thunell* (2005) observed for the 30–33°C temperature interval the same exponential as well as preexponential constant for the white variety we found for the Mg/Ca *vs.* annual temperature calibration for *G. ruber* pink (Figure 3.6; Table 3.7), which was not separately calibrated up to now. Offset by 1–2°C to lower temperatures, we found a temperature dependency of Mg^{2+} incorporation for *G. sacculifer* resembling that of *Nürnberg et al.* (2000), calibrated for the 20–25°C temperature range, and similar to that of *Dekens et al.* (2002) (Figure 3.6; Table 3.7).

The temperatures of the tropical Atlantic and Caribbean thermocline are best recorded by *G. menardii* and *N. dutertrei*. Our *N. dutertrei* calibration (Figure 3.6; Table 3.7) resembles the y-axis intercept of the *Dekens et al.* (2002) calibration, but exhibits a diminished Mg^{2+} incorporation. It is notable that both regression lines match well at the cold end (<21°C) of our calibration but diverge towards the warm end. The calibration of thermocline-dwelling *G. menardii*

is similar to that of *G. ruber* white using annual temperatures and *G. ruber* pink using seasonal temperatures. In the literature, there is no species-specific calibration available for *G. menardii*, yet our calibration is in good agreement with the multispecies equation of *Anand et al.* (2003) (including *G. menardii*).

G. truncatulinoides dextral and *G. crassaformis* record the temperatures of the tropical Atlantic and Caribbean waters below the seasonal thermocline. In comparison with the calibration of *McKenna and Prell* (2004), which is based on electron microprobe analyses, our *G. truncatulinoides* dextral calibration is characterized by much higher Mg/Ca ratios. Our species-specific calibration, however, is the first considering bulk calcite Mg/Ca. The *G. crassaformis* calibration (Figure 3.6; Table 3.7) shows a considerably higher y–axis intercept b combined with a slightly decreased temperature dependency than the multispecies calibrations of *Elderfield and Ganssen* (2000) (including *G. truncatulinoides*) and *Anand et al.* (2003) (including *G. truncatulinoides* and *G. crassaformis*).

Our *G. tumida* Mg/Ca *vs.* temperature calibration (Figure 3.6; Table 3.7) shows a fairly weaker temperature dependency with respect to the other planktonic species studied. The calibration reveals a relatively higher y-axis intercept b than the non-empirical calibration of *Rickaby and Halloran* (2005), which is based on the assumption that the temperature sensitivity (9% per 1°C) is the same for all planktonic foraminifera.

3.4.2 Combination of Species-Specific Mg/Ca *vs.* Temperature Calibrations

In accordance to previous studies, Mg/Ca ratios of the studied planktonic foraminiferal species reveal a ~7–11% increase per 1°C (Figure 3.6; Table 3.7), with lower temperature dependencies of subthermocline-dwelling *G. tumida* and deep-dwelling *G. truncatulinoides* dextral. The preexponential constants are significantly different for calcification temperatures <15°C with respect to those >19°C, whereas the exponential constants are relatively similar (~0.07–0.11). In detail, Mg/Ca *vs.* temperature calibrations of shallow- and thermocline-dwelling species reveal lower y-axis intercepts b (0.23–0.65) than the calibrations of the deep-dwelling species (0.83–1.31) (Figure 3.6; Table 3.7). Although the Mg/Ca ratios of the thermocline- (*G. menardii*, *N. dutertrei*) and deep-dwelling species (*G. truncatulinoides* dextral, *G. crassaformis*) are overlapping by more than 1 mmol/mol (Figure 3.6; Table 3.7), the assigned temperatures of the thermocline-dwelling species are at least 4°C higher than the maximum calcification temperatures assigned to the Mg/Ca of the deep-dwelling species (Figure 3.7). Consequently, a combination of all species-specific planktonic foraminiferal data sets into a multispecies Mg/Ca *vs.* temperature calibration cannot account for the pronounced differences in species-specific preexponential constants between shallow- and thermocline-dwelling species on the one hand, and the deep-dwelling species on the other (Figure 3.7).

The combined data sets of shallow-dwelling *G. ruber* pink and white, and *G. sacculifer*, and of thermocline-dwelling *G. menardii* and *N. dutertrei* exhibits a strong exponential relationship

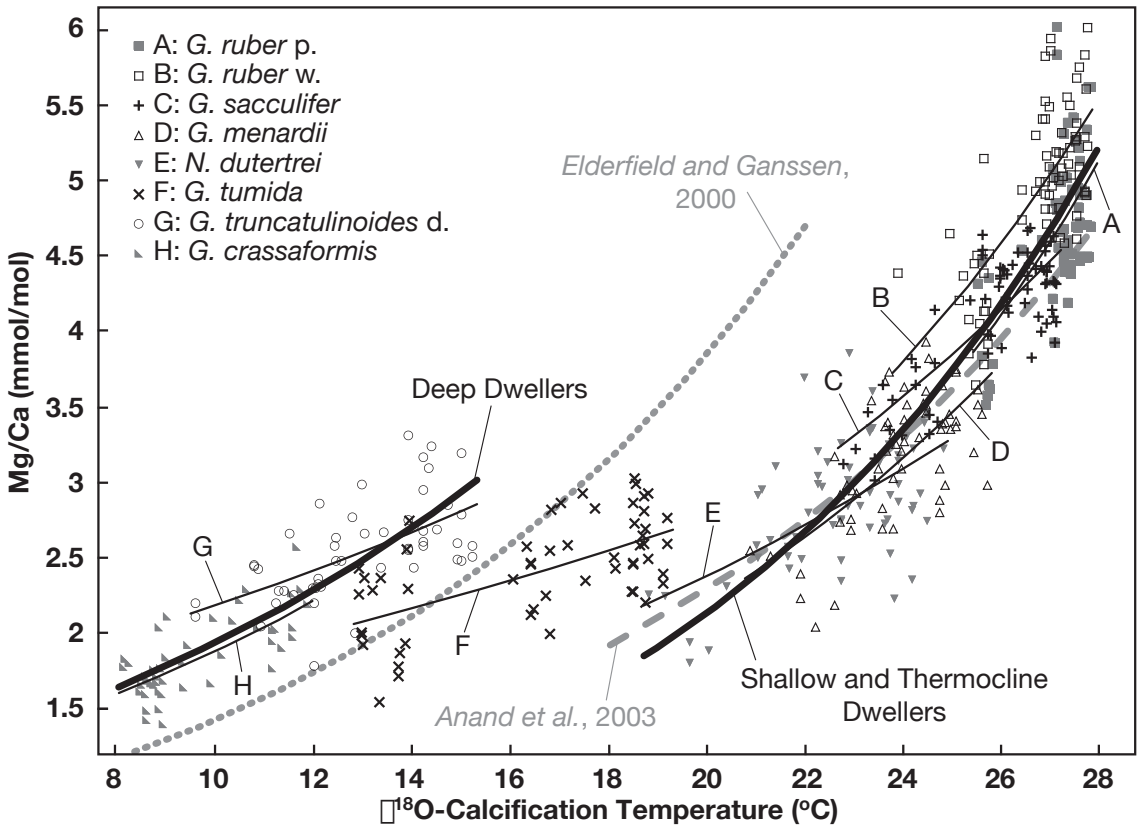

Figure 3.7 Planktonic foraminiferal Mg/Ca *vs.* annual temperature calibrations: Thin solid curves illustrate the species-specific calibrations of this study (Figure 3.6; Table 3.7). Right hand thick solid curve represents the multispecies calibration of shallow-dwelling *G. ruber* pink/white and *G. sacculifer*, and thermocline-dwelling *G. menardii* and *N. dutertrei* (Equation 3.4). Left hand thick solid curve indicates the dual-species calibration of deep-dwelling *G. truncatulinoides* dextral and *G. crassaformis* (Equation 3.5). Note the parallel offset of these calibration curves from each other by ~8°C. The multispecies calibrations of *Elderfield and Ganssen* (2000) (grey stippled curve) and *Anand et al.* (2003) (grey dashed curve) are given for comparison.

between the Mg/Ca ratios and annual temperatures (*NODC*, 2001) according to the equation

$$Mg/Ca \quad = \quad 0.223 \cdot exp^{(0.113 \cdot T)}; r = 0.90 \tag{3.4}$$

where Mg/Ca is in mmol/mol, temperature (T) in degree Celsius, and the calibration temperature range ~19–28°C. The 95% confidence interval of the preexponential constant is ±0.077, and the 95% confidence interval of the exponential constant is ±0.003. This multispecies calibration combines the species precipitating 'warm water' calcite at conditions of low y-axis intercepts b and temperatures of at least 19°C. It equals the *G. ruber* pink calibration and is similar to the multispecies calibration of *Anand et al.* (2003) from a 22–26°C temperature range including *G. truncatulinoides* and *G. crassaformis*. Only at the cold and warm ends of these multispecies calibrations, temperature differences increase to ~1°C. With respect to

our multispecies calibration, the species-specific *G. ruber* white calibration is parallel offset by ~1°C towards lower temperatures. Equation (4) represents at maximum 1°C higher temperatures than the species-specific calibrations of *G. sacculifer* and *N. dutertrei* at their cold ends, and at maximum 1°C lower temperatures than the calibrations of *G. sacculifer*, *G. menardii*, and *N. dutertrei* at their warm ends. These deviations match well with the uncertainty for calculated temperatures of ±1°C.

In contrast, the relationship between Mg/Ca ratios and annual temperatures (*NODC*, 2001) of the combined data set of deep-dwelling *G. truncatulinoides* dextral and *G. crassaformis* results in the exponential equation

$$Mg/Ca \quad = \quad 0.842 \cdot exp^{(0.083 \cdot T)}; r = 0.85 \tag{3.5}$$

with the calibration temperature range of ~8–15°C. The 95% confidence interval of the preexponential constant is ±0.059, and ±0.005 for the exponential constant. This dual-species calibration is parallel offset from the 'warm water' multispecies calibration (Equation 3.4) by ~8°C and combines those species precipitating 'cold water' calcite at conditions of high y-axis intercepts b and temperatures of at most 15°C. The combined calibration for the deep-dwelling species adopts the *G. crassaformis* calibration and is parallel offset by ~2°C towards lower temperatures from the *Elderfield and Ganssen* (2000) multispecies calibration (including *G. truncatulinoides*). The accuracy of calculated temperatures amounts to 1.3°C.

The *G. tumida* equation (covering the temperature range of ~13–19°C), however, deviates significantly from all species-specific and multispecies equations (Figure 3.7; Table 3.7). The assigned temperatures, at least for the temperature interval of ~16–19°C, are associated with very low or very high Mg/Ca ratios in comparison with the deep- or thermocline-dwelling species, respectively.

3.5 Conclusions

Paired Mg/Ca and δ^{18}O analyses were performed on eight planktonic foraminiferal species selected from 77 sediment surface samples covering large parts of the entire tropical Atlantic and Caribbean. Using various δ^{18}O-paleotemperature equations and modern temperature and salinity data, the calculation of δ^{18}O-derived mean calcification depths of the studied species implies preferred foraminiferal depth habitats within the surface mixed layer (*G. ruber* pink and white, *G. sacculifer*), the thermocline (*G. menardii*, *N. dutertrei*), and in subthermocline (*G. tumida*) and deep waters (*G. truncatulinoides* dextral, *G. crassaformis*). Increasing calcification depths towards the western side of the Atlantic Ocean are apparently associated with the increasing depth of the thermocline. Absolute calcification depth estimations, however, largely depend on the δ^{18}O-paleotemperature equation used for calculation.

Species-specific Mg/Ca ratios closely relate to the respective δ^{18}O-calcification temperatures derived from different δ^{18}O-paleotemperature equations. The choice of the respective δ^{18}O-

paleotemperature equation for the calculation of calcification temperatures, in this respect, is crucial to any Mg/Ca *vs.* δ^{18}O relationship. Applying *Shackleton* (1974) δ^{18}O-derived calcification depths, which for all species are in good agreement to published habitat specifications, we generated species-specific Mg/Ca *vs.* calcification temperature calibrations. Here, temperatures are obtained from mean calcification depths in the E-Atlantic, W-Atlantic, and Caribbean sector of the study area. In general, the resulting species-specific calibrations match well with existing species-specific calibrations revealing temperature sensitivities of ∼7–11% per 1°C.

The establishment of species-specific calibrations for sure will provide most accurate paleotemperature estimates. Nonetheless, we here suggest Mg/Ca *vs.* calcification temperature calibrations which are valid for either shallow- and thermocline-dwelling species or deep-dwelling species. These multispecies Mg/Ca *vs.* temperature calibrations will be most useful for species, whose Mg/Ca data were not yet calibrated or which are even extinct. Both multispecies calibrations, one in the 'warm water' (>19°C) mode with low y-axis intercepts and the other in the 'cold water' mode (<15°C) with high y-axis intercepts, are parallel offset by ∼8°C from each other with significant higher y-axis intercepts for the deep-dwelling species. Our data imply that a species solely calcifying 'warm (or cold) water' calcite falls on the calibration curve for shallow- and thermocline- (or deep-)dwelling species.

The Mg/Ca *vs.* calcification temperature calibrations of *G. tumida* with its shallow slope and large y-axis intercept clearly deviates from the shallow/thermocline and the deep multispecies calibrations curves. It might be speculated that the (sub)thermocline-dwelling *G. tumida* incorporates Mg^{2+} in the 'warm water' mode in regions with a deep-lying thermocline, as is observed for the Caribbean and the W-Atlantic. Instead, in ocean areas with a shallow thermocline as in the E-Atlantic Mg^{2+} incorporation in the 'cold water' mode overtakes. Further knowledge of planktonic foraminiferal calcification is urgently needed to unravel the suggested change in Mg^{2+}-incorporation modes. This is especially true when considering that foraminiferal tests may gradually precipitate at different water depth levels, and that regionally changing hydrographic conditions may affect calcite calcification depths.

3.6 Acknowledgements

We thank Stefan Mulitza, Joachim Schönfeld, Jeroen Groeneveld, and Reinhard Kozdon for discussions and comments, and Dieter Garbe-Schönberg, Silvia Koch, Lulzim Haxhiaj, Karin Kißling, Ulrike Nielsen, Daniel Oesterwind, and Stefan Dennenmoser for technical support and laboratory assistance. The GeoB samples were kindly provided by Stefan Mulitza (DFG Research Center Ocean Margins and Department of Geosciences, University of Bremen, Germany). The thoughtful reviews of ... significantly improved the manuscript. This research was funded by the German Ministry of Education and Research (BMBF, project No. 03G0164), by the German Research Foundation (DFG project Ti240-12), and by the Leibniz Award Du 129/33.

Chapter 4

Stable Isotopes of Planktonic Foraminifera from Tropical Atlantic/Caribbean Core-Tops: Implications for Reconstructing Upper-Ocean Stratification

Silke Steph[1,2], Marcus Regenberg[1], Ralf Tiedemann[2], Dirk Nürnberg[1], Stefan Mulitza[3]

[1]Leibniz Institute of Marine Sciences IFM-GEOMAR, Kiel, Germany

[2]Alfred Wegener Institute for Polar and Marine Research AWI, Bremerhaven, Germany

[3]Research Center Ocean Margins RCOM, University of Bremen, Germany

Manuscript for submission

Abstract. δ^{18}O and δ^{13}C values of nine tropical-subtropical planktonic foraminiferal species and varieties from different preferential habitat depths from 63 core-top samples along an east-west transect along the tropical Atlantic/Caribbean were used to identify key interspecific stable isotope gradients, which have a high potential to register changes in upper-ocean stratification in the geological record. East-west increase in thermocline depth is associated with a general increase in calcification depths of the examed species. The δ^{18}O gradients ($\Delta\delta^{18}$O) between *Globorotalia tumida* and *Globorotalia scitula* and shallow dwellers (i.e. *Globigerinoides sacculifer*, *Globigerinoides ruber* pink/white or deep dwellers (*Globorotalia crassaformis*, *Globorotalia truncatulinoides* dextral) strongly reflect westward deepening of the thermocline across the Atlantic/Caribbean. $\Delta\delta^{18}$O between *G. tumida* and *G. scitula* and the shallow dwellers decrease with increasing thermocline depth, whereas $\Delta\delta^{18}$O between *G. tumida* and *G. scitula* and deep

dwellers increase with increasing thermocline depth. Increasing thickness of the nutrient-depleted surface water masses from east to west is mirrored by a distinct increase in δ^{13}C gradients between shallow and deep dwellers.

4.1 Introduction

The reconstruction of changes in tropical upper-ocean stratification provides essential information for understanding past climate dynamics, including variations in the tropical wind field, changes in ocean heat transport and in the heat and gas exchange between ocean and atmosphere, and interactions between tropical climate and extratropical conditions. In paleoceanographic studies, planktonic foraminifera are frequently used for monitoring the variability of tropical upper ocean hydrography. They live vertically dispersed at different depth levels within the upper water column (*Fairbanks and Wiebe*, 1980a), recording environmental conditions in their stable oxygen and carbon isotope composition (δ^{18}O and δ^{13}C).

δ^{18}O values of foraminiferal calcite record the temperature signal as well as the δ^{18}O composition of ambient seawater ($\delta^{18}O_{seawater}$) at calcification (*Emiliani*, 1955; *Shackleton and Opdyke*, 1973; *Duplessy et al.*, 1991) in agreement with thermodynamic fractionation (e.g., *O'Neil et al.*, 1969; *Kim and O'Neil*, 1997). In addition, factors like the carbonate ion concentration, light levels, and calcification rate control foraminiferal δ^{18}O (*Spero and Lea*, 1993; *Spero et al.*, 1997; *Bemis et al.*, 1998). Outside the equatorial upwelling region, $\delta^{13}C_{DIC}$ (DIC = dissolved inorganic carbon) is expected to decrease with increasing water depth. Phytoplankton elevates surface $\delta^{13}C_{DIC}$ as it discriminates against $^{13}CO_2$ during photosynthesis, and heterotrophic organisms reintroduce ^{13}C-depleted CO_2 back into the DIC pool *via* respiration at depth (*Kroopnick*, 1974; *Spero et al.*, 2003).

Differences in δ^{18}O and δ^{13}C values of planktonic foraminifera from different preferential habitat depths should therefore permit the reconstruction of vertical temperature and nutrient gradients within the upper water column (e.g., *Emiliani*, 1954; *Ravelo and Fairbanks*, 1992; *Mulitza et al.*, 1997; *Patrick and Thunell*, 1997; *Ravelo and Andreasen*, 1999). Vertical temperature differences and the δ^{18}O gradients ($\Delta\delta^{18}$O) between shallow- and deeper-dwelling species are assumed to be large (small), if the thermocline is shallow (deep). Changes in $\delta^{13}C_{calcite}$ of planktonic foraminifera may be used for the reconstruction of changes in the vertical nutrient distribution within the upper water column (*Ravelo and Fairbanks*, 1995), since δ^{13}C of seawater can be related to nutrient concentrations (i.e. phosphate). Vertical nutrient gradients and δ^{13}C gradients ($\Delta\delta^{13}$C) between shallow- and deep-dwelling foraminifera are suggested to be large (small), if the nutricline is shallow (deep). The δ^{13}C composition of foraminiferal calcite, however, is not straightforward, as it can be strongly biased by offsets from $\delta^{13}C_{DIC}$, which are caused by 'vital effects', such as kinetic fractionation effects, photosynthetic activity of symbionts, and/or utilisation of metabolic CO_2 during shell growth (*Spero and Lea*, 1993; *Bemis et al.*, 2000).

The use of planktonic foraminiferal $\Delta\delta^{18}$O and $\Delta\delta^{13}$C as indicators of upper-ocean stratification is complicated by the fact that calcification of most species is not restricted to a certain

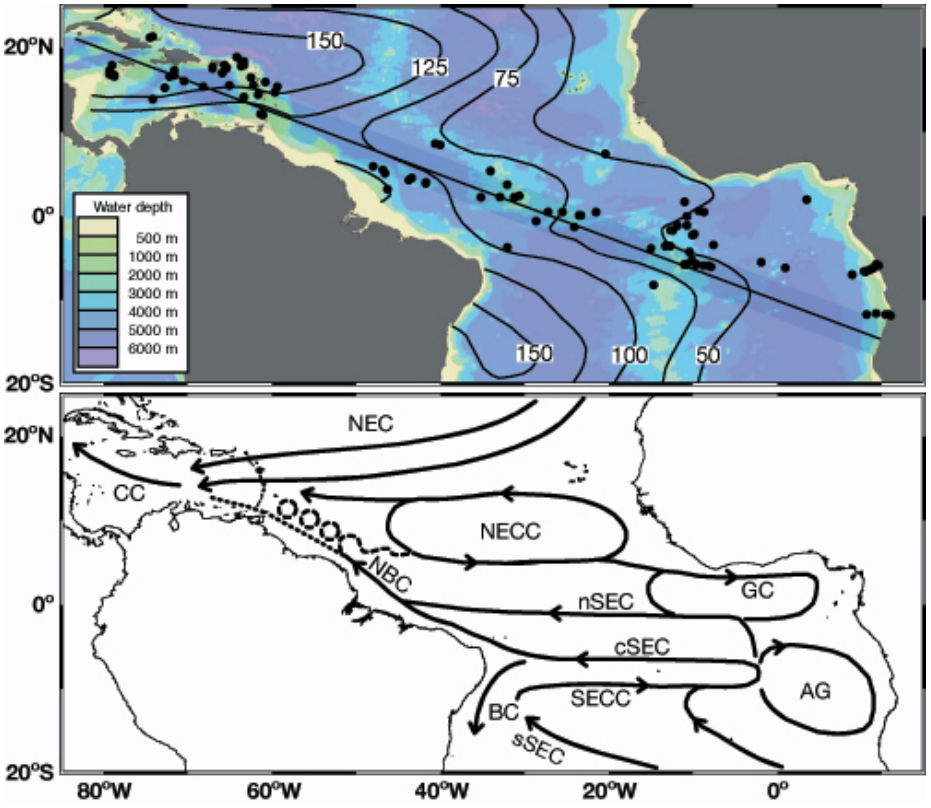

Figure 4.1 a) Bathymetric chart of the tropical Atlantic and Caribbean (Ocean Data View; *Schlitzer* (2002)) showing the locations of the core-top samples used in this study (black dots), and additional sites of *Mulitza* (1994) and *Rühlemann et al.* (2001). Thin lines illustrate the depth (m) of the annual 22°C isotherm, which aproximates the westward-dipping top of the modern thermocline. The thick line indicates the hydrographic section tracked by the core-top samples (Figure 4.2). Hydrographic data, shown in this publication to illustrate the tropical upper-ocean stratification, are taken from *NODC* (2001) stations within the shaded area around the profile. (b) Modern oceanographic setting of the tropical Atlantic and Caribbean, showing major surface currents. NEC: North Equatorial Current; SEC: South Equatorial Current; NBC: North Brazil Coastal Current; GC: Guyana Current; CC: Caribbean Current; LC: Loop Current.

depth level. Vertical migration through the water column (e.g., *Fairbanks et al.*, 1982; *Sautter and Thunell*, 1991a,b) with calcification at greater water depths may alter the stable isotope composition of foraminiferal tests (e.g., *Duplessy et al.*, 1981; *Lohmann*, 1995; *Kohfeld*, 1998). Therefore, changes in intraspecific stable isotope gradients may either result from variations of water mass signatures at a specific (fixed) depth level, or from migration of one or both species to shallower or deeper habitats.

With this study, we seek to test the use of the stable isotope compositions in planktonic foraminiferal calcite as tool for the reconstruction of changes in tropical upper-ocean stratification by calculation of interspecific δ^{18}O and δ^{13}C gradients. We compared the stable isotopic composition of nine planktonic foraminiferal species and varieties from sediment-surface samples positioned along an E-W transect along the tropical Atlantic/Caribbean (Figure 4.1) with the

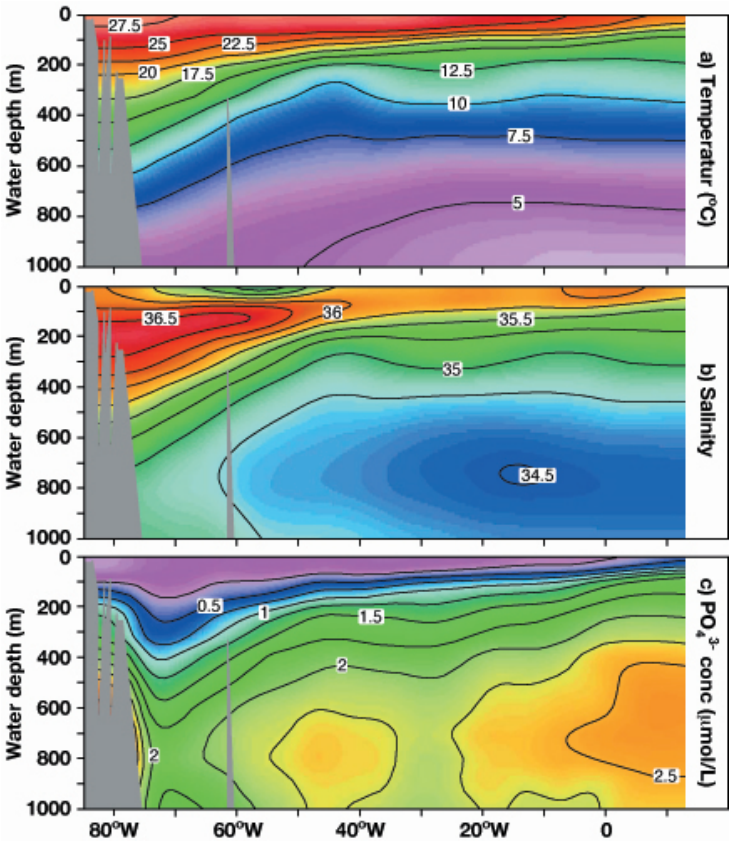

Figure 4.2 a) Annual temperature (°C), b) salinity, and c) phosphate concentration (μmol/L) ((*NODC*, 2001), (*Schlitzer*, 2002)) for the upper 1000 m of the tropical Atlantic and Caribbean water column, plotted along the hydrographic section shown in Figure 4.1a. The westward-dipping thermocline is illustrated by yellow colors in the temperature plot.

modern hydrographic data of the National Oceanographic and Data Center (*NODC*, 2001). This transect covers a broad depth range of the hydrographic regimes with a shallow thermocline in the eastern and central Atlantic and a deep thermocline in the western Atlantic and Caribbean. Comparing foraminiferal $\Delta\delta^{18}$O and $\Delta\delta^{13}$C with longitudinal changes in the vertical temperature and nutrient gradients, we were able to identify key species and key interspecific δ^{18}O and δ^{13}C gradients that are most sensitive to changes in thermocline depth and, thus, have the potential to monitor variations in upper-ocean stratification in the geological record.

4.2 Hydrography Along the Sampling Transect

We chose surface-sediments that are positioned on an E-W transect through the tropical Atlantic/Caribbean (13°E, 15°S – 83°W, 21°N; Figure 4.1a). Along this transect, seasonal TCD increases from east to west, mainly as a function of wind strength (*Philander and Pacanowski*, 1984, 1986a,b) and oceanic heat transport (Figures 4.1a, 4.2a). Easterly trade winds create a general westward flow of wind-driven surface currents across the basin. In the eastern and

Table 4.1 Locations, water depths, and calendar ages of the sediment-surface samples (0–1 cm) used in this study.

Station	Longitude	Latitude	Core Depth	^{14}C Age	Station	Longitude	Latitude	Core Depth	^{14}C Age
			m	years BP				m	years BP
GeoB1111-5	8°39'W	5°50.52'S	3757		M35012-6	63°37.6'W	18°18.3'N	1121	
GeoB1108-6	9°52.38'W	2°10.38'S	3897		M35014-1	63°44.2'W	17°50.5'N	1604	
GeoB1114-3	10°12.18'W	5°16.98'S	3422		M35010-2	64°05.4'W	18°56.0'N	2696	
GeoB1104-5	10°42.3'W	1°09.78'S	3724		M35008-1	64°09.8'W	18°01.9'N	2820	
GeoB1112-3	10°44.58'W	5°46.68'S	3128	2730±40[a]	SO164-23-3	65°08.09'W	15°34.01'N	4328	
GeoB1113-7	11°02.1'W	5°44.7'S	2373		M35018-1	65°22.2'W	17°34.5'N	1728	
GeoB1105-3	12°25.7'W	1°39.9'S	3232	2430±50[a]	M35019-1	65°26.1'W	17°40.3'N	1815	
GeoB1106-5	12°33.12'W	1°45.6'S	2471		M35020-2	65°40.2'W	17°55.8'N	2005	
GeoB1115-4	12°34.8'W	3°33.48'S	2921		M35023-3	65°40.9'W	17°36.2'N	1192	
GeoB1116-1	13°11.22'W	3°37.38'S	3471		M35023-4	65°41.0'W	17°36.2'N	1183	
GeoB1503-2	30°38.88'W	2°18.6'N	2298		M35024-6	66°00.1'W	17°02.6'N	4710	2510±45[b]
GeoB1505-3	33°00.42'W	2°16.38'N	3703	3090±40[a]	M35025-1	67°00.5'W	17°45.2'N	1778	699±30[b]
GeoB1508-1	34°01.5'W	5°19.98'N	3685		M35026.2	67°02.6'W	17°30.5'N	3815	1175±70[b]
GeoB1506-1	35°10.92'W	2°12.3'N	4267		SO164-22-2	68°12.0'W	15°24.0'N	4506	
GeoB4305-1	39°59.52'W	8°29.88'N	3042		SO164-21-3	70°30.0'W	16°06.0'N	3995	
GeoB4304-1	40°26.22'W	8°34.32'N	3365		SO164-20-2	71°29.22'W	16°45.49'N	3357	
GeoB1523-2	41°37.32'W	3°48.9'N	3291		SO164-04-2	71°39.09'W	17°16.38'N	1013	
GeoB1515-2	43°39.9'W	4°14.28'N	3125	1750±40[a]	SO164-03-3	72°12.31'W	16°32.40'N	2744	
GeoB1511-6	46°20.58'W	3°10.68'N	3162		SO164-02-3	72°47.06'W	15°18.29'N	2977	2205±25[c]
GeoB1513-2	46°55.62'W	5°25.92'N	3621		SO164-07-3	74°08.76'W	21°19.46'N	2722	720±35[c]
GeoB1512-1	48°02.58'W	5°54.18'N	3716		SO164-01-3	74°09.028'W	13°50.195'N	4025.7	
SO164-50-3	59°16.94'W	15°21.25'N	4002		SO164-19-3	74°20.98'W	21°14.7'N	1706	<AD 1954[c]
SO164-25-3	59°44.48'W	14°41.25'N	2720	1915±30[c]	SO164-18-1	74°21.0'W	21°13.61'N	1629	1350±25[c]
SO164-48-2	60°55.0'W	15°57.02'N	1286		M35030-1	78°36.6'W	16°45.3'N	1298	
M35002-1	61°10.6'W	12°01.9'N	1506		M35032-1	78°36.9'W	16°35.3'N	1363	
M35003-6	61°14.7'W	12°05.1'N	1299		M35034-3	79°03.5'W	16°54.2'N	1212	
M35004-1	61°39.7'W	14°24.6'N	2885		M35035-1	79°07.9'W	16°53.6'N	1252	
M35005-3	62°13.9'W	15°27.2'N	2289		M35039-1	79°08.7'W	17°55.6'N	1142	
M35006-6	62°27.2'W	16°25.3'N	888		M35038-1	79°13.8'W	17°15.7'N	1066	
SO164-24-3	63°25.43'W	14°11.89'N	1545		M35037-1	79°23.3'W	16°54.8'N	1190	
M35013-3	63°27.0'W	18°18.9'N	899		M35036-3	79°25.3'W	16°55.0'N	1196	
M35015-1	63°27.1'W	17°59.6'N	1230						

^{14}C dates from: [a] *Mollenhauer* (1999), [b] *Schmuker* (2000), and [c] *Regenberg et al.* (2006)

central tropical Atlantic, regional upwelling (resulting from seasonally changing trade winds and equatorial divergent flow) brings cool South Atlantic Central Water into the photic zone and creates a shallow thermocline and steep vertical temperature gradients (Figure 4.2a). The maximum of chlorophyll concentration occurs at the top of the thermocline, resulting from strong vertical nutrient gradients (Figure 4.2c). Wind-induced westward flow of tropical surface currents allows warm surface water to pile up in western parts of the basin west of 30°W, forming a deep mixed layer in the western Atlantic/Caribbean. In this area, the seasonal thermocline and nutricline are below the photic zone throughout the year (Figure 4.2a,c). With respect to the central Atlantic, the total temperature range and vertical phosphate gradient within the upper 300 m of the Caribbean water column are smaller by up to 5°C and 0.5 μmol/L, respectively. Changes in sea-surface temperature (SST) along the transect amount to ~4°C (Figure 4.22a), and are, hence, relatively weak compared to SST changes along latitudinal transects (e.g., *Mulitza et al.*, 1997).

The alignment of core-top stations roughly tracks the dominant westward-flowing tropical Atlantic surface current system of the South Equatorial Current (SEC), North Brazil Current (NBC), Guyana Current (GC), and the Caribbean Current (CC) (Figure 4.1b). Largest volume

Table 4.2 Species-specific averages ±standard deviations of the planktonic foraminiferal $\delta^{18}O$ values from the different study areas. In addition, the differences between the regional $\delta^{18}O$ averages are given. Related probability (p) values, if >0.05 (<0.05, bold face), indicate that the regionally restricted data sets are similar (significantly different from each other).

Species	Averages ±standard deviations			Difference between averages					
	E-Atlantic	W-Atlantic	Caribbean	W-Atlantic/ E-Atlantic		Caribbean/ W-Atlantic		Caribbean/ E-Atlantic	
	□^{18}O	□^{18}O	□^{18}O	□^{18}O	p value	□^{18}O	p value	□^{18}O	p value
G. ruber p.	-1.59 ±0.51	-1.93 ±0.32	-1.82 ±0.16	-0.35	**0.0088**	0.11	0.084	-0.23	**0.0082**
G. ruber w.	-1.39 ±0.16	-1.46 ±0.43	-1.76 ±0.21	-0.07	0.63	-0.30	**0.0017**	-0.37	**<0.0001**
G. sacculifer	-1.14 ±0.29	-1.51 ±0.21	-1.33 ±0.14	-0.37	**<0.0001**	0.18	**0.0005**	-0.19	**0.0007**
G. menardii	-0.04 ±0.43	-0.68 ±0.24	-0.57 ±0.32	-0.64	**0.0001**	0.11	0.27	-0.54	**<0.0001**
N. dutertrei	0.21 ±0.43	-0.30 ±0.44	-0.53 ±0.19	-0.51	**0.011**	-0.24	**0.0098**	-0.74	**<0.0001**
G. tumida	0.82 ±0.45	0.44 ±0.33	0.25 ±0.34	-0.38	**0.015**	-0.19	0.086	-0.57	**<0.0001**
G. scitula	1.63 ±0.14	1.01 ±0.35	0.28 ±0.38	-0.62	**<0.0001**	-0.73	**0.0002**	-1.34	**<0.0001**
G. truncatulinoides d.	1.33 ±0.29	1.24 ±0.51	1.24 ±0.32	-0.09	0.49	0.00	0.97	-0.09	0.31
G. crassaformis	1.89 ±0.38	2.05 ±0.31	1.65 ±0.19	0.16	0.14	-0.40	**<0.0001**	-0.24	**0.0097**

transport towards the west takes place within the SEC, which is driven by the southeast trade winds and covers a broad region from 3°N–25°S (with seasonal variations). In the tropical western Atlantic, the SEC feeds the NBC, heading northwestward along the South American Coast and providing a conduit for cross-equatorial transport of South Atlantic upper-ocean waters to the northern hemisphere as part of the Atlantic meridional overturning cell (*Johns et al.*, 2002). Strengh and direction of the NBC is largely depending on the seasonal movement of the ITCZ.

From January to May, when the ITCZ is in its southern position, the NBC continues northwest along the coast and feeds the GC (*Csanady*, 1990) that enters the Caribbean through the Lesser Antilles Passages and continues westward as the CC (*Wüst*, 1964; *Gordon*, 1967; *Roemmich*, 1981; *Hernandez-Guerra and Joyce*, 2000). It passes the Yucatan Channel and the Florida Straits, and merges with the Antilles Current to form the northward flowing Western Boundary Current (Figure 4.1b). Surface water transported *via* the GC is significantly influenced by freshwater discharges from the Amazon and Orinoco Rivers (*Morrison and Smith*, 1990; *Hellweger and Gordon*, 2002; *Johns et al.*, 2002; *Silva et al.*, 2005). In boreal summer and fall, when the ITCZ reaches its northern position, the NBC connects with the eastward flowing North Equatorial Countercurrent (NECC) at about 6°N, and eddies are formed in an offshore retroflection zone (*Müller-Karger et al.*, 1988; *Johns et al.*, 1990; *Schott et al.*, 1998; *Memery et al.*, 2000). The NECC is bounded to the north by the broad, westward flowing, wind-induced North Equatorial Current (NEC) that extends from about 7–20°N (*Schott et al.*, 2002) and is mainly fed by cooler northeast Atlantic waters. As the NEC travels across the open ocean, it is joined by waters originating south of the equator, thus, entraining waters from the Southern Atlantic into the Northern Atlantic. Most of the NEC waters flow northwest and supply the GC and the CC (*Bourles et al.*, 1999a,b; *Johns et al.*, 2002).

4.3 Materials and Methods

We analyzed 39 core-top samples from the Caribbean and 24 core-top samples from the tropical Atlantic (Figure 4.1a; Table 4.1). Caribbean surface-sediments used in this study were recovered during R/V SONNE cruise SO164 (*Nürnberg et al.*, 2003) and R/V METEOR cruise 35/1 (*Hemleben et al.*, 1998). Core-top samples from the tropical Atlantic were recovered during RV METEOR cruises M6/6, M9/4, M16/1, M20/2, M38/1 and M41/2 (*Wefer et al.*, 1988, 1991a,b; *Müller et al.*, 1988; *Bleil and Fischer*, 1998; *Schulz et al.*, 1998) (Table 4.1) and have already been used for previous studies (e.g., *Mulitza*, 1994; *Mulitza et al.*, 1997; *Schmidt and Mulitza*, 2002; *Mulitza et al.*, 2004). Faunal assemblages and oxygen isotope stratigraphy indicate that all core-top samples are of Holocene age (*Mulitza*, 1994) (Chapter 3). AMS^{14}C datings for 12 core-top samples suggest an age younger than ∼2000–3000 years (*Regenberg et al.*, 2006a) ((Chapters 2, 3; Table 4.1). In addition, we used existing tropical Atlantic core-top δ^{18}O and δ^{13}C data for *G. ruber*, *G. sacculifer*, *G. tumida*, and *G. crassaformis* to extend our dataset (*Mulitza*, 1994; *Rühlemann et al.*, 2001) (Table 4.1).

We measured the stable isotopic composition of nine planktonic foraminiferal taxa or varieties with different preferential habitat depths: *Globigerinoides ruber* pink and white, *Globigerinoides sacculifer* (without sac-like final chamber), *Globorotalia menardii*, *Neogloboquadrina dutertrei*, *Globorotalia tumida*, *Globorotalia scitula*, *Globorotalia truncatulinoides* dextral, and *Globorotalia crassaformis* (Figure 4.3). The vertical distribution of these species is supposed to cover the upper ∼400–500 m of the water column (e.g., *Elderfield and Ganssen*, 2000; *Anand et al.*, 2003; *Schiebel and Hemleben*, 2005). Generic assignments follow *Kennett and Srinivasan* (1983) and *Hemleben et al.* (1989). For the highly abundant mixed-layer dwellers *G. ruber* pink and white, and *G. sacculifer* (without sac-like final chamber), and for thermocline-dwelling *G. menardii*, ∼40 specimens were selected from the 355–400 μm fraction. We avoided smaller grain size fractions in order to minimize size-dependent fractionation effects that are supposed to be greatest for juveniles (e.g., *Ravelo and Fairbanks*, 1995). Tests were crushed and homogenized, and double measurements were done from the powder to obtain a stable mean isotope composition of the population in the sediment (*Ravelo and Andreasen*, 1999). For thermocline-dwelling *N. dutertrei*, for *G. tumida* (bottom of the photic zone), and for deep-dwelling *G. truncatulinoides* dextral and *G. crassaformis*, 8–12 specimens were separated from the 355–400 μm fraction. Intermediate-dwelling *G. scitula* has not been found in sufficient numbers in the larger grain sizes. Therefore, 30–40 specimens were selected from the 125–250 μm grain size fraction. All isotope measurements were run at IFM-GEOMAR (Kiel) on a Finnigan MAT 252 Mass Spectrometer with automated Kiel carbonate preparation device. Analytical precision was better than 0.07‰ for δ^{18}O and 0.04‰ for δ^{13}C ($\pm 1\sigma$, N=130). The values are reported relative to Pee Dee Belemnite (PDB). Calibration to PDB was calculated *via* the National Bureau of Standards (NBS) 19 and an internal laboratory standard.

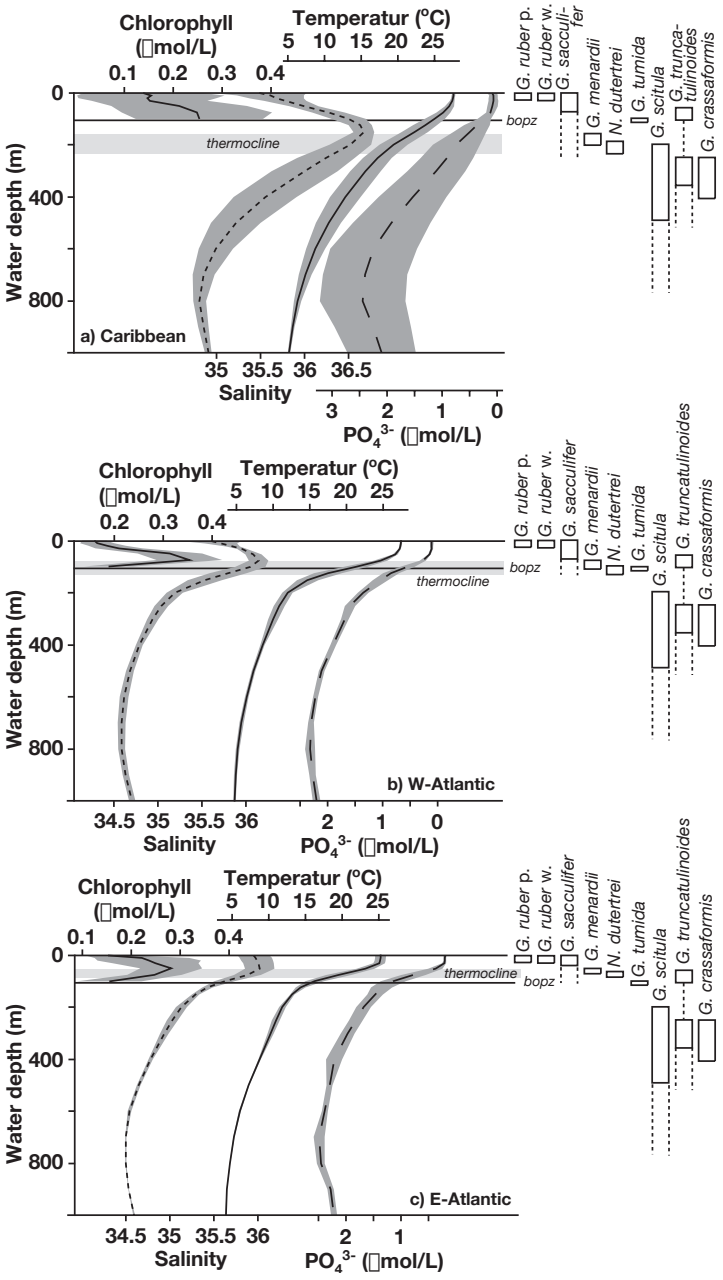

Figure 4.3 Modern annual-average properties of the upper water column for (a) the Caribbean, (b) the tropical western Atlantic, and (c) the tropical eastern Atlantic, and preferential habitat depths of the planktonic foraminiferal species used in this study. Atlas data on physical and chemical properties are taken from *NODC* (2001) for the Caribbean section (58.5°W–80.5°W), the W-Atlantic section (49.5°W–30.5°W), and the E-Atlantic section (17.5°W–0.5°E, excluding coastal upwelling regions) of the hydrographic transect shown in Figure 4.1. Thick lines are mean values, shaded areas indicate the range of standard devitation (from left to right: chlorophyll, salinity, temperature, phosphate concentrations). The gray bar shows the thermocline as zone with the highest vertical temperature gradient (22°C–18°C), and the black line indicates the bottom of the photic zone (bopz), which is at a relatively constant depth level within the tropics (80–100 m). Bars to the right show the range of preferential habitat depths of studied planktonic foraminiferal species. Habitat specifications are taken from the literature.

To evaluate the observed changes in stable isotope values and gradients between planktonic foraminiferal taxa used in this study, we estimated calcification depths for different species by comparing measured $\delta^{18}O_c$ values to predicted $\delta^{18}O_c$ values at different depth levels. Predicted $\delta^{18}O_c$ was calculated from 0–1000 m water depth using annual temperature and salinity data from *NODC* (2001). For the uppermost 100 m of the water column, salinity was converted to $\delta^{18}O_{seawater}$ with $\delta^{18}O_{seawater}$-salinity relationships for the Caribbean (0–100 m; $\delta^{18}O_{seawater}$ = 0.319·S - 10.511 (*Steph et al.*, 2006), and the tropical Atlantic (0–100 m; $\delta^{18}O_{seawater}$ = 0.265·S - 8.662, Chapter 3). From 100–1000 m water depth, $\delta^{18}O_{seawater}$-salinity relationships for the Caribbean (0.498·S - 17.116 (*Steph et al.*, 2006)) and the tropical Atlantic ($\delta^{18}O_{seawater}$ = 0.493·S - 16.919, Chapter 3) closely resemble the global $\delta^{18}O_{seawater}$-salinity relationship ($\delta^{18}O_{seawater}$ = 0.5·S - 17 (*Broecker*, 1989)). All $\delta^{18}O_{seawater}$-salinity relationships used in this study were generated using the $\delta^{18}O_{seawater}$ database of *Schmidt* (1999). $\delta^{18}O_{seawater}$ was scaled to PDB by subtracting 0.27‰ (*Hut*, 1987). Finally, predicted $\delta^{18}O_c$ was calculated by solving the $\delta^{18}O$-temperature relationships of *Shackleton* (1974) and *Mulitza et al.* (2004) for $\delta^{18}O$ of carbonate. For each core-top value, predicted $\delta^{18}O_c$ values from the corresponding 1° grid box have been assigned. The water depth in which predicted $\delta^{18}O_c$ matches measured $\delta^{18}O_c$ is assumed to approximate the calcification depth of each species. We did not correct measured $\delta^{18}O_c$ for offsets from equilibrium calcite, as the ranges of 'disquilibrium' given in the literature for individual species are large (e.g., *Niebler et al.*, 1999). In fact, the correction for a specific disequilibrium would consistently shift measured $\delta^{18}O_c$ for each species to higher or lower values, and therefore the estimated mean calcification depth to deeper or shallower levels. The application of 'disequilibrium corrections' for individual species would hence change absolute $\delta^{18}O$ gradients between species, whereas the longitudinal variations of $\delta^{18}O$ values and gradients due to changes in hydrography remain unaffected.

4.4 Results

4.4.1 Longitudinal Changes of $\delta^{18}O_c$ and Comparison to Predicted $\delta^{18}O_c$

In general, foraminiferal $\delta^{18}O$ increases with increasing preferential calcification depth of the planktonic foraminiferal species (e.g., *Emiliani*, 1954) mainly due to lower temperatures (Figure 4.3): The shallow dwellers *G. ruber* (pink/white) and *G. sacculifer* record the lowest $\delta^{18}O$ values, and $\delta^{18}O$ values of the deep dwellers *G. truncatulinoides* dextral and *G. crassaformis* are highest. The intermediate dwellers *G. menardii* and *N. dutertrei*, *G. tumida* (bottom of the photic zone) and *G. scitula* have $\delta^{18}O$ values intermediate to those of the shallow- and deep-dwelling species (Figure 4.4; Table 4.4).

The absolute depth of corresponding predicted $\delta^{18}O_{calcite}$ strongly depends on the $\delta^{18}O$-paleotemperature equations used for calculations (Figure 4.5a,b). In general, the comparison of measured $\delta^{18}O$ values to the water depth of corresponding predicted $\delta^{18}O_{calcite}$ suggests that the mean calcification depth of most species is not strictly coupled to a certain depth level, but

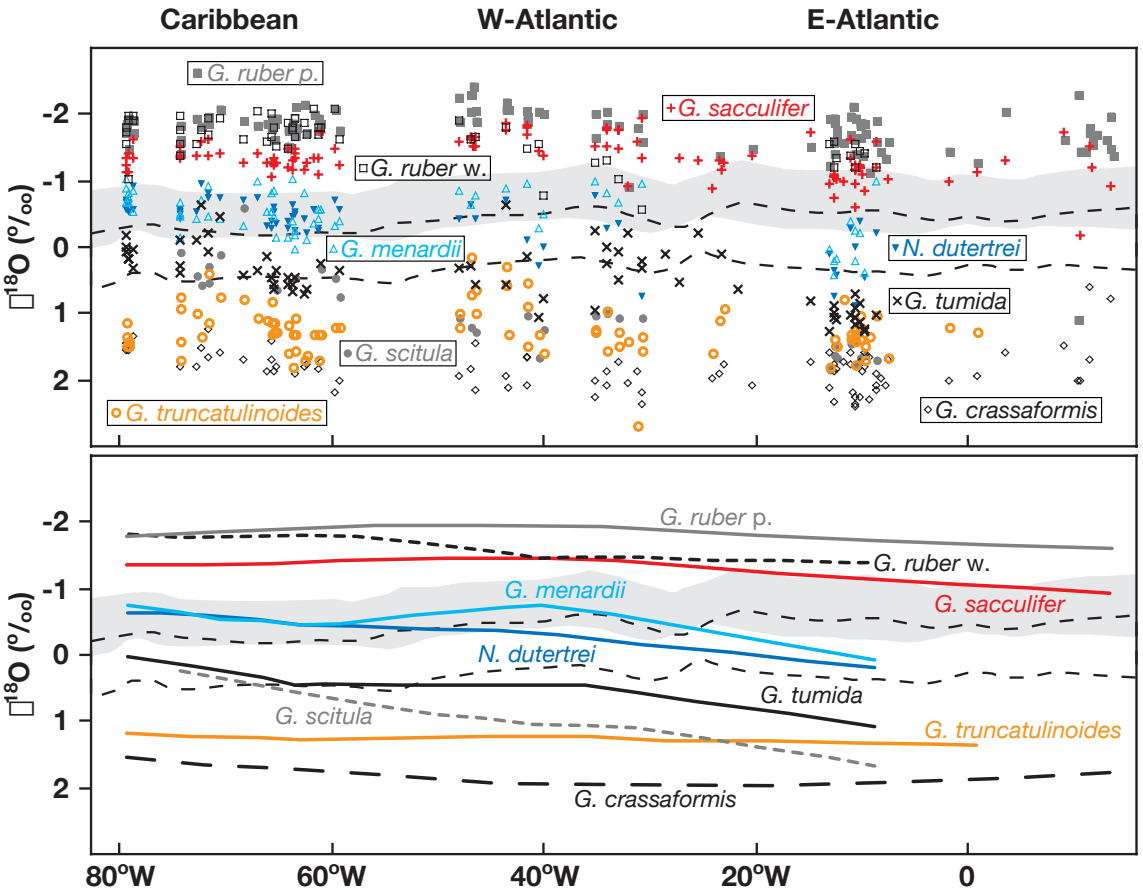

Figure 4.4 Top: Measured δ^{18}O values of the planktonic foraminiferal species used in this study *vs.* the longitudinal position of the core-top samples. Gray squares: *G. ruber* pink; white squares: *G. ruber* white; red positive signs: *G. sacculifer*; light blue triangles: *G. menardii*; blue inverse triangles: *N. dutertrei*; crosses: *G. tumida*; gray dots: *G. scitula*; orange circles: *G. truncatulinoides*; white diamonds: *G. crassaformis*. Predicted $\delta^{18}O_c$ for the thermocline (indicated by the 22°C and 18°C isotherms along the hydrographic section; Figure 4.2) was calculated after *Shackleton* (1974) (dashed lines) and *Mulitza et al.* (2004) (shaded area). According to their preferential habitat depths, δ^{18}O values of the shallow dwellers *G. ruber* (pink/white) and *G sacculifer* are generally lowest, and δ^{18}O values of the deep dwellers *G. truncatulinoides* dextral and *G. crassaformis* are highest. The thermocline dwellers *G. menardii* and *N. dutertrei*, *G. tumida* (bottom of the photic zone) and *G. scitula* show δ^{18}O values intermediate to those of the shallow and deep dwellers. Bottom: Trends of δ^{18}O changes along the E-W transect. We smoothed the data by using the locally weighted least squared error method (e.g., *Cleveland*, 1979) and applying a smoothing factor of 60%.

Table 4.3 Averaged gradients ±standard deviations between planktonic foraminiferal δ^{18}O values ($\Delta\delta^{18}$O) from the different study areas. In addition, the differences between the averaged regional $\Delta\delta^{18}$O are given. Related probability (p) values, if >0.05 (<0.05, bold face), indicate that the regionally restricted data sets are similar (significantly different from each other).

Gradient between species	Averages ±standard deviations			Difference between averaged gradients					
	E-Atlantic	W-Atlantic	Caribbean	E-Atlantic/ W-Atlantic		W-Atlantic/ Caribbean		E-Atlantic/ Caribbean	
	□□^{18}O	□□^{18}O	□□^{18}O	□□^{18}O	p value	□□^{18}O	p value	□□^{18}O	p value
shallow-shallow									
G. ruber w.-*G. ruber* p.	0.44 ±0.11	0.51 ±0.35	0.06 ±0.19	-0.07	0.56	0.44	**<0.0001**	0.38	**<0.0001**
G. sacculifer-*G. ruber* p.	0.55 ±0.36	0.41 ±0.24	0.50 ±0.20	0.13	0.18	-0.08	0.19	0.05	0.48
G. sacculifer-*G. ruber* w.	0.33 ±0.20	-0.07 ±0.38	0.43 ±0.23	0.39	**0.0076**	-0.50	**<0.0001**	-0.11	0.19
intermediate-intermediate									
N. dutertrei-*G. menardii*	0.25 ±0.31	0.39 ±0.50	0.04 ±0.31	-0.15	0.43	0.35	**0.0048**	0.21	0.069
G. tumida-*N. dutertrei*	0.90 ±0.42	0.82 ±0.52	0.80 ±0.27	0.08	0.7	0.02	0.88	0.10	0.39
G. tumida-*G. menardii*	1.15 ±0.40	1.20 ±0.32	0.86 ±0.46	-0.06	0.72	0.34	**0.026**	0.28	0.093
G. scitula-*G. menardii*	1.66 ±0.45	1.67 ±0.44	0.70 ±0.49	-0.01	0.95	0.97	**<0.0001**	0.96	**0.0003**
G. scitula-*N. dutertrei*	1.42 ±0.42	1.33 ±0.39	0.92 ±0.42	0.08	0.64	0.41	**0.034**	0.49	**0.021**
G. scitula-*G. tumida*	0.52 ±0.11	0.55 ±0.28	0.25 ±0.64	-0.03	0.74	0.30	0.18	0.27	0.22
deep-deep									
G. crassaformis-*G. truncatulinoides* d.	0.62 ±0.33	0.76 ±0.55	0.46 ±0.36	-0.14	0.39	0.30	0.067	0.16	0.17
intermediate-shallow									
G. menardii-*G. ruber* p.	1.79 ±0.40	1.29 ±0.34	1.25 ±0.35	0.50	**0.003**	0.04	0.72	0.54	**0.0001**
G. menardii-*G. ruber* w.	1.35 ±0.49	0.78 ±0.55	1.18 ±0.37	0.57	**0.016**	-0.41	**0.0039**	0.17	0.25
G. menardii-*G. sacculifer*	1.03 ±0.34	0.85 ±0.24	0.76 ±0.37	0.18	0.14	0.08	0.45	0.26	0.051
N. dutertrei-*G. ruber* p.	2.04 ±0.34	1.67 ±0.42	1.29 ±0.22	0.36	**0.037**	0.39	**0.0001**	0.75	**<0.0001**
N. dutertrei-*G. ruber* w.	1.60 ±0.40	1.13 ±0.35	1.22 ±0.24	0.46	**0.0079**	-0.09	0.32	0.37	**0.0005**
N. dutertrei-*G. sacculifer*	1.27 ±0.30	1.21 ±0.40	0.80 ±0.18	0.06	0.69	0.41	**<0.0001**	0.47	**<0.0001**
G. tumida-*G. ruber* p.	2.88 ±0.24	2.46 ±0.34	2.06 ±0.38	0.42	**0.0032**	0.41	**0.0027**	0.82	**<0.0001**
G. tumida-*G. ruber* w.	2.50 ±0.20	1.92 ±0.47	1.98 ±0.42	0.58	**0.0019**	-0.06	0.69	0.52	**0.0007**
G. tumida-*G. sacculifer*	2.04 ±0.41	2.03 ±0.30	1.59 ±0.31	0.01	0.96	0.44	**0.0002**	0.45	**0.0003**
G. scitula-*G. ruber* p.	3.45 ±0.15	2.96 ±0.43	2.20 ±0.43	0.50	**0.0021**	0.76	**0.0006**	1.25	**<0.0001**
G. scitula-*G. ruber* w.	3.01 ±0.17	2.44 ±0.44	2.05 ±0.43	0.57	**0.0009**	0.39	0.054	0.96	**<0.0001**
G. scitula-*G. sacculifer*	2.69 ±0.17	2.52 ±0.35	1.70 ±0.45	0.17	0.17	0.82	**0.0001**	0.99	**<0.0001**
deep-intermediate									
G. truncatulinoides d.-*G. menardii*	1.49 ±0.21	1.85 ±0.38	1.81 ±0.49	-0.35	**0.027**	0.04	0.79	-0.31	0.083
G. truncatulinoides d.-*N. dutertrei*	1.27 ±0.40	1.46 ±0.39	1.76 ±0.31	-0.18	0.32	-0.31	**0.0078**	-0.49	**0.0005**
G. truncatulinoides d.-*G. tumida*	0.39 ±0.13	0.68 ±0.46	0.98 ±0.37	-0.28	0.11	-0.30	**0.037**	-0.58	**0.0001**
G. truncatulinoides d.-*G. scitula*	-0.11 ±0.12	0.23 ±0.44	0.82 ±0.51	-0.34	**0.048**	-0.59	**0.0091**	-0.93	**0.0002**
G. crassaformis-*G. menardii*	2.11 ±0.52	2.87 ±0.41	2.24 ±0.24	-0.76	**0.0028**	0.63	**<0.0001**	-0.13	0.37
G. crassaformis-*N. dutertrei*	1.87 ±0.45	2.50 ±0.45	2.23 ±0.17	-0.63	**0.0094**	0.27	**0.027**	-0.36	**0.0034**
G. crassaformis-*G. tumida*	0.96 ±0.24	1.70 ±0.38	1.49 ±0.32	-0.74	**0.0001**	0.21	0.18	-0.53	**<0.0001**
G. crassaformis-*G. scitula*	0.45 ±0.22	1.28 ±0.31	1.38 ±0.43	-0.82	**<0.0001**	-0.11	0.56	-0.93	**<0.0001**
deep-shallow									
G. truncatulinoides d.-*G. ruber* p.	2.99 ±0.42	3.14 ±0.50	3.06 ±0.36	-0.15	0.35	0.08	0.49	-0.07	0.55
G. truncatulinoides d.-*G. ruber* w.	2.90 ±0.24	2.63 ±0.38	2.99 ±0.39	0.28	0.083	-0.36	**0.0056**	-0.08	0.57
G. truncatulinoides d.-*G. sacculifer*	2.42 ±0.26	2.74 ±0.48	2.58 ±0.31	-0.32	**0.021**	0.16	0.15	-0.16	0.072
G. crassaformis-*G. ruber* p.	3.43 ±0.68	3.94 ±0.48	3.54 ±0.25	-0.51	**0.018**	0.41	**0.0027**	-0.11	0.5
G. crassaformis-*G. ruber* w.	3.47 ±0.24	3.58 ±0.38	3.44 ±0.23	-0.11	0.45	0.14	0.24	0.03	0.76
G. crassaformis-*G. sacculifer*	3.03 ±0.37	3.58 ±0.34	3.01 ±0.18	-0.55	**0.0001**	0.57	**<0.0001**	0.02	0.78

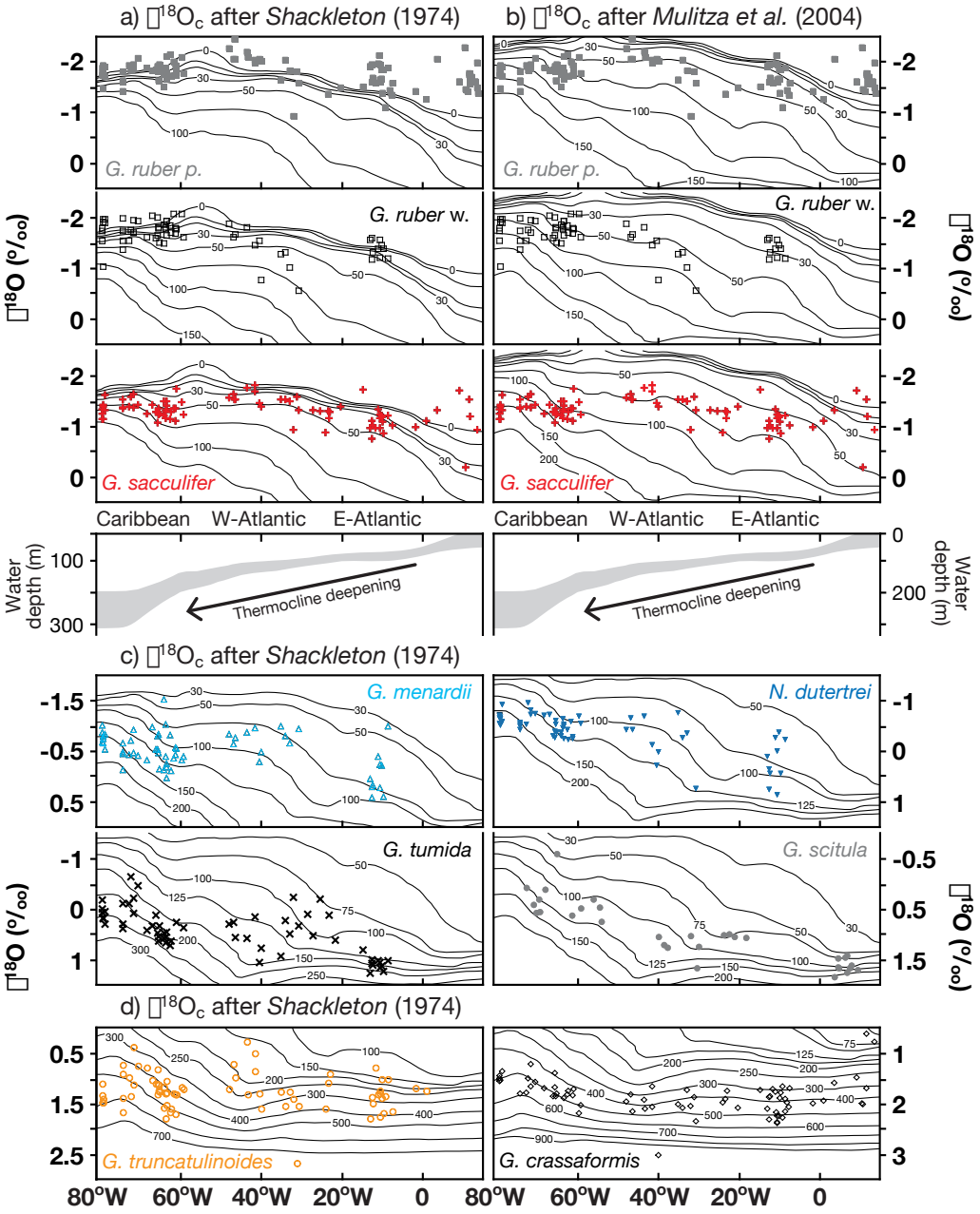

Figure 4.5 Measured planktonic foraminiferal δ^{18}O values for each species plotted *vs.* the longitudal position of core-top samples used in this study. In the background, the depth levels of predicted $\delta^{18}O_c$ calculated after (a, c, d) *Shackleton* (1974) and (b) *Mulitza et al.* (2004) along the hydrographic section shown in Figure 4.1 are given for the illustration of mean calcification depths. At the top of the figures, the westward-dip of the Atlantic/Caribbean thermocline is indicated by the depth range of the 18°C–22°C isotherm. Comparison of estimated calcification depths of the shallow dwellers given in (a) and (b) shows that the depth estimates strongly depend on the δ^{18}O-paleotemperature equation used for calculation. Relative changes in species-specific calcification depths, however, are consistent for each paleotemperature equation used, and suggest that mean calcification depths of most species are not strictly coupled to a certain depth level, but increase from east to west with increasing thermocline depth. (a), (b): Shallow dwellers; (c): Intermediate dwellers, and (d): Deep dwellers.

Table 4.4 Averaged gradients ±standard deviations between planktonic foraminiferal δ^{18}O values ($\Delta\delta^{18}$O) from the different study areas. In addition, the differences between the averaged regional $\Delta\delta^{18}$O are given. Related probability (p) values, if >0.05 (<0.05, bold face), indicate that the regionally restricted data sets are similar (significantly different from each other).

Gradient between species	Averages ±standard deviations			Difference between averaged gradients					
	E-Atlantic	W-Atlantic	Caribbean	E-Atlantic/ W-Atlantic		W-Atlantic/ Caribbean		E-Atlantic/ Caribbean	
	□□^{18}O	□□^{18}O	□□^{18}O	□□^{18}O	p value	□□^{18}O	p value	□□^{18}O	p value
shallow-shallow									
G. ruber w.-*G. ruber* p.	0.44 ±0.11	0.51 ±0.35	0.06 ±0.19	-0.07	0.56	0.44	**<0.0001**	0.38	**<0.0001**
G. sacculifer-G. ruber p.	0.55 ±0.36	0.41 ±0.24	0.50 ±0.20	0.13	0.18	-0.08	0.19	0.05	0.48
G. sacculifer-G. ruber w.	0.33 ±0.20	-0.07 ±0.38	0.43 ±0.23	0.39	**0.0076**	-0.50	**<0.0001**	-0.11	0.19
intermediate-intermediate									
N. dutertrei-G. menardii	0.25 ±0.31	0.39 ±0.50	0.04 ±0.31	-0.15	0.43	0.35	**0.0048**	0.21	0.069
G. tumida-N. dutertrei	0.90 ±0.42	0.82 ±0.52	0.80 ±0.27	0.08	0.7	0.02	0.88	0.10	0.39
G. tumida-G. menardii	1.15 ±0.40	1.20 ±0.32	0.86 ±0.46	-0.06	0.72	0.34	**0.026**	0.28	0.093
G. scitula-G. menardii	1.66 ±0.45	1.67 ±0.44	0.70 ±0.49	-0.01	0.95	0.97	**<0.0001**	0.96	**0.0003**
G. scitula-N. dutertrei	1.42 ±0.42	1.33 ±0.39	0.92 ±0.42	0.08	0.64	0.41	**0.034**	0.49	**0.021**
G. scitula-G. tumida	0.52 ±0.11	0.55 ±0.28	0.25 ±0.64	-0.03	0.74	0.30	0.18	0.27	0.22
deep-deep									
G. crassaformis-G. truncatulinoides d.	0.62 ±0.33	0.76 ±0.55	0.46 ±0.36	-0.14	0.39	0.30	0.067	0.16	0.17
intermediate-shallow									
G. menardii-G. ruber p.	1.79 ±0.40	1.29 ±0.34	1.25 ±0.35	0.50	**0.003**	0.04	0.72	0.54	**0.0001**
G. menardii-G. ruber w.	1.35 ±0.49	0.78 ±0.55	1.18 ±0.37	0.57	**0.016**	-0.41	**0.0039**	0.17	0.25
G. menardii-G. sacculifer	1.03 ±0.34	0.85 ±0.24	0.76 ±0.37	0.18	0.14	0.08	0.45	0.26	0.051
N. dutertrei-G. ruber p.	2.04 ±0.34	1.67 ±0.42	1.29 ±0.22	0.36	**0.037**	0.39	**0.0001**	0.75	**<0.0001**
N. dutertrei-G. ruber w.	1.60 ±0.40	1.13 ±0.35	1.22 ±0.24	0.46	**0.0079**	-0.09	0.32	0.37	**0.0005**
N. dutertrei-G. sacculifer	1.27 ±0.30	1.21 ±0.40	0.80 ±0.18	0.06	0.69	0.41	**<0.0001**	0.47	**<0.0001**
G. tumida-G. ruber p.	2.88 ±0.24	2.46 ±0.34	2.06 ±0.38	0.42	**0.0032**	0.41	**0.0027**	0.82	**<0.0001**
G. tumida-G. ruber w.	2.50 ±0.20	1.92 ±0.47	1.98 ±0.42	0.58	**0.0019**	-0.06	0.69	0.52	**0.0007**
G. tumida-G. sacculifer	2.04 ±0.41	2.03 ±0.30	1.59 ±0.31	0.01	0.96	0.44	**0.0002**	0.45	**0.0003**
G. scitula-G. ruber p.	3.45 ±0.15	2.96 ±0.43	2.20 ±0.43	0.50	**0.0021**	0.76	**0.0006**	1.25	**<0.0001**
G. scitula-G. ruber w.	3.01 ±0.17	2.44 ±0.44	2.05 ±0.43	0.57	**0.0009**	0.39	0.054	0.96	**<0.0001**
G. scitula-G. sacculifer	2.69 ±0.17	2.52 ±0.35	1.70 ±0.45	0.17	0.17	0.82	**0.0001**	0.99	**<0.0001**
deep-intermediate									
G. truncatulinoides d.-*G. menardii*	1.49 ±0.21	1.85 ±0.38	1.81 ±0.49	-0.35	**0.027**	0.04	0.79	-0.31	0.083
G. truncatulinoides d.-*N. dutertrei*	1.27 ±0.40	1.46 ±0.39	1.76 ±0.31	-0.18	0.32	-0.31	**0.0078**	-0.49	**0.0005**
G. truncatulinoides d.-*G. tumida*	0.39 ±0.13	0.68 ±0.46	0.98 ±0.37	-0.28	0.11	-0.30	**0.037**	-0.58	**0.0001**
G. truncatulinoides d.-*G. scitula*	-0.11 ±0.12	0.23 ±0.44	0.82 ±0.51	-0.34	**0.048**	-0.59	**0.0091**	-0.93	**0.0002**
G. crassaformis-G. menardii	2.11 ±0.52	2.87 ±0.41	2.24 ±0.24	-0.76	**0.0028**	0.63	**<0.0001**	-0.13	0.37
G. crassaformis-N. dutertrei	1.87 ±0.45	2.50 ±0.45	2.23 ±0.17	-0.63	**0.0094**	0.27	**0.027**	-0.36	**0.0034**
G. crassaformis-G. tumida	0.96 ±0.24	1.70 ±0.38	1.49 ±0.32	-0.74	**0.0001**	0.21	0.18	-0.53	**<0.0001**
G. crassaformis-G. scitula	0.45 ±0.22	1.28 ±0.31	1.38 ±0.43	-0.82	**<0.0001**	-0.11	0.56	-0.93	**<0.0001**
deep-shallow									
G. truncatulinoides d.-*G. ruber* p.	2.99 ±0.42	3.14 ±0.50	3.06 ±0.36	-0.15	0.35	0.08	0.49	-0.07	0.55
G. truncatulinoides d.-*G. ruber* w.	2.90 ±0.24	2.63 ±0.38	2.99 ±0.39	0.28	0.083	-0.36	**0.0056**	-0.08	0.57
G. truncatulinoides d.-*G. sacculifer*	2.42 ±0.26	2.74 ±0.48	2.58 ±0.31	-0.32	**0.021**	0.16	0.15	-0.16	0.072
G. crassaformis-G. ruber p.	3.43 ±0.68	3.94 ±0.48	3.54 ±0.25	-0.51	**0.018**	0.41	**0.0027**	-0.11	0.5
G. crassaformis-G. ruber w.	3.47 ±0.24	3.58 ±0.38	3.44 ±0.23	-0.11	0.45	0.14	0.24	0.03	0.76
G. crassaformis-G. sacculifer	3.03 ±0.37	3.58 ±0.34	3.01 ±0.18	-0.55	**0.0001**	0.57	**<0.0001**	0.02	0.78

increases with increasing TCD from east to west (Figure 4.5). Based on measured δ^{18}O values (Figures 4.4, 4.5) and the pattern of changes in δ^{18}O, the foraminiferal species investigated in this study can be devided into three groups:

G. ruber pink and white, and *G. sacculifer*

δ^{18}O values of the shallow-dwelling foraminifera *G. ruber* pink and white, and *G. sacculifer* reveal comparable patterns, showing lowest δ^{18}O for *G. ruber* pink (δ^{18}Orubp) and highest δ^{18}O for *G. sacculifer* (δ^{18}Osac) (Figure 4.4; Table 4.4). In the eastern and central Atlantic (10°E–20°W), δ^{18}O values of the shallow-dwelling foraminifera show no significant longitudinal changes. From 20°W to 50°W, mean δ^{18}O values of *G. ruber* pink and *G. sacculifer* decrease by 0.35‰ (Figure 4.5a,b; Table 4.4), most likely due to an increase of upper ocean temperature. In contrast, east and west Atlantic mean δ^{18}O values of *G. ruber* white ($\delta^{18}O_{rubw}$) do not differ significantly (Table 4.4). In the Caribbean (west of 60°W), the mean δ^{18}O values *G. ruber* pink and *G. sacculifer* are slightly higher (~0.1–0.2‰) than in the western Atlantic, whereas the mean $\delta^{18}O_{rubw}$ are lower by 0.3‰ (Figure 4.5a,b; Table 4.4). An increase in mean δ^{18}O values towards the Caribbean may be attributed either to higher salinity values in the Caribbean basin (Figure 4.2b) or to an increase in the calcification depth of the shallow dwellers, determining calcification in cooler subsurface waters (Figure 4.5a,b). These factors contribute to an underestimation of the east-west SST increase of 4°C (Figure 4.2a) in the δ^{18}O signal of shallow-dwelling species. A general increase in estimated calcification depths coincides with increasing TCD (from east to west) (Figure 4.5a,b), yet estimates of absolute calcification depths derived from the (*Shackleton*, 1974) (Figure 4.5a) and (*Mulitza et al.*, 2004) (Figure 4.5b) δ^{18}O-paleotemperature equations differ significantly from each other. Using the shackleton (1974) equation, ~75% of the measured $\delta^{18}O_{rubp}$ values and 50% of the $\delta^{18}O_{rubw}$ values are lower than those predicted for the sea surface (Figure 4.5a). This mismatch is strong in the eastern and central Atlantic, whereas in the Caribbean, calcification depths of *G. sacculifer* and *G. ruber* pink/white are estimated to ~30–100 m and to up to 75 m, respectively. Using the δ^{18}O-paleotemperature equation of *Mulitza et al.* (2004), estimated calcification depths are higher than those derived from the equation of *Shackleton* (1974), and *G. ruber* pink/white samples with lower δ^{18}O than predicted for the sea surface are restricted to the eastern Atlantic (Figure 4.5b). Calculated after the *Mulitza et al.* (2004) δ^{18}O-paleotemperature equation, estimated calcification depths in the eastern and central Atlantic reach up to 50 m for *G. ruber* (pink/white) and ~75 m for *G. sacculifer* and are, thus, comparable to the habitat depths determined by plankton tows (Figure 4.3). In the Caribbean, estimated calcification depth increases to up to 150 m for *G. ruber* pink/white and 200 m for *G. sacculifer* (Figure 4.5b). The δ^{18}O signal recorded in the tests of the shallow-dwelling species corresponds roughly to predicted δ^{18}O values at depth of the chlorophyll maximum (Figure 4.3), implying that the shallow-dwelling foraminifera may exploit the chlorophyll maximum as food source like previously suggested by (e.g., *Fairbanks et al.*, 1982; *Kohfeld et al.*, 1996; *Schiebel et al.*, 2001).

G. menardii, *N. dutertrei*, *G. tumida*, and *G. scitula*

In general, the $\delta^{18}O$ patterns of *G. menardii* ($\delta^{18}O_{men}$), *N. dutertrei* ($\delta^{18}O_{dut}$), *G. tumida* ($\delta^{18}O_{tum}$), and *G. scitula* ($\delta^{18}O_{sci}$) show a gradual decrease in $\delta^{18}O$ with increasing TCD from east to west (Figure 4.4; Table 4.4). This trend is strongest for $\delta^{18}O_{sci}$ (Figure 4.5c). In the eastern Atlantic (10°W), absolute $\delta^{18}O_{sci}$ values are similar to those of the deep dweller *G. crassaformis* ($\delta^{18}O_{cras}$). Mean $\delta^{18}O_{sci}$ decreases by 0.6‰ from the eastern Atlantic (10°W) to the western Atlantic (30–50°W), and by another 0.7‰ towards the Caribbean (west of 60°W) (Figure 4.5c; Table 4.4). The estimated calcification depth of *G. scitula*, however, does not change significantly across the Atlantic, and varies between 75–200 m in the eastern Atlantic and 125–200 m in the Caribbean, which is shallower than suggested by *Hemleben and Spindler* (1983), *Ortiz et al.* (1992), and *Niebler et al.* (1999) (Figure 4.3). Therefore, the east-west $\delta^{18}O$ decrease recorded by *G. scitula* can mainly be attributed to subsurface warming at a relatively constant depth level. $\delta^{18}O_{tum}$ shows a pattern similar to that of *G. scitula*, whereas the total decrease in $\delta^{18}O_{tum}$ towards the west is lower than that recorded by *G. scitula* (Figure 4.5c). Compared to *G. scitula*, mean $\delta^{18}O_{tum}$ decreases only slightly (∼0.2‰) from the western Atlantic (30–50°W) into the Caribbean (west of 60°W). Furthermore, $\delta^{18}O$ variability of *G. tumida* is significantly higher than that recorded by *G. scitula*, especially in the western Atlantic (up to 1.5‰ between 20–40°W). This may partly be caused by the fact that the number of specimens of *G. scitula* measured in each sample is 4 times higher than that of *G. tumida* (Chapter 4.3), which probably reduces the variability inherent to fossil foraminiferal populations. Comparison of measured and predicted $\delta^{18}O$ suggests a minor increase in calcification depths of *G. tumida* across the Atlantic (from ∼125–200 m in the eastern Atlantic to 150–250 m in the Caribbean (Figure 4.5c)). Only samples from the western Atlantic (20–40°W) with exceptionally low $\delta^{18}O_{tum}$ values indicate shallower calcification close to the BOPZ (75–125 m), which was suggested as preferential habitat of *G. tumida* (*Ravelo and Fairbanks*, 1992) (Figure 4.3). This implies that *G. tumida* predominantly records subsurface warming at a relatively constant depth level below the BOPZ. $\delta^{18}O$ of the thermocline dwellers *G. menardii* and *N. dutertrei* decreases by 0.5–0.6‰ from the eastern (10°W) to the western Atlantic (30–50°W). This trend is more pronounced in *G. menardii* possibly because the variability of $\delta^{18}O_{dut}$ is significantly higher, especially in the western Atlantic (-0.7‰ to +0.7‰ in $\delta^{18}O_{dut}$ compared to -1.0 to -0.3‰ in $\delta^{18}O_{men}$) (Figure 4.5c). West of 60°W, the mean $\delta^{18}O_{dut}$ values show a small decrease (0.2‰), while $\delta^{18}O_{men}$ increases by ∼0.1‰ (similar to what is observed in the $\delta^{18}O$ pattern of the shallow-dwelling species). Comparison of measured and predicted $\delta^{18}O_{calcite}$ indicates that the calcification depth of the thermocline dwellers increases with increasing TCD from 50–100 m (50–125 m) in the eastern Atlantic to 75–200 m (100–200 m) in the Caribbean for *G. menardii* (*N. dutertrei*) (Figure 4.5c). This confirms the suggestion that the habitat of these species is coupled to TCD (e.g., *Curry and Matthews*, 1981a,b; *Curry et al.*, 1983; *Sautter and Thunell*, 1991a; *Ravelo and Fairbanks*, 1992) (Figure 4.3). The associated migration to deeper habitats with increasing TCD may therefore reduce the effect of subsurface warming and thermocline deepening across the Atlantic on the $\delta^{18}O$ signal of the thermocline dwellers (i.e.

compared to $\delta^{18}O_{sci}$). Nonetheless, the mean $\delta^{18}O$ decrease of ~0.7‰ from east to west recorded by *N. dutertrei* indicates a significant increase in calcification temperature with increasing TCD, since it cannot be attributed to a decrease in thermocline salinity (Figure 4.2b). This contradicts the assumption that *N. dutertrei* tends to calcify within a very narrow temperature range (e.g., *Curry and Matthews*, 1981a,b; *Curry et al.*, 1983; *Sautter and Thunell*, 1991a; *Ravelo and Fairbanks*, 1992).

G. truncatulinoides dextral and *G. crassaformis*

The effect of longitudinal changes in upper-ocean stratification on the $\delta^{18}O$ pattern of the deep dwellers *G. crassaformis* and *G. truncatulinoides*, which predominantly calcify well below the seasonal thermocline, is weaker than that observed for shallow and intermediate dwellers (Figure 4.5d). The $\delta^{18}O$ values of *G. crassaformis* ($\delta^{18}O_{cras}$) show relatively large variations (2‰ to 0.7‰) in the eastern Atlantic (0–20°E). In the eastern and western Atlantic, $\delta^{18}O_{cras}$ is more or less constant, whereas towards the Caribbean (west of 60°W), mean $\delta^{18}O_{cras}$ decreases by 0.4‰ (Table 4.4). The estimated calcification depth of *G. crassaformis* generally lies between 250 m and 600 m in the eastern and western Atlantic and between 400 m and 600 m in the Caribbean (e.g., *Schmuker and Schiebel*, 2002; *Anand et al.*, 2003) (Figure 4.3). The only exception are two samples from the eastern Atlantic that suggest calcification in very shallow water depths of 50–75 m, which is consistent with some shallow ocurrence of *G. crassaformis* in the eastern Atlantic observed by *Kemle von Mücke and Oberhänsli* (1999). The decrease in $\delta^{18}O_{cras}$ within the Caribbean therefore probably results from warming at the depth level of the permanent thermocline (Figures 4.2a, 4.5d). The longitudinal $\delta^{18}O$ pattern observed in *G. truncatulinoides* dextral ($\delta^{18}O_{trunc}$) is similar to that of *G. crassaformis*, although the variability in $\delta^{18}O_{trunc}$ is much higher and mean $\delta^{18}O$ values of *G. truncatulinoides* dextral do not decrease significantly towards the Caribbean, which may be caused by an increase in the estimated calcification depth of *G. truncatulinoides* dextral from 125–300 m in the eastern and western Atlantic to 250–400 m in the Caribbean (Figure 4.5d). *Mulitza et al.* (1997) suggested that the estimated calification depth of *G. truncatulinoides* dextral represents a mean of different calcification depths. Accordingly, the facts that initial parts of the calcite tests of *G. truncatulinoides* are built shallower in the water column, and that encrustation takes place in deeper water later during its lifecycle (e.g., *Mulitza et al.*, 1997; *LeGrande et al.*, 2004) (Figure 4.3), may attribute to the comparatively large scatter in the $\delta^{18}O$ values of *G. truncatulinoides* dextral.

4.4.2 $\delta^{18}O$ Gradients Between Planktonic Foraminifera With Different Preferential Habitats

Whereas the $\delta^{18}O$ values of single foraminiferal species provide information about changes in the calcification temperature at a specific depth level (taking into account that the calcification depth of individual species can change when hydrographic conditions change), $\delta^{18}O$ gradients between planktonic foraminiferal species with different preferential calcification depths yield

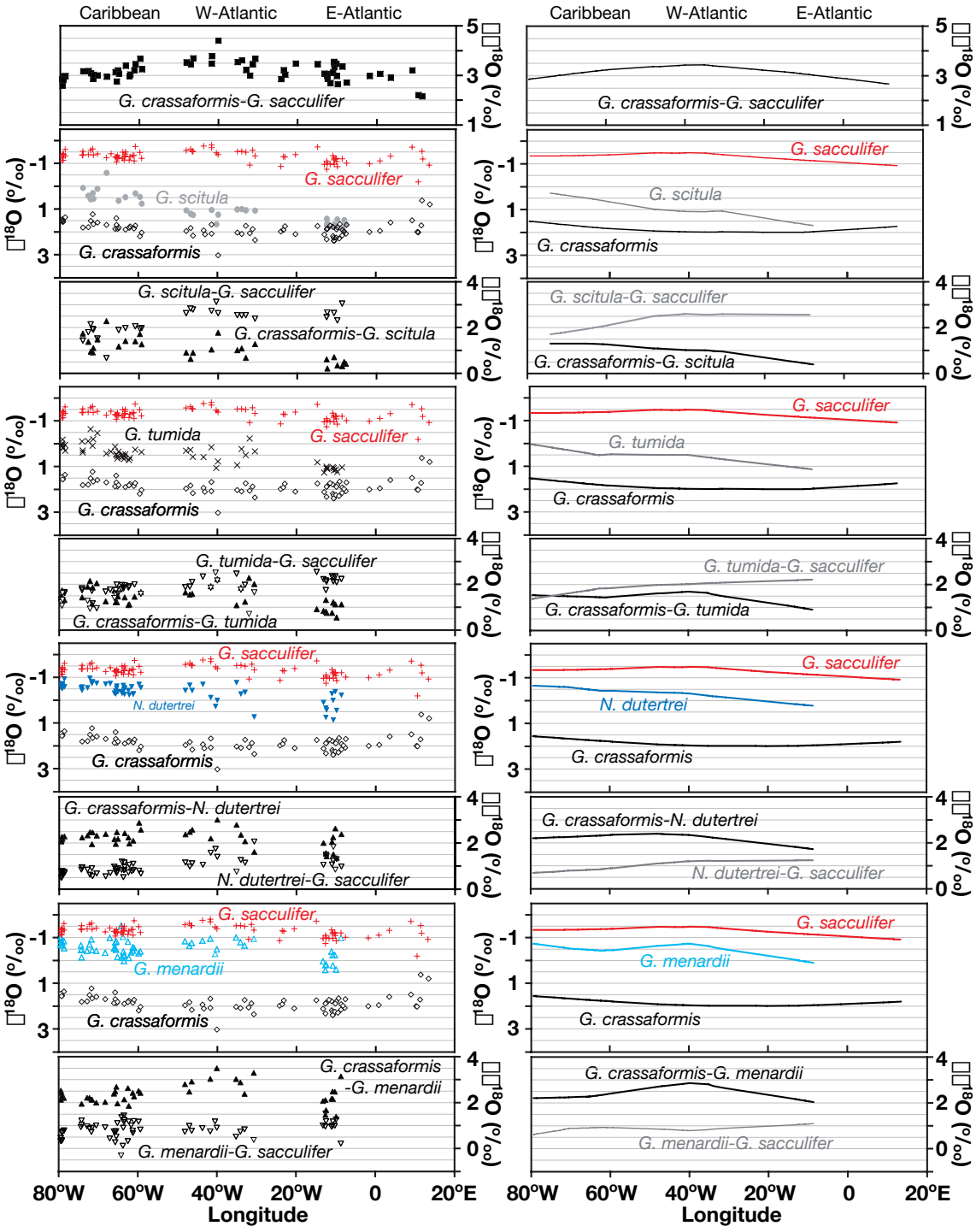

Figure 4.6 δ^{18}O values of *G. sacculifer* (positive signs) and *G. crassaformis* (white diamonds), δ^{18}O values of the intermediate dwellers *G. menardii* (white triangles), *N. dutertrei* (gray inverse triangles), *G. tumida* (crosses), and *G. scitula* (gray circles), and the δ^{18}O gradients between intermediate dwellers and *G. sacculifer* (white inverse triangles) and between *G. crassaformis* and intermediate dwellers (black triangles); plotted *vs.* the longitudinal position of core-top samples. Left: measured δ^{18}O values and calculated gradients for each station. Right: Trends of δ^{18}O patterns and δ^{18}O gradients along the E-W transect. We smoothed the data by using the locally weighted least squared error method (e.g., *Cleveland*, 1979) and applying a smoothing factor of 60%.

information about vertical temperature gradients in the upper water column. One important precondition for the use of this method is that depth stratification of different species relative to each other remains more or less constant in different hydrographic regimes (Figures 4.3, 4.4). The mean $\Delta\delta^{18}$O for the eastern and western Atlantic and for the Caribbean, as well as the differences in $\Delta\delta^{18}$O between the different regions are shown in Table 4.4 for all species used in this study. We consider $\Delta\delta^{18}$O between different groups of planktonic foraminifera with similar δ^{18}O patterns to be most significant (shallow, intermediate, and deep dwellers; Table 4.4). The δ^{18}O gradients between foraminifera of the same group are often smaller than the scatter in measured δ^{18}O values of single species and result in large uncertainties concerning the evaluation of interspecific $\Delta\delta^{18}$O (Table 4.4).

Since the highest sensitivity to changes in upper-ocean stratification and TCD across the tropical Atlantic is given for δ^{18}O patterns of foraminiferal species with intermediate calcification depths (Chapter 4.4.1; Figure 4.5c; Table 4.4), we exemplarely show the $\Delta\delta^{18}$O between each of the intermediate-dwelling species (*G. menardii*, *N. dutertrei*, *G. tumida*, *G. scitula*) and the shallow dweller *G. sacculifer* ($\Delta\delta^{18}O_{intermediate-sacc}$) as well as $\Delta\delta^{18}$O between each of the intermediate-dwelling species and the deep dwellers *G. crassaformis* ($\Delta\delta^{18}O_{cras-intermediate}$) and *G. truncatulinoides* dextral ($\Delta\delta^{18}O_{trunc-intermediate}$) (Figures 4.6, 4.7). The δ^{18}O patterns and absolute δ^{18}O values of the shallow-dwelling species, especially *G. ruber* pink and *G. sacculifer*, along the E-W transect are similar. Hence, the use of both species for the calculation of intraspecific $\Delta\delta^{18}$O produces similar results (Table 4.4). We chose *G. sacculifer* as representative for the group of shallow dwellers for the following reasons: (1) The eastern Atlantic δ^{18}O values of *G. ruber* pink are often lower than predicted for the sea surface (Figure 4.5a,b), This leads to uncertainties concerning the evaluation of $\Delta\delta^{18}$O, although the $\Delta\delta^{18}$O between the intermediate dwellers and the shallow dwellers are highest for *G. ruber* pink (Table 4.4). (2) The western Atlantic δ^{18}O values of *G. ruber* white are relatively high compared to the longitudinal δ^{18}O trends observed in *G. ruber* pink and *G. sacculifer* (Figure 4.5a,b; Table 4.4), resulting in a relatively strong decrease in $\Delta\delta^{18}$O between *G. ruber* white and the intermediate dwellers between the eastern and western Atlantic, but to a smaller and statistically less significant decrease in $\Delta\delta^{18}$O between the western Atlantic and the Caribbean. (3) For paleoceanographic studies, the advantage of *G. sacculifer* is given by its relatively long fossil record, reaching back into the early Miocene (*Kennett and Srinivasan*, 1983), whereas *G. ruber* white does not constantly occur during the early Pliocene (e.g., *Chaisson and Ravelo*, 2000), and the last occurrence date of *G. ruber* pink is 0.12 Ma in Pacific and Indian Ocean samples (*Thompson et al.*, 1979). In general, $\Delta\delta^{18}$O between shallow and intermediate dwellers significantly decreases from east to west (with increasing TCD; Figures 4.6, 4.7; Table 4.4), whereas $\Delta\delta^{18}$O between deep and intermediate dwellers increases with increasing TCD (Figures 4.6, 4.7). These changes in $\Delta\delta^{18}$O are highest and statistically significant for $\Delta\delta^{18}O_{sci-shallow}$, $\Delta\delta^{18}O_{deep-sci}$, as well as for $\Delta\delta^{18}O_{tum-shallow}$, $\Delta\delta^{18}O_{deep-tum}$, and for the δ^{18}O gradients between *N. dutertrei* and shallow- and deep dwellers (Figures 4.6, 4.7; Table 4.4). The longitudinal changes in $\Delta\delta^{18}O_{men-shallow}$ and $\Delta\delta^{18}O_{deep-men}$, however, are lower in absolute values and statistically less justified (Table 4.4).

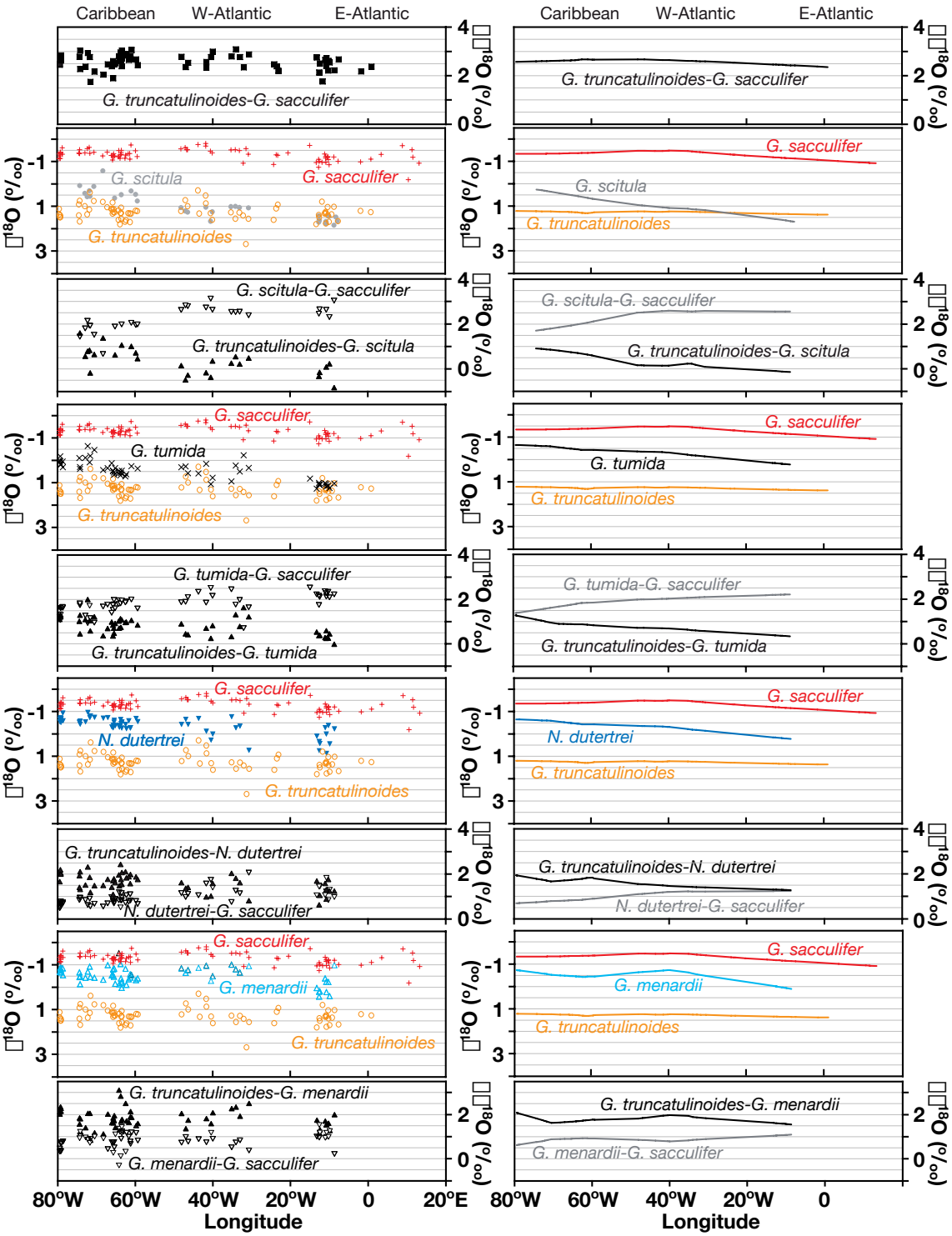

Figure 4.7 δ^{18}O values of *G. sacculifer* (positive signs) and *G. truncatulinoides* (white circles), δ^{18}O values of the intermediate dwellers *G. menardii* (white triangles), *N. dutertrei* (gray inverse triangles), *G. tumida* (crosses), and *G. scitula* (gray circles), and δ^{18}O gradients between the intermediate dwellers and *G. sacculifer* (white inverse triangles) and between *G. truncatulinoides* and the intermediate dwellers (black triangles); plotted *vs.* the longitudinal position of core-top samples. Left: measured δ^{18}O values and calculated gradients for each station. Right: Trends of δ^{18}O patterns and δ^{18}O gradients along the E-W transect. We smoothed the data by using the locally weighted least squared error method (e.g., *Cleveland*, 1979) and applying a smoothing factor of 60%.

4.4.3 Longitudinal Changes of δ^{13}C and Comparison to Modern Phosphate Concentrations

$\delta^{13}C_{seawater}$ is related to nutrient concentrations, since it is influenced by organic production and remineralization in near-constant proportion to nutrients. Thus, comparison of $\delta^{13}C_{calcite}$ of specific planktonic foraminiferal species (Figure 4.8) with phosphate concentrations (woa01, 2001) at their estimated calcification depth (Figure 4.2c) may provide information about the use of planktonic foraminiferal δ^{13}C for the detection of changes in the nutrient concentration at specific water depth levels. It is, thus, commonly assumed that the most positive δ^{13}C values correspond to the nutrient-depleted surface mixed-layer, and that lowest δ^{13}C values occur at greater depths, where the nutrient supply and recycling is highest. This pattern is generally reflected by our data, except for *G. tumida*. The δ^{13}C values of *G. tumida* ($\delta^{13}C_{tum}$) are higher then expected for its deep habitat (Figures 4.3, 4.8), whereas the δ^{13}C values of *G. scitula* ($\delta^{13}C_{sci}$) are relatively too low (Figures 4.3, 4.8). The relationship between measured δ^{18}O and δ^{13}C (Figure 4.9) corroborates these results, as δ^{13}C generally decreases with increasing δ^{18}O (decreasing calcification temperature due to increasing calcification depth). The linear correlation between $\delta^{13}C_{sci}$ and $\delta^{18}O_{sci}$, however, is striking (Figure 4.9), and suggests that incorporation of ^{13}C into the calcite test of *G. scitula* is strongly depending on calcification temperature. Considering the temperature-equation of *Shackleton* (1974), the relationship is similar to that observed for *Globigerinoides bulloides* (0.11‰ per 1°C), which likely results from incorporation of more respired CO_2 into shell carbon at higher metabolic rates (*Bemis et al.*, 2000). Therefore, we assume that δ^{13}Csci provides basically no information about changes in the nutrient composition of ambient seawater, and we will hence not consider δ^{13}Csci in the following discussion. Based on the pattern of changes in δ^{13}C along the E-W transect, the planktonic foraminiferal species used in this study can be divided in 2 groups (Figure 4.10; Table 4.5):

G. ruber (pink/white), *G. sacculifer*, *G. menardii*, and *N. dutertrei*

In general, the shallow-dwellers *G. ruber* (pink/white), *G. sacculifer* and the intermediate dwellers *G. menardii*, and *N. dutertrei* show a small increase in δ^{13}C (<0.2‰) from the eastern to the western Atlantic (10–50°W) which is consistent with thickening of the nutrient-poor surface mixed-layer (phosphate concentrations <0.5 μmol/mol; Figures 4.2c, 4.10) and a general decrease in δ^{13}C between the tropical western Atlantic and Caribbean (0.2 to 0.35‰), whereas the δ^{13}C variability strongly increases west of 60°W. The decrease in mean δ^{13}C towards the Caribbean (Table 4.5) and the high Caribbean δ^{13}C variability observed in *G. ruber* (pink/white), *G. sacculifer*, *G. menardii*, and *N. dutertrei* (Figure 4.10) are not consistent with changes in the nutrient concentration (Figure 4.10). In the Caribbean basin, the nutrient-depleted surface mixed-layer (phosphate conc. <0.5 μmol/mol) reaches down to more than 150 m (Figures 4.2c, 4.10), and is, thus, generally deeper than the habitat of the shallow dwellers *G. ruber* (pink/white) and *G. sacculifer*. Accordingly, the δ^{13}C values of these species should be high. In the Caribbean, however, low phosphate concentrations at the estimated calcification depth of the shallow dwellers

Table 4.5 Species-specific averages ±standard deviations of the planktonic foraminiferal δ^{13}C values from the different study areas. In addition, the differences between the regional δ^{13}C averages are given. Related probability (p) values, if >0.05 (<0.05, bold face), indicate that the regionally restricted data sets are similar (significantly different from each other).

Species	Averages ±standard deviations			Difference between averages					
	E-Atlantic	W-Atlantic	Caribbean	W-Atlantic/ E-Atlantic		Caribbean/ W-Atlantic		Caribbean/ E-Atlantic	
	□^{13}C	□^{13}C	□^{13}C	□^{13}C	p value	□^{13}C	p value	□^{13}C	p value
G. ruber p.	1.50 ±0.33	1.75 ±0.31	1.54 ±0.34	0.25	**0.0075**	-0.21	**0.026**	0.04	0.6
G. ruber w.	1.80 ±0.12	1.75 ±0.20	1.41 ±0.31	-0.04	0.54	-0.34	**0.0004**	-0.38	**0.0004**
G. sacculifer	1.74 ±0.37	1.90 ±0.34	1.67 ±0.27	0.16	0.16	-0.22	**0.012**	-0.07	0.41
G. menardii	1.61 ±0.16	1.84 ±0.18	1.53 ±0.21	0.23	**0.004**	-0.31	**<0.0001**	-0.08	0.26
N. dutertrei	1.74 ±0.16	1.89 ±0.16	1.51 ±0.21	0.15	**0.038**	-0.37	**<0.0001**	-0.23	**0.0031**
G. tumida	1.73 ±0.11	1.96 ±0.11	1.87 ±0.14	0.23	**<0.0001**	-0.08	0.07	0.14	**0.0054**
G. scitula	-0.03 ±0.13	-0.15 ±0.11	-0.41 ±0.23	-0.12	**0.028**	-0.27	**0.0015**	-0.38	**0.0003**
G. truncatulinoides d.	0.78 ±0.16	0.92 ±0.16	1.20 ±0.17	0.14	**0.012**	0.28	**<0.0001**	0.43	**<0.0001**
G. crassaformis	0.93 ±0.14	1.19 ±0.13	1.10 ±0.10	0.26	**<0.0001**	-0.09	**0.02**	0.17	**<0.0001**

roughly correlate to low δ^{13}C values. In addition, regional variations in phosphate concentration at the estimated calcification depth of the shallow dwellers *G. ruber* (pink/white) and *G. sacculifer* are relatively small (Figure 4.10). Local variations in phosphate concentrations at the habitat depth of the thermocline dwellers are higher, and maximum phosphate concentrations are higher than in the western Atlantic and Caribbean (Figure 4.3). Local changes in Caribbean nutrient concentrations can, thus, possibly contribute to the variability of δ^{13}C in *G. menardii* ($\delta^{13}C_{men}$) and *N. dutertrei* ($\delta^{13}C_{dut}$). At large, however, the reasons for the high variability in Caribbean δ^{13}C, and especially for the low δ^{13}C values of the shallow dwellers *G. ruber* pink/white and *G. sacculifer*, remain enigmatic. Core-top stations with particularly low δ^{13}C values are located close to the northern part of the Antilles island arc (for *G. ruber* pink/white, *G. sacculifer*, *G. menardii*, and *N. dutertrei*), and in the central Colombian Basin (with the exception of *G. sacculifer*). As the core-top stations with low δ^{13}C values are not restricted to near-shore areas, we cannot attribute low δ^{13}C values solely to coastal upwelling or enhanced nutrient input from land. Freshwater input from the Amazon and Orinoco Rivers may serve as potential source for low δ^{13}C values, as it contains large amounts of remineralized organic material. However, although Amazon and Orinoco river water can be traced into the central Caribbean (∼75°W (*Hellweger and Gordon*, 2002)), it is difficult to explain the regional variations in Caribbean δ^{13}C by different amounts of freshwater input. We also cannot exclude that different ages of Caribbean core-tops may contribute to the scatter in δ^{13}C of shallow and thermocline dwellers (and especially to the low δ^{13}C values) in the Caribbean basins, since only seven Caribbean core-top samples are radiocarbon-dated (ages vary between recent and 2.5 kyrs; Table 4.1). On the one hand, core tops with deglacial age (or the admixture of reworked older material) may reduce the δ^{13}C values of calcite. On the other hand, a high amount of foraminifera with post-anthropogenic age can lower the δ^{13}C values of shallow- and intermediate dwelling foraminifera, since post-anthropogenic δ^{13}C

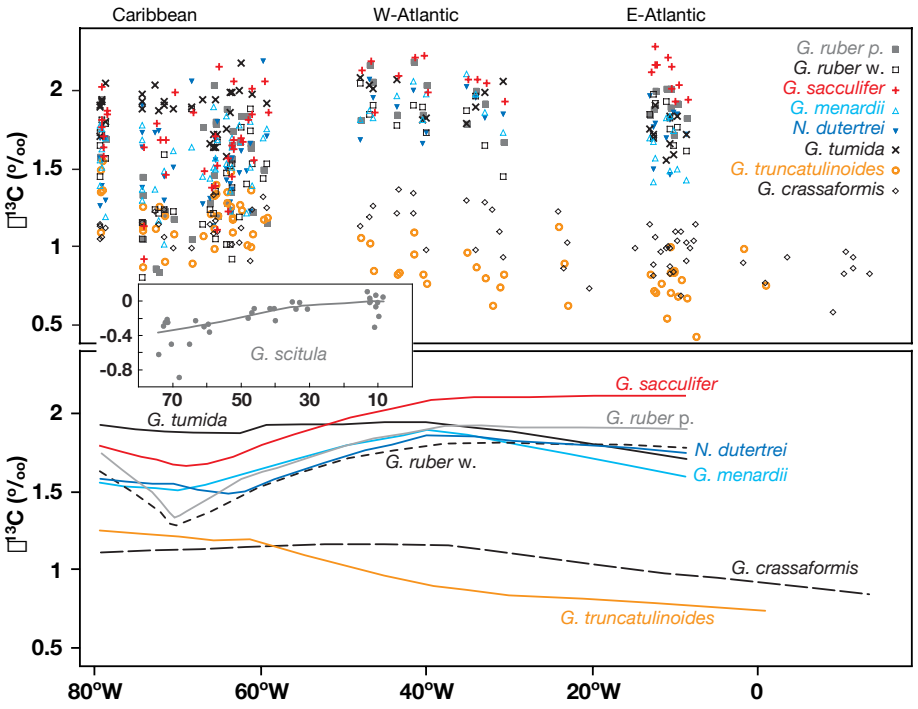

Figure 4.8 Top: Measured planktonic foraminiferal δ^{13}C values plotted *vs.* the longitudal position of the core-top samples. Gray squares: *G. ruber* (pink); white squares: *G. ruber* (white); red positive signs: *G. sacculifer*; light blue triangles: *G. menardii*; blue inverse triangles: *N. dutertrei*; crosses: *G. tumida*; gray dots: *G. scitula*; orange circles: *G. truncatulinoides* dextral; white diamonds: *G. crassaformis*. In general, the δ^{13}C values decrease with increasing preferential habitat depth (Figure 4.3); except for *G. tumida*, whose δ^{13}C values are too high with respect to its relatively deep habitat, and for *G. scitula*; whose δ^{13}C values are exceptionally low. Bottom: Trends of δ^{13}C changes along the E-W transect. We smoothed the data by using the locally weighted least squared error method (e.g., *Cleveland*, 1979) and applying a smoothing factor of 60%.

within the upper ocean is lowered by up to 0.8‰ due to the uptake of atmospheric CO_2 with low δ^{13}C values (Suess-Effect (*Keeling*, 1979; *Böhm et al.*, 1996)).

G. tumida, *G. truncatulinoides* dextral, and *G. crassaformis*

The pattern of longitudinal changes in δ^{13}C of *G. tumida* and of the deep dwellers *G. truncatulinoides* and *G. crassaformis* is opposite to that observed in the shallow-dwellers and in the thermocline dwellers *G. menardii* and *N. dutertrei* (Figure 4.10; Table 4.5). In general, the mean $\delta^{13}C_{tum}$, $\delta^{13}C_{trunc}$ and $\delta^{13}C_{cras}$ values increase from east to west. *G. tumida* shows a small increase in δ^{13}C between the eastern and western Atlantic (0.23‰) and a minor decrease towards the Caribbean (<0.1‰), whereas the scatter of $\delta^{13}C_{tum}$ in the Caribbean region is relatively low compared to *G. ruber* (pink/white), *G. sacculifer*, *G. menardii*, and *N. dutertrei*. Similar to $\delta^{13}C_{tum}$, a prominent increase in the mean δ^{13}C of *G. crassaformis* occurs only between the eastern and western Atlantic (0.26‰), whereas mean δ^{13}C of *G. truncatulinoides* dextral decreases

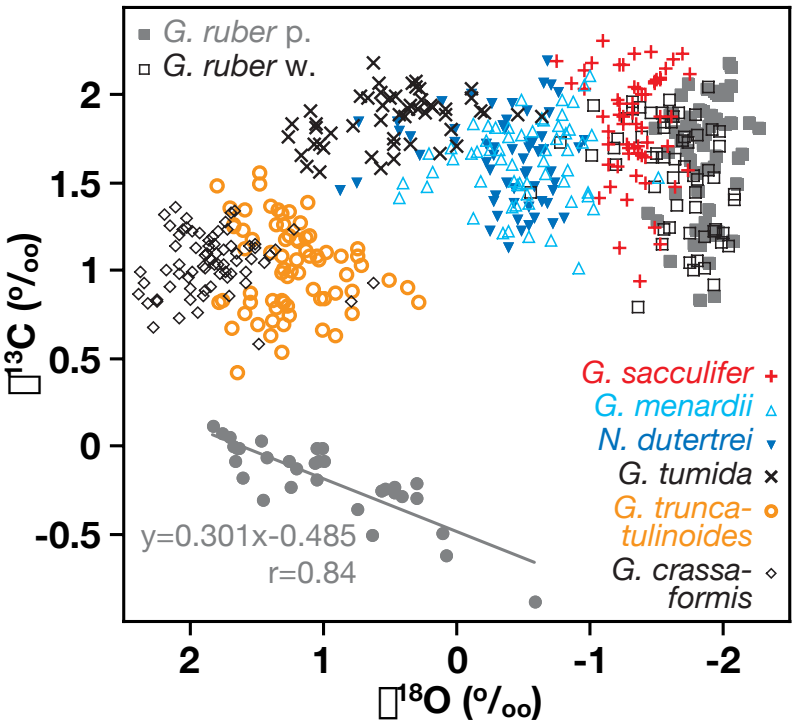

Figure 4.9 δ^{13}C values of the foraminiferal species used in this study *vs.* δ^{18}O values. Gray squares: *G. ruber* (pink); white squares: *G. ruber* (white); red positive signs: *G. sacculifer*; light blue triangles: *G. menardii*; blue inverse triangles: *N. dutertrei*; crosses: *G. tumida*; gray dots: *G. scitula*; orange circles: *G. truncatulinoides*; white diamonds: *G. crassaformis*. In general, δ^{13}C increases with dereasing δ^{18}O. However, the δ^{13}C values of *G. tumida* are relatively high with respect to its low δ^{18}O values, and the linear relationship of δ^{13}C and δ^{18}O observed in *G. scitula* suggests that the incorporation of ^{13}C into the calcite test strongly depends on calcification temperature.

by 0.14‰ between the eastern and western Atlantic, and by 0.28‰ between the western Atlantic and the Caribbean (Figure 4.10; Table 4.5). The variability in δ^{13}C is significantly smaller than observed for the shallow and intermediate dwellers, and does not change significantly between the different hydrographic regions. *Ravelo and Fairbanks* (1995) suggested that fractionation of δ^{13}C in the carbonate shells of *G. truncatulinoides* dextral and *G. crassaformis* is temperature-dependent, whereas lower δ^{13}C values correspond to higher temperatures. This mechanism, however, cannot account for the observed increase in δ^{13}C within the western Atlantic and Caribbean, as the corresponding decrease in the Caribbean δ^{18}O values of *G. truncatulinoides* dextral and *G. crassaformis* most likely results from a temperature increase at the depth of calcification (Figures 4.2a, 4.5c). Comparison with phosphate concentrations along the transect rather implies that the δ^{13}C increase towards the west reflects an increase in $\delta^{13}C_{DIC}$ at the estimated calcification depth of *G. crassaformis* and *G. truncatulinoides* dextral, which probably results from a decrease in nutrient concentrations in concert with warming of the permanent thermocline.

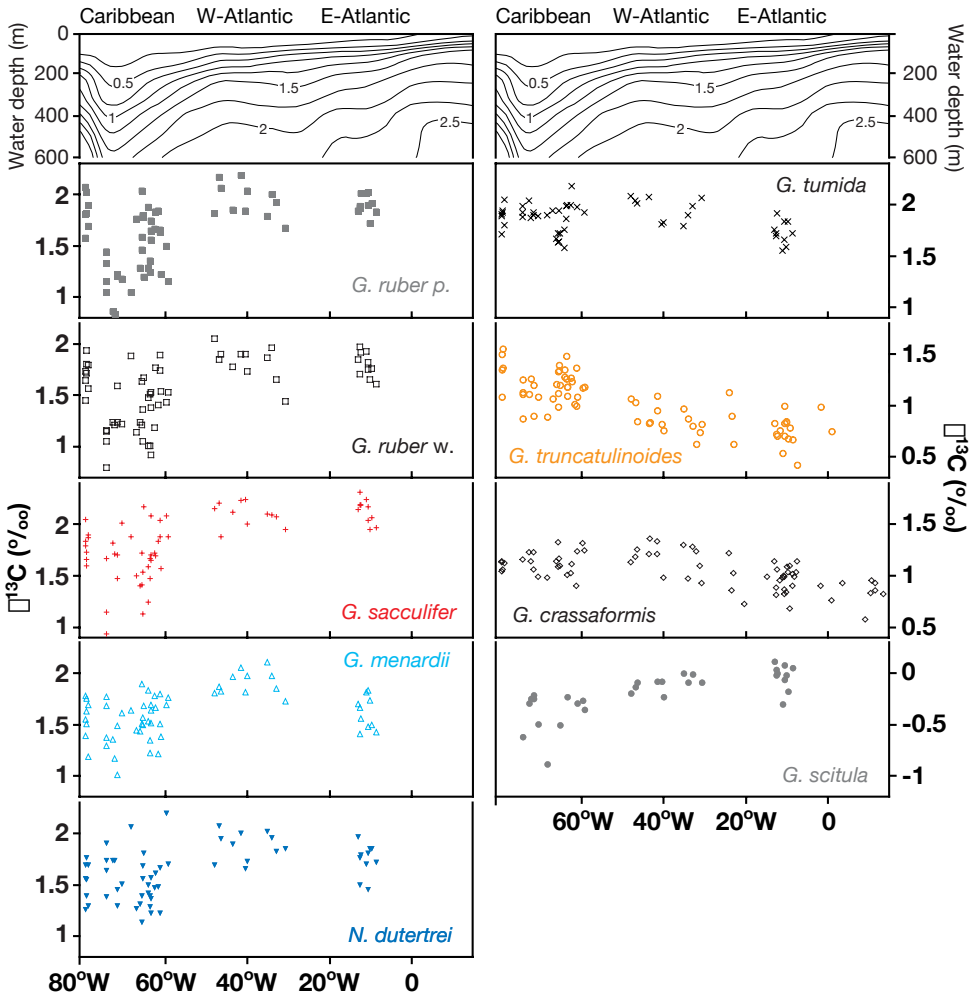

Figure 4.10 Measured planktonic foraminiferal δ^{13}C values for each species *vs.* the longitudal position of core-top samples used in this study. The phosphate concentrations (μmol/L) (*NODC*, 2001) for the upper 600 m of the tropical Atlantic and Caribbean water column are given for comparison on top of the figure.

4.4.4 δ^{13}C gradients between planktonic foraminifera with different preferential habitats

Changes in δ^{13}C gradients between shallow- and deep-dwelling planktonic foraminifera may provide information about changes in vertical nutrient gradients that result from mixing of nutrient-rich intermediate-water and nutrient-poor surface-water. However, 'vital effects' result in disequilibria from $\delta^{13}C_{DIC}$, which complicates the interpretation of $\Delta\delta^{13}$C between individual foraminiferal species (e.g., *Shackleton and Vincent*, 1978; *Fairbanks et al.*, 1982; *Ravelo and Fairbanks*, 1995; *Spero and Lea*, 1993; *Mulitza et al.*, 1999; *Bemis et al.*, 2000). These 'vital effects' are only partly understood. They include kinetic fractionation effects, photosynthetic activity of symbionts, and/or utilisation of metabolic CO_2 during shell growth (*Spero and Lea*, 1993; *Bemis et al.*, 2000). Apparent disequilibria from $\delta^{13}C_{DIC}$ can also result from size-related

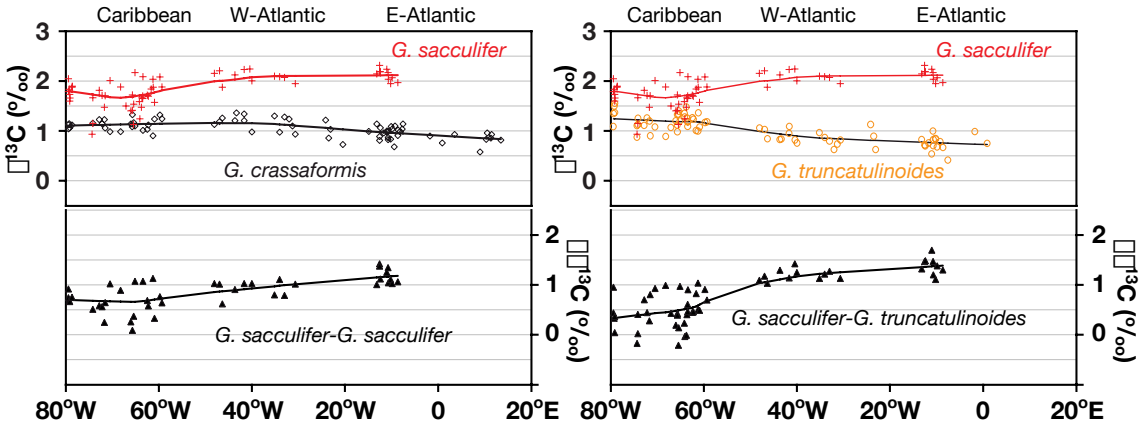

Figure 4.11 Left: (top) δ^{13}C values of *G. sacculifer* (positive signs) and *G. crassaformis* (white diamonds) and the δ^{13}C gradient between *G. sacculifer* and *G. crassaformis* (bottom; black triangles) *vs.* longitudinal position of the core-top samples. Right: (top) δ^{13}C values of *G. sacculifer* (crosses) and *G. truncatulinoides* (white circles) and the δ^{13}C gradient between *G. sacculifer* and *G. truncatulinoides* (bottom; black triangles) plotted *vs.* longitudinal position of the core-top samples. Solid lines show the trends of δ^{13}C patterns and δ^{13}C gradients along the E-W transect. We smoothed the data by using the locally weighted least squared error method (e.g., *Cleveland*, 1979) and applying a smoothing factor of 60%.

variations in foraminiferal species, or from changes in the calcification depth over the course of their lifecycle (e.g., *Ravelo and Fairbanks*, 1995; *Mulitza et al.*, 1999).

Thus, we focus on a more general comparison of measured vertical δ^{13}C to changes in vertical nutrient gradients (Figures 4.8, 4.10). Figure 4.8 indicates that $\Delta\delta^{13}$C between shallow, deep, and intermediate dwellers decreases with increasing TCD from east to west, consistent with a decrease in the nutrient gradient between the (nutrient-poor) sea-surface and ~600 m water depth (assumed deepest habitat of *G. crassaformis*) (Figure 4.2c).

We exemplarly use $\Delta\delta^{13}$C between the shallow dweller *G. sacculifer* and the deep dwellers *G. truncatulinoides* and *G. crassaformis* to clarify this trend (Figure 4.11). Between the tropical eastern and western Atlantic, the $\Delta\delta^{13}$C between *G. sacculifer* and deep dwellers decreases by up to 0.5‰, as the depth of the seasonal thermocline, and therefore the thickness of the nutrient-depleted surface mixed-layer increases (Figures 4.10, 4.11). Changes in $\Delta\delta^{13}$C between *G. sacculifer* and *G. crassaformis* are small from the western Atlantic into the Caribbean (50–60°W), where deep vertical mixing of nutrient-depleted surface waters reaches down to depths of more than 200 m due to an exceptionally deep position of the seasonal thermocline. The $\Delta\delta^{13}$C between *G. sacculifer* and *G. truncatulinoides*, however, exhibits another prominent decrease of about 0.5‰. Although this change in vertical $\Delta\delta^{13}$C is consistent with changes in the vertical nutrient distribution, we are aware of the fact that this decrease cannot only be attributed to a lowering of the nutrient composition within the permanent thermocline (Chapter 4.4.4), but results to a significant part from the exceptionally low Caribbean δ^{13}C values measured in *G. sacculifer* that remain questionable.

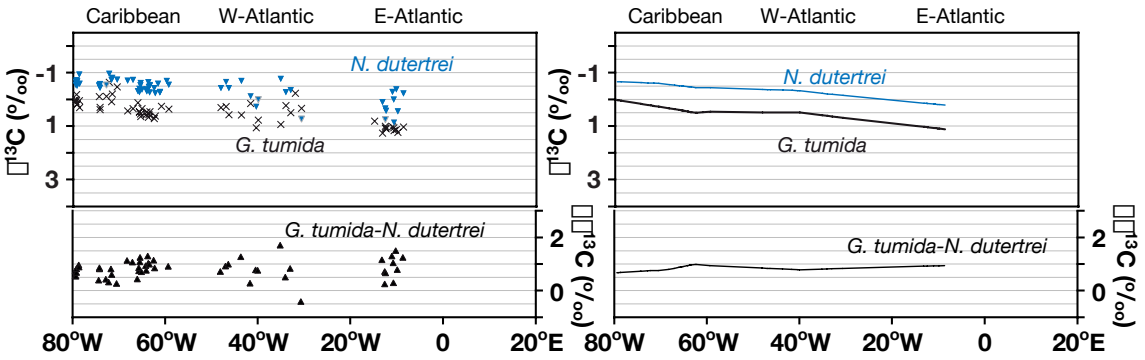

Figure 4.12 Top: δ^{18}O values of *N. dutertrei* (blue inverse triangles) and *G. tumida* (black crosses) and the δ^{18}O gradient between *G. tumida* and the *N. dutertrei* (black triangles) plotted *vs.* longitudinal position of the core-top samples. Left: measured δ^{18}O values and calculated gradients for each station. Right: Trends of δ^{18}O patterns and δ^{18}O gradients along the E-W transect. We smoothed the data by using the locally weighted least squared error method (e.g., *Cleveland*, 1979) and applying a smoothing factor of 60%.

4.4.5 Implications for Paleoceanographic Studies

Comparison of multispecies foraminiferal stable isotope values from Atlantic/Caribbean core-top samples with modern hydrographic data (*NODC*, 2001) displays them as a useful tool for monitoring changes in tropical upper-ocean stratification. Despite variations in the calcification depths, which generally increase with increasing TCD (Figure 4.5), $\Delta\delta^{18}$O between intermediate-dwelling species and shallow-dwelling (deep-dwelling) species decreases (increases) with increasing TCD. We identified the $\Delta\delta^{18}$O between shallow dwellers (*G. ruber* (pink/white); *G. sacculifer*) and the intermediate dwellers *G. tumida* and *G. scitula*, as well as the $\Delta\delta^{18}$O between *G. tumida* and *G. scitula* and the deep dwellers *G. crassaformis* and *G. truncatulinoides* dextral to be most suitable for the reconstruction of upper-ocean stratification (Figures 4.6, 4.7; Table 4.4). The $\Delta\delta^{18}$O between the thermocline dweller *N. dutertrei* and shallow and deep dwellers also changes significantly with changing TCD (Figures 4.6, 4.7; Table 4.4), although the calcification depth of *N. dutertrei* increases significantly with increasing TCD (Figure 4.5c), whereby migration to deeper (i.e. relatively cooler) waters may reduce the effect of subsurface warming on $\delta^{18}O_{dut}$ values.

Based on the assumption that *N. dutertrei* always calcifies within the thermocline (close to the same temperature), and that *G. tumida* always calcifies in a specific water depth close to the BOPZ, previous studies showed that the δ^{18}O gradient between *G. tumida* and *N. dutertrei* is sensitive to changes in TCD (*Ravelo and Andreasen*, 1999). $\Delta\delta^{18}O_{tum-dut}$ should therefore be small (large) when the thermocline is deep (shallow). This study, however, shows that the mean $\Delta\delta^{18}O_{tum-dut}$ of the different hydrographic regimes are insignificantly sensitive to changes in TCD (Table 4.4), furthermore both $\delta^{18}O_{tum}$ and $\delta^{18}O_{dut}$ decrease with increasing TCD (Figure 4.12). This indicates that *N. dutertrei* calcifies in warmer waters when the thermocline is deep, although its calcification depth increases towards the west (Figure 4.5c). Moreover, *Ravelo and Andreasen* (1999) proposed

that the $\Delta\delta^{18}O$ between *G. crassaformis* and *N. dutertrei* is indicative of changes in TCD. They suggested that *G. crassaformis* calcifies in relatively cold waters deep below the mixed layer, if the thermocline is deep, and in warmer waters close to the BOPZ, if the thermocline is shallow. Hence, $\Delta\delta^{18}O_{cras-dut}$ should be large, when TCD is high, and small, when TCD is low. This study shows that $\Delta\delta^{18}O_{cras-dut}$ indeed increases with increasing TCD, but mainly due to a decrease in $\delta^{18}O_{dut}$ rather than an increase in $\delta^{18}O_{cras}$ (Figures 4.5c,d, 6; Tables 4.4, 4.4). In contrast to the assumption of *Ravelo and Andreasen* (1999), the decrease of $\delta^{18}O_{cras}$ in the Caribbean suggests that the calcification temperature of *G. crassaformis* increases when the depth of the seasonal thermocline is exceptionally high. Although we can detect qualitative changes in TCD based on planktonic foraminiferal $\Delta\delta^{18}O$, the quantification of TCD changes using $\Delta\delta^{18}O$ is complicated, since the observed changes in the $\Delta\delta^{18}O$ are subject to factors that are not (or only indirectly) linked to changes in TCD:

1. Changes in mixed-layer temperatures and related changes in the $\delta^{18}O$ values of shallow-dwelling foraminifera can bias the $\Delta\delta^{18}O$ between shallow and intermediate dwellers (*Ravelo and Andreasen*, 1999). For example, the small increase in $\delta^{18}O$ of shallow-dwelling *G. ruber* pink and *G. sacculifer* towards the Caribbean causes overestimation of the observed decrease in $\Delta\delta^{18}O$ between shallow- and intermediate-dwelling species induced by increasing TCD (Figures 4.6, 4.7; Tables 4.4, 4.4). In addition, temperature changes within the permanent thermocline and related changes in the $\delta^{18}O$ values of deep-dwelling species influence the $\Delta\delta^{18}O$ between deep- and intermediate-dwelling species. The decrease in $\delta^{18}O_{cras}$ of $\sim$0.4‰ towards the Caribbean, therefore, leads to underestimation of the observed increase in $\delta^{18}O$ gradients between deep and intermediate dwellers caused by an increasing TCD (Figure 4.6; Tables 4.4, 4.4). The observed east-west decrease in mean $\Delta\delta^{18}O$ between *G. crassaformis* and *G. sacculifer* of 0.57‰ from the western Atlantic into the Caribbean points to these uncertainties (Figure 4.6; Table 4.4). In the ideal case, this gradient should be relatively constant although TCD changes (as observed in $\Delta\delta^{18}O_{trunc-sacc}$; Figure 4.7; Table 4.4).

2. Changes in the calcification depth of different planktonic foraminiferal species may cause variations in intraspecific $\Delta\delta^{18}O$. As suggested by *Ravelo and Andreasen* (1999), migration of the shallow-dwelling species to a deeper (relatively cooler) habitat in regions with higher TCD (western Atlantic and Caribbean; Figure 4.5) decreases the $\Delta\delta^{18}O$ beween shallow and intermediate dwellers. Furthermore, migration of *G. crassaformis* to a deeper (and relatively cooler) habitat increases the $\Delta\delta^{18}O$ between deep and intermediate dwellers as observed for the Caribbean. As the comparison of measured $\delta^{18}O$ and predicted $\delta^{18}O_{calcite}$ suggests that the intermediate dwellers also migrate to deeper habitats, when TCD increases (more pronounced for the thermocline dwellers, less pronounced for *G. scitula* and *G. tumida*), quantification of habitat effects on changes in interspecific $\Delta\delta^{18}O$ remains difficult.

3. Changes in vertical $\delta^{18}O_{seawater}$ gradients (Figure 4.2b) may generate changes in intraspecific $\delta^{18}O$ gradients. For example, the longitudinal increase in subsurface salinity towards the west, especially at the calcification depth of the intermediate dwellers (Figures 4.2, 4.3), should elevate the $\delta^{18}O$intermediate in the western Atlantic and Caribbean. Thus, the observed decrease

in $\Delta\delta^{18}$O between intermediate- and shallow-dwelling species (due to subsurface warming) is probably underestimated. Mg/Ca-paleotemperature reconstructions may provide a useful tool to get hold of the salinity portion in the δ^{18}O signal of different planktonic foraminiferal species.

4. Additional information regarding changes in upper-ocean stratification can be extracted from the δ^{13}C signal of planktonic foraminifera. For example, our dataset shows that δ^{13}C of the deep dwellers *G. crassaformis* and *G. truncatulinoides* increases with increasing TCD (Figures 4.8, 4.10; Table 4.5), probably due to a decrease in the nutrient contents within the permanent thermocline. However, exceptionally low δ^{13}C values of shallow- and thermocline-dwelling species within the Caribbean clearly show that changes in planktonic foraminiferal δ^{13}C are subject to factors other than changes in nutrient TCD (e.g., input of nutrient-enriched river water; changes in the isotopic composition of atmospheric CO_2). Furthermore, the uncertainties regarding species-specific disequilibria from $\delta^{13}C_{DIC}$ (*Ravelo and Fairbanks*, 1995; *Mulitza et al.*, 1999; *Mielke*, 2001) are large. Hence, we assume that δ^{13}C values and $\Delta\delta^{13}$C changes can support and complement the interpretation of δ^{18}O values with respect to vertical nutrient gradients, but cannot be used exclusively for reconstructions of tropical TCD.

4.4.6 Conclusions

We examined δ^{18}O and δ^{13}C values of nine foraminiferal species and varieties with different preferential habitat depths from 63 core-top samples along an E-W transect across the tropical Atlantic/Caribbean in order to further test the stable isotopic composition of planktonic foraminifera as paleoceanographic tool for reconstructions of changes in upper-ocean stratification. The major conclusions and implications for paleoceanographic reconstructions include:

Comparison of measured δ^{18}O values to the water depth of corresponding predicted $\delta^{18}O_{calcite}$ suggests that estimated calcification depth of most species is not strictly coupled to a certain depth level, but increases from east to west with increasing TCD. Absolute calcification depth, however, strongly depends on the δ^{18}O-paleotemperature equation used for calculating predicted $\delta^{18}O_{calcite}$.

The $\Delta\delta^{18}$O between *G. tumida* and *G. scitula* and shallow dwellers (i.e. *G. sacculifer*, *G. ruber* (pink/white)) or deep dwellers (*G. crassaformis*, *G. truncatulinoides* dextral) clearly mirrors the east-west increase in TCD across the Atlantic/Caribbean. $\Delta\delta^{18}$O between *G. tumida* and *G. scitula* and shallow dwellers decreases with increasing TCD, and $\Delta\delta^{18}$O between *G. tumida* and *G. scitula* and deep dwellers increases with increasing TCD.

Increasing TCD across the Atlantic is also accompanied by a decrease in the δ^{18}O values of the thermocline dwellers *N. dutertrei* and *G. menardii*, which results in a decrease of $\Delta\delta^{18}$O between thermocline dwellers and shallow-dwelling species, and an increase in $\Delta\delta^{18}$O between thermocline dwellers and deep-dwelling foraminifera. This implies that, at least in the tropical Atlantic, the thermocline dwellers do not always calcify close to the same temperature in different hydrographic regimes as suggested before for *N. dutertrei* (*Ravelo and Fairbanks*, 1992; *Ravelo and Andreasen*, 1999). The observed changes in the δ^{18}O gradients between *G. menardii* and the

shallow and deep dwellers are smaller than those observed in the $\Delta\delta^{18}$O between *G. scitula*, *G. tumida*, and *N. dutertrei*, and shallow- and deep-dwelling species. This may probably be attributed to distinct migration of the thermocline dweller to deeper habitats when TCD increases.

Quantification of TCD changes based on $\Delta\delta^{18}$O still suffers from the effect of (1) simultaneous changes in sea-surface temperatures, (2) temperature changes at the calcification depth of deep-dwelling species, and (3) temporal or regional changes in the calcification depth (all species tend to calcify deeper in the water column, when the thermocline is deep). Furthermore, vertical and spatial changes in salinity may bias the intraspecific $\Delta\delta^{18}$O. Thus, multispecies Mg/Ca-paleotemperature reconstructions, and the extraction of the salinity signal from the δ^{18}O signal of foraminiferal calcite may provide important additional information regarding the evaluation of vertical δ^{18}O gradients. With respect to these uncertainties, changes in $\Delta\delta^{18}$O can up to now only provide information about relative changes in TCD.

Incorporation of δ^{13}C into the carbonate tests of *G. scitula* seems to be strongly temperature-dependent, with a linear relationship similar to that observed for G. bulloides (0.11‰ per 1°C (*Bemis et al.*, 2000)). Thus, we assume that δ^{13}C of *G. scitula* provides no major information about changes in nutrient concentrations of ambient seawater.

Interpretation of δ^{13}C values and $\Delta\delta^{13}$C between different planktonic foraminifera is complicated by 'vital effects', which result in δ^{13}C offsets from $\delta^{13}C_{DIC}$. Despite these uncertainties, a general decrease in $\Delta\delta^{13}$C between shallow- and deep-dwelling species from the western Atlantic towards the Caribbean is consistent with decreasing vertical nutrient gradients associated with increasing TCD. The east-west decrease in $\Delta\delta^{13}$C mainly results from an increase in the δ^{13}C values of the deep-dwelling *G. truncatulinoides* dextral and *G. crassaformis*, and a general decrease in δ^{13}C values of the shallow and intermediate dwellers, which is complicated by a large scatter in Caribbean δ^{13}C. Since the increase in δ^{13}C values of the deep dwellers towards the Caribbean matches the decrease in the nutrient contents within the permanent thermocline, the δ^{13}C values of *G. truncatulinoides* dextral and *G. crassaformis* might be a valuable indicator for changes in nutrient concentrations below the seasonal thermocline. Yet, the reasons for the large scatter in the Caribbean δ^{13}C of the shallow and intermediate dwellers (and especially for the low δ^{13}C values) remain speculative.

4.5 Acknowledgements

We thank Joachim Schönfeld, Reinhard Kozdon, and Lars Reuning for discussions and criticism, and Lulzim Haxhiaj, Ulrike Nielsen, and Daniel Oesterwind for technical support and laboratory assistance. Funding for this project was provided by the Deutsche Forschungsgemeinschaft through project Ti240-12 (being part of the DFG-Research Unit, FOR 451: Impact of Gateways on Ocean Circulation, Climate and Evolution at Kiel University), by the German Ministry of Education and Research (BMBF) under project No. 03G0164, and by the Leibniz Award Du 129/33.

Chapter 5

Early Diagenetic Overprint in Caribbean Sediment Cores and its Effect on the Geochemical Composition of Planktonic Foraminifera

Marcus Regenberg[1], Dirk Nürnberg[1], Joachim Schönfeld[1], Gerd-Jan Reichart[2]

[1]Leibniz Institute of Marine Sciences IFM-GEOMAR, Kiel, Germany

[2]Faculty of Earth Sciences, Utrecht University, Netherlands

Manuscript in preparation

Abstract. Early diagenetic features are noticed in the vicinity of carbonate platforms. Planktonic foraminifera of two tropical Atlantic deep-sea sediment cores show the strict relation between micro-scale euhydral crystallites of inorganic precipitates, higher oxygen isotope values and Mg/Ca ratios, and lower Sr/Ca ratios than expected for their pelagic environment in the time interval of ∼100,000–550,000 calendar years before present. Laser ablation Mg/Ca (Sr/Ca) of crystallite-bearing foraminiferal chamber walls revealed 4–6 times elevated (2–3 times depleted) ratios, when ablating the diagenetic overgrowth. Crystalline overgrowth in proportions of 10–20% are estimated to cause the observed geochemical alteration. The extent of foraminiferal Mg/Ca alteration, moreover, seems to be controlled by the composition of the bulk sediment, especially the content of high-magnesium calcite. Anomalous ratios of >6 mmol/mol only occur, when high-magnesium calcite has dissolved within the sediment. The older parts (back to ∼800 kyrs) of the records are characterized by similar trends of Mg/Ca and Sr/Ca. We discuss possible scenarios to accommodate the obtained geochemical information.

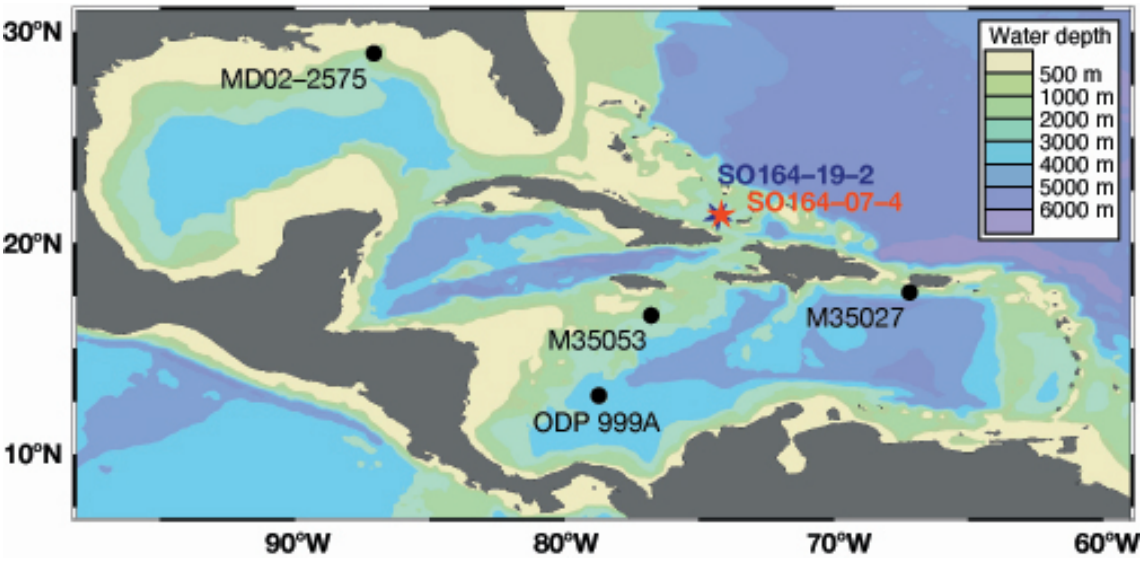

Figure 5.1 Bathymetric chart of the Caribbean and the Gulf of Mexico generated with Ocean Data View (*Schlitzer*, 2002): Stars indicate the site locations of the examined sediment cores SO164–07–4 and SO164–19–2. For comparison, data of sites MD02-2575 (847 m water depth), M35027 (1814 m), M35053 (1698 m), and ODP 999A (2827 m) are shown in this study.

5.1 Introduction

A persistent problem in many paleoceanographic studies is the potential of diagenetic processes to compromise the fidelity of geochemical proxies in deep-sea carbonates and microfossils, such as foraminifera. Principally, two processes of deep-sea carbonate diagenesis can be distinguished from each other: First, the geochemical composition may be biased by dissolution processes on the sediment's carbonate mineralogy (e.g., *Droxler*, 1984; *Sabine and Mackenzie*, 1995; *Haddad and Droxler*, 1996; *Malone et al.*, 2001; *Frank and Bernet*, 2000; *Jansen et al.*, 2002), and on the foraminiferal isotope and element content (e.g., *Lorens et al.*, 1977; *Lohmann*, 1995; *Rosenthal et al.*, 1997; *Dekens et al.*, 2002; *Regenberg et al.*, 2006a) (Chapter 2). Second, the geochemical composition may be altered by precipitation and reprecipitation of calcite from sediment pore fluid (e.g., *Baker et al.*, 1982; *Norris and Wilson*, 1998; *Hover et al.*, 2001; *Rudnicki et al.*, 2001). Dissolution and/or inorganic reprecipitation is determined by the saturation state of seawater or pore fluid with respect to the solid phase (e.g., *Morse*, 2003; *Funk et al.*, 2003; *Regenberg et al.*, 2006a) (Chapter 2). Inorganic (or diagenetic) calcite in terms of overgrowth may mask the primary oceanographic signal of planktonic foraminiferal tests. Both, inorganic calcite overgrowth and dissolution of foraminiferal tests during shallow burial tend to bias the oxygen isotope composition (δ^{18}O) to more positive values (*Killingley*, 1983; *Mulitza et al.*, 2004).

A paramount aim of geochemical studies with diagenetic issue is the quantification of the alteration. One strategy for quantifying the extent of diagenesis is the application of numerical models to assess pore-fluid and precipitate isotope compositions (e.g., *Killingley*, 1983; *Richter and DePaolo*, 1987; *Schrag et al.*, 1992; *Schrag*, 1999; *Rudnicki et al.*, 2001). Basically,

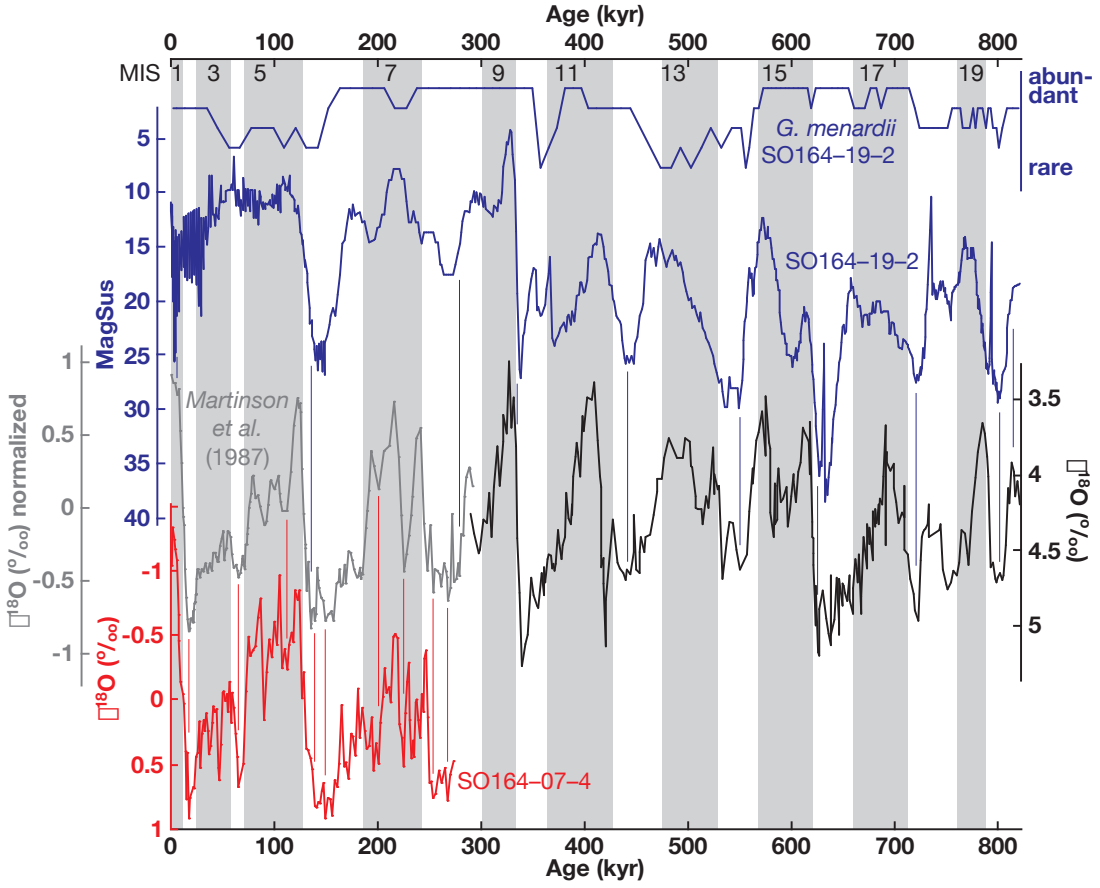

Figure 5.2 Stratigraphical framework of sites SO164–07–4 and SO164–19–2 based on the oxygen isotope curve of *G. sacculifer* and the magnetic susceptibility (MagSus) curve, respectively: For graphical correlation back to ∼290 ka, the stacked reference curve of *Martinson et al.* (1987) was used; for the older parts, we used the benthic oxygen isotope record of ODP Site 677 (*Shackleton et al.*, 1990). Tie points are indicated by thin vertical lines. For site SO164–19–2, we additionally estimated the relative abundance of *G. menardii* as indicator of warm isotope stages. Odd numbered marine isotope stages (MIS) are indicated by shading.

these studies address deep-burial sediments from depths of >300 m. Another approach for the quantification of diagenetic alteration deals with the Element/Ca ratios and their alignment to measured pore-fluid composition by application of partition coefficients (e.g., *Tripati et al.*, 2003; *Sexton et al.*, 2006).

Here, we found unexpected shallow-burial diagenesis in tropical Atlantic and Caribbean deep-sea sediments from different water depths (∼1700–2700 m; Figure 5.1) marginally described before (*Müller*, 1999). We applied oxygen isotope and Element/Ca analysis on bulk planktonic foraminiferal tests revealing anomalous ratios compared to data sets reflecting past environmental conditions. Since information on the bulk foraminiferal geochemical composition altered by diagenesis combines the actual biogenic calcite signal and the composition of the inorganic precipitate, we additionally prepared laser ablation inductively coupled plasma mass spectrometry

capable to generate high resolving Element/Ca-ratio profiles of foraminiferal tests (*Eggins et al.*, 2003; *Hathorne et al.*, 2003; *Reichart et al.*, 2003). This technique allows to determine end-member compositions of the diagenetic precipitates. Associated carbonate mineralogy of the bulk sediment affords the possibility to characterize the processes involved in sediment alteration.

5.2 Materials and Methods

Piston cores SO164–07–4 and SO164–19–2 were recovered during R/V SONNE cruise 164 (*Nürnberg et al.*, 2003) from Windward Passage (21°19'27.6"N, 74°08'46.2"W at 2722 m and 21°14'42.6"N, 74°20'59.4"W at 1704 m, respectively (Figure 5.1)). Syringe sampling (∼10 mL) of the upper ∼9.5 m of site SO164–07–4 and ∼6.5 m of site SO164–19–2, respectively, took place every 5 cm. Samples taken from the ∼2.2 m of intercalated calcite-turbidite sequences of site SO164–07–4 were discarded.

5.2.1 Analysis of Carbonate Phases

The relative abundance of a variety of minerals present in the sediment samples was quantified by X-ray diffraction (XRD). XRD was typically performed on ∼0.5 g of the bulk sediment. Each sample was carefully grinded for five minutes in an agate mortar in order to homogenize the grain size to ∼5–10 μm. The analysis was carried out on a Philips PW 1710 X-ray diffractometer (IFM-GEOMAR, Kiel) containing a cobalt anode Kσ tube at 40 KV and 35 mA. The samples were scanned from 25–40° at a scanning speed of 0.01 steps per second to cover the significant peaks of the various carbonate minerals. The peak-area method was deployed to quantify the aragonite content using the computer based integration program MacDiff of *Petschick* (2001). The aragonite/calcite peak-area ratios were converted into relative weight percentages using an in-house calibration curve. Weight percentages of HMC and LMC were directly calculated by their peak-area ratios.

5.2.2 δ^{18}O Analysis

For stable isotope analysis, 10 specimens of planktonic foraminifera *Globigerinoides sacculifer* (without sac-like final chamber) were selected from the 315–400 μm size fraction. All isotope analyses were run on a Finnigan MAT 252 Mass Spectrometer with automated Kiel carbonate preparation device at IFM-GEOMAR (Kiel). The mass spectrometer was calibrated *via* the National Bureau of Standards (NBS) 19 and an internal laboratory standard to the Vienna Pee Dee Belemnite (PDB) scale. Isotope values are reported in ‰ PDB. The external reproducibility of in-house carbonate standards was ∼0.08‰ for δ^{18}O.

5.2.3 Element/Ca Analysis

Twenty to twenty-five specimens (∼550–800 μg) of *Globigerinoides ruber* white, *G. sacculifer* (without sac-like final chamber), and *Neogloboquadrina dutertrei* were selected from the

315–400 μm size fraction. Clay removal (water and methanol wash) and organic-matter oxidation (hydrogen peroxide treatment) were applied to gently crushed samples, followed by a weak acid leach and final dissolution of the fragments. For detailed description of the Mg-cleaning protocol (*Barker et al.*, 2003), see *Regenberg et al.* (2006a) (Chapter 2).

Element/Ca ratios were performed on two inductively coupled plasma optical emission spectrometry (ICP OES) devices showing no significant offsets in Mg/Ca (*Regenberg et al.*, 2006a) (Chapter 2). All *G. sacculifer* samples, and parts of the *G. ruber* white and *N. dutertrei* samples, were analyzed on an ICP OES (ISA Jobin Yvon, Spex Instruments S.A. GmbH) at IFM-GEOMAR, Kiel, using 10 ppm of yttrium as internal standard. Analytical errors for calcium and strontium were ~0.15%, for magnesium ~0.45%, for manganese ~10%, and for iron ~15%. The remainder of the *G. ruber* white and *N. dutertrei* samples were measured on an ICP OES (Spectro CirosCCD SOP) at the Institute for Geosciences, Kiel. Analytical errors for Mg/Ca and Sr/Ca ratios were ~0.1%. For manganese and iron, analytical errors amount to ~0.5% and ~2%, respectively.

5.2.4 Chronostratigraphy

The stratigraphical framework for the upper ~9.5 m (including ~2.2 m of turbidite sediment) of site SO164–07–4 (Figure 5.2) was established by graphically correlating prominent maxima and minima in the planktonic oxygen isotope record of *G. sacculifer* to the stacked reference curve of *Martinson et al.* (1987).The age model for the upper ~6.5 m of site SO164–19–2 (Figure 5.2) is based on the graphic correlation of the magnetic susceptibility curve younger than ~290 ka with the stacked reference curve of *Martinson et al.* (1987). For graphical correlation back to ~820 kyrs, the magnetic susceptibility curve was correlated to the benthic isotope record of ODP Site 677 (*Shackleton et al.*, 1990). Definition of marine isotope stages (MIS) follows *Bassinot et al.* (1994), graphic correlation was performed with AnalySeries Version 1.1 (*Paillard et al.*, 1996). To further constrain the chronostratigraphy of site SO164–19–2, we studied the presence/absence of the planktonic foraminifera *Globorotalia menardii*, serving as time stratigrahic markers and climatic indicators in Pleistocene sediments from the tropical Atlantic (*Ericson and Wollin*, 1956, 1968; *Ruddiman*, 1971). Abundance peaks and barren zones correspond, to some extent, with warm and cold marine isotopic stages, respectively (Figure 5.2).

5.2.5 LA-ICP MS

For laser ablation inductively coupled plasma mass spectrometry (LA-ICP MS), we selected cleaned *G. ruber* white, *G. sacculifer*, and *N. dutertrei* fragments from the 315–400 μm size fraction of five different samples. Multiple laser ablation profiles were performed on different foraminiferal fragments from the same sample to elucidate in-test heterogeneities. In total, 18 profiles were ablated.

Using an Excimer 193 nm deep ultra violet laser (Lambda Physik) with Geolas optics (*Günther et al.*, 1997), craters of ~80 μm in diameter were ablated during analysis. Energy density at the

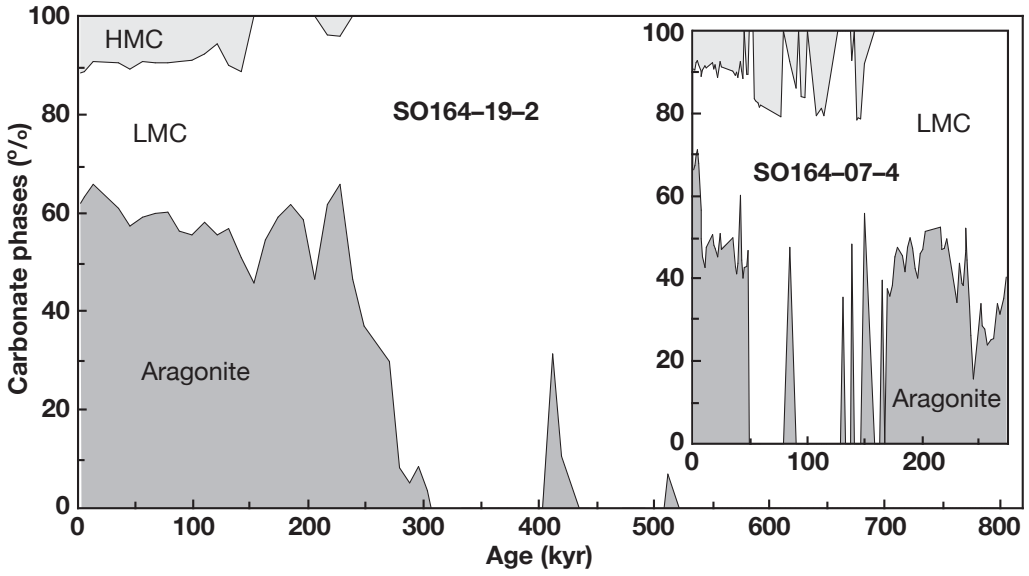

Figure 5.3 Carbonate mineralogy of sites SO164–19–2 and SO164–07–4 (inlet) for the last ∼820 kyrs and ∼270 kyrs, respectively: Proportions of low-magnesium calcite (LMC), high-magnesium calcite (HMC), and aragonite are given in weight %.

sample surface was kept at 2 mJ/cm^2, shot repetition rate at 8 Hz. Laser ablation of calcite requires ablation at ultra violet wave lengths since higher wave lengths result in uncontrolled cleavage. The ablated material was transported on a continuous He flow and mixed with an Ar make up gas before injection into the Ar plasma of the quadrupole ICP MS instrument (Micromass Platform at the Faculty of Geosciences, Utrecht University, Netherlands). A collision and reaction cell was used to improve results by reducing spectral interferences on the minor isotopes of Ca (^{42}Ca, ^{43}Ca, and ^{44}Ca). Interelemental fractionation was insignificant due to the relative low depth to width ratio of the ablation craters produced (*Mason and Mank*, 2001). The use of a collision cell also prevented interference of clusters like $^{12}C^{16}O^{16}O$. Although the Excimer UV-193 usually does not show any matrix effects, possible matrix effects, nevertheless, were checked with matrix matched standards. Calibration was performed against U.S. National Institute of Standards and Technology SRM 612 glass using the concentration data of *Pearce et al.* (1997), with Ca as an internal standard. Calcium carbonate is well suited for LA-ICP MS because Ca can be used as an internal standard at 40 weight percentages. We used ^{44}Ca for quantification, ^{42}Ca and ^{43}Ca for internal monitoring. Using Ca as an internal standard allows direct comparison to trace metal to Ca ratios from traditional wet-chemical studies. Concentrations of Mg and Sr were calculated using ^{24}Mg and ^{26}Mg, and ^{88}Sr. Although the accuracy for the more abundant ^{24}Mg is higher, both Mg isotopes agree within a few percent.

With initiation of the ablation process, preferential ablation of material from surfaces that lie orthogonal to the incident laser beam results in greater ablation from the tops of interpore ridges and spine bases (*Eggins et al.*, 2003). This means that the ablation crater is not flat but follows the curvature of the foraminiferal test, and, therefore, should reveal elevated element concentrations in

a diagenetic coating when present. Further in the ablation process the craters become increasingly flatter bottomed. This results in a smoothing of the signal when the ablation reaches the pores on the other side of the test. To certify that no smoothing of a possible coating peak occurred, the fragments of each sample were measured both from the inner side toward the outer side and *vice versa*.

5.3 Results

5.3.1 Carbonate Mineralogy

The composition of the bulk-sediment carbonate of sites SO164–19–2 and SO164–07–4 changes through time (Figure 5.3). For site SO164–19–2, the content of HMC (with Mg^{2+} concentrations >4 mol.% (*Morse*, 2003)) on the carbonate phases amounts to 6–12% from the core top back until ∼140 kyrs with an additional peak at ∼220 kyrs. From the core top back until ∼270 kyrs, aragonite contributes with 50–60% to the carbonate content. A marked decrease leads to the absence of aragonite (and HMC) from the sediments prior to ∼300 kyr, except for two aragonite peaks at ∼280 kyrs and ∼410–420 kyrs. Higher resolution site SO164–07–4 shows the permanent presence of aragonite and HMC from the core top back until ∼48 kyrs at 40–70% and 7–12%, respectively. Further back to ∼116 kyrs, HMC is present in most of the samples in proportions of 8–21%, while aragonite is only present at ∼85 kyrs. Prior to ∼116 kyrs, HMC is absent except for the time interval of ∼139–149 kyrs. From ∼131–169 kyrs, aragonite is only present in single peaks, whereas prior to ∼169 kyrs, aragonite is permanent present in proportions of 16–52%.

5.3.2 δ^{18}O, Mg/Ca, and Sr/Ca Records of Sites SO164–19–2 and SO164–07–4

The δ^{18}O, Mg/Ca, and Sr/Ca records of sites SO164–19–2 and SO164–07–4 reveal atypical patterns compared to proxy records available in the literature. Site SO164–19–2 covers the glacial/interglacial cycles back to ∼820 kyrs in low resolution (Figure 5.4). Core top, Holocene, and interglacial isotope stage δ^{18}O values are consistent with the corresponding values of site SO164–07–4. Reaching values as high as 1.62‰ and prior to MIS 3 not lower than about -0.5‰, δ^{18}O is far offset from the Caribbean ODP Site 999 δ^{18}O record of *G. ruber* white (*Schmidt et al.*, 2006) showing highest values of ∼0.1‰ during MIS 2 and MIS 12 (Figure 5.4). From MIS 14–20, variation in δ^{18}O is considerably dampened, values are around 0.5‰.

Mg/Ca ratios of site SO164–19–2 show a completely different trend compared to the *G. ruber* white record of ODP Site 999 (*Schmidt et al.*, 2006). Expected lower Mg/Ca during MIS 2–4 with respect to core-top and Holocene ratios are not observed (Figure 5.4). From *G. ruber* white Mg/Ca of ∼5.5 mmol/mol during this time interval and throughout MIS 5, an intense increase to ratios >8 mmol/mol occurs during MIS 6. Among a hugh variability of ∼3 mmol/mol, Mg/Ca further increases to >10 mmol/mol during MIS 10–12. This trend is well reflected in the Mg/Ca records of *G. sacculifer* and *N. dutertrei* of site SO164–19–2 (Figure 5.4), whereas the latter is

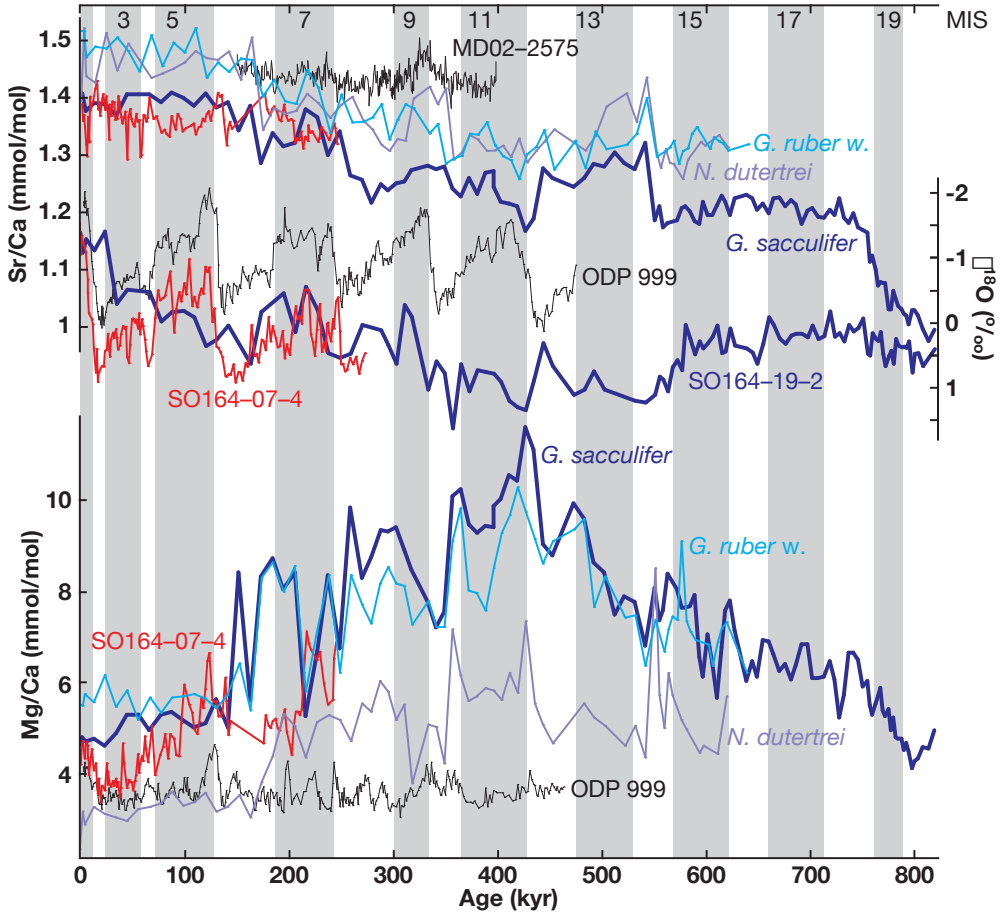

Figure 5.4 Sr/Ca and Mg/Ca curves of *G. ruber* white, *G. sacculifer*, and *N. dutertrei* (top and bottom panels, respectively), and the *G. sacculifer* oxygen isotope curve of site SO164–19–2 for the last ∼820 kyrs. The trends of the δ^{18}O and Mg/Ca records deviate substantially from Caribbean *G. ruber* white curves of ODP Site 999 (*Schmidt et al.*, 2006). Likewise, the *G. ruber* white Sr/Ca ratios are lower than those of *G. ruber* white of site MD02–2575 from the Gulf of Mexico *Karas and Nürnberg*, pers. comm.), at least prior to MIS 7. Higher resolution *G. sacculifer* curves of site SO164–07–4 follow the atypical trends of site SO164–19–2 records.

almost constantly offset by ∼2.5–3 mmol/mol to lower ratios. Decreasing Mg/Ca particularly during MIS 13 level off the ratios of *G. sacculifer* to ∼6–7 mmol/mol during MIS 16–18. Lower ratios than core-top Mg/Ca are observed for MIS 20. Comparing the younger part of the record to the *G. sacculifer* Mg/Ca of site SO164–07–4, a similar trend at least during MIS 5 and MIS 7 to the *G. sacculifer* and *G. ruber* white records of site SO164–19–2 can be seen (Figure 5.4).

G. sacculifer Sr/Ca ratios of ∼1.4 mmol/mol are observed back until MIS 7 with excursions to ∼1.3 mmol/mol during MIS 6. A similar trend is shown by the *G. sacculifer* Sr/Ca curve of site SO164–07–4. During MIS 8, Sr/Ca decreases to ratios of ∼1.25–1.3 mmol/mol. This level persists until MIS 14 with excursions to minimum ratios of ∼1.2 mmol/mol. During MIS 14, Sr/Ca decreases to a level of ∼1.2 mmol/mol. In the oldest parts, Sr/Ca further decreases to ratios <1 mmol/mol. For the entire record, Sr/Ca of *G. ruber* white and *N. dutertrei* of site SO164–

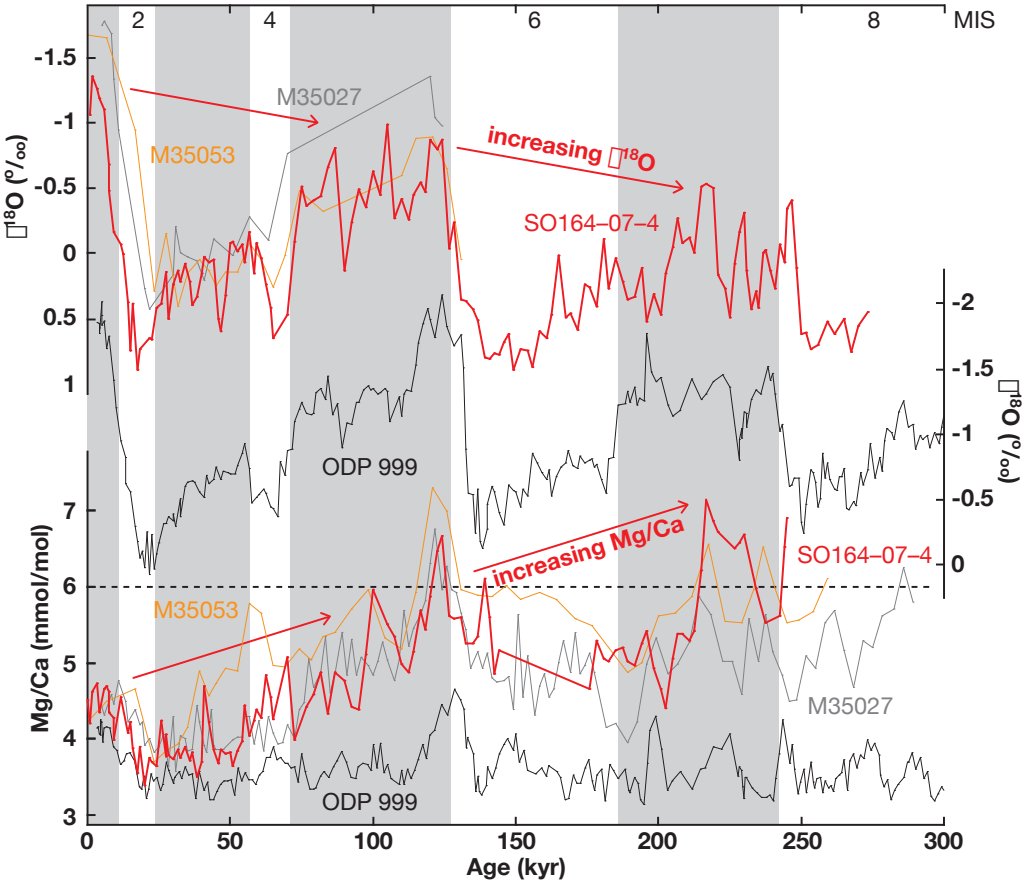

Figure 5.5 Oxygen isotope and Mg/Ca curves of *G. sacculifer* of site SO164–07–4 for the last ~250 kyrs: For comparison, Caribbean *G. sacculifer* curves of sites M35027 and M35053 (*Müller*, 1999), and *G. ruber* white curves of ODP Site 999 (*Schmidt et al.*, 2006) are given. Increased δ^{18}O and anomalously high Mg/Ca with respect to Holocene values at least during MIS 5 and 7 of sites SO164–07–4, M35027, and M35053 do not follow the expected trend observed for ODP Site 999. Note that Mg/Ca of >6 mmol/mol would convert to open-ocean temperatures of >30.5°C.

19–2 are offset to higher ratios by ~0.5–1 mmol/mol and follow the trend of *G. sacculifer*. The decreasing trend in all planktonic foraminiferal Sr/Ca records prior to MIS 6 contradicts the *G. ruber* white Sr/Ca record of site MD02–2575 from the Gulf of Mexico (data obtained from *Cyrus Karas and Dirk Nürnberg*, pers. comm.), which remains at the same level of ~1.4–1.5 mmol/mol from MIS 6–11.

5.3.3 Atypical Trends in Caribbean δ^{18}O and Mg/Ca Records

The *G. sacculifer* δ^{18}O record of site SO164–07–4 shows two complete glacial cycles back to MIS 8 at ~270 kyrs (Figures 5.2, 5.5). δ^{18}O values across Terminations I and II display glacial/interglacial differences of ~2.2‰ and ~1.6‰, respectively. Other (sub)tropical Atlantic, Caribbean, and Bahamian records (*Curry and Oppo*, 1997; *Wolff et al.*, 1998; *Rühlemann et al.*, 1999; *Kroon et al.*, 2000; *Schmidt et al.*, 2004, 2006), in contrast, indicate that differences across

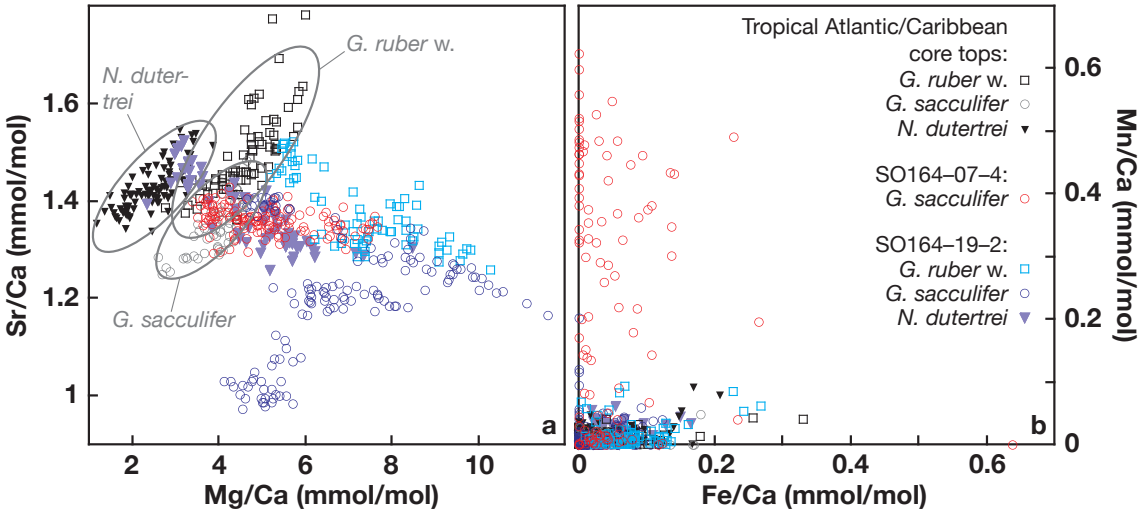

Figure 5.6 a) Mg/Ca *vs.* Sr/Ca ratios and b) Fe/Ca *vs.* Mn/Ca ratios of sediment-surface (black and grey symbols) and downcore *G. ruber* white, *G. sacculifer*, and *N. dutertrei* (colored symbols). Marked elliptical areas characterize the modern Mg/Ca and Sr/Ca of tropical Atlantic/Caribbean core-top samples, which resemble open-ocean temperatures of ∼19–28°C (*Regenberg et al.*, 2006a) (Chapters 2, 3). Low Fe/Ca (∼0.2 mmol/mol) and Mn/Ca (∼0.1 mmol/mol), unanimously obtained for the core-top foraminifera, indicate that contaminating phases can be neglected as source of Mg^{2+} at least for site SO164–19–2. Annotation of a) is the same as for b).

both terminations are similar. The difference across Termination III of ∼1.2‰ better matches with the range of ∼1.1‰ observed for Caribbean ODP Site 999 (*Schmidt et al.*, 2006) (Figure 5.5). The Holocene attains minimum δ^{18}O of about -1.5‰, which is exceeded in interglacial MIS 5 and MIS 7 with values of about -1.0‰ and -0.5‰, respectively. In contrast to other studies (*Kroon et al.*, 2000; *Schmidt et al.*, 2006), the Holocene stands out in the record with the most negative δ^{18}O values. Highest values during glacial MIS 2, MIS 6, and MIS 8 are close to 0.9‰. In lower resolution, the *G. sacculifer* δ^{18}O records of sites M35027 and M35053 (*Müller*, 1999) go back to MIS 5, with more depleted Holocene values than site SO164–07–4, but with similar increased values during MIS 5 (Figure 5.5).

Mean Holocene *G. sacculifer* Mg/Ca ratios yield ∼4.5 mmol/mol (Figure 5.5). These Mg/Ca ratios correspond to reasonable temperatures of ∼27.0°C, when applying the species-specific paleotemperature equation of Chapter 3. Mg/Ca of site SO164–07–4 decreases to ∼3.7 mmol/mol (∼24.4°C) during the Last Glacial Maximum (LGM, 18–24 kyr). This Holocene/LGM change in Mg/Ca of ∼0.8 mmol/mol is consistent with previous estimates for the Caribbean (*Hastings et al.*, 1998; *Schmidt et al.*, 2004, 2006). From the Holocene to MIS 3, Mg/Ca of site SO164–07–4 is nearly parallel offset by ∼0.2 mmol/mol from the *G. ruber* white record of Caribbean ODP Site 999 (*Schmidt et al.*, 2004, 2006). Prior to MIS 4, Mg/Ca reveals lowest values of ∼5 mmol/mol. From this level, Mg/Ca increases to as much as 6.66 mmol/mol during MIS 5e and 7.13 mmol/mol during MIS 7, corresponding to temperatures of ∼32.2°C and ∼33.1°C, respectively. Prior to MIS 4, Mg/Ca diverges from the ratios of ODP Site 999 (*Schmidt et al.*,

2006). During MIS 5, MIS 6, and late MIS 7, the offset amounts to ∼1.5–2 mmol/mol, increasing to ∼3 mmol/mol for the oldest parts. The Mg/Ca records of sites M35027 and M35053 (*Müller*, 1999) generally show the same atypical trend like those of site SO164–07–4. In general, the downcore increasing trend in δ^{18}O, obviously for the interglacials, is synchronized to the increasing trend in Mg/Ca (Figure 5.5).

5.3.4 Negligible Influence of Contaminating Phases on Mg/Ca Ratios

With respect to the Mg/Ca and Sr/Ca ratios of tropical Atlantic and Caribbean sediment-surface samples (*Regenberg et al.*, 2006a) (Chapters 2, 3), downcore records of sites SO164–07–4 and SO164–19–2 reveal elevated Mg/Ca and lowered Sr/Ca (Figure 5.6a). To evaluate the possible contribution of contaminating phases high in magnesium, iron, and/or manganese (i.e. clay minerals, Mn-oxide coatings) to the original planktonic foraminiferal Mg/Ca and Sr/Ca, we measured the Fe/Ca and Mn/Ca ratios of our foraminiferal sample solutions. These phases may coat or adhere to the surfaces of tests. *Barker et al.* (2003) found Fe/Ca and Mn/Ca of around 0.2 mmol/mol and 0.1 mmol/mol, respectively, typically for foraminiferal tests devoid of contaminating phases. These ratios, which imply negligible elevation of Mg/Ca, are observed for the sediment-surface and site SO164–19–2 samples (Figure 5.6b). For site SO164–07–4, elevated foraminiferal Mn/Ca of up to 0.6 mmol/mol may be indicative of contamination by Mn-oxide coatings. The suggested contribution of Mg^{2+} from coatings to the foraminiferal Mg/Ca of ∼1% (*Barker et al.*, 2003), however, cannot account alone for the atypically high Mg/Ca (up to 7.13 mmol/mol) of site SO164–07–4 (Figure 5.6a).

5.3.5 Micro-Scale Crystallites on Planktonic Foraminiferal Tests

In order to understand the geochemical composition of the planktonic foraminiferal tests atypically for open-ocean conditions (Figures 5.4, 5.5, 5.6a), we prepared scanning electron microscope (SEM) images of selected cleaned and uncleaned fragments of specimens revealing typical Mg/Ca ratios and anomalously high Mg/Ca, respectively. Tests of those specimens revealing typical Mg/Ca (Figure 5.7a,c) show inner and outer chamber-wall surfaces of well preserved biogenic texture with smooth surfaces, wide pores, and well defined outer ridges. In contrast, surfaces of those specimens revealing anomalously high Mg/Ca (Figure 5.7) are overgrown with micro-scale euhydral crystallites of secondary precipitates, which cover the outer ridges and fill the pores. The diagenetic overgrowth covers the inner surface even after the intense Mg-cleaning procedure. SEM images of chamber-wall cross sections of specimens without overgrowth display the microgranular texture that is characteristic of biogenic calcite. The intact wall structure comprises wide pores reaching throughout the wall and smooth inner surfaces (Figure 5.8a,c). Chamber-wall cross sections of specimens with overgrowths reveal that the crystallites narrow the pores and almost close them at their insides (Figure 5.8). Figure 5.8b displays an uncleaned fragment identifying the diagenetic crystallites as distinct rims with a sharply bordered contact to the biogenic calcite.

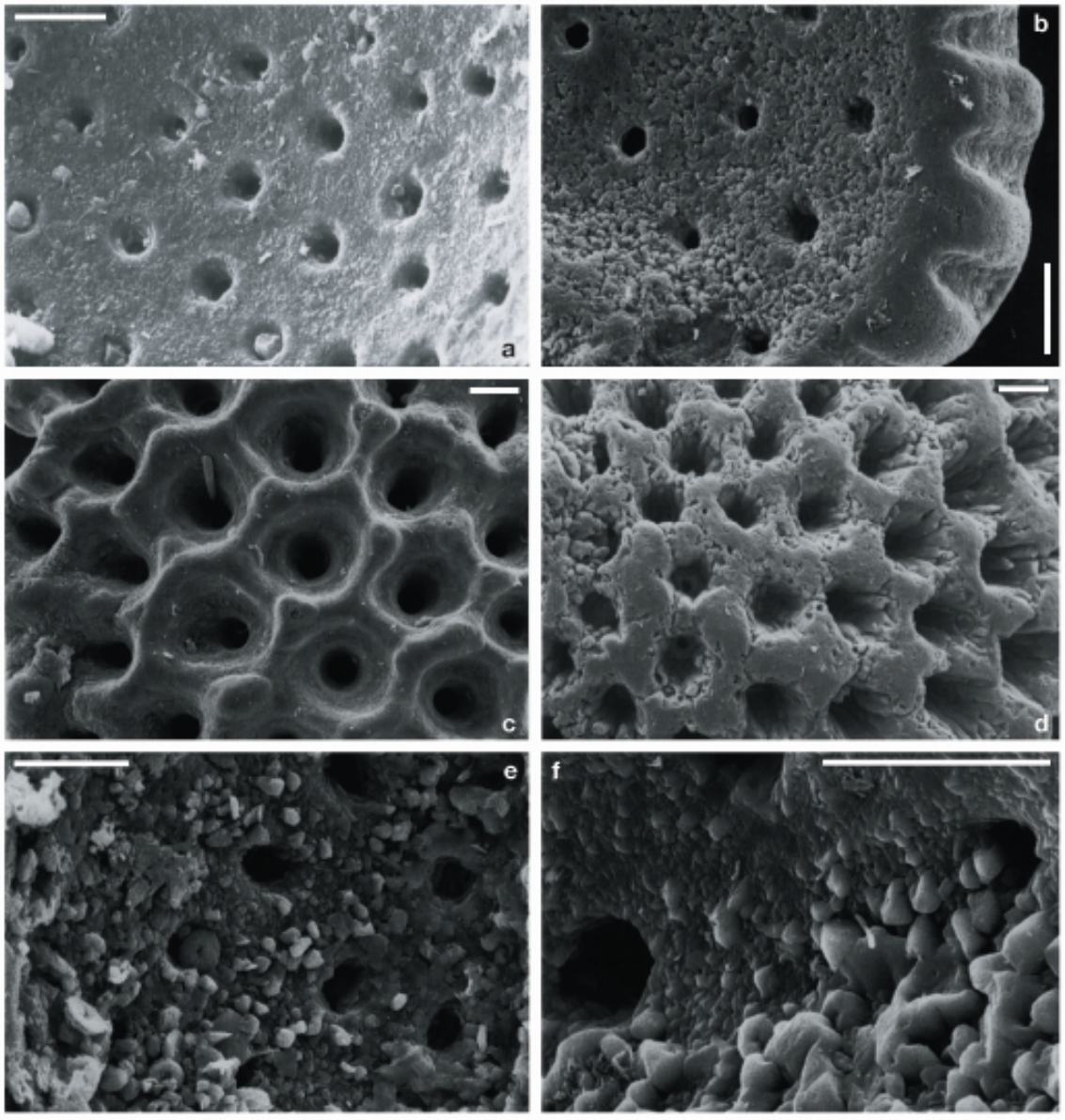

Figure 5.7 SEM images of the wall-surface texture of opened planktonic foraminiferal chambers: a) *G. ruber* white of site SO164–07–4, 118 cm (∼23 kyrs), uncleaned; b) *G. ruber* white of site SO164–19–2, 130 cm (∼259.5 kyrs), cleaned; c) *G. sacculifer* of site SO164–07–4, 118 cm (∼23 kyrs), cleaned; d) *G. ruber* white of site SO164–19–2, 260 cm (∼473 kyrs), cleaned; e and f) *N. dutertrei* of site SO164–19–2, 315 cm (∼563.5 kyrs), uncleaned and cleaned, respectively. Scale bar = 10 μm.

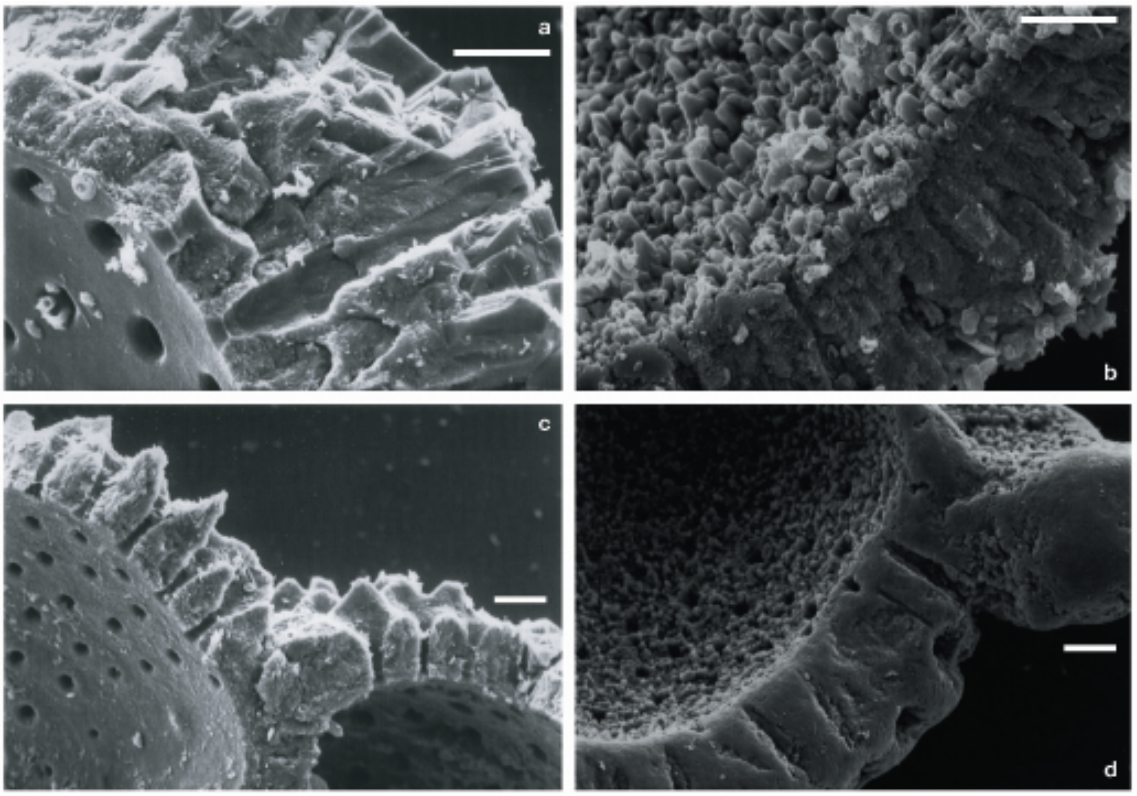

Figure 5.8 SEM images of wall-cross sections of opened planktonic foraminiferal chambers: a) *N. dutertrei* of site SO164–07–4, 3 cm (∼0.9 kyrs), uncleaned; b) *G. ruber* white of site SO164–19–2, 260 cm (∼473 kyrs), uncleaned; c) *G. ruber* white of site SO164–07–4: 3 cm (∼0.9 kyrs), uncleaned; d) *G. ruber* white of site SO164–19–2, 260 cm (∼473 kyrs), cleaned. Scale bar = 10 μm.

5.3.6 Geochemical Composition of the Diagenetic Overgrowth

To further constrain the possible influence of the crystallites on the planktonic foraminiferal geochemistry, we analyzed the elemental composition of foraminiferal chamber walls of site SO164–19–2 applying high resolution LA-ICP MS. We observed a significant different Mg/Ca and Sr/Ca signal for the outermost ratios compared to the remainder of the chamber walls (Figure 5.9). Whether close to the inner or outer surfaces, Mg/Ca ratios are 4–6 times elevated and Sr/Ca 2–3 times depleted with respect to the profile averages. For the time interval of ∼260–470 kyrs, chamber-wall surface Mg/Ca is at least 10 mmol/mol (highest observed ratios are >40 mmol/mol; Figure 5.9), Sr/Ca shows relatively uniform ratios of ∼0.5–0.8 mmol/mol (Figure 5.10).

5.4 Discussion

The δ^{18}O, Mg/Ca, and Sr/Ca records of downcore planktonic foraminiferal samples of sites SO164–07–4 and SO164–19–2 show to some extent atypical values with respect to data sets reflecting past environmental conditions (Chapter 5.3.1; Figures 5.4, 5.5). Within the same

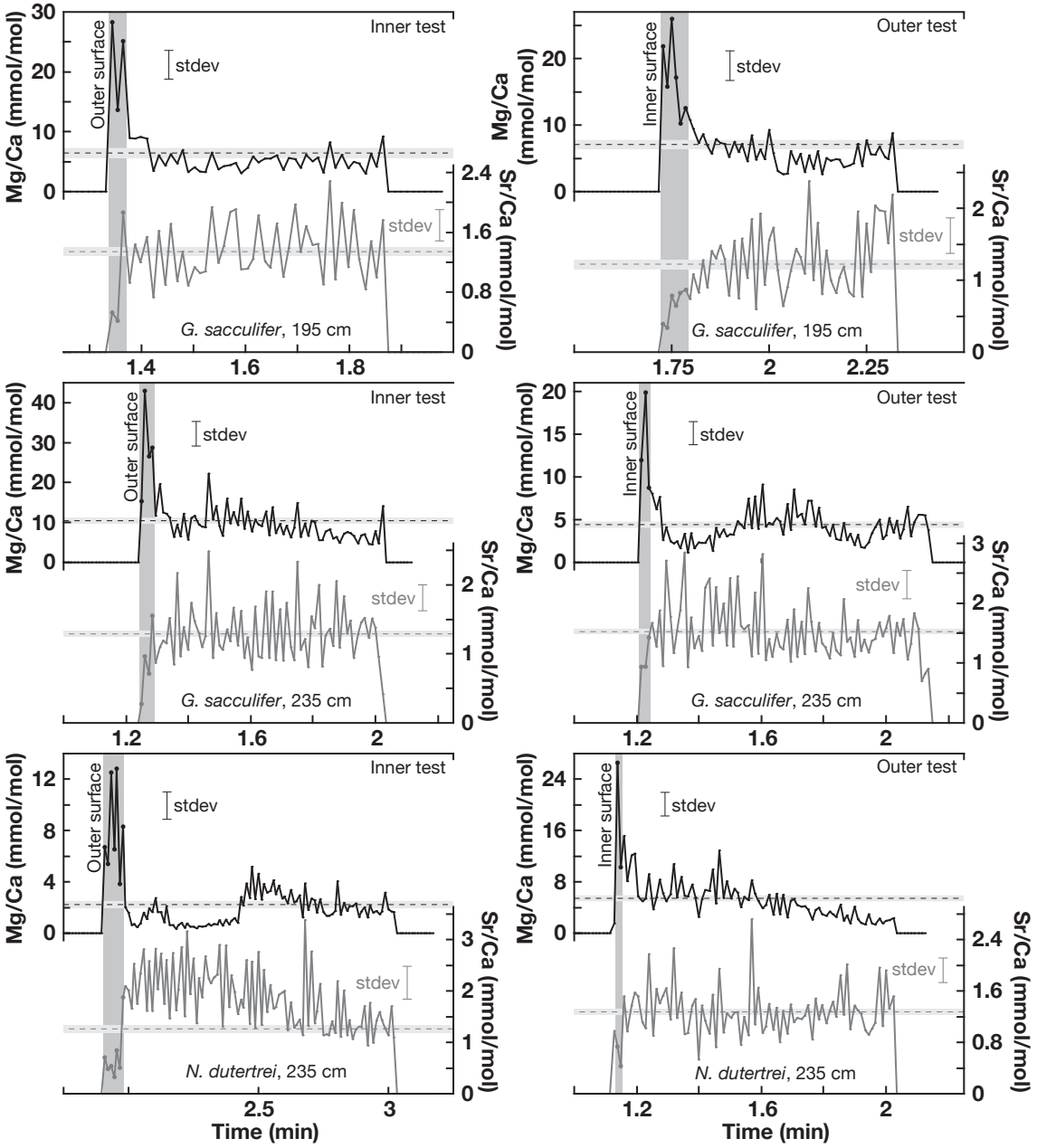

Figure 5.9 Time-resolved LA-ICP MS Mg/Ca (upper panels) and Sr/Ca ratios (lower panels) of cleaned foraminiferal samples with diagenetic overgrowths of site SO164–19–2, ablated perpendicular to the chamber-wall surfaces: Sample 195 cm (∼365 kyrs), sample 235 cm (∼427 kyrs). Standard deviations of single ratios are given as error bars (stdev). Horizontal dashed lines illustrate mean ratios averaged for the entire profile of each plot, standard deviations of the respective means are given as horizontal bars. Vertical grey bars illustrate surface-near ratios revealing elevated Mg/Ca and lowered Sr/Ca compared to the remainder ratios. Left hand profiles are ablated from the outer side of the tests towards the inner side, right hand profiles *vice versa*.

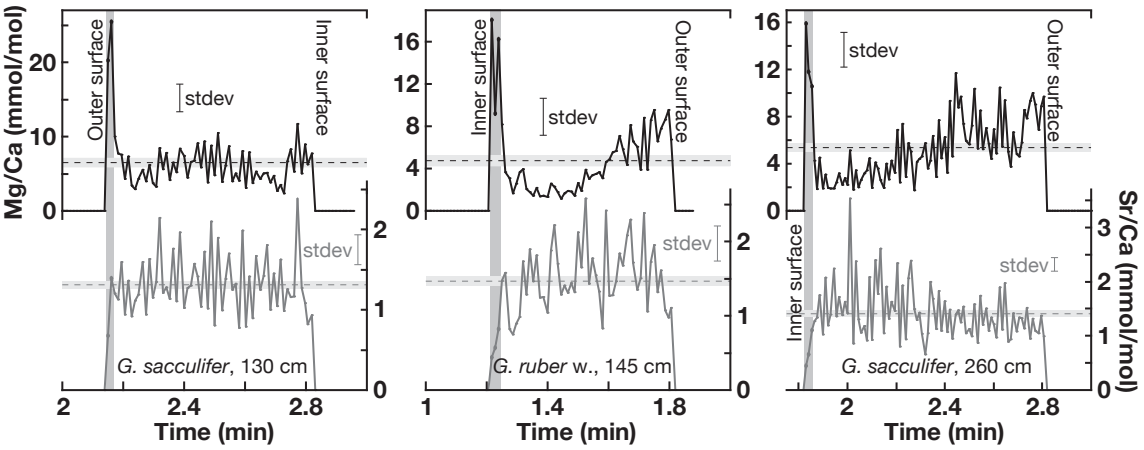

Figure 5.10 Time-resolved LA-ICP MS Mg/Ca and Sr/Ca ratios of cleaned foraminiferal samples with diagenetic overgrowths of site SO164–19–2: Sample 130 cm (∼260 kyrs), sample 145 cm (∼288 kyrs), sample 260 cm (∼ 473 kyrs). For detailed description, see Figure 5.9.

samples, δ^{18}O values as well as Mg/Ca ratios are higher than expected, Sr/Ca, contrarily, shows the inverse trend with lower ratios than expected.

In principal, the oxygen isotope composition of the actual planktonic foraminiferal test is determined by the composition and (higher) temperature of the pelagic waters, in which the calcite was formed. Since precipitation of the overgrowth during diagenesis is expected to occur near the sediment/bottom-water interface and its oxygen isotope composition is driven by thermodynamic fractionation (e.g., *O'Neil et al.*, 1969; *Kim and O'Neil*, 1997), δ^{18}O tends to more positive values (e.g., *Killingley*, 1983; *Schrag et al.*, 1995; *Crowley and Zachos*, 2000; *Pearson et al.*, 2001; *Wade and Kroon*, 2002). Like in this study, higher than expected foraminiferal δ^{18}O values from deep-sea sites in conjunction with diagenetic crystalline overgrowth have been observed, yet merely for sample material from great sediment-burial depth (e.g., *Pearson et al.*, 1997; *Norris and Wilson*, 1998; *Price et al.*, 1998; *Wade and Kroon*, 2002; *Tripati et al.*, 2003; *Sexton et al.*, 2006).

The common approach to understand the contribution to the calcite composition derived from inorganic precipitates is using downcore pore-fluid data for the calculation and numerical modeling of theoretical precipitate compositions (e.g., *Killingley*, 1983; *Schrag et al.*, 1992; *Schrag*, 1999; *Rudnicki et al.*, 2001; *Tripati et al.*, 2003; *Sexton et al.*, 2006). In contrast to these studies, we attempt to quantify the influence of the diagenetic overgrowth with the results from laser-ablation analysis, as downcore pore fluid data are not available for the presented sites and the fluid behavior at the very shallow burial depth of the deep-sea sediments is hardly understood (e.g., *Mullins et al.*, 1985; *Morse*, 2003).

5.4.1 Mg/Ca and Sr/Ca Data: Assessing the extent of diagenetic alteration

Considering the visual evidence for diagenetic alteration of planktonic foraminiferal tests (Figures 5.7, 5.8) in combination with the results of the laser ablation (Figures 5.9, 5.10),

Table 5.1 Mass-balanced Mg/Ca and Sr/Ca ratios of an assumed planktonic foraminiferal sample overgrown with diagenetic crystallites. Proportions of overgrowth are given with respect to foraminiferal calcite. Assumed crystallite ratios are obtained from LA-ICP MS results.

Over-growth	Combined signature of planktonic foraminifera and overgrowth (mmol/mol)				
%	[a]Mg/Ca	[b]Mg/Ca	[c]Mg/Ca	[d]Sr/Ca	[e]Mg/Ca
0	4	4	4	1.4	1.4
5	4.3	4.8	5.8	1.36	1.37
10	4.6	5.6	7.6	1.31	1.34
15	4.9	6.4	9.4	1.27	1.31
20	5.2	7.2	11.2	1.22	1.28

[a]Assumed Mg/Ca (mmol/mol): Planktonic foraminifera = 4; crystallites = 10
[b]Assumed Mg/Ca (mmol/mol): Planktonic foraminifera = 4; crystallites = 20
[c]Assumed Mg/Ca (mmol/mol): Planktonic foraminifera = 4; crystallites = 40
[d]Assumed Sr/Ca (mmol/mol): Planktonic foraminifera = 1.4; crystallites = 0.5
[e]Assumed Sr/Ca (mmol/mol): Planktonic foraminifera = 1.4; crystallites = 0.8

the explanation for anomalously high Mg/Ca ratios is the presence of inorganic calcite: The outermost measurements, even if time-resolved, closely correspond with the outermost position of the diagenetic crystallites. Inorganic calcite contains about an order of magnitude more Mg^{2+} than planktonic foraminiferal calcite (e.g., *Katz*, 1973; *Baker et al.*, 1982; *Mucci and Morse*, 1983; *Mucci*, 1987). We detected 10–40 mmol/mol for the crystallites, typically <7 mmol/mol for the actual test (Figures 5.9, 5.10). Thus, only little proportion of overgrowth, which still remains on the foraminiferal test even after the Mg-cleaning procedure, would be sufficient to raise the ratio of foraminiferal sample calcite.

Sr/Ca ratios of the ablated chamber-wall cross sections reveal 2–3 times depleted ratios for the inorganic crystallites, which is ∼0.5–0.8 mmol/mol. Depending on the species, typical ratios of planktonic foraminifera without overgrowth are in the order of 1.2–1.7 mmol/mol (Figure 5.6). Since biogenic calcite contains significantly more Sr^{2+} than inorganic (*Baker et al.*, 1982; *Carpenter and Lohmann*, 1992), lower Sr/Ca indicates larger proportions of secondary inorganic calcite (*Bralower et al.*, 1997).

In order to estimate the proportion of diagenetic overgrowth necessary to alter the Mg/Ca and Sr/Ca ratios of the actual foraminiferal test by degrees indicated by the downcore records (Figure 5.4), we applied mass balance. End-member phases are an assumed planktonic foraminifera with Mg/Ca of 4 mmol/mol and Sr/Ca of 1.4 mmol/mol, roughly appropriate for interglacial *G. sacculifer*, and three possible Mg/Ca (10, 20, 40 mmol/mol) and two possible Sr/Ca signals (0.5, 0.8 mmol/mol) for the overgrowth, obtained from laser ablation (Table 5.1). We suggest that a proportion of 10–20% of crystallites is sufficient to increase (decrease) the Mg/Ca (Sr/Ca) the way we observed for sites SO164–07–4 (∼7 mmol/mol; Figure 5.5) and SO164–19–2 back until MIS 13 (∼11 mmol/mol; Figure 5.4).

Prior to MIS 13, this straightforward interrelationship between Mg/Ca ratios and Sr/Ca is not visible anymore, both show similar trends with an intense decrease from MIS 18–20. Since

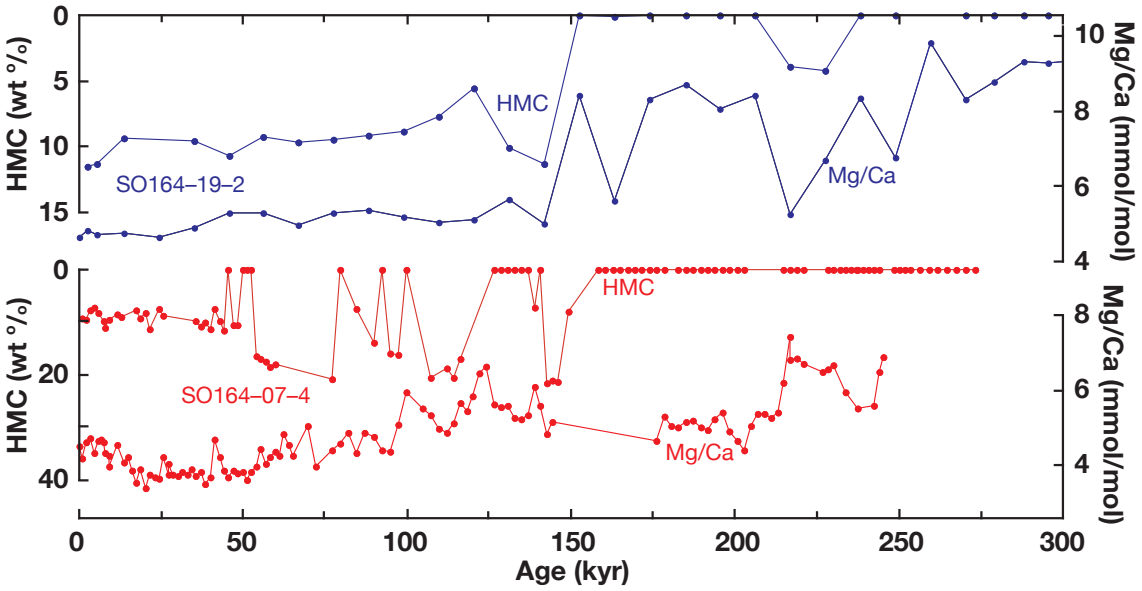

Figure 5.11 *G. sacculifer* Mg/Ca ratios and high-magnesium calcite proportion on the carbonate phases of sites SO164–07–4 and SO164–19–2 for the last 300 kyrs: Note that HMC weight percentages are inversely plotted.

we have got neither SEM images nor laser-ablation data from the older part of the record, we cannot illucidate the changing patterns of geochemical compositions. It might be speculated that the system for pore fluid changes the way that dissolution and reprecipitation of carbonate has taken place, which results in increased Sr^{2+} and Mg^{2+} concentrations of coexisting pore fluids (*Schrag et al.*, 1995). A diffusive flux of ions out the top of the sediment column (*Schrag et al.*, 1995) might have depleted the pore fluid (and elevated the overlying fluids). Such carbonate recrystallization is suggested to have relatively minor effects on $\delta^{18}O$ values of pore fluid (*Schrag et al.*, 1992). The recorded $\delta^{18}O$ trend during this time interval with values around 0.5‰ and lack of considerable changes implies that the original planktonic foraminiferal signal has almost completely been overprinted or recrystallized.

5.4.2 Control of high-magnesium calcite on Mg/Ca ratios?

Aragonite and high-magnesium calcite (HMC) get important in areas around carbonate platforms, which distribute these shallow-water carbonates even down to the deep sea (*Morse*, 2003). Relatively high proportions of aragonite and HMC (Figure 5.3) seem to confirm a recent influence of carbonate production on platforms (i.e. most likely the Bahama platform) on the deep-sea region of the presented sites. Nevertheless, reported aragonite production on the Bahama platform and export towards the deeper basins around the platform during sea-level highstands (*Kroon et al.*, 2000; *Rendle et al.*, 2000; *Slowey et al.*, 2002), possibly mirrored in the aragonite contents of site SO164–07–4, are certainly not reflected in the downcore trend of the carbonate phases of shallow site SO164–19–2. Moreover, absence of aragonite and HMC in sediments of

site SO164–19–2 prior to ∼300 kyrs may result from selective dissolution of both phases, which was observed for deeper water (>1000 m) Bahamian periplatform slope sediments (*Mullins et al.*, 1985; *Haak and Schlager*, 1989). Associated reprecipitation of low-magnesium calcite in the respective sediments (*Mullins et al.*, 1985) in combination with possible supply of Mg2+ through diffusive flux of ions (*Schrag et al.*, 1995) from the deeper sediment column could provide a source to alter the planktonic foraminiferal geochemical composition to the observed extent. Probably, this is why planktonic foraminiferal Mg/Ca ratios and HMC content of sites SO164–07–4 and SO164–19–2 reveal negatively correlated trends (Figure 5.11) with occurrence of anomalously high Mg/Ca above ∼6 mmol/mol, only when HMC is absent from the sediments.

5.5 Conclusions

Planktonic foraminiferal δ^{18}O, Mg/Ca, and Sr/Ca records of two deep-sea sediment cores (SO164–07–4, 2722 m; SO164–19–2, 1704 m) from tropical Windward Passage of the last glacial/interglacial cycles reveal values atypical for pelagic environmental conditions. Contemporaneously, δ^{18}O values and Mg/Ca ratios are higher than expected, Sr/Ca shows lower ratios than expected. Contamination by Mg^{2+}-bearing Mn-oxide coatings and clay could have been ruled out.

Scanning electron microscope images display distinct micro-scale euhydral crystallites of inorganic precipitates on tests with the atypical geochemical composition. Laser ablation measurements of foraminiferal chamber walls identified significant different Mg/Ca (4–6 times elevated) and Sr/Ca signals (2–3 times depleted) for the inorganic precipitates in comparison with the actual foraminiferal test.

Back until marine isotope stage 13, crystalline overgrowth proportions of 10–20%, which cannot by removed by the cleaning procedure applied for foraminiferal Mg/Ca analysis, are sufficient to alter the Mg/Ca and Sr/Ca of the foraminiferal sample calcite to the observed extent. The absence of aragonite and high-magnesium calcite in the sediments prior to ∼300 kyrs is likely coupled with selective dissolution within the sediments. It might be speculated that the combined processes of dissolution of these two phases and reprecipitation of low-magnesium calcite contributes as a source for diagenetic alteration of the planktonic foraminiferal geochemical composition. Considering changed interrelationships between the planktonic foraminiferal geochemical parameters prior to marine isotope stage 13, we suggest a diffusive flux of ions out the top of the sediment column (*Schrag et al.*, 1995) to supply the pore fluid of the overlying sediments. In these sediments, however, planktonic foraminiferal Mg/Ca ratios and high-magnesium calcite presence in the respective sediments show the exclusion of anomalously high Mg/Ca (>6 mmol/mol), when HMC is present.

As diagenetic alteration, especially in such shallow-burial sediments, is controlled by very local conditions and processes, similarities of the planktonic foraminiferal δ^{18}O and Mg/Ca records SO164–07–4, and M35027 as well as M35053 are remarkable (Figures 5.5). The vicinity of these sites to carbonate platforms implies similar processes in sediments with

dissolution of significant proportions of aragonite and, most important, high-magnesium calcite, and reprecipitation of low-magnesium calcite.

5.6 Acknowledgements

We thank John J. G. Reijmer, Jeroen Groeneveld, Sybille Noe, Lars Reuning, and Silke Steph for insightful discussions. SEM images were prepared at the Institute for Geosciences, Kiel, with the aid of Ute Schuldt and Lester Lembke-Jene. We also thank Beate Bader, Dieter Garbe-Schönberg, Lulzim Haxhiaj, Jutta Heinze, Karin Kißling, Silvia Koch, for laboratory know-how and technical support. Financial support for this research was provided by the German Ministry of Education and Research (BMBF, project No. 03G0164).

Chapter 6

Summary & Conclusions

Calcification Depths of Modern Planktonic Foraminiferal

Since planktonic foraminiferal species pass through differing life cycles including partly large vertical migration through the upper water column with calcification at different stages (e.g., *Bé*, 1977; *Hemleben et al.*, 1989; *Lohmann*, 1995; *Schiebel and Hemleben*, 2005), the geochemical composition of proxy indicators may be complicated due to a mixing of the originating signal. Nevertheless, planktonic foraminifera from the examined tropical Atlantic and Caribbean sediment-surface samples (0–1 cm) are observed to reflect the modern hydrographic conditions. Both, the magnesium content as well as the oxygen isotope composition of the planktonic foraminiferal tests unanimously show the systematic succession of the different species according to their expected increased calcification depths. Furthermore, a general westward-directed increase in calcification depths of the examined species is depending on the hydrographic regime in terms of thermocline depth, which increases from the E-Atlantic towards the Caribbean.

Preservation of the Planktonic Foraminiferal Mg/Ca Ratios

The magnesium content in a calcite planktonic foraminiferal test, expressed as Mg/Ca ratio, has been shown to reflect seawater temperature at the depth of calcification (*Elderfield and Ganssen*, 2000; *Nürnberg*, 2000; *Anand et al.*, 2003). Since Mg/Ca is also subject to dissolution (*Lorens et al.*, 1977; *Rosenthal et al.*, 1997; *Martin et al.*, 2002), the assessment of its extent is crucial to any temperature reconstruction *Dekens et al.* (2002). From the close modern interrelationship of decreasing planktonic foraminiferal Mg/Ca, increasing water depth, and decreasing carbonate ion concentration in the Caribbean, we extracted a dissolution pattern indicating that initial ratios are only preserved at depths well above the lysocline (at least 1.5 km). Depending on the foraminiferal species, we found that Mg/Ca starts to decrease linearly, when the carbonate ion concentration at sedimentation falls below 26–18 μmol/kg. For the recalculation of the initial Mg/Ca from a dissolution-affected ratio, we developed routines, which account for the carbonate ion concentration (or water depth) at sedimentation b with respect to the critical carbonate ion

concentration (or water depth) level, where dissolution starts:

- Correction-equation for depth-induced decrease is
  $Mg/Ca_{initial} = Mg/Ca_{dissolution-affected} + (d - d_{critical})/b$.
- Correction-equation for carbonate ion concentration $\Delta[CO_3{}^{2-}]$-induced decrease is
  $Mg/Ca_{initial} = Mg/Ca_{measured} + (\Delta[CO_3^{2-}]_{critical} - \Delta[CO_3^{2-}])/b$.

Determination of Upper Ocean Temperatures

The alignment of oxygen isotope compositions (δ^{18}O), also an indicator of seawater temperature (e.g., *Urey*, 1947; *O'Neil et al.*, 1969; *Lea*, 2003; *Zhou and Zheng*, 2003), and Mg/Ca ratios within the same biogenic carrier holds the possibility to establish well-defined temperature dependencies for either of the proxies. On the basis of dissolution-unaffected planktonic foraminiferal Mg/Ca of multiple species from different preferred calcification depths, we attempt to calibrate the ratios with δ^{18}O-derived calcification temperatures. Investigation of the respective calcification depths approved the temperatures calculated after the δ^{18}O-paleotemperature of *Shackleton* (1974) to most accurately fit the habitat specifications of the species from literature (e.g., *Williams et al.*, 1981; *Deuser and Ross*, 1989; *Niebler et al.*, 1999; *Schmuker and Schiebel*, 2002). Mg/Ca was calibrated for the overall range in calcification temperatures of 8–28°C. Similar exponential temperature sensitivities of 7–11% per 1°C for all species examined are faced by significantly different preexponential constants for the shallow- and thermocline-dwelling species (0.23–0.65 for *G. ruber* pink and white, *G. sacculifer*; *G. menardii* and *N. dutertrei*) with respect to the deep dwellers (0.83–1.31 for *G. truncatulinoides* dextral and *G. crassaformis*). Focussing on a multispecies Mg/Ca paleothermometry, we extracted two relationships,

- a 'warm water' calibration from shallow- and thermocline-dwelling species
  ($Mg/Ca = 0.223 \cdot exp(0.113T)$) for temperatures above 19°C, and
- a 'cold water' calibration from deep-dwelling species
  ($Mg/Ca = 0.842 \cdot exp(0.083T)$) for temperatures below 15°C.

Description of Upper-Ocean Stratification

The tropical Atlantic upper water column is temperature- and nutrient-stratified with a westward increasing thermocline depth below a thickening mixed layer. Changing depth of a variable thermocline depths would, thus, provide information about the heat content stored in the warm water of the mixed layer (*Philander and Pacanowski*, 1986b; *McPhaden*, 2003). A high potential to register such changes in upper ocean stratification is involved in planktonic foraminiferal oxygen and carbon isotope compositions (δ^{18}O and δ^{13}C) from different preferred calcification depths by using the isotope differences between the species. In terms of grouped foraminifera,

modern interspecific δ^{18}O gradients between intermediate dwellers (*G. tumida* and *G. scitula*) and shallow (deep) dwellers clearly reflect the east-west increase in thermocline depth by showing decreased (increased) values with a deepening of the thermocline. The same pattern as for the intermediate species is observed for the thermocline-dwelling species. For the δ^{13}C differences between shallow- and deep-dwelling species, a decrease of the gradients towards the Caribbean is consistent with modern decreasing vertical nutrient gradients associated with the increasing thermocline depth.

Characterization of Diagenetic Precipitates

Almost all deep-sea carbonate-rich sediments are composed of calcite low in magnesium (>99 weight percent of $CaCO_3$) with primarily derived material from pelagic skeletal organisms such as coccolithophores and foraminifera, and a varying proportion of aragonite from pteropods and heteropods. This is different for areas around carbonate platforms, where platform-derived aragonite and high-magnesium calcite are exported toward the deeper basins (e.g., *Rendle et al.*, 2000; *Kroon et al.*, 2000; *Slowey et al.*, 2002). Alteration of such deeper-basin carbonates at the Bahamas results from selective dissolution of aragonite and high-magnesium calcite, and reprecipitation of low-magnesium calcite (*Mullins et al.*, 1985). Shallow-burial diagenetic reprecipitates from the upper meters of the sediments, however, are found as micro-scale euhydral crystallites on planktonic foraminiferal test in sediment cores from the Windward Passage (channel between Caribbean and Atlantic). The geochemical composition of the crystallites is 4–6 times increased for Mg/Ca ratios and 2–3 times decreased for Sr/Ca with respect to the actual foraminiferal test as revealed by laser-ablation profiles. Continuous elevation of the planktonic foraminiferal Mg/Ca above 6 mmol/mol is caused by a crystallite proportion of 10–20 percent and synchronizes the absence of high-magnesium calcite from the sediment. Prior ∼550 thousand years, changed geochemical characteristics suggest diffusive flux of ions (*Schrag et al.*, 1995) supportive for the diagenetic alteration in the overlying sediment column. The observed sensitivity of planktonic foraminiferal Mg/Ca to little amounts of inorganic calcite, which are sufficient to compromise its application as temperature indicator, is disastrous for Mg/Ca paleothermometry. Furthermore, this sensitivity of Mg/Ca as well as Sr/Ca can be turned into the opportunity for a control of a diagenetic influence on sediment cores.

Bibliography

Anand, P., and H. Elderfield (2005), Variability of Mg/Ca and Sr/Ca between and within the planktonic foraminifers *Globigerina bulloides* and *Globorotalia truncatulinoides*, *Geochem. Geophys. Geosys.*, *6*(11), doi:10.1029/2004GC000811. 2.4.3, 2.4.4

Anand, P., H. Elderfield, and M. H. Conte (2003), Calibration of Mg/Ca thermometry in planktonic foraminifera from sediment trap time series, *Paleoceanography*, *18*(2), doi:10.1029/2002PA000846. 1.2, 1.3.1, 2.1, 2.2, 2.4.2, 2.4.3, 2.4, 2.4.3, 2.5, 2.4.5, 3.1, 3.4.1, 3.7, 3.4.1, 3.7, 3.4.2, 4.3, 4.4.1, 6

Anderson, D. M., and D. Archer (2002), Glacial-interglacial stability of ocean pH inferred from foraminifer dissolution rates, *Nature*, *416*, 70–73. 2.4.5

Baker, P. A., J. M. Gieskes, and H. Elderfield (1982), Diagenesis of carbonates in deep-sea sediments: Evidence from Ca/Sr ratios and interstitial dissolved Sr^{2+} data, *J. Sediment. Petrol.*, *52*, 71–82. 5.1, 5.4.1

Barker, S., and H. Elderfield (2002), Foraminiferal Calcification Response to Glacial-Interglacial Changes in Atmospheric CO_2, *Science*, *297*, 833–836. 2.4.5

Barker, S., M. Greaves, and H. Elderfield (2003), A study of cleaning procedures used for foraminiferal Mg/Ca paleothermometry, *Geochem. Geophys. Geosys.*, *4*(9), doi:10.1029/2003GC000559. 2.3.3, 3.2.2, 5.2.3, 5.3.4

Bassinot, F. C., L. D. Labeyrie, E. Vincent, X. Quidelleur, N. J. Shackleton, and Y. Lancelot (1994), The astronomical theory of climate and the age of the Brunhes-Matuyama magnetic reversal, *Earth Planet. Sci. Lett.*, *126*, 91–108. 5.2.4

Bé, A. W. H. (1977), An ecological, zoogeographic and taxonomic review of recent planktonic foraminifera, in *Oceanic Micropaleontology, Vol. 1*, edited by A. T. S. Ramsay, pp. 1–100, Academic Press, London. 1.3.1, 2.3.2, 6

Bé, A. W. H. (1980), Gametogenic calcification in a spinose planktonic foraminifer *Globigerinoides sacculifer* (Brady), *Mar. Micropal.*, *5*, 283–310. 1.3.1, 2.3.2

Bé, A. W. H., and D. B. Ericson (1963), Aspects of calcification in planktonic foraminifera, *Ann. N. Y. Acad. Sci.*, *109*, 65–81. 1.3.1, 2.3.2

Bé, A. W. H., and L. Lott (1964), Shell growth and structure of planktonic foraminifera, *Science*, *145*, 823–824. 1.3.1, 2.3.2

Bé, A. W. H., O. R. Anderson, W. W. J. Faber, and D. A. Caron (1983), Sequence of morphological and cytoplasmic changes during gametogenesis in the planktonic foraminifera *Globigerinoides sacculifer* (Brady), *Micropaleontology*, *29*, 310–325. 1.3.1, 2.3.2

Bemis, B. E., H. J. Spero, J. Bijma, and D. W. Lea (1998), Reevaluation of the oxygen isotopic composition of planktonic foraminifera: Experimental results and revised paleotemperature equations, *Paleoceanography*, *13*(2), 150–160. 3.3, 3.3.1, 3.4, 3.5, 4.1

Bemis, B. E., H. J. Spero, D. W. Lea, and J. Bijma (2000), Temperature influence on the carbon isotopic composition of *Orbulina universa* and *Globigerina bulloides* (planktonic foraminifera), *Mar. Micropal.*, *38*, 213–228. 4.1, 4.4.3, 4.4.4, 4.4.6

Bender, M. L., R. B. Lorens, and D. F. Williams (1975), Sodium, Magnesium and Strontium in the Tests of Planktonic Foraminifera, *Micropaleontology*, *21*(4), 448–459, doi:10.2307/1485293. 2.4.4

Bentov, S., and J. Erez (2005), Novel oberservations on biomineralization processes in foraminifera and implications for Mg/Ca ratio in the shells, *Geology*, *33*(11), 841–844, doi: 10.1130/G21800.1. 2.4.4

Bentov, S., and J. Erez (2006), Impact of biomineralization processes on the Mg content of foraminiferal shells: A biological perspective, *Geochem. Geophys. Geosys.*, *7*(1), Q01P08, doi: 10.1029/2005GC001015. 2.4.4

Benway, H. M., B. A. Haley, G. P. Klinkhammer, and A. C. Mix (2003), Adaptation of a flow-through leaching procedure for Mg/Ca paleothermometry, *Geochem. Geophys. Geosys.*, *4*(2), 8403, doi:10.1029/2002GC000312. 1.3.1

Berger, W. H. (1968), Planktonic foraminifera: Selective solution and paleoclimate interpretation, *Deep-Sea Res.*, *15*, 31–43. 2.4.4

Berger, W. H. (1970), Planktonic foraminifera: Selective solution and the lysocline, *Mar. Geol.*, *8*, 111–138. 2.4.4

Berger, W. H. (1971), Sedimentation of planktonic foraminifera, *Mar. Geol.*, *11*, 325–358. 2.4.4

Bijma, J., J. Erez, and C. Hemleben (1990), Lunar and semi-lunar reproductive cycles in some spinose planktonic foraminifers, *J. Foram. Res.*, *20*(2), 117–127. 1.3.1, 2.3.2

Bijma, J., C. Hemleben, and K. Wellnitz (1994), Population dynamics of the planktic foraminifer *Globigerinoides sacculifer* (Brady) from the central Red Sea, *Deep-Sea Res. I*, *41*(3), 485–510. 1.3.1, 2.3.2

Bleil, U., and G. Fischer (Eds.) (1998), *Research Vessel METEOR Cruise No. 38 (1997): Geo Bremen South Atlantic 1997*, Institut für Meereskunde der Universität Hamburg, Leitstelle METEOR, Hamburg. 4.3

Böhm, F., M. M. Joachimski, H. Lehnert, G. Morgenroth, W. Kretschmer, J. Vacelet, and W.-C. Dullo (1996), Carbon isotope records from extant Caribbean and South Pacific sponges: Evolution of δ^{13}C in surface water DIC, *Earth Planet. Sci. Lett.*, *139*, 291–303. 4.4.3

Bourles, B., Y. Gouriou, and R. Chuchla (1999a), On the circulation in the upper layer of the western equatorial Atlantic, *J. Geophys. Res.*, *104*(C9), 21,151–21,170, doi:10.1029/1999JC900058. 4.2

Bourles, B., R. L. Molinari, E. Johns, W. D. Wilson, and K. D. Leaman (1999b), Upper layer currents in the western tropical North Atlantic (1989–1991), *J. Geophys. Res.*, *104*(C1), 1361–1376, doi:10.1029/1998JC900025. 4.2

Bouvier-Soumagnac, Y., and J.-C. Duplessy (1985), Carbon and oxygen isotopic composition of planktonic foraminifera from laboratory culture, plankton tows and recent sediment: Implications for the reconstruction of paleoclimatic conditions and of the global carbon cycle, *J. Foram. Res.*, *15*(4), 302–320. 3.3, 3.3.1, 3.4, 3.5

Bralower, T. J., P. D. Fullagar, C. K. Paull, G. S. Dwyer, and R. M. Leckie (1997), Mid-Cretaceous strontium-isotope stratigraphy of deep-sea sections, *GSA Bull.*, *109*(10), 1421–1442. 5.4.1

Broecker, W. S. (1989), The salinity contrast between the Atlantic and Pacific oceans during glacial time, *Paleoceanography*, *4*, 207–212. 3.2, 3.3.1, 4.3

Broecker, W. S., and E. Clark (2002), Carbonate ion concentration in glacial-age deep waters of the Caribbean Sea, *Geochem. Geophys. Geosys.*, *3*(3), doi:10.1029/2001GC000231. 2.4.5

Broecker, W. S., and E. Clark (2003), $CaCO_3$ dissolution in the deep sea: Paced by insolation cycles, *Geochem. Geophys. Geosys.*, *4*(7), 1059, doi:10.1029/2002GC000450. 3.2.2

Brown, K., and K. Azmy (2005), Morphological and geochemical analysis of recent Caribbean Globorotaliid foraminifera, in *Geophys. Res. Abstracts*, vol. 7, sRef-ID: 1607-7962/gra/EGU05-A-05254. 2.3.2

Brown, S. J., and H. Elderfield (1996), Variations in Mg/Ca and Sr/Ca ratios of planktonic foraminifera caused by postdepositional dissolution: Evidence of shallow Mg-dependent dissolution, *Paleoceanography*, *11*(5), 543–551. 2.1, 2.4.2, 2.4.4

Bulgakov, N. P., and O. D. Lomakin (1995), Local sound channels in the Caribbean Sea, *Oceanology*, *34*(6), 744–749. 2.2

Carpenter, S. J., and K. C. Lohmann (1992), Sr/Mg ratios of modern calcite: Empirical indicators of ocean chemistry and precipitation rate, *Geochim. Cosmochim. Acta*, *56*, 1837–1849. 5.4.1

Chaisson, W., and A. C. Ravelo (2000), Pliocene development of the East-West hydrographic gradient in the Equatorial Pacific, *Paleoceanography*, *15*(5), 1999PA000442. 4.4.2

Chaisson, W. P., and A. C. Ravelo (1997), Changes in upper water-column structure at Site 925, Late Miocene-Pleistocene: Planktonic foraminifer assemblage and isotopic evidence, in *Proc. ODP, Sci. Results*, vol. 154, edited by N. J. Shackleton, W. B. Curry, C. Richter, and T. J. Bralower, pp. 255–268, College Station, TX (Ocean Drilling Program). 2.3.2, 2.4.3

Cleveland, W. S. (1979), Robust locally weighted regression and smoothing scatterplots, *J. Am. Stat. Assoc.*, *74*, 829–836. 3.4, 4.4, 4.6, 4.7, 4.8, 4.11, 4.12

Corredor, J. E., and J. M. Morell (2001), Seasonal variation of physical and biogeochemical features in eastern Caribbean Surface Water, *J. Geophys. Res.*, *106*(C3), 4517–4525. 2.2

Cronblad, H. G., and B. A. Malmgren (1981), Climatically controlled variation of Sr and Mg in Quaternary planktic foraminifera, *Nature*, *291*, 61–64. 2.1

Crowley, T. J., and J. C. Zachos (2000), Comparison of zonal temperature profiles for past warm periods, in *Warm Climates in Earth History*, edited by B. T. Huber, K. G. MacLeod, and S. L. Wing, pp. 50–76, Cambridge University Press, Cambridge, doi:10.2277/052164142X. 5.4

Csanady, G. T. (1990), Retroflection and leakage in the North Brazil Current - Critical-point analysis, *J. Mar. Res.*, *48*, 701–728. 4.2

Curry, W. B., and T. J. Crowley (1987), The ^{13}C of equatorial Atlantic surface waters: Implications for the ice age pCO_2 levels, *Paleoceanography*, *2*(5), 489–517. 1.3.1, 2.3.2

Curry, W. B., and R. K. Matthews (1981a), Equilibrium ^{18}O fractionation in small size fraction planktic foraminifera: Evidence from Recent Indian Ocean sediments, *Mar. Micropal.*, *6*, 327–337. 4.4.1

Curry, W. B., and R. K. Matthews (1981b), Paleo-oceanographic utility of oxygen isotopic measurements on planktic foraminifera: Indian Ocean core-top evidence, *Palaeogeogr., Palaeoclimatol., Palaeoecol.*, *33*, 173–191. 4.4.1

Curry, W. B., and D. W. Oppo (1997), Synchronous, high-frequency oscillations in tropical sea surface temperatures and North Atlantic Deep Water production during the last glacial cycle, *Paleoceanography*, *12*, 1–14. 5.3.3

Curry, W. B., R. C. Thunell, and S. Honjo (1983), Seasonal changes in the isotopic composition of planktonic foraminifera collected in Panama Basin sediment traps, *Earth Planet. Sci. Lett.*, *64*, 33–43. 2.3.2, 4.4.1

de Villiers, S. (2003), Dissolution effects on foraminiferal Ma/Ca records of sea surface temperature in the western equatorial Pacific, *Paleoceanography*, *18*(3), 1070, doi:10.1029/2002PA000802. 2.1

Dekens, P. S., D. W. Lea, D. K. Pak, and H. J. Spero (2002), Core top calibration of Mg/Ca in tropical foraminifera: Refining paleotemperature estimation, *Geochem. Geophys. Geosys.*, *3*(4), doi:10.1029/2001GC000200. 1.2, 1.3.1, 2.1, 2.2, 2.4.2, 2.5, 2.4.3, 2.4.4, 3.1, 3.2.2, 3.4.1, 3.4.1, 3.6, 5.1, 6

Deuser, W. G. (1987), Seasonal variations in isotopic composition and deep-water fluxes of the tests of perennially abundant planktonic foraminifera of the Sargasso Sea: Results from sediment trap collections and their paleoceanographic significance, *J. Foram. Res.*, *17*, 14–27. 2.3.2, 2.4.3

Deuser, W. G., and E. H. Ross (1989), Seasonally abundant planktonic foraminifera of the Sargasso Sea: succession, deep-water fluxes, isotopic compositions, and paleoceanographic implications, *J. Foram. Res.*, *19*, 268–293. 2.3.2, 2.4.3, 3.4.1, 6

Dickson, A. G. (1990), Standard potential of the reaction: Ag(Cl)(s) + 1/2 H_2(g) = Ag(s) + HCl(aq), and the standard acidity constant ot the ion HSO_4^- in synthetic seawater from 273.15 to 318.15 K, *J. Chem. Thermodyn.*, *22*, 113–127. 1.4.2

Dickson, A. G., and F. J. Millero (1987), A comparison of the equilibrium constants for the dissociation of carbonic acid in seawater media, *Deep-Sea Res.*, *34*, 1733–1743. 1.4.2

Droxler, A. W. (1984), Late quaternary glacial cycles in the Bahamian deep basins and in the adjacent Atlantic Ocean, Ph.D. thesis, Miami Univ., Coral Gables, USA. 5.1

Duckworth, D. L. (1977), Magnesium concentrations in the tests of the planktonic foraminifer *Globorotalia truncatulinoides*, *J. Foram. Res.*, *4*, 304–312. 2.4.4

Duplessy, J.-C., P. L. Blanc, and A. W. H. Bé (1981), Oxygen-18 enrichment of planktic foraminifera due to gametogenic calcification below the euphotic zone, *Science*, *213*, 1247–1249. 1.3.1, 2.3.2, 4.1

Duplessy, J.-C., L. Labeyrie, A. Juillet-Leclerc, F. Maitre, J. Dupart, and M. Sarnthein (1991), Surface salinity reconstruction of the North Atlantic ocean during the last glacial maximum, *Oceanol. Acta*, *14*, 311–324. 4.1

Eggins, S., P. DeDeckker, and J. Marshall (2003), Mg/Ca variation in planktonic foraminifera tests: implications for reconstructing palaeo-seawater temperature and habitat migration, *Earth Planet. Sci. Lett.*, *212*, 291–306. 1.3.1, 2.3.2, 2.4.4, 5.1, 5.2.5

Elderfield, H., and G. Ganssen (2000), Past temperature and δ^{18}O of surface ocean waters inferred from foraminiferal Mg/Ca ratios, *Nature*, *405*, 442–445, doi:10.1038/35013033. 1.2, 1.3.1, 2.1, 2.4.3, 3.1, 3.4.1, 3.7, 3.4.1, 3.7, 3.4.2, 4.3, 6

Elderfield, H., M. Vautravers, and M. Cooper (2002), The relationship between shell size and Mg/Ca, Sr/Ca, δ^{18}O, and δ^{13}C of species of planktonic foraminifera, *Geochem. Geophys. Geosys.*, *3*(8), doi:10.1029/2001GC000194. 2.3.1, 2.4.3, 3.2.2

Emiliani, C. (1954), Depth habitats of some species of pelagic foraminifera as indicated by oxygen isotope ratios, *Am. Jour. Sci.*, *252*, 149–158. 3.1, 4.1, 4.4.1

Emiliani, C. (1955), Pleistocene temperatures, *J. Geol.*, *63*, 538–578. 4.1

Erez, J., and S. Honjo (1981), Comparison of isotopic composition of planktonic foraminifera in plankton tows, sediment traps and sediments, *Palaeogeogr., Palaeoclimatol., Palaeoecol.*, *33*, 129–156. 1.3.1, 2.3.2, 2.4.3

Erez, J., and B. Luz (1983), Experimental paleotemperature equation for planktonic foraminifera, *Geochim. Cosmochim. Acta*, *47*, 1025–1031. 3.3, 3.3.1, 3.4, 3.5

Ericson, D. B., and G. Wollin (1956), Micropaleontological and isotopic determinations of Pleistocene climates, *Micropaleontology*, *2*, 257–270. 5.2.4

Ericson, D. B., and G. Wollin (1968), Pleistocene climates and chronology in deep-sea sediments, *Science*, *162*, 1227–1234. 5.2.4

Fairbanks, R. G., and P. H. Wiebe (1980a), Foraminifera and chlorophyll maximum – vertical distribution, seasonal succession and paleoceanographic significance, *Science*, *209*, 1524–1526. 1.3.1, 2.3.2, 2.4.3, 2.4.3, 3.4.1, 4.1

Fairbanks, R. G., P. H. Wiebe, and A. W. H. Bé (1980b), Vertical distribution and isotopic composition of living planktonic foraminifera in the western North Atlantic, *Science*, *207*, 61–63. 1.3.1, 2.3.2, 2.4.3, 2.4.3, 3.4.1

Fairbanks, R. G., M. Sverdlove, R. Free, P. H. Wiebe, and A. W. H. Bé (1982), Vertical distribution and isotopic fractionation of living planktonic foraminifera from the Panama Basin, *Nature*, *298*, 841–844. 1.3.1, 2.3.2, 2.4.3, 2.4.3, 3.4.1, 4.1, 4.4.1, 4.4.4

Feely, R. A., C. L. Sabine, K. Lee, W. Berelson, J. Kleypas, V. J. Fabry, and F. J. Millero (2004), Impact of Anthropogenic CO_2 on the $CaCO_3$ System in the Oceans, *Science*, *305*, 362–366. 2.4.4

Feely, R. A., et al. (2002), *In situ* calcium carbonate dissolution in the Pacific Ocean, *Glob. Biogeochem. Cycles*, *16*(4), doi:10.1029/2002GB001866. 2.4.4

Field, D. B. (2004), Variability in vertical distributions of planktonic foraminifera in the California Current: Relationships to vertical ocean structure, *Paleoceanography*, *19*, PA2014, doi:10.1029/2003PA000970. 3.4.1

Flower, B. P., D. W. Hastings, H. W. Hill, and T. M. Quinn (2004), Phasing of deglacial warming and Laurentide Ice Sheet meltwater in the Gulf of Mexico, *Geology*, *32*(7), 597–600. 2.4.3

Frank, T. D., and K. Bernet (2000), Isotopic signature of burial diagenesis and primary lithological contrasts in periplatform carbonates (Miocene, Great Bahama Bank), *Sedimentology*, *47*, 1119–1134. 5.1

Fratantoni, D. M., R. J. Zantopp, W. E. Johns, and J. L. Miller (1997), Updated bathymetry of the Anageda-Jungfern Passage complex and implications for Atlantic inflow to the abyssal Caribbean Sea, *J. Mar. Res.*, *55*, 847–860. 2.2

Funk, J. A., T. von Dobeneck, T. Wagner, and S. Kasten (2003), Late Quaternary Sedimentation and Early Diagenesis in the Equatorial Atlantic Ocean: Patterns, Trends and Processes Deduced from Rock Magnetic and Geochemical Records, in *The South Atlantic in the Late Quaternary: Reconstruction of Material Budgets and Current Systems*, edited by G. Wefer, S. Mulitza, and V. Ratmeyer, pp. 461–497, Springer-Verlag, Berlin, Heidelberg, New York, Tokyo. 5.1

Ganssen, G., and D. Kroon (2000), The isotopic signature of planktonic foraminifera from NE-Atlantic surface sediments: Implications for the reconstruction of past oceanic conditions, *J. Geol. Soc. Lond.*, *157*, 693–699. 2.3.2

Gordon, A. L. (1967), Circulation of the Caribbean Sea, *J. Geophys. Res.*, *72*, 6207–6223. 4.2

Günther, D., R. Frischknecht, C. A. Heinrich, and H. J. Kahlert (1997), Capabilities of a 193 nm ArF excimer laser for LA-ICP-MS micro analysis of geological materials, *J. Anal. At. Spectrom.*, *12*, 939–944. 5.2.5

Haak, A. B., and W. Schlager (1989), Compositional variations in calciturbedites due to sea-level fluctuations, late Quaternary, Bahamas, *Int. J. Earth Sci.*, *78*(2), 477–486, doi:10.1007/BF01776186. 5.4.2

Haddad, G. A., and A. W. Droxler (1996), Metastable $CaCO_3$ dissolution at intermediate water depths of the Caribbean and western North Atlantic: Implications form intermediate water circulation during the past 200,000 years, *Paleoceanography*, *11*(6), 701–716. 2.4.5, 5.1

Hastings, D. W., S. R. Emerson, J. Erez, and B. R. Nelson (1996), Vanadium in foraminiferal calcite: Evaluation of a method to determine paleo-seawater vanadium concentrations, *Geochim. Cosmochim. Acta*, *60*(19), 3701–3715. 2.4.2

Hastings, D. W., S. R. Emerson, J. Erez, and B. R. Nelson (1998), Foraminiferal magnesium in *Globigerinoides sacculifer* as a paleotemperature proxy, *Paleoceanography*, *13*(2), 161–169. 2.1, 5.3.3

Hathorne, E. C., O. Alard, R. H. James, and N. W. Rogers (2003), Determination of intratest variability of trace elements in foraminifera by laser ablation inductively coupled plasma-mass spectrometry, *Geochem. Geophys. Geosys.*, *4*(12), 8408, doi:10.1029/2003GC000539. 5.1

Hecht, A. D., E. V. Eslinger, and L. B. Garmon (1975), Experimental studies on the dissolution of planktonic foraminifera, in *Dissolution of Deep-Sea Carbonates*, vol. Spec. Publ. 13, edited by W. V. Sliter, A. W. H. Bé, and W. H. Berger, pp. 56–69, Cushman Found. Foram. Res., Washington, D.C. 2.4.2

Hellweger, F. L., and A. L. Gordon (2002), Tracing Amazon River water into the Caribbean Sea, *J. Mar. Res.*, *60*, 537–549. 4.2, 4.4.3

Hemleben, C., and M. Spindler (1983), Recent advances in research in living planktonic foraminifera, *Utrecht Microp. Bull.*, *30*, 141–170. 4.4.1

Hemleben, C., M. Spindler, and O. R. Anderson (Eds.) (1989), *Modern Planktonic Foraminifera*, 363 pp., Springer-Verlag, Berlin, Heidelberg, New York. 1.3.1, 2.3.2, 2.4.3, 3.2, 4.3, 6

Hemleben, C., R. Zahn, and D. Meischner (Eds.) (1998), *Research Vessel METEOR Cruise No. 35 (1996): Caribbean Sea, Sargasso Sea*, Institut für Meereskunde der Universität Hamburg, Leitstelle METEOR, Hamburg. 2.3.1, 4.3

Hernandez-Guerra, A., and T. M. Joyce (2000), Water masses and circulation in the surface layers of the Caribbean at 66°W, *Geophys. Res. Lett.*, *27*, 3497–3500. 4.2

Hilbrecht, H. (Ed.) (1996), *Extant planktic foraminifera and the physical environment in the Atlantic and Indian Oceans*, vol. Neue Folge, No. 300, 93 pp., Mitteilungen aus dem Geologischen Institut der Eidgen. Technischen Hochschule und der Universität Zürich, Zürich. 2.3.2

Hover, V. C., L. M. Walter, and D. R. Peacor (2001), Early marine diagenesis of biogenic aragonite and Mg-calcite: new constraints from high-resolution STEM and AEM analyses of modern platform carbonates, *Chem. Geol.*, *175*. 5.1

Hut, G. (Ed.) (1987), *Consultants group meeting on stable isotope reference samples for geochemical and hydrological investigations*, 42 pp., Int. At. Energy Agency, Vienna. 3.3.1, 4.3

Jansen, H., R. E. Zeebe, and D. A. Wolf-Gladrow (2002), Modeling the dissolution of settling $CaCO_3$ in the ocean, *Glob. Biogeochem. Cycles*, *16*(2), 1027, doi:10.1029/2000GB001279. 2.6, 5.1

Johns, W. E., T. N. Lee, F. A. Schott, R. J. Zantopp, and R. H. Evans (1990), The North Brazil Current retroflection: Seasonal structure and eddy variability, *J. Geophys. Res.*, *95*, 22,103–22,119. 4.2

Johns, W. E., T. L. Townsend, D. M. Fratantoni, and W. D. Wilson (2002), On the Atlantic inflow to the Caribbean Sea, *Deep-Sea Res. I*, *49*, 211–243. 2.2, 4.2, 4.2

Joyce, T. M., R. S. Pickart, and R. C. Millard (1999), Long-term hydrographic changes at 52 and 66° W in the North Atlantic Subtropical Gyre & Caribbean, *Deep-Sea Res. II*, *46*, 245–278. 2.2

Kameo, K. (2002), Late Pliocene Caribbean surface water dynamics and climatic changes based on calcareous nannofossil records, *Palaeogeogr., Palaeoclimatol., Palaeoecol.*, *179*, 211–226. 2.2

Katz, A. (1973), The interaction of magnesium with calcite during crystal growth at 25–90°C and one atmosphere, *Geochem. Cosmochim. Acta*, *37*, 1563–1586. 1.3.1, 3.1, 5.4.1

Keeling, C. D. (1979), The Suess Effect: ^{13}Carbon-^{14}Carbon Interrelations, *Environ. Internat.*, *2*, 229–300. 4.4.3

Kemle von Mücke, S., and H. Oberhänsli (1999), The distribution of living planktic foraminifera in relation to southeast Atlantic oceanography, in *Use of Proxies in Paleoceanography: Examples from the South Atlantic*, edited by G. Fischer and G. Wefer, pp. 91–115, Springer-Verlag, Berlin, Heidelberg. 2.3.2, 2.4.3, 3.4.1, 4.4.1

Kennett, J. P., and M. S. Srinivasan (Eds.) (1983), *Neogene Planktonic Foraminifera, A Phylogenetic Atlas*, 265 pp., Hutchinson Ross, Stroudsburg, Pennsylvania. 2.3.2, 3.2, 4.3, 4.4.2

Killingley, J. S. (1983), Effects of diagenetic recrystallization on ^{18}O/^{16}O values of deep-sea sediments, *Nature*, *301*, 594–597. 5.1, 5.1, 5.4

Kim, S. T., and J. R. O'Neil (1997), Equilibrium and nonequilibrium oxygen isotope effects in synthetic carbonates, *Geochim. Cosmochim. Acta*, *61*, 3461–3475. 1.3.1, 3.3, 3.3.1, 3.4, 3.5, 4.1, 5.4

Klinkhammer, G. P., B. A. Haley, A. C. Mix, H. M. Benway, and M. Cheseby (2004), Evaluation of automated flow-through time-resolved analysis of foraminifera for Mg//Ca paleothermometry, *Paleoceanography*, *19*(4), PA4030, doi:10.1029/2004PA001050. 1.3.1

Kohfeld, K. E. (1998), Geochemistry and ecology of polar planktonic foraminifera, and applications to paleoceanographic reconstructions, Ph.D. thesis, Columbia University. 4.1

Kohfeld, K. E., R. G. Fairbanks, S. L. Smith, and I. D. Walsh (1996), *Neogloboquadrina pachyderma* (sinistral coiling) as paleoceanographic tracers in polar oceans: Evidence from Northeast Water Polynya plankton tows, sediment traps, and surface sediments, *Paleoceanography*, *11*(6), 96PA02617. 4.4.1

Kroon, D., and K. Darling (1995), Size and upwelling control of the stable isotope composition of *Neogloboquadrina dutertrei* (d'Orbigny), *Globigerinoides ruber* (d'Orbigny), and *Globigerina bulliodes* (d'Orbigny): Examples from the Panama Basin and the Arabian Sea, *J. Foram. Res.*, *25*, 39–52. 2.3.2

Kroon, D., J. J. G. Reijmer, and R. Rendle (2000), 2. Mid- to Late-Quaternary variations in the oxygen isotope signature of *Globigerinoides ruber* at Site 1006 in the western subtropical Atlantic, in *Proc. ODP, Sci. Results*, vol. 166, edited by P. K. Swart, G. P. Eberli, M. J. Malone, and J. F. Sarg, pp. 13–22, College Station, TX (Ocean Drilling Program). 5.3.3, 5.4.2, 6

Kroopnick, P. (1974), The dissolved O_2-CO_2-^{13}C system in the eastern equatorial Pacific, *Deep-Sea Res.*, *21*, 211–227. 1.3.1, 4.1

Larsen, J. C. (1992), Transport and heat flux of the Florida Current at 27° N derived from the cross-steam voltages and profiling data: Theory and observation, *Phil. Trans. Roy. Soc. Lond. A*, *338*, 169–236. 2.2

Lea, D. W. (2003), Elemental and Isotopic Proxies of Past Ocean Temperatures, in *Treatise on Geochemistry - The Oceans and Marine Geochemistry*, vol. 6, edited by H. Elderfield, pp. 365–390, Elsevier Ltd., Oxford. 2.1, 3.1, 6

Lea, D. W., T. A. Mashiotta, and H. J. Spero (1999), Controls on the magnesium and strontium uptake in planktonic foraminifera determined by live culturing, *Geochim. Cosmochim. Acta*, *63*(16), 2369–2379. 1.3.1, 2.1, 3.1, 3.4.1

Lea, D. W., D. K. Pak, and H. J. Spero (2000), Climate impact of late quaternary equatorial Pacific sea surface temperature variations, *Science*, *289*, 1719–1724. 1.3.1, 2.1, 2.5, 2.4.4, 3.1, 3.4.1, 3.4.1, 3.6

LeGrande, A. N., J. Lynch-Stieglitz, and E. C. Farmer (2004), Oxygen isotopic composition of *Globorotalia truncatulinoides* as a proxy for intermediate depth intensity, *Paleoceanography*, *19*(4), PA4025, doi:10.1029/2004PA001045. 1.3.1, 3.4.1, 4.4.1

Lewis, E., and D. W. R. Wallace (Eds.) (1998), *co2sys – Program Developed for CO_2 System Calculations*, Carbon Dioxide Information Analysis Center, Oak Ridge National Laboratory, U.S. Department of Energy, Oak Ridge, Tennessee, oRNL/CDIAC-105. 1.4.2, 2.6, 2.4.4

Lin, H., L. C. Peterson, J. T. Overpeck, S. E. Trumbore, and D. W. Murray (1997), Late Quaternary climate change from δ^{18}O records of multiple species of planktonic foraminifera: High-resolution records from the anoxic Cariaco Basin, Venezuela, *Paleoceanography*, *12*(3), 415–427. 2.3.2

Loeblich, A. R., and H. Tappan (1964), Protista 2, in *Treatise on Invertebrate Paleontology, Part C*, edited by R. C. Moore, pp. 1–900, University of Kansas Press, Lawrence, Kansas. 1.3

Lohmann, G. (1995), A model for variation in the chemistry of planktonic foraminifera due to secondary calcification and selective dissolution, *Paleoceanography*, *10*(3), 445–457. 1.3.1, 2.3.2, 4.1, 5.1, 6

Lončarić, N., F. J. C. Peeters, D. Kroon, and G.-J. A. Brummer (2006), Oxygen isotope ecology of recent planktic foraminifera at the central Walvis Ridge (SE Atlantic), *Paleoceanography*, *21*(3), PA3009, doi:10.1029/2005PA001207. 1.3.1, 3.4.1

Lorens, R. B., D. F. Williams, and M. L. Bender (1977), The early nonstructual chemical diagenesis of foraminiferal calcite, *J. Sediment. Petrol.*, *47*, 1602–1609. 2.4.2, 2.4.4, 5.1, 6

Malone, M. J., N. C. Slowey, and G. M. Henderson (2001), Early diagenesis of shallow-water periplatform carbonate sediments, leeward margin, Great Bahama Bank (Ocean Drilling Program Leg 166), *GSA Bull.*, *113*(7), 881–894. 5.1

Martin, P. A., D. W. Lea, Y. Rosenthal, N. J. Shackleton, M. Sarnthein, and T. Papenfuss (2002), Quaternary deep sea temperature histories derived from benthic foraminiferal Mg/Ca, *Earth Planet. Sci. Lett.*, *198*, 193–209. 6

Martinson, D. G., N. G. Pisias, J. D. Hays, J. Imbrie, J. T. C. More, and N. J. Shackleton (1987), Age dating and the orbital theory of the ice ages: Development of a high-resolution 0 to 300,000-year chronostratigraphy, *Quat. Res.*, *27*, 1–29. 5.2, 5.2.4

Mashiotta, T. A., D. W. Lea, and H. J. Spero (1999), Glacial-interglacial changes in Subantarctic sea surface temperature and δ^{18}O-water using foraminiferal Mg, *Earth Planet. Sci. Lett.*, *170*, 417–432. 2.1, 3.1, 3.4.1

Mason, P. R. D., and A. J. G. Mank (2001), Depth-resolved analysis in multi-layered glass and metal materials using laser ablation inductively coupled plasma mass spectrometry (LA-ICP-MS), *J. Anal. At. Spectrom.*, *16*, 1381–1388. 5.2.5

McConnell, M. C., and R. C. Thunell (2005), Calibration of the planktonic foraminiferal Mg/Ca paleothermometer: Sediment trap results from the Guaymas Basin, Gulf of California, *Paleoceanography*, *20*, doi:10.1029/2004PA001077. 1.3.1, 2.1, 2.5, 3.1, 3.4.1, 3.4.1, 3.6

McKenna, V. S., and W. L. Prell (2004), Calibration of the Mg/Ca of *Globorotalia truncatulinoides* (R) for the reconstruction of marine temperature gradients, *Paleoceanography*, *19*(2), PA2006, doi:10.1029/2000PA000604. 1.3.1, 1.3.1, 2.1, 2.3.2, 2.4.3, 2.5, 2.4.3, 2.4.4, 3.4.1, 3.6, 3.4.1

McPhaden, M. J. (2003), Tropical Pacific Ocean heat content variations and ENSO persistence barriers, *Geophys. Res. Lett.*, *30*(9), 1480, doi:10.1029/2003GL016872. 6

Mehrbach, C., C. H. Culberson, J. E. Hawley, and R. M. Pytkowicz (1973), Measurement of the apparent dissociation constants of carbonic acid in seawater at atmospheric pressure, *Limnol. Oceanogr.*, *18*, 897–907. 1.4.2

Memery, L., M. Arhan, X. A. Alvarez-Salgado, M. J. Messias, H. Mercier, C. G. Castro, and A. F. Rios (2000), The water masses along the western boundary of the south and equatorial Atlantic, *Progress in Oceanogr.*, *47*, 69–98. 4.2

Miao, Q., R. C. Thunell, and D. M. Anderson (1994), Glacial-Holocene carbonate dissolution and sea surface in the South China and Sulu seas, *Paleoceanography*, *9*(2), 269–290. 2.4.4

Mielke, K. M. (2001), Reconstructing surface carbonate chemistry and temperature in paleoceans: Geochemical results from laboratory experiments and the fossil record, Master's thesis, Univ. of Calif. 1.3.1, 3.3, 3.3.1, 3.4, 3.5, 4.4.5

Molinari, R., E. Johns, and J. F. Festa (1990), The annual cycle of meridional heat flux in the Atlantic Ocean at 26.5° N, *J. Phys. Oceanogr.*, *20*, 476–482. 2.2

Mollenhauer, G. (1999), Einfluss von Bioturbation, Produktivität und Zirkulation auf C-Datierungen an planktischen Foraminiferen, Master's thesis, Univ. of Bremen. 3.1

Morrison, J. M., and W. D. Nowlin (1982), General distribution of water masses within the Eastern Caribbean Sea during the winter of 1972 and fall of 1973, *J. Geophys. Res.*, *87*(C6), 4207–4229. 2.2

Morrison, J. M., and O. P. Smith (1990), Geostrophic transport variability along the Aves Ridge in the eastern Caribbean Sea during 1985 and 1986, *J. Geophys. Res.*, *95*, 699–710. 2.2, 4.2

Morse, J. W. (2003), Formation and Diagenesis of Carbonate Sediments, in *Treatise on Geochemistry - The Oceans and Marine Geochemistry*, vol. 7, edited by F. T. Mackenzie, pp. 67–85, Elsevier Ltd., Oxford. 5.1, 5.3.1, 5.4, 5.4.2

Mucci, A. (1987), Influence of temperature on the composition of magnesian calcite overgrowths precipitated from seawater, *Geochim. Cosmochim. Acta*, *51*, 1977–1984. 1.3.1, 5.4.1

Mucci, A., and J. W. Morse (1983), The incorporation of Mg^{2+} and Sr^{2+} into calcite overgrowths: influences of growth rate and solution composition, *Geochim. Cosmochim. Acta*, *47*, 217–233. 3.1, 5.4.1

Mulitza, S. (Ed.) (1994), *Spätquartäre Variationen der oberflächennahen Hydrographie im westlichen äquatorialen Atlantik*, vol. 57, 97 pp., Fachbereich Geowissenschaften, Berichte, University of Bremen, Germany. 1.3, 3.2, 4.1, 4.3

Mulitza, S., A. Dürkoop, W. Hale, and G. Wefer (1997), Planktonic foraminifera as recorders of past surface-water stratification, *Geology*, *25*(4), 335–338. 2.3.2, 2.4.3, 3.4.1, 4.1, 4.2, 4.3, 4.4.1

Mulitza, S., H. Arz, S. Kemle-von Mücke, C. Moos, H.-S. Niebler, J. Pätzold, and M. Segl (1999), The South Atlantic carbon isotope record of planktic foraminifera, in *Use of Proxies in Paleoceanography: Examples from the South Atlantic*, edited by G. Fischer and G. Wefer, pp. 427–445, Springer-Verlag, Berlin, Heidelberg, New York, Tokyo. 1.3.1, 4.4.4, 4.4.5

Mulitza, S., D. Boltovskoy, B. Donner, H. Meggers, A. Paul, and G. Wefer (2003), Temperature:δ^{18}O relationships of planktonic foraminifera collected from surface waters, *Palaeogeogr. Palaeoclimatol. Palaeoecol.*, *202*, 143–152. 3.3, 3.3.1, 3.4, 3.5

Mulitza, S., B. Donner, G. Fischer, A. Paul, J. Pätzold, C. Rühlemann, and M. Segl (2004), The South Atlantic Oxygen Isotope Record of Planktic Foraminifera, in *The South Atlantic in the Late Quaternary: Reconstruction of Material Budgets and Current Systems*, edited by G. Wefer, S. Mulitza, and V. Ratmeyer, pp. 121–142, Springer-Verlag, Berlin, Heidelberg, New York, Tokyo. 1.3.1, 2.3.2, 3.3, 3.3.1, 3.4, 3.3.1, 3.5, 4.3, 4.3, 4.4, 4.5, 4.4.1, 5.1

Müller, A. (Ed.) (1999), *Mg/Ca- und Sr/Ca-Verhältnisse in biogenem Carbonat planktischer Foraminiferen und benthischer Ostracoden*, vol. 313, 182 pp., Berichte aus dem Institut für Meereskunde, University of Kiel, Germany. 5.1, 5.5, 5.3.3, 5.3.3

Müller, T. J., W. Zenk, and G. Wefer (Eds.) (1988), *Research Vessel METEOR Cruise No. 9 (1988/89): Barlavento-Expedition*, Institut für Meereskunde der Universität Hamburg, Leitstelle METEOR, Hamburg. 4.3

Müller-Karger, F. E., C. R. McClain, and P. L. Richardson (1988), The dispersal of the Amazon's water, *Nature*, *333*, 56–59. 4.2

Mullins, H. T., S. W. Wise Jr., A. F. Gardulski, E. J. Hinchey, P. M. Masters, and D. I. Siegel (1985), Shallow subsurface diagenesis of Pleistocene periplatform ooze: northern Bahamas, *Sedimentology*, *32*(4), 473–494, doi:10.1111/j.1365-3091.1985.tb00465.x. 5.4, 5.4.2, 6

Niebler, H.-S., H.-W. Hubberten, and R. Gersonde (1999), Oxygen Isotope Values of Planktic Foraminifera: A Tool for the Reconstruction of Surface Water Stratification, in *Use of Proxies in Paleoceanography: Examples from the South Atlantic*, edited by G. Fischer and G. Wefer, pp. 165–189, Springer-Verlag, Berlin, Heidelberg. 1.2, 3.4.1, 4.3, 4.4.1, 6

NODC (2001), National Oceanographic and Data Center, World Ocean Atlas 2001: Objective Analyses, Data Statistics, and Figures, *CD-ROM Documentation*, Natl. Oceanic and Atmos. Admin., Silver Spring, Md., http://www.nodc.noaa.gov/. 2.1, 2.2, 2.3, 2.4.3, 2.4, 2.5, 3.1, 3.1, 3.3.1, 3.4, 3.3.2, 3.5, 3.5, 3.4.1, 3.6, 3.7, 3.4.2, 3.4.2, 4.1, 4.2, 4.3, 4.10, 4.4.5

Norris, R. D., and P. A. Wilson (1998), Low-latitude sea-surface temperatures for the mid-Cretaceous and the evolution of planktic foraminifera, *Geology*, *26*(9), 823–826. 5.1, 5.4

Nürnberg, D. (1995), Magnesium in tests of *Neogloboquadrina pachyderma* sinistral from high Northern and Southern latitudes, *J. Foram. Res.*, *25*(4), 350–368. 2.1, 2.4.3, 2.4.4, 3.1

Nürnberg, D. (2000), Taking the Temperature of Past Ocean Surfaces, *Science*, *289*, 1698–1699. 2.1, 3.1, 6

Nürnberg, D., and J. Groeneveld (2006), Pleistocene variability of the Subtropical Convergence at East Tasman Plateau: Evidence from planktonic foraminiferal Mg/Ca (ODP Site 1172A), *Geochem. Geophys. Geosys.*, *7*(4), Q04P11, doi:10.1029/2005GC000984. 2.1, 3.1

Nürnberg, D., J. Bijma, and C. Hemleben (1996a), Assessing the reliability of magnesium in foraminiferal calcite as a proxy for water mass temperatures, *Geochim. Cosmochim. Acta*, *60*(5), 803–814. 1.3.1, 1.3.1, 2.1, 2.3.2, 2.5, 2.4.3, 2.4.4, 3.1, 3.4.1

Nürnberg, D., J. Bijma, and C. Hemleben (1996b), Erratum, *Geochim. Cosmochim. Acta*, *60*(13), 2483–2484. 2.1, 2.5, 2.4.3, 3.1, 3.4.1

Nürnberg, D., A. Müller, and R. R. Schneider (2000), Paleo-sea surface temperature calculations in the equatorial East Atlantic from Mg/Ca ratios in planktic foraminifera: A comparison to sea surface temperature estimates from Uk'37, oxygen isotopes, and foraminiferal transfer function, *Paleoceanography*, *15*(1), 124–134. 1.3.1, 2.1, 3.4.1, 3.6

Nürnberg, D., J. Schönfeld, W.-C. Dullo, and C. Rühlemann (Eds.) (2003), *RV SONNE: Cruise report SO164 RASTA (2002)*, 109, 151 pp., GEOMAR Report, Kiel. 1.4, 2.3.1, 3.2, 4.3, 5.2

O'Neil, J. R., R. N. Clayton, and T. K. Mayeda (1969), Oxygen isotope fractionation in divalent metal carbonates, *J. Chem. Phys.*, *51*(12), 5547–5558. 1.3.1, 3.3.1, 4.1, 5.4, 6

Ortiz, J. D., A. C. Mix, S. Hostetler, and M. Kashgarian (1992), April and August northeast Atlantic surface water masses reflected in planktic foraminifera, *Neth. J. Sea Res.*, *28*, 261–283. 4.4.1

Ortiz, J. D., A. C. Mix, and R. W. Collier (1995), Environmental control of living symbiotic and asymbiotic foraminifera of the California Current, *Paleoceanography*, *10*(6), 95PA02088. 2.3.2

Ortiz, J. D., A. C. Mix, W. Rugh, J. M. Watkins, and R. W. Collier (1996), Deep-dwelling planktonic foraminifera of the Northeast Pacific reveal environmental control of oxygen and carbon isotopic disequilibria, *Geochim. Cosmochim. Acta*, *60*, 4509–4523. 2.3.2

Ortiz, J. D., A. C. Mix, S. Hostetler, and M. Kashgarian (1997), The California Current of the Last Glacial Maximum at 42° N: Reconstruction based on multiple proxies, *Paleoceanography*, *12*(2), 96PA02878. 2.3.2

Pahnke, K., and R. Zahn (2005), Southern Hemisphere Water Mass Conversion Linked with North Atlantic Climate Variability, *Science*, *307*, 1741–1746. 2.1, 3.1

Paillard, D., L. Labeyrie, and P. Yiou (1996), Macintosh program performs time-series analysis, *Eos Trans. AGU*, *77*, 379, Electronic supplement available at: http://www.agu.org/eos_elec/96097e.html. 5.2.4

Patrick, A., and R. C. Thunell (1997), Tropical Pacific sea surface temperatures and upper water column thermal structure during the last glacial maximum, *Paleoceanography*, *12*(5), 97PA01553. 4.1

Pearce, N. J. G., W. T. Perkins, J. A. Westgate, M. P. Gorton, S. E. Jackson, C. R. Neal, and S. P. Chenery (1997), A compilation of new and published major and trace element data for NIST SRM 610 and NIST SRM 612 glass reference materials, *Geostandards Newsletter*, *21*, 115–144. 5.2.5

Pearson, P. N., N. J. Shackleton, G. P. Weedon, and M. A. Hall (1997), 29. Multispecies planktonic foraminifer stable isotope stratigraphy through Oligocene/Miocene boundary climatic cycles, Site 926, in *Proc. ODP, Sci. Results*, vol. 154, edited by N. J. Shackleton, W. B. Curry, C. Richter, and T. J. Bralower, pp. 441–449, College Station, TX (Ocean Drilling Program). 5.4

Pearson, P. N., P. W. Ditchfield, J. Singano, K. G. Harcourt-Brown, C. J. Nicholas, R. K. Olsson, N. J. Shackleton, and M. A. Hall (2001), Warm tropical sea surface temperatures in the Late Cretaceous and Eocene epochs, *Nature*, *413*, 481–487. 5.4

Petschick, R. (Ed.) (2001), *MacDiff – The user-friendly X-ray powder diffractometry analysis tool for Macintosh computers.*, available at: http://servermac.geologie.uni-frankfurt.de/Staff/Homepages/Petschick/RainerE.html. 1.4.1, 5.2.1

Philander, S. G. H., and R. C. Pacanowski (1984), Simulation of the seasonal cycle in the tropical Atlantic Ocean, *Geophys. Res. Lett.*, *11*(8), 802–804. 4.2

Philander, S. G. H., and R. C. Pacanowski (1986a), A Model of the Seasonal Cycle in the Tropical Atlantic, *J. Geophys. Res.*, *91*(C12), 14,192–14,206. 4.2

Philander, S. G. H., and R. C. Pacanowski (1986b), The Mass and Heat Budget in a Model of the Tropical Atlantic Ocean, *J. Geophys. Res.*, *91*(C12), 14,212–14,220. 4.2, 6

Price, G. D., B. W. Sellwood, R. M. Corfield, L. Clarke, and J. E. Cartlidge (1998), Isotopic evidence for palaeotemperatures and depth stratification of Middle Cretaceous planktonic foraminifera from the Pacific Ocean, *Geol. Mag.*, *135*(2), 183–191. 5.4

Ravelo, A. C., and D. H. Andreasen (1999), Using planktonic foraminifera as monitors of the tropical surface ocean, in *Reconstructing Ocean History - A window into the future*, edited by F. Abrantes and A. C. Mix, pp. 217–244, Plenum Press, New York. 1.2, 4.1, 4.3, 4.4.5, 4.4.6

Ravelo, A. C., and R. G. Fairbanks (1992), Oxygen isotopic composition of multiple species of planktonic foraminifera: Recorders of the modern photic zone temperature gradient, *Paleoceanography*, *7*(6), 815–831. 1.2, 2.3.2, 2.4.3, 2.4.3, 3.4.1, 4.1, 4.4.1, 4.4.6

Ravelo, A. C., and R. G. Fairbanks (1995), Carbon isotope fractionation in multiple species of planktonic foraminifera from core-tops in the tropical Atlantic, *J. Foram. Res.*, *25*, 53–74. 1.2, 1.3.1, 4.1, 4.3, 4.4.3, 4.4.4, 4.4.5

Ravelo, A. C., R. G. Fairbanks, and S. G. H. Philander (1990), Reconstructing tropical Atlantic hydrography using planktonic foraminifera and an ocean model, *Paleoceanography*, *5*, 409–431. 1.2

Regenberg, M., D. Nürnberg, S. Steph, J. Groeneveld, D. Garbe-Schönberg, R. Tiedemann, and W.-C. Dullo (2006a), Assessing the dissolution effect on planktonic foraminiferal Mg/Ca ratios: Evidence from Caribbean core-tops, *Geochem. Geophys. Geosys.*, *7*(1), doi:10.1029/2005GC001019. 1.2, 3.1, 3.1, 3.2, 3.2.2, 3.2.2, 3.3, 3.4, 4.3, 5.1, 5.2.3, 5.6, 5.3.4

Regenberg, M., S. Steph, D. Nürnberg, R. Tiedemann, and S. Mulitza (2006b), Calibrating Mg/Ca of Multiple Planktonic Foraminiferal Species with δ^{18}O-Calcification Temperatures: Paleothermometry for the Upper Water Column, *Earth Planet. Sci. Lett.*, *submitted*, EPSL-D-06-00991. 1.2

Reichart, G.-J., F. Jorissen, P. Anschutz, and P. R. D. Mason (2003), Single foraminiferal test chemistry records the marine environment, *Geology*, *31*(4), 355–358, doi:10.1130/0091-7613(2003)031. 1.3.1, 5.1

Reimer, P. J., M. G. L. Baillie, E. Bard, and et al. (2004), IntCal04 Terrestrial radiocarbon age calibration, 26–0 ka BP, *Radiocarbon*, *46*, 1029–1058. 2.1

Rendle, R. H., J. J. G. Reijmer, D. Kroon, and G. M. Henderson (2000), 6. Mineralogy and sedimentology of the Pleistocene to Holocene on the leeward margin of the Great Bahama Bank, in *Proc. ODP, Sci. Results*, vol. 166, edited by P. K. Swart, G. P. Eberli, M. J. Malone, and J. F. Sarg, pp. 61–76, College Station, TX (Ocean Drilling Program). 5.4.2, 6

Richter, F. M., and D. J. DePaolo (1987), Numerical models for diagenesis and the Neogene Sr isotopic evolution of seawater from DSDP Site 590B, *Earth Planet. Lett.*, *83*, 27–38. 5.1

Rickaby, R., and P. Halloran (2005), Cool La Niña during the warmth of the Pliocene?, *Science*, *307*, 1948–1952, doi:10.1126/science.1104666. 2.5, 3.4.1, 3.6, 3.4.1

Roemmich, D. (1981), Circulation in the Caribbean Sea: A well-resolved inverse problem, *J. Geophys. Res.*, *86*, 7993–8005. 4.2

Rosenthal, Y., and E. A. Boyle (1993), Factors controlling the flouride content of planktonic foraminifera: An evaluation of its paleoceanographic applicability, *Geochim. Cosmochim. Acta*, *57*, 335–346. 2.4.2, 2.4.4

Rosenthal, Y., and G. P. Lohmann (2002), Accurate estimation of sea surface temperatures using dissolution-corrected calibrations for Mg/Ca paleothermometry, *Paleoceanography*, *17*(3), doi: 10.1029/2001PA000749. 1.2, 1.3.1, 2.1, 3.1, 3.2.2

Rosenthal, Y., E. A. Boyle, and N. Slowey (1997), Temperature control on the incorporation of magnesium, strontium, fluorine, and cadmium into benthic foraminiferal shells from Little Bahama Bank: Prospects for thermocline paleoceanography, *Geochim. Cosmochim. Acta*, *61*(17), 3633–3643. 3.2.2, 5.1, 6

Rosenthal, Y., G. P. Lohmann, K. C. Lohmann, and R. M. Sherrell (2000), Incorporation and preservation of Mg in *Globigerinoides sacculifer*: Implications for reconstructing the temperature and $^{18}O/^{16}O$ of seawater, *Paleoceanography*, *15*(1), 135–145. 1.3.1, 2.1, 2.3.2, 2.2, 2.4.4, 3.1

Rosenthal, Y., S. Perron-Cashman, C. H. Lear, and et al. (2004), Interlaboratory comparison study of Mg/Ca and Sr/Ca measurements in planktonic foraminifera for paleoceanographic research, *Geochem. Geophys. Geosys.*, *5*(4), doi:10.1029/2003GC000650. 2.2

Ruddiman, W. F. (1971), Pleistocene sedimentation in the equatorial Atlantic: Stratigraphy and faunal paleoclimatology, *Geol. Soc. Am. Bull.*, *82*, 283–302. 5.2.4

Rudnicki, M. D., P. A. Wilson, and W. T. Anderson (2001), Numerical models of diagenesis, sediment properties, and pore fluid chemistry on a paleoceanographic transect: Blake Nose, Ocean Drilling Program Leg 171B, *Paleoceanography*, *16*(6), 563–575. 5.1, 5.1, 5.4

Rühlemann, C., S. Mulitza, P. J. Müller, G. Wefer, and R. Zahn (1999), Warming of the tropical Atlantic Ocean and slowdown of thermohaline circulation during the last deglaciation, *Nature*, *402*, 511–514. 5.3.3

Rühlemann, C., B. Diekmann, S. Mulitza, and M. Frank (2001), Late Quaternary changes of western equatorial Atlantic surface circulation and Amazon lowland climate recorded in Ceara Rise deep-sea sediments, *Paleoceanography*, *16*(3), 293–305, doi:10.1029/1999PA000474. 1.3, 3.2, 4.1, 4.3

Russell, A. D., S. Emerson, B. K. Nelson, J. Erez, and D. W. Lea (1994), Uranium in foraminiferal calcite as a recorder of seawater uranium concentrations, *Geochim. Cosmochim. Acta*, *58*, 671–681. 2.4.2

Russell, A. D., B. Hönisch, H. J. Spero, and D. W. Lea (2004), Effects of seawater carbonate ion concentration and temperature on shell U, Mg, and Sr in cultured planktonic foraminifera, *Geochim. Cosmochim. Acta*, *68*(21), 4347–4361, doi:10.1016/j.gca.2004.03.013. 2.1

Sabine, C. L., and F. T. Mackenzie (1995), Bank-Derived Carbonate Sediment Transport and Dissolution in the Hawaiian Archipelago, *Aquatic Geochem.*, *1*, 189–230. 5.1

Sadekov, A. Y., S. M. Eggins, and P. de Deckker (2005), Characterization of Mg/Ca distributions in planktonic foraminifera species by electron microprobe mapping, *Geochem. Geophys. Geosys.*, *6*(12), Q12P06, doi:10.1029/2005GC000973. 1.3.1, 2.4.4

Sautter, L. R., and R. C. Thunell (1991a), Seasonal variability in the oxygen and carbon isotopic composition of planktonic foraminifera from an upwelling environment: sediment trap results from the San Pedro Basin, Southern California Bight, *Paleoceanography*, *6*, 307–334. 2.3.2, 2.4.3, 4.1, 4.4.1

Sautter, L. R., and R. C. Thunell (1991b), Planktonic foraminiferal response to upwelling and seasonal hydrographic conditions: Sediment trap results from the San Pedro Basin, Southern California Bight, *J. Foram. Res.*, *21*, 347–363. 2.4.3, 3.4.1, 4.1

Savin, S. M., and R. G. Douglas (1973), Stable Isotope and Magnesium Geochemistry of Recent Planktonic Foraminifera from the South Pacific, *GSA Bull.*, *84*(7), 2327–2342. 2.1, 2.3.2, 2.4.4, 3.1, 3.2.2

Schiebel, R., and C. Hemleben (2005), Modern planktic foraminifera, *PalŁontologische Zeitschrift*, *79*(1), 135–148. 1.1, 4.3, 6

Schiebel, R., J. Waniek, M. Bork, and C. Hemleben (2001), Entrainment and redistribution of nutrients and chlorophyll stimulating planktic foraminiferal production, *Deep-Sea Res. I*, *48*, 721–740. 4.4.1

Schlitzer, R. (Ed.) (2002), *Ocean Data View*, available at: http://www.awi-bremerhaven.de/GEO/ODV. 2.1, 3.1, 4.1, 4.2, 5.1

Schmidt, G. A. (1999), Error analysis of paleosalinity calculations, *Paleoceanography*, *14*(3), 1999PA900008. 3.3.1, 3.2, 3.3.1, 4.3

Schmidt, G. A., and S. Mulitza (2002), Global calibration of ecological models for planktic foraminifera from coretop carbonate oxygen-18, *Mar. Micropal.*, *44*, 125–140. 4.3

Schmidt, G. A., G. R. Bigg, and E. J. Rohling (1999), Global Seawater-δ^{18}O Database. 3.2

Schmidt, M. W., H. J. Spero, and D. W. Lea (2004), Links between salinity variation in the Caribbean and North Atlantic thermohaline circulation, *Nature*, *428*, 160–163. 2.1, 2.1, 2.4.5, 3.1, 5.3.3, 5.3.3

Schmidt, M. W., M. J. Vautravers, and H. J. Spero (2006), Western Caribbean sea surface temperatures during the late Quaternary, *Geochem. Geophys. Geosys.*, *7*(2), doi:10.1029/2005GC000957. 3.1, 5.3.2, 5.4, 5.5, 5.3.3, 5.3.3

Schmuker, B. (2000), Recent Planktic Foraminifera in the Caribbean Sea: Distribution, Ecology and Taphonomy, Ph.D. thesis, ETH Zürich, Switzerland. 2.1, 2.3.2, 3.1

Schmuker, B., and R. Schiebel (2002), Planktic foraminifers and hydrography of the eastern and northern Caribbean Sea, *Mar. Micropal.*, *428*, 387–403. 2.2, 2.3.2, 2.4.3, 2.4, 2.4.3, 2.5, 3.4.1, 4.4.1, 6

Schott, F. A., T. N. Lee, and R. Zantopp (1988), Variability of structure and transport of the Florida Current in the period range of days to seasonal, *J. Phys. Oceanogr.*, *18*(9), 1209–1230. 2.2

Schott, F. A., J. Fischer, and L. Stramma (1998), Transports and pathways of the upper-layer circulation in the western tropical Atlantic, *J. Phys. Oceanogr.*, *28*(10), 1904–1928. 4.2

Schott, F. A., P. Brandt, M. Hamann, J. Fischer, and L. Stramma (2002), On the boundary flow off Brazil at 5–10°S and its connection to the interior tropical Atlantic, *Geophys. Res. Lett.*, *29*(17), 1840, doi:10.1029/2002GL014786. 4.2

Schrag, D. P. (1999), Effects of diagenesis on the isotopic record of late Paleogene tropical sea surface temperatures, *Chem. Geol.*, *161*, 215–244. 5.1, 5.4

Schrag, D. P., D. J. DePaolo, and F. M. Richter (1992), Oxygen isotope exchange in a two-layer model of oceanic crust, *Earth Planet. Sci. Lett.*, *111*, 305–317. 5.1, 5.4, 5.4.1

Schrag, D. P., D. J. DePaolo, and F. M. Richter (1995), Reconstructing past sea surface temperatures: Correcting for diagenesis of bulk marine carbonate, *Geochim. Cosmochim. Acta*, *59*(11), 2265–2278. 5.4, 5.4.1, 5.4.2, 5.5, 6

Schulz, H. D., C. W. Devey, J. Pätzold, and G. Fischer (Eds.) (1998), *Research Vessel METEOR Cruise No. 41 (1998): Geo Bremen/GPI Kiel South Atlantic 1998*, Institut für Meereskunde der Universität Hamburg, Leitstelle METEOR, Hamburg. 4.3

Schweitzer, P. N., and G. P. Lohmann (1991), Ontogeny and habitat of modern menardiiform planktonic foraminifera, *J. Foram. Res.*, *21*, 332–346. 1.3.1, 2.3.2, 2.4.3

Sexton, P. F., P. A. Wilson, and P. N. Pearson (2006), Microstructual and geochemical perspectives on planktic foraminiferal preservation: "Glassy! versus "Frosty", *Geochem. Geophys. Geosys.*, *7*(12), Q12P19, doi:10.1029/2006GC001291. 5.1, 5.4

Shackleton, N. J. (1974), Attainment of isotopic equilibrium between ocean water and the benthonic foraminifera genus *Uvigerina*: Isotopic changes in the ocean during the last glacial, *Cent. Nat. Rech. Sci. Colloq. Int.*, *219*, 203–209. (document), 1.3.1, 3, 3.3, 3.3.1, 3.4, 3.3.1, 3.4.1, 3.5, 3.4.1, 3.6, 3.7, 3.5, 4.3, 4.4, 4.5, 4.4.1, 4.4.3, 6

Shackleton, N. J., and N. D. Opdyke (1973), Oxygen isotope and paleomagnetic stratigraphy of equatorial Pacific core V28-238: Oxygen isotope temperatures and ice volume on a 10^5 and 10^6 year time scale, *Quat. Res.*, *3*, 39–55. 3.1, 4.1

Shackleton, N. J., and E. Vincent (1978), Oxygen and carbon isotope studies in recent foraminifera from the southwest Indian Ocean, *Mar. Micropal.*, *3*, 1–13. 1.3.1, 4.4.4

Shackleton, N. J., A. Berger, and W. R. Peltier (1990), An alternative astronomical calibration of the lower Pleistocene timescale based on ODP Site 677, *Trans. R. Soc. Edinburgh Earth Sci.*, *81*, 251–261. 5.2, 5.2.4

Silva, A., M. Araujo, C. Medeiros, M. Silva, and B. Bourles (2005), Seasonal changes in the mixed and barrier layers in the western equatorial Atlantic, *Brazil. J. Oceanogr.*, *53*(3/4), 83–98. 4.2

Slowey, N. C., R. J. Wilber, G. A. Haddad, and G. M. Henderson (2002), Glacial-to-Holocene sedimentation on the western slope of Great Bahama Bank, *Mar. Geol.*, *185*, 165–176. 5.4.2, 6

Spero, H. J., and D. W. Lea (1993), Intraspecific stable isotope variability in the planktonic foraminifera *Globigerinoides sacculifer*: Results from laboratory experiments, *Mar. Micropal.*, *22*, 221–234. 4.1, 4.4.4

Spero, H. J., and D. F. Williams (1989), Opening the carbon isotope vital effect black box, 1, Seasonal temperatures in the euphotic zone, *Paleoceanography*, *4*(6), 593–601. 1.3.1, 2.3.2

Spero, H. J., J. Bijma, and D. W. L. B. E. Bemis (1997), Effect of seawater carbonate concentration on foraminiferal carbon and oxygen isotopes, *Nature*, *390*, 497–500. 4.1

Spero, H. J., K. M. Mielke, E. M. Kalve, D. W. Lea, and D. K. Pak (2003), Multispecies approach to reconstructing eastern equatorial Pacific thermocline hydrography during the past 360 kyr, *Paleoceanography*, *18*(1), 1022, doi:10.1029/2002PA000814. 1.3.1, 3.3, 3.3.1, 3.4, 3.5, 4.1

Stalcup, M. C., W. G. Metcalf, and R. G. Johnson (1975), Deep Caribbean inflow through the Anageda-Jungfern Passage, *J. Mar. Res.*, *33*(Suppl.), 15–35. 2.2

Steinke, S., H.-Y. Chiu, P.-S. Yu, C.-C. Shen, L. Löwenmark, H.-S. Mii, and M.-T. Chen (2005), Mg/Ca ratios of two *Globigerinoides ruber* (white) morphotypes: Implications for reconstructing past tropical/subtropical surface water conditions, *Geochem. Geophys. Geosys.*, *6*(11), doi:10.1029/2005GC000926. 2.4.3

Steph, S. (2005), Pliocene stratigraphy and the impact of Panama uplift on changes in Caribbean and tropical East Pacific upper ocean stratification (6–2.5 Ma), Ph.D. thesis, University of Kiel. 3.2, 3.3.1

Steph, S., R. Tiedemann, J. Groeneveld, D. Nürnberg, L. Reuning, and G. Haug (2006), Changes in Caribbean surface hydrography during the Pliocene shoaling of the Central American Seaway, *Paleoceanography*, *in press*. 3.2, 3.3.1, 4.3

Stuiver, M., P. J. Reimer, and R. W. Reimer (Eds.) (2005), *CALIB 5.0. [www program and documentation]*, available at: http://radiocarbon.pa.qub.ac.uk/calib. 2.1

Tedesco, K. A., and R. Thunell (2003), Seasonal and interannual variations in planktonic foraminiferal flux and assemblage composition in the Cariaco Basin, Venezuela, *J. Foram. Res.*, *33*(3), 192–210. 2.3.2, 2.4.3

Thompson, P. R., A. W. H. Bé, J.-C. Duplessy, and N. J. Shackleton (1979), Disappearance of pink-pigmented *Globigerinoides ruber* at 120,000 yr BP in the Indian and Pacific oceans, *Nature*, *280*, 554–558. 4.4.2

Thunell, R., E. Tappa, C. Pride, and E. Kincaid (1999), Sea-surface temperature anaomalies associated with the 1997–1998 El Niño recorded in the oxygen isotope composition of planktonic foraminifera, *Geology*, *27*(9), 843–846. 3.3, 3.3.1, 3.4, 3.5

Tripati, A. K., M. L. Delaney, J. C. Zachos, and L. D. Anderson (2003), Tropical sea-surface temperature reconstruction for the early Paleogene using Mg/Ca ratios of planktonic foraminifera, *Paleoceanography*, *18*(4), 1101, doi:10.1029/2003PA000937. 5.1, 5.4

Tyrrell, T., and R. E. Zeebe (2004), History of carbonate ion concentration over the last 100 million years, *Geochim. Cosmochim. Acta*, *68*(17), 3521–3530. 2.4.4

Urey, H. C. (1947), The thermodynamic properties of isotopic substances, *J. Chem. Soc.*, pp. 562–581. 1.3.1, 6

von Langen, P. J., D. K. Pak, H. J. Spero, and D. W. Lea (2005), Effects of temperature on Mg/Ca in neogloboquadrinid shells determined by live culturing, *Geochem. Geophys. Geosys.*, *6*(10), Q10P03, doi:10.1029/2005GC000989. 3.1, 3.4.1

Wade, B. S., and D. Kroon (2002), Middle Eocene regional climate instability: Evidence from the western North Atlantic, *Geology*, *30*(11), 1011–1014. 5.4

Walter, L. M., and J. W. Morse (1985), The dissolution kinetics of shallow marine carbonates in seawater: a laboratory study, *Geochim. Cosmochim. Acta*, *49*, 1503–1514. 2.4.4

Wang, L., M. Sarnthein, J.-C. Duplessy, H. Erlenkeuser, S. Jung, and U. Pflaumann (1995), Paleo sea surface salinities in the low-latitude Atlantic: The δ^{18}O record of *Globigerinoides ruber* (white), *Paleoceanography*, *10*(4), 95PA00577. 3.2

Watanabe, T., A. Winter, and T. Oba (2001), Seasonal changes in sea surface temperature and salinity during the Little Ice Age in the Caribbean Sea deduced from Mg/Ca and ^{18}O/^{16}O ratios in corals, *Mar. Geol.*, *173*, 21–35. 2.4.3

Watkins, J. M., and A. C. Mix (1998), Testing the effects of tropical temperature, productivity, and mixed-layer depth on foraminiferal transfer functions, *Paleoceanography*, *13*(1), 97PA02904. 2.3.2

Wefer, G., G. F. Lutze, T. J. Müller, O. Pfannkuche, W. Schenke, G. Siedler, and W. Zenk (Eds.) (1988), *Research Vessel METEOR Cruise No. 6 (1987/88): Atlantik 87/88*, Institut für Meereskunde der Universität Hamburg, Leitstelle METEOR, Hamburg. 4.3

Wefer, G., U. Bleil, F. Schott, and H.-B. Hirschleber (Eds.) (1991a), *Research Vessel METEOR Cruise No. 16 (1991): Atlantik 91*, Institut für Meereskunde der Universität Hamburg, Leitstelle METEOR, Hamburg. 4.3

Wefer, G., K. Hinz, and H. D. Schulz (Eds.) (1991b), *Research Vessel METEOR Cruise No. 20 (1991/92): Ostatlantik 91/92*, Institut für Meereskunde der Universität Hamburg, Leitstelle METEOR, Hamburg. 4.3

Wefer, G., W. H. Berger, J. Bijma, and G. Fischer (1999), Clues to ocean history: a brief overview of proxies., in *Use of Proxies in Paleoceanography: Examples from the South Atlantic*, edited by G. Fischer and G. Wefer, pp. 1–68, Springer-Verlag, Berlin, Heidelberg. 1.1

Whitko, A. N., D. W. Hastings, and B. P. Flower (2002), Past sea surface temperatures in the tropical South China Sea based on a new foraminiferal Mg calibration, *MARsci*, doi:MARSci. 2002.01.020101. 1.3.1, 2.1, 2.4.3, 2.5, 2.4.4, 3.1, 3.4.1, 3.6

Williams, D. F., A. W. H. Bé, and R. G. Fairbanks (1981), Seasonal stable isotopic variations in living planktonic foraminifera from Bermuda plankton tows, *Palaeogeogr., Palaeoclimatol., Palaeoecol.*, *33*, 71–102. 2.4.3, 6

Wolff, T., S. Mulitza, H. W. Arz, J. Pätzold, and G. Wefer (1998), Oxygen isotope *versus* CLIMAP (18 ka) temperatures: A comparison from the tropical Atlantic, *Geology*, *26*, 675–678. 5.3.3

Wüst, G. (1963), On the stratification and the circulation in the cold water sphere of the Antillean-Caribbean basins, *Deep-Sea Res.*, *10*, 165–187. 2.2

Wüst, G. (Ed.) (1964), *Stratification and Circulation in the Antillean-Caribbean Basins, Part 1: Spreading and Mixing of the Water Types with an Oceanographic Atlas*, 201 pp., Columbia University Press, London, New York. 2.2, 4.2

Zhou, G.-T., and Y.-F. Zheng (2003), An experimental study of oxygen isotope fractionation between inorganically precipitated aragonite and water at low temperatures, *Geochim. Cosmochim. Acta*, *67*(3), 387–399. 1.3.1, 6